TRPM2 ion channel trafficking and its role in mitochondrial fragmentation and cell death

Nada Khaled S Abuarab

Submitted in accordance with the requirements for the degree of Doctor of Philosophy

The University of Leeds
School of Biomedical Sciences

December 2015

Declaration

The candidate confirms that the work submitted is her own, except where work which has formed part of jointly-authored publications has been included. The contribution of the candidate and the other authors to this work has been explicitly indicated in the text. The candidate confirms that appropriate credit has been given within the thesis where reference has been made to the work of others. This copy has been supplied on the understanding that it is copyright material and that no quotation from the thesis may be published without proper acknowledgement.

Publications

- Rucha Karnik, Melanie J, Ludlow, **Nada Abuarab**, Andrew J. Smith, Matthew E. L. Hardy, David J. S. Elliott, Asipu Sivaprasadarao, *Endocytosis of hERG is clathrin-independent and involves Arf6.* Plos One, 2013. 8(12).

- Paul T Manna, Tim S Munsey, **Nada Abuarab**, Fangfang Li, Aruna Asipu, Gareth Howell, Alicia Sedo, Wei Yang, Jacqui Naylor, David J Beech, Lin-Hua Jiang, Asipu Sivaprasadarao, *TRPM2 mediated intracellular Zn^{2+} release triggers pancreatic beta cell death.* Biochem J, 2015. 466:537-546.

Manuscript under revision

- Fangfang Li, **Nada Abuarab**, Asipu Sivaprasadarao, *Reciprocal regulation of actin cytoskeleton remodelling and cell migration by calcium and zinc: role of TRPM2 channels*. 2015.

Manuscript in preparation

- **Nada Abuarab**, Tim S Munsey, Lin-Hua Jiang, Jing Li and Asipu Sivaprasadarao, *Zn^{2+} entry through mitochondrial TRPM2 channels promotes Drp-1 recruitment and mitochondrial fragmentation*.

Acknowledgements

First and foremost I offer my sincerest gratitude to my supervisor, Professor Asipu Sivaprasadarao, for his valuable suggestions during the planning and development of this research work, his willingness to give his time so generously and his intellectual support. One simply could not wish for a better or friendlier supervisor.

I would like to express my gratitude to Dr. Jing Li and Dr. Melanie Ludlow for all their valuable advice and friendly help during my lab work. I would also like to thank all of the Professor Sivaprasadarao research group members both past and present, Dr. Judith Hynes, Mr. Tim Munsey, Mrs. Hong-Lin Rong and Dr. Fangfang Li for their assistance and support during my project.

I would also like to thank Dr. Lin-Hua Jiang for being my second supervisor. I also humbly thank Dr. Sreenivasan Ponnambalam for being my assessor. I also wish to thank Dr. Jamel Mankouri for providing many fantastic antibodies.

My PhD would not be possible without the generous scholarship from King Saud bin Abdulaziz University for Health Sciences–National Guard Hospital and the UK-Saudi Bureau in London.

Most of all, I am indebted to my family. Gratitudes in Arabic.

لأبي الغالي خالد أبوعرب ، أعظم إنسان عرفته ، ياأنقى قلب وياأصدق الخلق. كنت ولازلت دوما تاج على رأسي أفتخر به. إليك أهدي هذا الجهد.. ليزداد فخرك بي.

لأمي الحبيبة الغالية ومعلمتي فتحيه ولي ، علمتني كيف أكتب وكيف أتعلم وكيف أتحمل ، فشكرا لك لكل حرف علمتني أن أكتبه في دفتري الصغير فساعدني أن أكتب هذا الدفتر الكبير.. شكرا لحبك وعطاءك وتشجيعك اللا محدود.

لأبني الغالي ومهجة قلبي فيصل ، شكرا لكل اللحظات التى أضحكتني فيها في وسط ضيق الحياة .. آسفه على كل الساعات والأيام التى قضيتها بعيده عنك .. أحبك جداً جداً.

لأختي الكبرى يسرى، كنتي دائما سنداً لي ولإبني في غربتي.. شكرا لعطاءك ودعمك وحبك.

لإخواتي شهد ورغد وأخي إبراهيم .. شكرا لدعمكم ودعواتكم وحبكم .. على الود نلتقي قريبا إن شاءالله.

الخميس 10 ديسمبر 2015
ندى خالد أبوعرب
ليدز- المملكة المتحدة

Abstract

Mitochondria play a central role in oxidative stress-induced cell death. By increasing the production of reactive oxygen species, such as H_2O_2, oxidative stress causes mitochondrial fragmentation and apoptosis. It was hypothesised that Transient Receptor Potential Melastatin 2 (TRPM2) channels play a role in mitochondrial fragmentation and cell death. The rationale behind this hypothesis was the published evidence that oxidative stress stimulates TRPM2 channels, resulting in an increase in the cytosolic levels of Ca^{2+} and Zn^{2+}, and that both these ions are detrimental to mitochondrial health and cell survival. To test the hypothesis, human umbilical vein endothelial cells (HUVECs) and endothelial cells isolated from wild-type and TRPM2 knock-out mice were used. TRPM2 actions were suppressed using pharmacological agents and small interfering RNA (siRNA). Fluorescent reporters were used to examine changes in intracellular ion distribution and organelle morphology. Molecular biology, biochemical and imaging techniques were used to examine the dynamics of ions and organelles.

Exposure of HUVECs to H_2O_2 or high glucose stress led to TRPM2 activation, resulting in extracellular Ca^{2+} entry, lysosomal membrane permeability (LMP) and the release of lysosomal free Zn^{2+}. Unexpectedly, this was accompanied by the accumulation of Zn^{2+} in the mitochondria. The rise in mitochondrial Zn^{2+} led to extensive mitochondrial fragmentation, mitochondrial outer membrane permeabilisation (MMP) and cell death. Silencing of TRPM2 channels with siRNA prevented intracellular Zn^{2+} redistribution, mitochondrial fragmentation and cell death. Endothelial cells derived from TRPM2 knock-out mice were resistant to oxidative stress-induced mitochondrial fragmentation. Biochemical and immunostaining experiments revealed an unexpected presence of TRPM2 channels in mitochondria, where they mediated mitochondrial Zn^{2+} uptake. Accumulation of Zn^{2+} in the mitochondria led to mitochondrial fragmentation by promoting the recruitment of cytoplasmic Drp1, an enzyme responsible for mitochondrial fission. Taken together, the results of this thesis revealed a novel mechanism for how oxidative stress can cause excessive mitochondrial fragmentation and cell death: the mechanism involves activation of TRPM2 channels leading to increased Ca^{2+} entry,

LMP and release of lysosomal Zn^{2+}; Zn^{2+} thus released is taken up by the mitochondria, leading to Drp1 recruitment, mitochondrial fragmentation and finally cell death.

Since mitochondrial fragmentation is associated with several age-related chronic illnesses, including neuronal (Alzheimer's, Parkinson's), cardiovascular (atherosclerosis, myocardial infarction) and metabolic/inflammatory (diabetes) disorders, these results suggest that the TRPM2 channel is a novel target that could be explored for therapeutic intervention of age-related illnesses.

Abbreviations

ACA	N-(p-Amylcinnamoyl) anthranilic
ADP	Adenosine-5'-diphophate
ATP	Adenosine-5'-triphophate
ADPR	Adenosine diphosphate ribose
Apaf-1	Apoptotic protease activating factor-1
Bcl-2	B-cell lymphoma 2
BPH-1	Benign prostatic hyperplasia cells
CaM	Calmodulin
CAP	Capsaicin
CAT	Catalase
Cy3	Cyanine 3
cyt *c*	Cytochrome *c*
Drp1	Dynamin-related protein 1
DMSO	Dulbecco's modified eagle medium
DPBS	Dulbecco's phosphate buffered saline
EDTA	Ethylenediamine-tetraacetic acid
EGTA	Ethylene glycol tetraacetic acid
eNOS	Endothelial nitric oxide synthase
ER	Endoplasmic reticulum
ERAD	ER-associated degradation
Fis1	Fission protein 1
FITC	Fluorescein isothiocyanate
GFP	Green fluorescent protein
GPX	Glutathione reductase
HA	Haemagglutinin A
HBSS	Hanks' Balanced Salt Solution
HEK-MSR	Human embryonic kidney cells expressing macrophage scavenger receptor
HEK-TRPM2	Human embryonic kidney (HEK293) cells expressing tetracycline

	inducible human TRPM2
HeLa	Line derived from cervical cancer cells taken from Henrietta Lacks
HEPES	4-(2-hydroxyethyl)-1-piperazineethanesulfonic acid
HO	Hydroxyl radical
HRP	Horseradish peroxidase
hTRPM2	Human TRPM2
HUVECs	Human Umbilical Vein Endothelial Cells
H_2O_2	Hydrogen peroxide
INS-1	Insulinoma cell
LB	Luria-Bertani broth
LMP	Lysosomal membrane permeability
LAMP-1	Lysosomal associated membrane protein 1
MFF	Mitochondria fission factor
Mfn	Mitofusin
MMP	Mitochondrial membrane permeability
Ml	Millilitre
MPT	Mitochondrial permeability transition pore
MLSP	Maximum life span potential
NAD	Nicotinamide adenine dinucleotide
Ng	Nanogram
NO	Nitric oxide
OPA1	Optic atrophy 1
PARG	Poly (ADP-ribose) glycohydrolase
PARP	Poly (ADP-ribose) polymerase
PBS	Phosphaye buffered saline
PCR	Polymerase chain reactions
PFA	Paraformaldehyde
Rpm	Revolutions per minutes
ROS	Reactive oxygen species
SBS	Standard Barth's Solution
SDS	Sodium dodecyl sulphate

SODs	Superoxide dismutases
TAE	Tris-acetate-EDTA buffer
Tm	Primer annealing temperature
TPEN	N,N,N',N'-tetrakis(2-pyridylmethyl)ethane-1,2-diamine
TRIS	Tris(hydroxymethyl)aminomethane
TRP	Transient receptor potential
TRPM2	Transient receptor potential melastatin 2
TRPV1	Transient receptor potential vanilloid 1
UV	Ultraviolet light
ZnT	Zinc transport

Amino acid abbreviations

Amino acid	Three-letter code	One-letter code
Alanine	Ala	A
Arginine	Arg	R
Asparagine	Asn	N
Aspartic acid	Asp	D
Cysteine	Cys	C
Glutamic acid	Glu	E
Glutamine	Gln	Q
Glycine	Gly	G
Histidine	His	H
Isoleucine	IIe	I
Leucine	Leu	L
Lysine	Lys	K
Methionine	Met	M
Phenylalanine	Phe	F
Proline	Pro	P
Serine	Ser	S
Threonine	Thr	T
Tryptophan	Trp	W
Tyrosine	Tyr	Y
Valine	Val	V

Table of contents

List of figures

List of tables

1 Introduction

Diabetes is a major risk factor for cardiovascular disease. Increase in blood glucose levels is associated with endothelial dysfunction, where mitochondria play a key role. High glucose has been shown to induce overproduction of reactive oxygen species (ROS) and thereby induce mitochondrial fragmentation and dysfunction of endothelial cells. However, the exact mechanism for how ROS induces mitochondrial fragmentation is not fully understood. The TRPM2 channel is a ROS sensitive ion channel that regulates intracellular Ca^{2+} and Zn^{2+} dynamics. The overall aim of this thesis is to examine the role of TRPM2 channels and intracellular changes in Ca^{2+} and Zn^{2+} dynamics on mitochondrial dynamics and endothelial cell viability. The aim of this chapter is to provide an overview of ROS, TRPM2 channels and mitochondrial dynamics.

1.1 Historical overview

Free radicals such as superoxide ($O_2^{\bullet-}$), hydroxyl ($OH^{\bullet}$) and nitric oxide ($NO^{\bullet}$) are derived from normal aerobic essential metabolism (Droge, 2002; Harman, 1956). Several decades ago, Harman noted that organisms (animals and plants) with a higher metabolic rate have a much shorter lifespan compared to those with a slower metabolism (Harman, 1956). However, the link between metabolism and aging was unclear. Harman introduced the free-radical theory of aging and degenerative diseases (Harman, 1956). This theory suggests that the generation of endogenous oxygen free radicals contributes to the process of cellular damage (Harman, 1956). However, the hypothesis of endogenous oxidants was controversial until superoxide dismutases (SODs) were discovered in 1968 (McCord and Fridovic, 1969). SODs are a family of enzymes which catalyse the dismutation of the superoxide radical anion ($O_2^{\bullet-}$) to H_2O_2 and oxygen (McCord and Fridovic, 1969). The discovery of SODs (McCord and Fridovic.I, 1969) and their mechanism provided support to Harman's hypothesis (Harman, 1956) that an organism would live longer if it had low oxidative stress or a higher level of antioxidants to mitigate oxidative stress.

Since the discovery of SODs, many studies have focused on superoxide radicals ($O_2^{\bullet-}$) and SODs and their physiological and pathophysiological roles. Superoxide radicals have been implicated in a variety of diseases including neurodegenerative diseases (Reiter, 1995), diabetes (Maritim et al., 2003), cancer (Church et al., 1993), inflammatory diseases (Salin and McCord, 1975) and ischemia (McCord et al., 1985). However, more recent studies have found that superoxide radicals can function in signal transduction in mammalian cells as well as regulating cell division and proliferation, migration and angiogenesis (Buetler et al., 2004; Werner, 2004).

Later studies have shown that mitochondria are a major source of $O_2^{\bullet-}$ and H_2O_2 production (Ku et al., 1993; Sohal et al., 1990). Mitochondrial generation of oxidative stress from the kidneys, heart and liver has been correlated with maximum life span potential (MLSP). The higher the metabolic rate, the higher the endogenous production of ROS in mitochondria from shorter-lived animal species compared to mitochondria from longer-lived animal species (Ku et al., 1993; Sohal et al., 1990). While these findings supported a free-radical theory of aging, no positive relationship was found between antioxidant defences and MLSP in species (Ku et al., 1993; Sohal et al., 1990). These findings have led to the view that the differences in aging rates may be due to differences in levels of oxidant production rather than antioxidant levels (Ku et al., 1993; Sohal et al., 1990).

A rise in the level of ROS has been linked to mitochondrial DNA fragmentation, membrane lipid damage and permeability changes, mitochondrial dysfunction and cell death (apoptosis) (Madesh and Hajnoczky, 2001; Richter, 1993; Wei et al., 2001). It was recognised that many cellular genes are activated to stimulate or suppress oxidative stress-induced apoptosis; these include genes encoding bcl-2, p53, TRPM2, RP-2, RP-8 and APO-1/FAS (Richter, 1993). It was also found that oxidative stress-induced cell death triggers extracellular Ca^{2+} entry and a rise in cytosolic levels (Farber, 1990). However, the exact mechanisms are unclear (Farber, 1990). Numerous studies have focused on the role of Ca^{2+} or Zn^{2+} ions in organelle stress-induced cell death

(Boya et al., 2003; Boya and Kroemer, 2008; Malaiyandi et al., 2005; Manna et al., 2015; Sun et al., 2012; Wiseman et al., 2007).

1.2 Oxidative stress

ROS are molecular oxygen (O_2) metabolites which have higher reactivity than O_2 (Finkel and Holbrook, 2000). They include unstable oxygen radicals such as superoxide anion radicals ($O_2^{\bullet -}$), hydrogen peroxide (H_2O_2) and hydroxyl radicals ($HO^{\bullet}$) (Finkel and Holbrook, 2000). ROS are continually produced during normal essential metabolism (Finkel and Holbrook, 2000). ROS at low levels (physiological level) play an important role in regulating cellular metabolic processes and other cellular processes including cell proliferation, differentiation and migration (Uttara et al., 2009; Waris and Ahsan, 2006). However, excessive ROS production is associated with a wide range of pathological conditions such as type 2 diabetes, neurodegenerative diseases, atherosclerosis and chronic inflammatory processes (Uttara et al., 2009; Waris and Ahsan, 2006). An imbalance between ROS production and antioxidants in favour of ROS is called oxidative stress (Uttara et al., 2009; Waris and Ahsan, 2006). Oxidative stress can be increased due to many environmental factors such as chemotherapeutic agents, cytokines and radiation, including ultraviolet (UV), ultrasound and microwave radiation (Sies, 1997; Waris and Ahsan, 2006). ROS are produced at several sites within the cell. These include the cytoplasm, mitochondria and endoplasmic reticulum.

1.2.1 Cytoplasmic ROS and NADPH oxidase

NADPH oxidase (NOX) is an important source of intracellular ROS generation. It is a multimeric enzyme comprising seven different mammalian isoforms which are known as NOX 1-5 (Sumimoto, 2008) and Duox1 and 2 (Mouche et al., 2007). NOX uses NADPH as a substrate to convert molecular oxygen into ROS (Martyn et al., 2006). NOX 4 is the only isoform that generates H_2O_2 instead of superoxide ($O_2^{\bullet -}$) (Martyn et al., 2006). NOX proteins are expressed in different tissues such as spleen, kidney and vascular smooth muscle (Sumimoto, 2008). ROS production by NOX activation is regulated by different stimuli such as growth factors, cytokines, free fatty acids, glucose and ions,

including Ca^{2+} and Zn^{2+} (Jiang et al., 2011a; Li and Shah, 2004; Sumimoto, 2008). Elevated intracellular Ca^{2+} (discussed in further detail later in this thesis) could act as an upstream signal in NOX activation and cytoplasmic ROS generation (Sumimoto, 2008). Protein kinase C (PKC) is a key regulator of NOX (Cosentino-Gomes et al., 2012). Ca^{2+} activates PKC (Jiang et al., 2011a; Sumimoto, 2008). Activated PKC is translocated from the cytoplasm to the cell membrane and phosphorylates P47 phox (Sumimoto, 2008) and P67phox (Jiang et al., 2011a). Phosphorylated P47phox or p67phox induces activation of NOX and triggers generation of superoxide anions (Jiang et al., 2011a; Sumimoto, 2008). As mentioned previously, superoxide is converted to H_2O_2 by superoxide dismutase (SOD) (Martyn et al., 2006). Studies have linked higher NOX activity to a variety of disease states such as diabetic vascular disease, neurodegenerative diseases (Alzheimer's disease and Parkinson's disease) and ischemic damage (Chen et al., 2011; Lambeth, 2007). Inhibition of NOX activity has been shown to have a protective role against diseases, indicating a significant pathophysiological role for excess cytoplasmic ROS (Chen et al., 2011; Lambeth, 2007).

1.2.2 Mitochondrial ROS

The majority of intracellular ROS is generated by mitochondria during normal metabolism (Finkel, 2012). Generation of mitochondrial superoxide radicals occurs at two sites in the electron transport chain; there are complex I (NADH dehydrogenase) and complex III (ubiquinone-cytochrome *c* reductase) (Finkel and Holbrook, 2000). Under normal conditions, complex III is the main source of ROS. Complex III produces $O_2^{\bullet-}$ in the mitochondrial matrix (Finkel and Holbrook, 2000). Superoxide dismutases (SOD1 and SOD2) convert $O_2^{\bullet-}$ into H_2O_2. H_2O_2 is then eliminated by enzymes such as catalase (CAT) and glutathione reductase (GPX). This leads to the regeneration of water and molecular oxygen (Finkel and Holbrook, 2000), as shown in Figure 1.1. Thus, the higher the metabolism rate, the greater the ROS production (Finkel and Holbrook, 2000). Mitochondrial biology is considered to be a potential therapeutic target, as the

mitochondria play important roles in cell death, inflammation, metabolism and ROS generation.

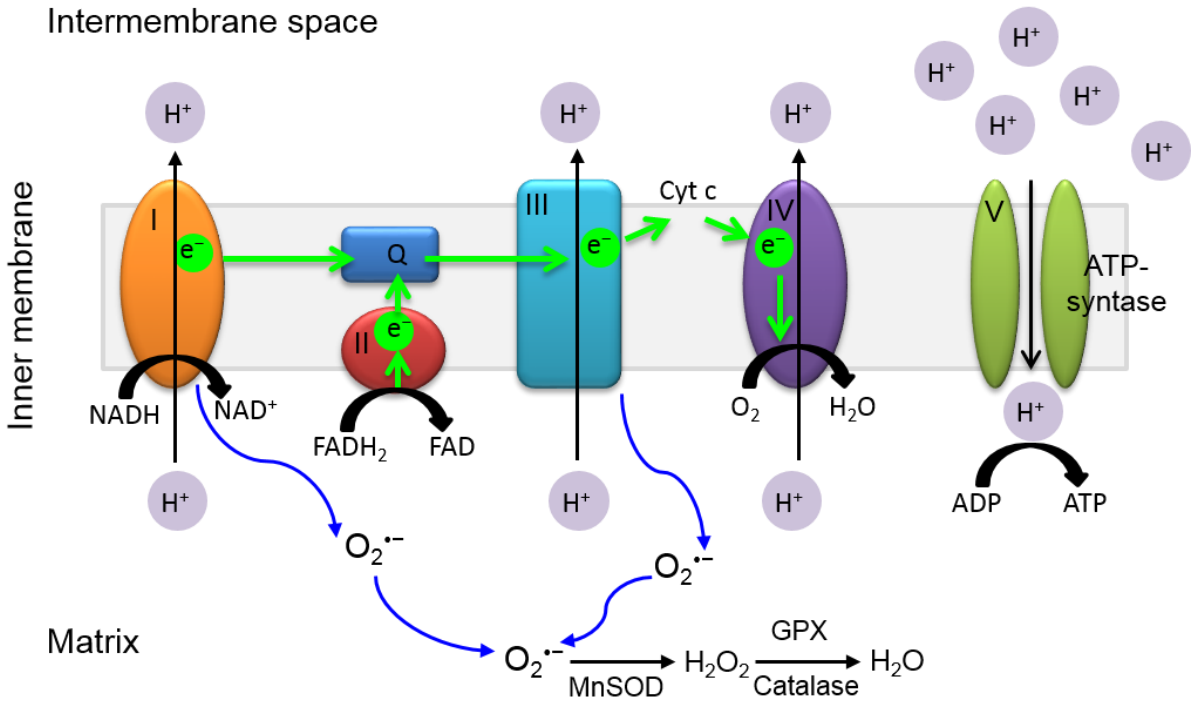

Figure 1.1 Mitochondrial respiratory chain and ROS generation, redrawn from (Yu and Bennett, 2014)

The electron transport chain receives electrons (e^-) from NADH and $FADH_2$. It mediates electron transfer from complex I to complex IV by ubiquinone (Q) and cytochrome *c* (cyt *c*). At complex IV, molecular oxygen is reduced by transported electrons, leading to the formation of water and a proton (H^+) gradient across the inner mitochondrial membrane. At complex V, the proton (H^+) gradient is used to convert ADP to ATP (ATP synthase). ROS are byproducts of the respiratory chain. At complex I and complex III, superoxide ($O_2^{\bullet-}$) is formed. Matrix manganese superoxide dismutase (MnSOD) converts $O_2^{\bullet-}$ to H_2O_2. H_2O_2 is subsequently reduced to H_2O by glutathione peroxidase (GPX) or catalase.

1.2.3 Endoplasmic reticulum ROS

The endoplasmic reticulum (ER) is an organelle that is responsible for the synthesis and correct folding of proteins for cell survival and normal physiological functions (Zhang

and Kaufman, 2008). Notably, 25% of cellular ROS are generated during the formation of disulphide bonds (oxidizing site) during oxidative protein folding (Wang et al., 2014; Zhang and Kaufman, 2008). The accumulation of unfolded and misfolded proteins in the ER initiates ROS accumulation and induces ER stress. Mitochondrial ROS production can also be enhanced by ER stress. ER stress induces Ca^{2+} leak from the ER stores. Ca^{2+} thus released enters mitochondria where it induces mitochondrial membrane depolarisation, ROS production and cell death (Denmeade et al., 2012).

Recently, ER stress-inducers have been investigated as potential anticancer drugs by pharmaceutical companies (Denmeade et al., 2012). There are many drugs capable of inducing ER stress and cancer cell death; these include bortezomib, celecoxib and thapsigargin (Denmeade et al., 2012; Kardosh et al., 2008).

1.3 Organelles and oxidative stress

1.3.1 Oxidative stress and lysosomes

Lysosomes are dynamic organelles discovered more than 50 years ago by Christian de Duve during his study on the distribution of intracellular enzymes using centrifugal fractionation techniques (de Duve, 2005; De Duve et al., 1955). Lysosomes contain hydrolytic enzymes including proteases, lipases, nucleases, glycosidases, phospholipases, phosphatases and sulfatases (Boya and Kroemer, 2008; Turk and Turk, 2009). They are responsible for the degradation of the macromolecules that come from autophagy or the endocytic trafficking pathway (Turk and Turk, 2009). Therefore, lysosomes are also referred to as “suicide bags” (Turk and Turk, 2009). It has been thought that lysosomes are involved not only in the degradation of macromolecules but also in apoptosis (Boya and Kroemer, 2008; Turk and Turk, 2009). Oxidative stress induces partial lysosomal membrane permeabilisation (LMP) which leads to the release many lysosomal proteases into the cytosol (Boya and Kroemer, 2008; Turk and Turk, 2009). These proteases, including cathepsins such as cathepsin B, cathepsin D and cathepsin L, contribute to the apoptosis signalling pathway (Turk and Turk, 2009).

The complete breakdown of lysosomes and the release of lysosomal proteases at a high concentration induce necrosis. However, though it is known that oxidative stress induces LMP (Boya et al., 2003; Boya and Kroemer, 2008; Repnik et al., 2014), the underlying mechanisms are not clear. It has been thought that LMP is a result of oxidants' nonspecific attack on the lysosomal membrane lipids. However, recent studies suggest a biochemical mechanism whereby lipases (such as phospholipase A2, sphingomyelinase and phospholipase C) act on lysosomal membranes (Boya and Kroemer, 2008; Repnik et al., 2014). These lipases are activated by the cytosolic entry of extracellular Ca^{2+}. However, the identity of Ca^{2+} channels or the transporters responsible for Ca^{2+} entry and LMP is not known.

1.3.2 Oxidative stress and mitochondria

Mitochondria exist as a network of large and branched tubules. They are highly dynamic and undergo continual fusion and fission in order to maintain their function and morphology (Chen and Chan, 2005) (discussed in further detail later in this thesis). However, many studies have shown that extracellular or mitochondrial oxidative stress disrupts the function and morphology of mitochondria (Chan, 2006; Chen and Chan, 2005). An imbalance between fission and fusion events is associated with a number of diseases such as diabetes (Archer, 2013), neurodegenerative diseases (Archer, 2013; Wang et al., 2009), ischemia reperfusion injury (Archer, 2013; Ong et al., 2010) and endothelial dysfunction (Shenouda et al., 2011).

Oxidative stress leads to increased cytosolic Ca^{2+} concentration. This in turn activates other mechanisms, including Ca^{2+} buffering by organelles (Rosenstock et al., 2004). Ca^{2+} uptake by mitochondria is one of the mechanisms that contributes to the buffering of cytosolic Ca^{2+} (Rosenstock et al., 2004). It has been reported that an increase in Ca^{2+} uptake by mitochondria triggers a decrease in the mitochondrial membrane potential (Rosenstock et al., 2004). The resulting increase in Ca^{2+} uptake also leads to mitochondria permeability transition (MPT), which is a nonspecific permeability pore in the inner membrane of mitochondria (Rosenstock et al., 2004). A change in

mitochondrial membrane potential initiates cytochrome *c* release from the inner mitochondrial membrane (IMM) (Ott et al., 2002). Cytochrome *c* release to extra-mitochondrial milieu occurs in a two-step process (Ott et al., 2002). In the first step, cytochrome *c* binds to two pools that attach to the IMM (Ott et al., 2002). One is loosely attached to the IMM through electrostatic interaction with the anionic phospholipid. This can be stimulated through changes in the pH or surface charge density or ionic strength. The second pool is tightly bound to the IMM by hydrophobic interaction, and it can be mobilized by the oxidation mitochondrial lipids (remodelling of membrane structure). Once the association of cytochrome *c* to the IMM is initiated, the soluble cytochrome *c* translocates to the cytoplasm where it interacts with other proteins. Cytochrome *c* binds to apoptotic protease activating factor-1 (Apaf-1) in the cytoplasm (Boya et al., 2003; Slee et al., 1999). The resulting protein complex activates caspase-9, which initiates programmed cell death by activating caspase-3 and caspase-7 (Boya et al., 2003; Slee et al., 1999). Activated caspase-3 translocates into the nucleus and induces DNA fragmentation (Janicke et al., 1998). Collectively, caspases (aspartic proteases) destroy cytoplasmic and nuclear proteins, leading to apoptosis (Janicke et al., 1998).

It has also been found that oxidative stress is associated with increased mitochondrial fragmentation, which is considered a sign of early-stage apoptosis (Karbowski and Youle, 2003). Oxidative stress-induced changes in the mitochondrial morphology from tubular to fragmented mitochondria is explained later in this chapter.

1.3.3 Oxidative stress and endoplasmic reticulum

The ER is a dynamic compartment and the main site of Ca^{2+} storage in the cell (Meldolesi and Pozzan, 1998). Most transmembrane proteins are folded in the ER as they enter the ER as unfolded polypeptide chains (Ron and Walter, 2007). The ER contains chaperons, glycosylation enzymes and oxidoreductases, which catalyse protein folding, glycosylation and disulphide bond formation, respectively, in the lumen of the ER (Haynes et al., 2004; Travers et al., 2000). However, misfolded proteins

accumulate in the lumen of the ER. This activates an intracellular stress response pathway called unfolded protein response (UPR) (Ron and Walter, 2007; Travers et al., 2000). UPR upregulates a range of genes that are required for protein folding, ER-Golgi trafficking, ER-associated degradation (ERAD) and ER expansion (Haynes et al., 2004; Malhotra and Kaufman, 2007; Ron and Walter, 2007; Travers et al., 2000). ERAD is a process that promotes the degradation of misfolded protein in the cytosol by proteasomes involving ubiquitination of misfolded proteins (Ron and Walter, 2007).

Unfolded protein accumulation in the ER induces ER stress. During ER stress, Ca^{2+} is released from the ER to the cytoplasm by BAX and BAK oligomers (Malhotra and Kaufman, 2007). Ca^{2+} released from the ER is taken up by mitochondria, leading to increased mitochondrial ROS production and inner mitochondrial membrane depolarisation and cytochrome *c* release (Malhotra and Kaufman, 2007).

ER stress-induced cell death occurs via pro-apoptotic components such as the BCL2 family and caspases (caspases 2, 3, 4, 7, 9 and 12) (Dahmer, 2005; Di Sano et al., 2006; Hitomi et al., 2004). ER stress and calpain activate caspase 12, which is associated with the ER membrane (Tan et al., 2006). Caspase 12 activation in turn activates caspase 9, which activates caspase 3, finally causing cell death (Dahmer, 2005; Hitomi et al., 2004; Tan et al., 2006), as shown in Figure 1.2. Moreover, BAX and BAK (discussed in further detail later in this thesis), which are pro-apoptotic BCL2 family members, form a pore in the membrane of the ER through which Ca^{2+} is released. The mechanism by which Ca^{2+} induces mitochondria mediated apoptosis has been described above.

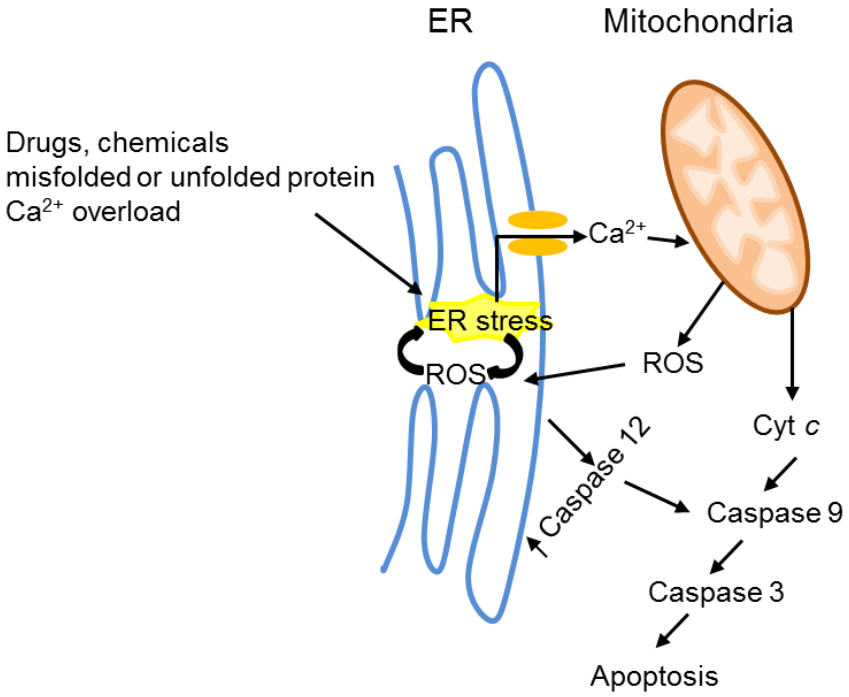

Figure 1.2 ER stress and ROS-induced cell death, redrawn from (Novo and Parola, 2012)
Environmental factors induce ER stress and ROS generation that increase Ca^{2+} release from the ER. The released Ca^{2+} is taken up by mitochondria, leading to mitochondrial ROS generation and mitochondrial outer membrane permeabilisation (MOMP). MOMP activates a pro-apoptotic pathway and increases cytochrome *c* (cyt *c*) release from mitochondria into the cytoplasm, leading to caspase-9 activation followed by caspase-3 activation. ROS increase in the ER also activates caspase 12, which in turn activates caspase 9 and caspase 3. Thus, ROS generated from the ER and mitochondria both contribute to apoptosis through a common pathway involving caspases 9 and 3.

1.3.4 Oxidative stress and protein trafficking

There are two different routes of normal intracellular protein trafficking to lysosomes. In the first route, proteins travel from the Golgi apparatus to late endosomes and then to lysosomes (Harter and Mellman, 1992; Mathews et al., 1992). In the second route, proteins start in the Golgi apparatus and travel to the plasma membrane and then to early endosomes, late endosomes and lysosomes (Harter and Mellman, 1992). However, recent studies have indicated that the presence of oxidative stress induces

the aforementioned organelle stress as well as lysosomal trafficking and fusion with the plasma membrane (lysosome exocytosis) (Li et al., 2012). This trafficking pathway during oxidative stress is Ca^{2+} dependent, as the exocytosis of lysosomes could be prevented by chelating Ca^{2+} with EGTA (Li et al., 2012; Rodriguez et al., 1997). Thus oxidative stress via intracellular Ca^{2+} plays a key role in the trafficking of lysosomes to the membrane. It has also been reported that oxidative stress affects endocytic trafficking. This was demonstrated by the significant decrease in the number of cell-surface transferrin (Tf)-binding sites and increase in the recycling of internalised Tf back to the plasma membrane in the presence of oxidants (Cheng and Vieira, 2006).

All of the above evidence indicates that cellular protein trafficking by lysosomes and internalisation is affected during oxidative stress. However, the relevance of these effects on cell physiology is unclear.

1.4 Oxidative stress and calcium ion channels

Ca^{2+} is an intracellular messenger that controls multiple cellular processes such as gene transcription, cell proliferation, differentiation, growth, membrane excitability, exocytosis and muscle contraction (Arundine and Tymianski, 2003; Berridge, 1993; Berridge et al., 1998; Clapham, 1995). Cytosolic Ca^{2+} can be elevated because of Ca^{2+} entry from the intracellular space or Ca^{2+} release from organelles. As such, calcium ion channels are not only found in the external membrane plasma membrane but also in the membranes of intracellular organelles such as the ER (Clapham, 1995), lysosomes (Rizzuto and Pozzan, 2006) and mitochondria (Clapham, 1995). The normal concentration of intracellular Ca^{2+} is about 100 nM; however, Ca^{2+} concentration can be elevated to 1 µM when the cell is stimulated (Fan et al., 2011).

Ca^{2+} elevation can be achieved by different mechanisms including calcium pumps (Strehler and Treiman, 2004), exchangers (Blaustein and Lederer, 1999) and ion channels (Clapham, 2007). Plasma membrane Ca^{2+}/ATPase (PMCA) helps to keep the intracellular Ca^{2+} at a low level by pumping Ca^{2+} out of the cytoplasm;

sacro/endoplasmic reticulum Ca^{2+}/ATPase (SERCAs) pumps Ca^{2+} into sarco/endoplasmic reticulum to reduce cytosolic Ca^{2+} (Strehler and Treiman, 2004). The Na^{+}/Ca^{2+} exchangers (NCX) (Blaustein and Lederer, 1999) exchange one Ca^{2+} ion for three Na^{+} ions (Blaustein and Lederer, 1999).

There are several types of Ca^{2+} ion channels in the plasma membrane which have different gating mechanisms. Voltage-gated calcium ion channels are activated when the membrane is depolarised; they allow Ca^{2+} entry (Catterall, 2011). Store-operated channels (SOCs) are activated in response to store depletion (low concentration of ER Ca^{2+}) (Putney, 2005). SOCs are made up of STIM-1 (stromal interaction molecule-1) and Orai1 subunits. Orai1 is a Ca^{2+} ion channel present in the plasma membrane (Feske, 2007). STIM-1 is located in the ER. In response to store depletion, STIM-1 associates with Orai1; this association leads to the activation of Orai-1 and extracellular Ca^{2+} entry (Feske, 2007; Putney, 2005).

However, the cytosolic Ca^{2+} concentration can be controlled by chelation of intracellular Ca^{2+} by Ca^{2+}-binding proteins (Burgoyne, 2007). Ca^{2+}-binding proteins are classified into buffering proteins and sensors (Burgoyne, 2007). Ca^{2+}-buffering proteins have EF-hands with which they bind Ca^{2+} (Burgoyne, 2007). Examples include calbindin, a Ca^{2+}-binding protein found in the brain (Mattson et al., 1991). Ca^{2+} sensors are EF-hand proteins that regulate the activity of other proteins (Burgoyne, 2007); examples include phospholipase C (PLC), IP3 receptor, the ryanodine receptor and calmodulin (Burgoyne, 2007; Clapham, 2007).

Free Ca^{2+} is sequestered by intracellular organelles such as the ER and mitochondria. As mentioned previously, Ca^{2+} sequestering into the ER is mediated by the SERCA pump (Strehler and Treiman, 2004), whereas Ca^{2+} entry into mitochondria is via voltage-dependent anion channel 2 (VDAC2) and the mitochondrial calcium uniporter (MCU) located in the outer and inner membranes of the mitochondria respectively (Min et al., 2012; Kirichok et al., 2004).

Transient receptor potential (TRP) channels represent a major superfamily that regulates Ca^{2+} entry into cells. Several members of TRP channels are activated by oxidative stress, including transient receptor potential vanilloid 1 (TRPV1) and transient receptor potential melastatin 2 channel (TRPM2). The following section explains the function of these channels.

1.4.1 Transient receptor potential (TRP) channels

TRP channels play key roles in the calcium-signalling processes by regulating cellular Ca^{2+} by permitting Ca^{2+} entry through the plasma membrane and/or its release from intracellular stores (Nagamine et al., 1998; Nilius et al., 2007; Venkatachalam and Montell, 2007).

The TRP family consists of two main groups and seven subfamilies based on differences in the amino acid sequence (Venkatachalam and Montell, 2007). Group 1 includes the TRPC (canonical), TRPV (vanilloid), TRPM (melastatin), TRPN and TRPA (ankyrin) subfamilies; these subfamilies have the strongest sequence homology between them (Venkatachalam and Montell, 2007) (Figure 1.3). Group 2 comprises the TRPP (polycystin) and TRPML (mucolipin) subfamilies, which have a large loop that separates the first two transmembrane domains. In addition, they have significant sequence homology in the transmembrane segments (Venkatachalam and Montell, 2007).

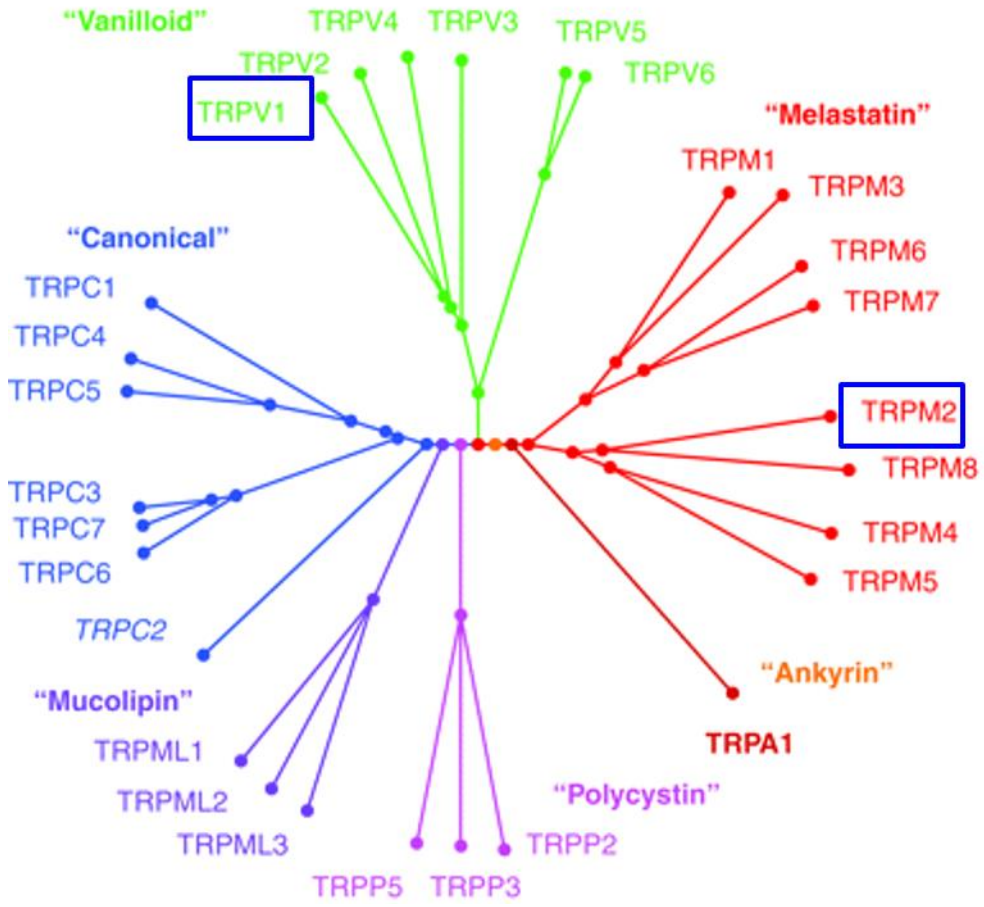

Figure 1.3 TRP-channel superfamily phylogenetic tree

The identified subfamilies in mammals are TRPC (canonical), TRPV (vanilloid), TRPM (melastatin), TRPA (ankyrin), TRPP (polycystin) and TRPML (mucolipin). Boxed ion channels are activated by oxidative stress, and their activation induces cell death, reproduced from (Gees et al., 2010).

1.4.1.1 Transient receptor potential vanilloid 1 channel (TRPV1)

TRPV1 is a Ca^{2+}-permeable, non-selective cation channel (Lishko et al., 2007). TRPV1 channels are like other TRP channels. They consist of six transmembrane domains with a pore-forming loop between transmembrane domains 5 and 6 and cytoplasmic N- and C-termini (Lishko et al., 2007). TRPV1 is highly expressed in the hippocampus and cortex, and it has been found in the hypothalamus, locus coeruleus, superior colliculus,

spinal cord and pancreatic islet cells (Caterina et al., 1997; Ho et al., 2012; Roberts et al., 2004). TRPV1 can be activated by different stimuli such as low pH, noxious heat, capsaicin and oxidative stress (Caterina et al., 1997). Activation of TRPV1 channels results in an overload of cytosolic Ca^{2+}, leading to oxidative stress mitochondrial damage and cell death (Amantini et al., 2007).

1.4.1.2 Transient receptor potential melastatin 2 channel (TRPM2)

The TRPM2 channel was discovered in 1998 (Nagamine et al., 1998). It was previously named TRPC7 (Nagamine et al., 1998) or LTRPC2 (Hara et al., 2002; Perraud et al., 2001). It is a voltage-independent, calcium-permeable, non-selective cation channel (Perraud et al., 2001). It has unique gating properties conferred by the presence of a functional adenosine diphophoribose hydrolase domain in its C-terminus (Jiang et al., 2011b; Kuhn et al., 2005; Lange et al., 2009; Nilius, 2007). TRPM2 is therefore referred to as a chanzyme, which means it is an ion channel fused to an enzymatic domain (Lange et al., 2009; Venkatachalam and Montell, 2007). The focus of this thesis is on the TRPM2 channel; therefore, this channel is discussed in more detail.

The aberrant functioning of TRPM2 channels can give rise to several types of disease (discussed in further detail later in this thesis) (Nilius, 2007). Diseases due to ion channel dysfunction are called channelopathies. However, there are few reports showing a direct link between mutations in TRPM2 and human diseases (Nilius, 2007). TRPM2, however, is thought to play an important role in diseases such as diabetes mellitus, atherosclerosis, Parkinson's disease and Alzheimer's disease (Takahashi et al., 2011). This review focuses on the main characteristics of the TRPM2 gene, its expression, localisation, architecture, permeation properties and activation through important stimuli that can gate the channel. This review also outlines the role of TRPM2 in diseases and the pharmacology of the channel.

The TRPM2 gene

The human TRPM2 gene is located on chromosome 21 (Nagamine et al., 1998) within the disease-rich 21q22.3 locus. This locus is linked to various types of inherited

diseases such as bipolar affective disorder and nonsyndromic hereditary deafness (Nagamine et al., 1998; Perraud et al., 2003; McQuillan et al., 2006). The human TRPM2 gene comprises 32 exons, making it approximately 100 kb long (Nagamine et al., 1998). The gene is highly expressed in brain cells (McQuillan et al., 2006).

TRPM2 expression and localisation in the mammalian cell

In addition to the brain, TRPM2 is expressed in various other tissues, including spleen, bone marrow, liver, heart, endothelium, heart, pancreas and lung (Fonfria et al., 2004; Takahashi et al., 2011; Togashi et al., 2006). TRPM2 is also present in several cell lines, including the neutrophil cell line, CRI-G1 insulinoma cells, microglia and the U937 monocyte cell line (Kolisek et al., 2005; Togashi et al., 2006). In mammalian cells, TRPM2 is normally expressed at the plasma membrane. However, in some cell types, it is expressed in late endosomes and lysosomes (Lange et al., 2009; Sumoza-Toledo et al., 2011). For example, TRPM2 is expressed in the endolysosomal vesicles in dendritic cells (DCs), while in neutrophils, TRPM2 is expressed in the plasma membrane (Abe and Puertollano, 2011; Lange et al., 2009; Sumoza-Toledo et al., 2011). In the INS-1 pancreatic β-cell line, TRPM2 is expressed in lysosomes (Lange et al., 2009; Manna et al., 2015).

TRPM2 channel architecture

TRPM channels have limited amino acid sequence homology to other members of the TRP ion-channel family (Nilius et al., 2003). It is a tetrameric protein with four subunits, each comprising six transmembrane (S1-S6) segments (Nilius, 2007; Takahashi et al., 2011; Venkatachalam and Montell, 2007). The pore forming-part of the channel is made from loops between the S5 and S6 segments (Nilius, 2007; Nilius et al., 2003) (Figure 1.4).

There are four key TRPM2 residues that play a role in determining divalent cation permeation properties (Xia et al., 2008). These are Glu-960, Gln-981, Asp-987 and Glu-1022 residues (Xia et al., 2008) (Figure 1.4). There are two conserved cysteine residues

at positions 996 and 1008 in the putative pore region in human TRPM2; these are essential for TRPM2 function (Mei et al., 2006).

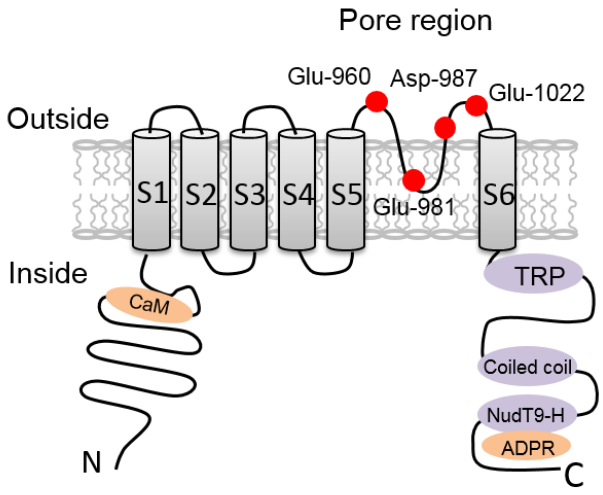

Figure 1.4 Topology of a TRPM2 subunit showing six transmembrane (TM) domains (S1-S6) with N and C-terminal regions; redrawn from (Takahashi et al., 2011)

The N-terminal region includes the calmodulin (CaM) binding region, while the C-terminal region includes the coiled-coil region, NudT9-H region and TRP region. The pore region (S5-S6) has residues (Glu-960, Glu-981, Asp-987 and Glu-1022) that control the permeation property of the TRPM2 channel.

The N-terminal in TRPM2 is important for protein trafficking and for correct assembly of channel subunits. The TRPM2 C-terminal has a coiled-coil domain, which is about 100 amino acids long, a linker region of about 30 amino acids and a NudT9-H domain of about 270 amino acids (Perraud et al., 2001). The so-called Nudix box is positioned in the NudT9-H domain, which consists of 22 amino acids (Perraud et al., 2001). The Nudix box is important for the enzymatic hydrolysis of nucleoside diphosphates (Perraud et al., 2001).

TRPM2 permeation properties and activation

Both whole-cell and single-channel current measurements demonstrated that TRPM2 is a non-selective cation channel (Perraud et al., 2001). It has a high level of permeation to potassium, sodium, caesium, and calcium ions (Perraud et al., 2001). Using the

FluoZin-3 probe, Ye and co-wrkers demonstrated TRPM2 channels can promote Zn^{2+} permeation (Ye et al., 2014). Studies have shown that oxidant activation of TRPM2 channels and the consequent rise in cytosolic Ca^{2+} levels can lead to plasma membrane depolarisation (Wehage et al., 2002).

TRPM2 channels are activated by oxidative stress (Hara et al., 2002; Wilkinson et al., 2008). While oxidants such as H_2O_2 can directly activate the channel by oxidising a methionine (Met-214) residue located in the N-terminus of TRPM2, much of H_2O_2 induced channel activation is indirect being mediated by ADP-ribose (ADPR) (see later). Furthermore, Ca^{2+}, which enters through the plasma membrane channel, can allosterically activate the channel (Hara et al., 2002; Perraud et al., 2001). Other activating intracellular signals include cyclic ADPR (cADPR) and nicotinic acid adenine dinucleotide phosphate (NAADP). They are thought to work as co-activators in combination with ADPR (Beck et al., 2006), although this is somewhat controversial (see later).

Signals that activate TRPM2 channels

ADPR, cADPR and NAD

Oxidant induced production of ADPR occurs in the nucleus as well as mitochondria. Oxidants cause damage to DNA, triggering activation of DNA repair enzymes: poly (ADPR) polymerase (PARP) and poly (ADPR) glycohydrolase (PARG) (Lange et al., 2009; Wilkinson et al., 2008). PARP catalyses the transfer of ADPR moieties from NAD^+ to nuclear proteins by a process known as polyADP ribosylation. PARG causes the release of ADPR from the polyADP-ribosylated proteins. ADPR diffuses from the nucleus into the cytoplasm to activate the TRPM2 channel. The other source of ADPR is mitochondria, where it is produced by the action of NADase on NAD^+ (Ayub and Hallett, 2004; Wilkinson et al., 2008). NAD^+ is normally restricted to the matrix of mitochondria because of the impermeability of mitochondrial membranes (Ayub and Hallett, 2004). However, during oxidative stress, when mitochondrial Ca^{2+} uptake increases, the permeability of the inner membrane to NAD^+ increases due to the opening of the mitochondrial permeability transition pore (MPTP). This leads to an

increase in the access of NAD^+ to the outer membrane NADase and release of ADPR into the cytosol through the permeable outer mitochondrial membrane (Ayub and Hallett, 2004).

TRPM2 activation occurs when ADPR binds to the C-terminal NudT9-H domain (Perraud et al., 2001; Venkatachalam and Montell, 2007). This then seems to be followed by the hydrolysis of ADPR, presumably terminating the TRPM2 activity (Takahashi et al., 2011; Venkatachalam and Montell, 2007). However, the enzymatic activity of TRPM2 has not yet been demonstrated (Takahashi et al., 2011). Although NAD^+ was thought to activate TRPM2 channels directly, Kolisek and co-workers have demonstrated that TRPM2 activation by NAD^+ occurs later than ADPR activation and at a much higher concentration (Kolisek et al., 2005). Thus the current consensus is that the effect of NAD^+ on TRPM2 is indirect via ADPR. Other reported activator of TRPM2 channel is cyclic ADP-ribose (cADPR) (Kolisek et al., 2005) and NAADP (Beck et al., 2006). However, a recent study reported that cADPR and NAADP do not enhance activation by ADPR, raising doubts on the role cADPR and NAADP as coactivators of the channel (BalazsToth and Csanady, 2010), see Table 1.1.

Ca^{2+}

McHugh and colleagues have reported that intracellular Ca^{2+} is crucial for ADPR-mediated TRPM2 activation (McHugh et al., 2003). It was suggested that Ca^{2+} acts as a cofactor and modulator in gating TRPM2 (Kolisek et al., 2005; McHugh et al., 2003). As intracellular Ca^{2+} rises, TRPM2 sensitivity to ADPR increases. This allows gating of the TRPM2 channel at lower concentrations of ADPR (Kolisek et al., 2005). Other studies however suggest that TRPM2 gating by intracellular Ca^{2+} can occur without the involvement of ADPR (Du et al., 2009). The direct effect of intracellular Ca^{2+} was confirmed by mutating the ADPR binding site on the TRPM2 channel and using alternative spliced isoforms (Du et al., 2009).

Table 1.1 TRPM2 channel activators

Ligand	Affinity	Unit	Concentration ranges (M)	Reference
NAD	-	-	$3x10^{-4}$ - $1x10^{-3}$	(Hara et al., 2002; Heiner et al., 2003; Sano et al., 2001; Togashi et al., 2006)
H_2O_2	-	-	$5x10^{-7}$ - $5x10^{-5}$	(Fonfria et al., 2004; Smith et al., 2003; Hara et al., 2002; Kraft et al., 2004; Wehage et al., 2002)
cADPR	5.0	pEC_{50}	-	(Kolisek et al., 2005; Lee, 2012; Togashi et al., 2006)
ADP ribose	3.9-4.4	pEC_{50}	-	(Perraud et al., 2001)
NAADP	3.1	pEC_{50}	-	(Beck et al., 2006)

Temperature

Activity of the TRPM2 channel is also sensitive to temperature (Kashio et al., 2011; Togashi et al., 2006). Kashio and colleagues demonstrated that H_2O_2 is capable of lowering the temperature threshold for TRPM2 activation. This is a unique mechanism which was referred to as “sensitization” (Kashio et al., 2011). In the absence of H_2O_2, the temperature threshold for TRPM2 activation is in the supraphysiological range (Kashio et al., 2011). The H_2O_2 sensitization is mediated by the oxidation of Met-214 residue located in the N-terminus of the channel. Mutation of this residue to alanine prevents sensitization completely (Kashio et al., 2011).

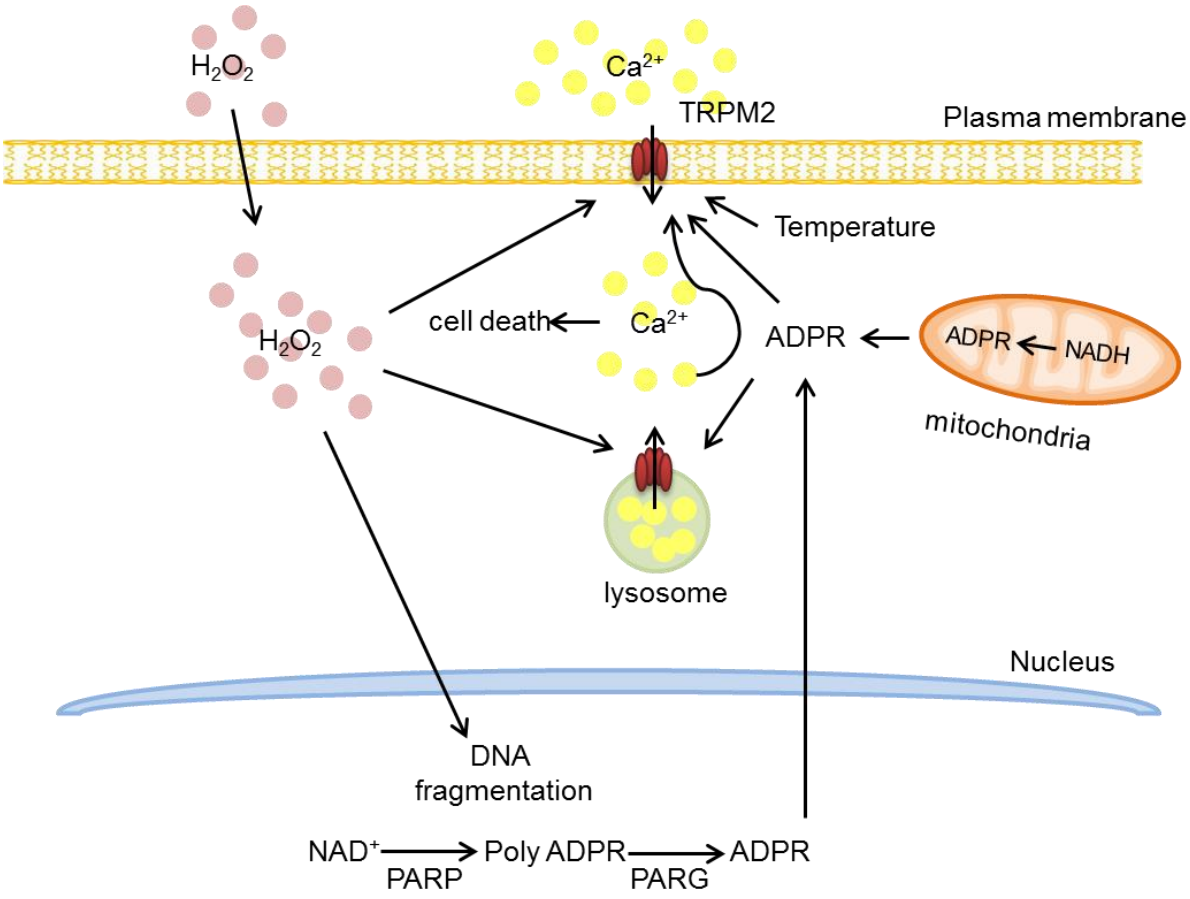

Figure 1.5 Signalling mechanisms for TRPM2 activation and inducing cell death

H_2O_2 can cross the plasma membrane, leading to direct activation of TRPM2 channels. H_2O_2 activation of the channel, however, is largely brought about by the production of ADPR in mitochondria and the nucleus. It causes production of ADPR from NADH in the mitochondria by activating NADase. In the nucleus, ADPR is generated by the activation of PARP/PARG pathway in response to H_2O_2 induced DNA damage. H_2O_2 lowers the temperature threshold required for TRPM2 activation. TRPM2 activation promotes Ca^{2+} influx across the plasma membrane and/or Ca^{2+} release from lysosomes. Ca^{2+} can allosterically activate the channel by acting on the cytosolic domain of the channel. A rise in intracellular free Ca^{2+} eventually leads to cell death.

Pharmacology of TRPM2 channels

To date, there are no specific TRPM2 inhibitors. However, there are several blockers which work effectively but not specifically on TRPM2. These blockers are antifungal imidazoles, such as clotrimazole and econazole, and flufenamic acid (FFA), which is a non-steroidal anti-inflammatory compound (Hill et al., 2004). FFA is widely used and completely inhibits the TRPM2 channel at 200 µM (Jiang et al., 2011b; Lee et al., 1996). AMP is considered as an ADPR negative feedback regulator (Kolisek et al., 2005). Thus, AMP can inhibit ADPR-mediated gating of the TRPM2 channel (Kolisek et al., 2005). 2-aminoethoxydiphenyl borate (2-APB) is also an effective blocker that induces partial inhibition at a low concentration (10 µM) but complete inhibition at a higher concentration (100 µM) (Togashi et al., 2008). ACA (N-(p-Amylcinnamoyl) anthranilic) is another potent inhibitor of TRPM2 channels (Kraft et al., 2006). In addition, TRPM2 function can be inhibited by the PARP inhibitor (N-(6-oxo-5,6-dihydro-phenanthridin-2-yl)-N,N-dimethylacetamide) (PJ34). PJ34 protects from H_2O_2 activation of TRPM2 channels, intracellular Ca^{2+} elevation and cell death (Fonfria et al., 2004) (Table 1.2).

Table 1.2 TRPM2 channel inhibitors

Ligand	**Affinity**	**Unit**	**Inhibitory concentration range (M)**	**Reference**
flufenamic acid	-	-	$5x10^{-5}$ - $1x10^{-3}$	(Hill et al., 2004a; Togashi et al., 2008)
clotrimazole	-	-	$3x10^{-6}$ - $3x10^{-5}$	(Hill et al., 2004b)
econazole	-	pIC_{50}	$3x10^{-6}$ - $3x10^{-5}$	(Hill et al., 2004b)
2-APB	6.1	pIC_{50}	-	(Togashi et al., 2008)
ACA	5.8	pIC_{50}	-	(Kraft et al., 2006)

TRPM2 and diseases

As mentioned previously, tissue damage can occur through activation of TRPM2 by oxidative stress. This could lead to different pathophysiological conditions, such as autoimmune disease, neurodegenerative disorders (Parkinson's disease and Alzheimer's), atherosclerosis and diabetes mellitus (Abe and Puertollano, 2011).

Oxidants also play a role in the regulation of macromolecules and circulating cells within the vasculature (Johnson et al., 1989). ROS are generated at the site of inflammation and injury (Di et al., 2012). The TRPM2 channel mediates oxidative stress-induced endothelial hyperpermeability (Dietrich and Gudermann, 2008; Hecquet and Malik, 2009). Understanding the role of TRPM2 in ROS induced Ca^{2+}-entry in endothelial cells may lead to more effective pharmacologic intervention of endothelial pathophysiology through manipulation of TRPM2 function (Dietrich and Gudermann, 2008). Thus, TRPM2 and oxidative stress play an important role in the pathophysiology of vascular diseases.

TRPM2 is expressed in pancreatic β-cells. Activation of TRPM2 channels has been linked to the regulation of insulin secretion and consequent reduction of blood glucose levels (Uchida et al., 2011). TRPM2 channels also mediate and H_2O_2-induced apoptosis of insulin-secreting β-cells (Lange et al., 2009; Manna et al., 2015). Thus TRPM2 channels are thought to play a key role in diabetes progression (Uchida et al., 2011).

In neurodegenerative diseases, which are complex disorders, a multitude of factors, such as environmental triggers, interact with genetic susceptibility genes (Hermosura et al., 2008). It has been reported that Western Pacific amyotrophic lateral sclerosis (ALS) and parkinsonism–dementia (PD) are tightly associated with environmental factors such as low levels of Ca^{2+} and Mg^{2+} in soil or water (Hermosura et al., 2008). Hermosura et al. reported that a genetic variant of the TRPM2 gene might be responsible for the diseases. The variant channel contains the P1018L mutation in the S5-S6 loop of the channel. Functional analysis revealed that, compared with the wild-type channel, the P1018L mutant channel inactivates rapidly. The authors suggest that attenuation of

intracellular Ca^{2+} contributes to the diseases via a mechanism that is unclear. Interestingly, knock-out of TRPM2 channels in mice does not produce either of the two disease phenotypes. The authors conclude that future studies using P1018L transgenic mice may provide the answers to the puzzle.

TRPM2 is expressed in many cell types of the immune system including dendritic cells, monocytes and macrophages (Di et al., 2012). It has been reported that phagocyte NADPH oxidase and ROS generation play an important role in host defence (Di et al., 2012). However, overproduction of ROS induces inflammatory injury. Di et al. found that the TRPM2 channel mediates NADPH oxidase-mediated ROS production in phagocytes. The results revealed that TRPM2 inactivation inhibits NADPH oxidase activity and protects from tissue injury (Di et al., 2012).

H_2O_2 is important in some diseases such as cancer because of its ability to cause cell death. In addition, it has been reported that ROS signalling pathways are involved in increasing anti-tumour activity (Alexandre et al., 2006). Thus, H_2O_2-mediated mechanisms can be targeted for the development of cancer therapeutics (Alexandre et al., 2006).

Although there have been numerous reports implicating Ca^{2+} in cell death, recent findings with neuronal and pancreatic β-cells indicate a role not only for Ca^{2+}, but also for Zn^{2+}, (Manna et al., 2015; Ye et al., 2014). Therefore, the next section discusses Zn^{2+} regulation by oxidative stress and its role in cell death.

1.5 Zn^{2+} homeostasis and oxidative stress

Zinc is the second most abundant trace element in the human body (Frederickson et al., 2005; Vallee and Falchuk, 1993). It plays an important role in normal growth, protein metabolism, membrane integrity, wound healing, gene expression and collagen synthesis (Islam and Loots, 2007). It is mostly bound to proteins and enzymes where it supports their structure and function. Since free Zn is cytotoxic, it is largely buffered by the Zn^{2+}-buffering protein metallothionein (MT)-1 (Frederickson et al., 2005; Vallee and

Falchuk, 1993; Wiseman et al., 2007). However, unbound zinc also plays an important role as a signalling molecule in cell function (Frederickson et al., 2005). Zinc deficiency leads to abnormalities in the skin and hair and in immune function (Frederickson et al., 2005). Zinc is highly available in the pancreatic β cells and in the brain (10 μg of zinc per gram of wet tissue) compared with its availability in other organs. The average estimated intracellular concentration is approximately 150 μM of total Zn^{2+} (Frederickson, 1989; Wallwork, 1987). However, zinc at high concentrations has a cytotoxic affect which has been linked to various diseases including neurodegenerative diseases (Parkinson's disease and Alzheimer's disease), atherosclerosis and type 1 diabetes (Frederickson et al., 2005; Manna et al., 2015; Morris and Levenson, 2012; Vallee and Falchuk, 1993; Wiseman et al., 2007).

Zn^{2+} homeostasis is affected by environmental factors such as oxidative stress (Frazzini et al., 2006). Intracellular Zn^{2+} rise occurs due to Zn^{2+} entry via transporters or ion channels (Frazzini et al., 2006; Morris and Levenson, 2012). Zn^{2+} can also be released from an intracellular source such as the Zn^{2+}-sequestering protein MT-1 (Wiseman et al., 2007). It was reported that oxidative stress leads to Zn^{2+} release from the MT-1 protein in the cytoplasm and overexpression of MT-1 prevents H_2O_2-induced apoptosis through sequestration of free Zn^{2+} (Wiseman et al., 2007). However, a recent report demonstrated that H_2O_2-induced apoptosis of pancreatic β-cells can be fully prevented by the inhibition or knock-out of TRPM2 channels (Manna et al., 2015). Manna et al. (2015) suggested that MT-1 is unlikely to play a role in oxidative stress-induced cell apoptosis. It is possible that supra-physiological concentrations of H_2O_2 (>1 mM) might be required to release Zn^{2+} from the MT-1 protein to cause cell death (Wiseman et al., 2007), while lower concentrations of H_2O_2 might cause cell death via a TRPM2-dependent, MT-1-independent pathway (Manna et al., 2015).

It has been also reported that excess intracellular Zn^{2+} can be removed by the mitochondria (Frazzini et al., 2006; Morris and Levenson, 2012). However, a rise in the mitochondrial Zn^{2+} concentration can lead to a marked reduction in mitochondrial function and drive mitochondrial ROS generation (Frazzini et al., 2006; Morris and

Levenson, 2012). Accumulation of Zn^{2+} in the mitochondria promotes release of pro-apoptotic factors including Apoptosis Inducing Factor (AIF) and cytochrome *c* and cell death (Frazzini et al., 2006; Morris and Levenson, 2012). The combination of oxidative stress and Zn^{2+} accumulation thus appears to induce ROS production and cell damage (Frazzini et al., 2006; Morris and Levenson, 2012).

It used to be thought that Zn^{2+} dynamics play a minor role in pathophysiology compared with Ca^{2+} dynamics (Inoue et al., 2015). However, studies have shown that many Ca^{2+}-permeable channels, such as voltage-dependent calcium channels (VDCCs), N-methyl-D-aspartate receptors (NMDA) and TRPM2, are also permeable to Zn^{2+} (Inoue et al., 2015; Morris and Levenson, 2012; Yu et al., 2012). Since Zn^{2+} is cytotoxic, it was suggested that Zn^{2+} could make significant contributions to pathophysiological processes (Inoue et al., 2015).

As Zn^{2+} is crucial for normal physiology, studies have focussed on how zinc is transported into and out of the cell. In 1995, zinc transporter 1 (ZnT1), the first member of the mammalian zinc transporter gene was identified (Palmiter and Findley, 1995). There are two families of proteins involved in zinc transport, namely the ZnT family (9 members) and Zip family proteins (14 members) (McMahon and Cousins, 2000). The ZnT family proteins allow zinc efflux from cells or zinc influx into intracellular vesicles (McMahon and Cousins, 2000). The Zip family proteins increase intracellular zinc by mediating zinc entry from an extracellular source or zinc release from an intracellular compartment (McMahon and Cousins, 2000). Most ZnT proteins have been found in the intracellular compartments such endosomes, lysosomes, Golgi apparatus and endoplasmic reticulum, with the exception of ZnT1, which is expressed in the plasma membrane (Kukic et al., 2014; Palmiter and Findley, 1995). Although the majority of Zip proteins have been found in the plasma membrane, Zip7 is located in the Golgi apparatus (Cousins et al., 2006; Huang et al., 2005).

As mentioned previously, TRPM2 is activated by oxidative stress. Using FluoZin-3-AM as a Zn^{2+} probe, studies have shown that TRPM2 channels in the plasma membrane

can induce Zn^{2+} entry into cells (Yu et al., 2012). Very little free Zn^{2+} is normally present in the cytoplasm, with the majority of Zn^{2+} being bound to proteins (e.g. metallothioneins) or sequestered into organelles such as lysosomes (Sensi et al., 2009). Manna et al. reported that Ca^{2+} entry due to plasma membrane TRPM2 activation leads to lysosomal Zn^{2+} release and Zn^{2+}-induced β-cell death (Manna et al., 2015). However, it has proven difficult to demonstrate Zn^{2+} permeation through TRPM2 channels using patch clamp electrophysiology because Zn^{2+} at 30 μM and higher was found to inactivate the channel (Yang et al., 2011) and higher concentrations of Zn^{2+} are required to generate enough driving force to measure Zn^{2+} currents.

1.6 Mitochondria

Mitochondrial morphology was revealed for the first time by electron microscopy in the early 1950s (Palade, 1953), when they were described as bean-shaped organelles (Chan, 2006; Okamoto and Shaw, 2005). Mitochondria are double membrane structures with an outer and inner membrane (Chan, 2006; Okamoto and Shaw, 2005). The inner membrane is folded into cristae (Chan, 2006; Okamoto and Shaw, 2005). Mitochondria have a range of morphologies from small spheres to long tubular structures (Chan, 2006; Okamoto and Shaw, 2005). The mitochondrial diameter is ~0.5 μm, while its length ranges from 1 to 10 μm (Chan, 2006; Okamoto and Shaw, 2005). A healthy mitochondrial network is essential for the survival of all eukaryotic cells. However, the network's structural integrity is constantly threatened by environmental and metabolic stresses. Mitochondria have the ability to cope with these threats by undergoing continuous cycles of fission and fusion (Archer, 2013; Dorn, 2015; Friedman and Nunnari, 2014; Youle and van der Bliek, 2012). As mitochondria are the most common organelles involved in programmed cell death due to oxidative stress, the following sections discuss the dynamics of mitochondria and how they change in response to pathological insults.

1.6.1 Dynamic shape of mitochondria

Mitochondrial shape, size and number are controlled by a balance between fission and fusion mechanisms (Bleazard et al., 1999; Chen et al., 2003; Sesaki and Jensen, 1999; Smirnova et al., 2001). Cells with more fusion than fission have longer and fewer mitochondria. Cells with more fission than fusion have smaller and more numerous mitochondria or fragmented mitochondria (Bleazard et al., 1999; Chen et al., 2003; Sesaki and Jensen, 1999; Smirnova et al., 2001).

1.6.1.1 The fusion machinery

The fission of mitochondria is balanced by sufficient mitochondrial fusion (Chen et al., 2003; Santel and Fuller, 2001). Fusion machinery is maintained by a two-step process, where the outer membrane and the inner membrane fuse in separate events involving three large GTPases: two mitofusins, Mitofusin1 (Mfn1) and Mitofusin2 (Mfn2), both of which are located in the outer membrane and responsible for outer membrane fusion (Chen et al., 2003; Santel and Fuller, 2001), and optic atrophy 1 (OPA1), which is located in the inner membrane and intermembrane space and is responsible for inner membrane fusion (Figure 1.6). These three proteins are the key proteins described to date.

Mitofusins 1 and 2 (Chen et al., 2003) promote mitochondrial fusion by cooperating or working individually (Chen et al., 2005). Their role in mitochondrial fusion has been studied using gene knock-out mice for Mfn1 and Mfn2 or by silencing Mfn1 or Mfn2 expression (Chen et al., 2005). A deficiency of Mfn1 or Mfn2 reduces the level of mitofusion significantly (Chen et al., 2005). However, the function of mitofusins is redundant (Chen et al., 2003). In other words, mitochondrial fragmentation due to a lack of Mfn1 can be rescued by overexpression of Mfn2, and, conversely, a lack of Mfn2 can be rescued by overexpression of Mfn1 (Chen et al., 2003). Furthermore, cells lacking in both Mfn1 and Mfn2 show severe mitochondrial fragmentation and a complete loss of tubular mitochondria (Chen et al., 2005). OPA1 is a crucial protein for the fusion of the inner mitochondrial membrane. Reducing OPA1 expression by RNA interference (RNAi)

induces mitochondrial fragmentation plus abnormalities and defects in cristae structure (Chen et al., 2005; Griparic et al., 2004). However, overexpression of OPA1 also induces mitochondrial fragmentation, but this is Drp1-dependent (Chen et al., 2005). mRNA splicing generates a long isoform and one or more short isoforms of OPA1. The combination of long and short isoforms is crucial for mitochondrial fusion (Song et al., 2007). However, overexpression of OPA1 could lead to an imbalance between the long and short isoforms of OPA1, leading to inappropriate mitochondrial fragmentation and poor maintenance of tubular mitochondrial morphology (Chen et al., 2005).

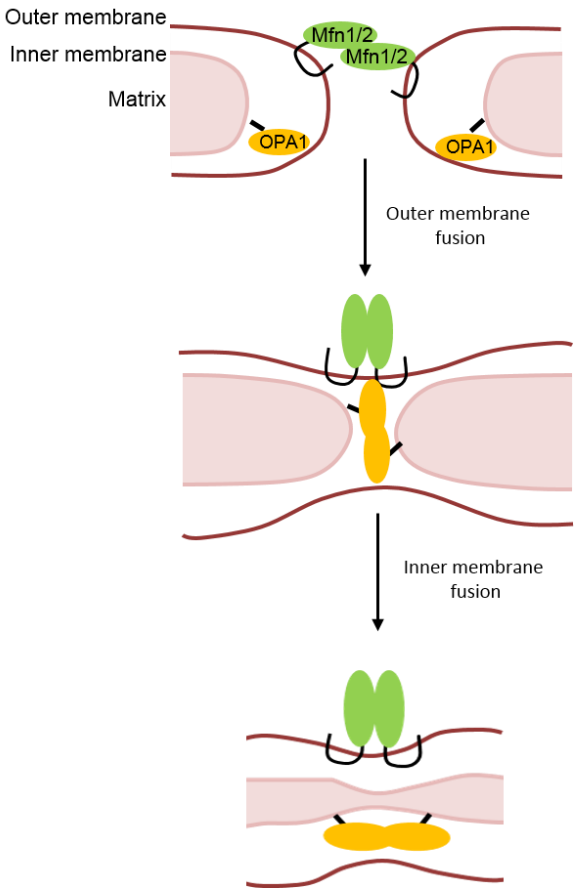

Figure 1.6 Mitochondrial fusion machinery, redrawn from (Mishra and Chan, 2014)

Three different proteins contribute to the fusion machinery: mitofusin1 and 2 (Mfn1 and Mfn2) and optic atrophy 1 (OPA1). Mfn1 and Mfn2 are transmembrane GTPases embedded in the outer mitochondrial membrane (OMM). They participate in the fusion of OMM. OPA1 is a dynamin-related protein embedded in the inner mitochondrial membrane (IMM) facing the intermembrane space. It contributes to the fusion of IMM.

1.6.1.2 The fission machinery

During apoptosis, the tubular mitochondria fragment into small and numerous mitochondria (Liesa et al., 2009). This fragmentation occurs because of increasing mitofission or decreasing mitofusion or both, and it leads to a change in the mitochondrial phenotype (Frank et al., 2001; Liesa et al., 2009). The most studied proteins involved in mitochondrial fragmentation are dynamin-related protein 1 (Drp1) and fission protein 1 homolog (FIS1) (James et al., 2003). These proteins are located in the mitochondrial outer membrane. Inhibition of the activity of Drp1 GTPase with dominant negative Drp1K39A prevents mitochondrial fragmentation during apoptosis (Frank et al., 2001; James et al., 2003). Overexpression of FIS1 induces mitochondrial fragmentation and cell apoptosis (James et al., 2003). Whether there are any fission-inducing proteins associated with the inner mitochondrial membrane is not known (Suen et al., 2008).

Drp1 is a regulator of mitochondrial fission in most eukaryotic organisms. It is a soluble protein that is expressed in different tissues such as heart, brain, kidney and pancreas (Smirnova et al., 1998; Yoon et al., 1998). Drp1 consists of an N-terminal GTPase, a medial domain (MD) and a C-terminal GTPase effector domain (GED) (Elgass et al., 2013). Drp1 proteins are recruited from the cytosol to the outer membrane of the mitochondria where they form a ring or spiral structure around the mitochondria, leading to the division of the mitochondrial membrane (Liesa et al., 2009). There are several mitochondrial proteins located in the outer mitochondrial membrane which act as a recruiter or receptor of Drp1; these include mitochondrial FIS1 mitochondria fission factor (MFF) and mitochondrial dynamics proteins (MIDs; MiD49 and MiD51) (Loson et al., 2013) (Figure 1.7).

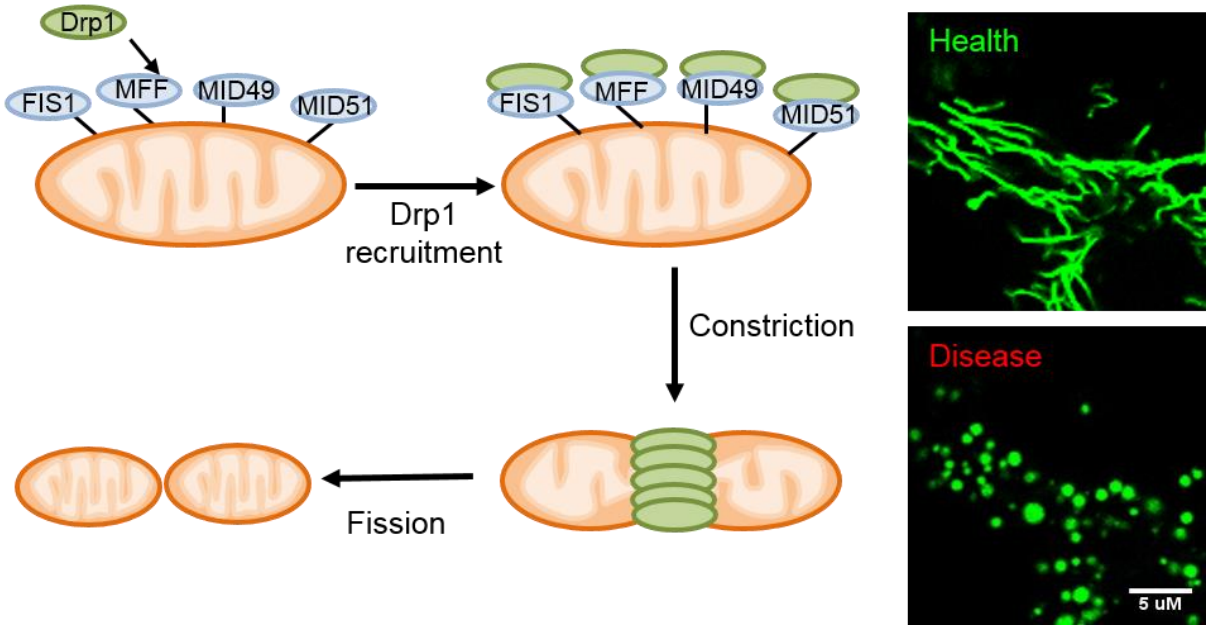

Figure 1.7 Mitochondria fission machinery, redrawn from (Mishra and Chan, 2014)
Dynamin-related protein 1 (Drp1) and its receptors (fission protein 1 (FIS1), mitochondrial fission factor (MFF) and mitochondrial dynamics proteins of 49 and 51 kDa (MiD49 and MiD51)) play a role in the fission mechanism. Drp1 is a large soluble GTPase in the cytosol. It is transported onto mitochondria and forms a ring at the division site of the outer mitochondrial membrane (OMM). The receptor proteins FIS1, MFF, MiD49 and Mid51 mediate Drp1 recruitment and mitochondrial fission.

1.6.2 Mitochondrial fragmentation and disease

The correct regulation of fission and fusion events is essential for mitochondrial function in ATP generation, Ca^{2+} signalling and regulation of apoptosis (Dorn, 2015; Friedman and Nunnari, 2014; Youle and van der Bliek, 2012). The disruption of the fusion-fission equilibrium contributes to a wide range of diseases, in particular the late-age onset diseases (Archer, 2013; Dorn, 2015) such as neuronal (Parkinson's, Alzheimer's) diseases, cardiovascular disease, diabetes and cancer (Archer, 2013; Friedman and Nunnari, 2014; Youle and van der Bliek, 2012). This disruption is attributed to the increase in cellular oxidative stress due to an increased production of ROS by the aging cell. Oxidative stress-induced mitochondrial fragmentation has been reported in neuronal (Grohm et al., 2012), cardiac (Cohen and Tong, 2010) and renal (Brooks et al.,

2009) cells exposed to ischemia/reperfusion injury, failing pancreatic β-cells (Molina et al., 2009), dysfunctional endothelial cells (Shenouda et al., 2011), insulin-resistant muscle cells (Jheng et al., 2012) and proliferating cancer cells (Rehman et al., 2012).

Importantly, many reports have indicated that inhibition of mitochondrial fragmentation can rescue the healthy phenotype (Chen et al., 2003; Rahn et al., 2013; Wakabayashi et al., 2009). These findings suggest that mitochondrial dynamics represent a valid drug target for a wide range of age-related illnesses. However, targeting the proteins involved in the fusion and fission events for therapeutic purposes may prove difficult because knock-out of these proteins has been shown to be embryonically lethal (Chen et al., 2003; Rahn et al., 2013; Wakabayashi et al., 2009).

1.6.2.1 Mitochondria as a drug target for diabetes complications

Diabetes mellitus, characterised by high blood glucose levels, can cause many vascular complications. Diabetic microvascular diseases cause nerve damage, terminal renal failure and blindness. Diabetic macrovascular damage leads to vascular diseases and its complications (Diabetes Control Complications Trial, 1995). One of the manifestations of cells exposed to hyperglycaemic conditions is ROS generation and consequent increase in mitochondrial fragmentation. However, the exact mechanism by which hyperglycaemia induces endothelial mitochondrial fragmentation and cell damage is not clear. Studies have indicated that high glucose-induced mitochondrial ROS production is also capable of inducing changes in the replication of the cell (Ono et al., 1988), mitochondrial permeability transition (MPT) and cell apoptosis (Buttke and Sandstrom, 1994).

Abnormal mitochondrial dynamics are associated with a variety of human diseases (Archer, 2013; Dorn, 2015; Friedman and Nunnari, 2014; Youle and van der Bliek, 2012). Thus, mitochondrial dynamics represent a therapeutic target against which pharmacologic or molecular modulators could be developed. Therefore, in the future, researchers could start targeting proteins involved in mitochondrial fragmentation and excessive mitochondrial ROS production. Indeed, a recent study has shown that a small

peptide inhibitor (P110) designed to inhibit the enzyme activity of Drp1 was able to prevent mitochondrial fragmentation. The inhibitor was able to do so by interfering with the protein-protein interaction between Drp1 and FIS1 (Qi et al., 2013). Another study has shown that pharmacological inhibition may be used to target mitochondrial ROS production and reverse the metabolic response in order to prevent tissue damage (Chouchani et al., 2014). However, no study has thus far shown whether targeting ion channels will prevent mitochondrial ROS production and mitochondrial fragmentation induced by high glucose.

1.7 Apoptosis

Oxidative stress and mitochondria play an important role in apoptosis. As mentioned earlier, mitochondria are the major site of ROS generation and they are also targets of ROS. ROS accumulation induces alteration in the mitochondrial membrane leading to a cascade of apoptotic events. However, there is another pathway of apoptosis known as extrinsic apoptosis (Elmore, 2007). This pathway is mediated by death receptor ligands. Extracellular stress such as that from chemotherapeutics and radiation can induce extracellular signals that stimulate ligands, including tumour necrosis factor (TNF) and Fas ligands, to bind specific transmembrane receptors (Elmore, 2007). These receptors are called death receptors (DR) (Elmore, 2007). The ligands interact with their cognate receptors forming complexes (e.g., FasL/FasR, TNF-α/TNFR1) called death initiation signalling complexes (DISC) (Elmore, 2007; Scaffidi et al., 1999). DISC lead to the activation of a caspase cascade, including activation of caspases -8 and -3, and induce cell death (Elmore, 2007).

Apoptosis is classified according to morphological changes and enzymological criteria (Elmore, 2007). It was described for first time with little knowledge of morphological changes in 1970s by Kerr, Wyllie and Currie (Kerr et al., 1972). Apoptosis is an essential process for normal development (Elmore, 2007). Dysregulation of apoptosis due to excess ROS is associated with a variety of diseases such as neurodegenerative diseases, autoimmune diseases, cardiovascular diseases and cancer (Elmore, 2007).

1.7.1 Apoptosis mechanism

As this study focuses on TRPM2 ion channels, mitochondrial fragmentation and cell death, this part of the introduction discusses the possible signalling pathways associated with mitochondria-dependent apoptosis (i.e., the intrinsic pathway). The mechanism of this pathway is regulated by the Bcl-2 family of proteins and controlled mitochondrial membrane permeability (Elmore, 2007). The anti-apoptotic proteins Bcl-2 and Bcl-X_L inserted in the outer mitochondrial membrane prevent cytochrome *c* release (Elmore, 2007; Kroemer and Reed, 2000). Under normal conditions, the pro-apoptotic members of the Bcl-2 family Bid and Bax, are located in the cytoplasm (Elmore, 2007; Kroemer and Reed, 2000). During stress, the cytosolic Bid is cleaved by caspase-8 and its active form (tBid) is translocated to the mitochondria. Then, in response to death stimuli (i.e., cell stress), Bax is translocated to the mitochondria and forms a channel or permeability-transition pore by itself (Elmore, 2007) or, in combination with VDAC, forms large channels (Kroemer and Reed, 2000). These channels promote cytochrome *c* release into the cytoplasm following death signalling (Elmore, 2007). The released cyt *c* binds to Apaf-1, and the complex leads to the activation of caspase 9, caspase-3 activation and apoptosis (Elmore, 2007) (Figure 1.8). The permeabilisation of the outer and inner mitochondrial membrane induces ATP depletion, loss of mitochondrial membrane potential ($\Delta\psi m$) and Ca^{2+} release (Elmore, 2007; Kroemer and Reed, 2000).

1.7.2 Morphological changes

Changes in the morphology of the cell during apoptosis have been documented by using light and electron microscopy (Kerr et al., 1972; Kroemer and Reed, 2000). During early apoptosis, cells are smaller in size (shrinkage), the cytoplasm is dense and the chromatin is condensed (Kerr et al., 1972; Kroemer and Reed, 2000). At the subcellular level, proteins are cleaved and the nucleus is fragmented (Kerr et al., 1972; Kroemer and Reed, 2000). As apoptosis advances, the cell gets fragmented into small bodies called “apoptotic bodies” (Kerr et al., 1972).

Apoptosis also triggers specific alternation in the plasma membrane as phosphatidylserine is redistributed from the inner to the outer leaflet of the plasma membrane (Brumatti et al., 2008). This alteration during apoptosis is due to an increase in intracellular Ca^{2+} concentration (Brumatti et al., 2008). This alteration can be detected with the most widely used marker Annexin V (apoptosis marker) (Brumatti et al., 2008). Annexin V is a recombinant phosphatidylserine-binding protein that interacts with phosphatidylserine residues (negatively charged phospholipids) exposed to the extracellular phase (Brumatti et al., 2008).

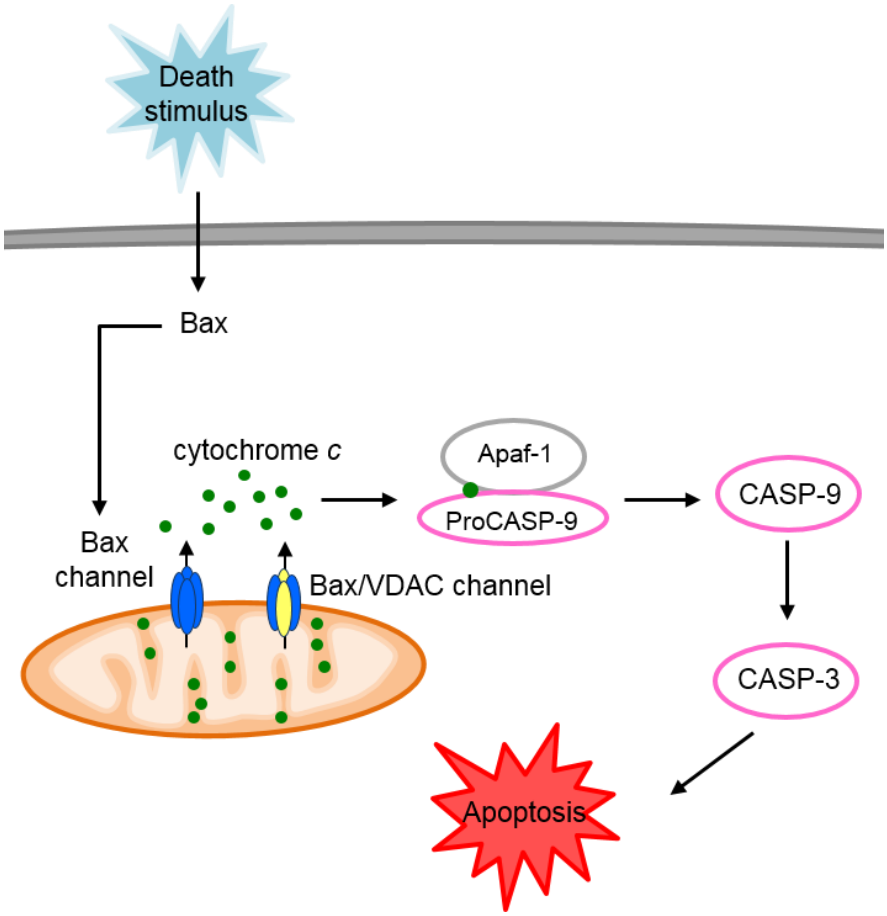

Figure 1.8 Proposed model of the molecular mechanism by which a death stimulus activates mitochondria-mediated apoptotic pathway

During stress stimulus, Bax is translocated from the cytoplasm to the mitochondria and forms a channel consisting of Bax or Bax and VDAC. The channel pore promotes cytochrome *c* release into the cytoplasm, where it binds Apaf-1 which in turn causes activation of caspase-9 and -3, resulting in cell apoptosis.

1.8 Endothelium in health and diseases

A study from the World Health Organization estimated that diabetes mellitus affects more than 170 million people in 2002. The prediction is that this number will increase to 366 million by 2030 (Rathmann and Giani, 2004). Type 1 diabetes and type 2 diabetes both exhibit similar clinical features, primarily including hyperglycaemia. Type 1 diabetes is caused by the failure of pancreatic β cells leading to insulin deficiency, whereas type 2 diabetes is caused by insulin resistance (American Diabetes Assocation, 2009). Diabetes mellitus can cause serious health problems and the dysfunction of various organs including the eyes, nerves, kidneys, heart and blood vessels (Amer Diabet, 2009). Vascular complications are divided into macrovascular complications (i.e., cardiovascular disease) and microvascular complications (i.e., retinopathy, neuropathy and nephropathy) (Duby et al., 2004; Jay et al., 2006; Li and Shah, 2003).

Endothelial cells form the inner lining of blood vessels and provide a protective barrier between the vessel wall and the circulating blood (Sumpio et al., 2002). The endothelium has an important role in releasing endothelium-induced relaxing factors including nitric oxide (NO) and endothelium-derived hyperpolarisation factor (EDHF) (Cai and Harrison, 2000; Kietadisorn et al., 2012). NO is synthesized by endothelial nitric oxide synthase (eNOS) from L-arginine and molecular oxygen. It plays an important role in maintaining smooth muscle relaxation and vascular function (Cai and Harrison, 2000; Kietadisorn et al., 2012). eNOS is localised at the plasma membrane caveolae in its inactive form (bound to caveolin 1 (Cav-1)) (Kietadisorn et al., 2012). Upon disassociation from Cav-1, eNOS becomes active. The functional form of eNOS, referred to as coupled eNOS, is a dimer (Kietadisorn et al., 2012). For optimal activity, eNOS requires tetrahydrobiopterin (BH4) (Cai and Harrison, 2000; Kietadisorn et al., 2012). BH4 is an important cofactor that helps in the conversion of L-arginine to NO (Cai and Harrison, 2000; Kietadisorn et al., 2012). However, in diabetes, eNOS is inactive because it largely exists in its monomeric form (i.e., uncoupled) due to BH4 deficiency (Cai and Harrison, 2000; Kietadisorn et al., 2012). Electrons are normally transferred from the reductase domain via the heme group of eNOS to L-arginine. The deficiency in BH4 leads to transfer electrons to molecular oxygen rather than to L-

arginine. This leads to the production of $O_2^{\bullet-}$ rather than NO. $O_2^{\bullet-}$ thus generated reacts with NO to form peroxinitrite ($ONOO^-$). $ONOO^-$ oxidizes BH4 and generates more $O_2^{\bullet-}$ production leading to endothelial dysfunction (Cai and Harrison, 2000; Kietadisorn et al., 2012) (Figure 1.9). It has been reported that increased synthesis of BH4 can restore eNOS function in diabetes (Cai et al., 2005). eNOS deficiency induces endothelial dysfunction which is a marker for atherosclerosis (Davignon and Ganz, 2004). At the cellular level, eNOS deficiency induces mitochondrial fragmentation, enlarged lysosomes and increased mitochondrial ROS production (Ueda et al., 2015).

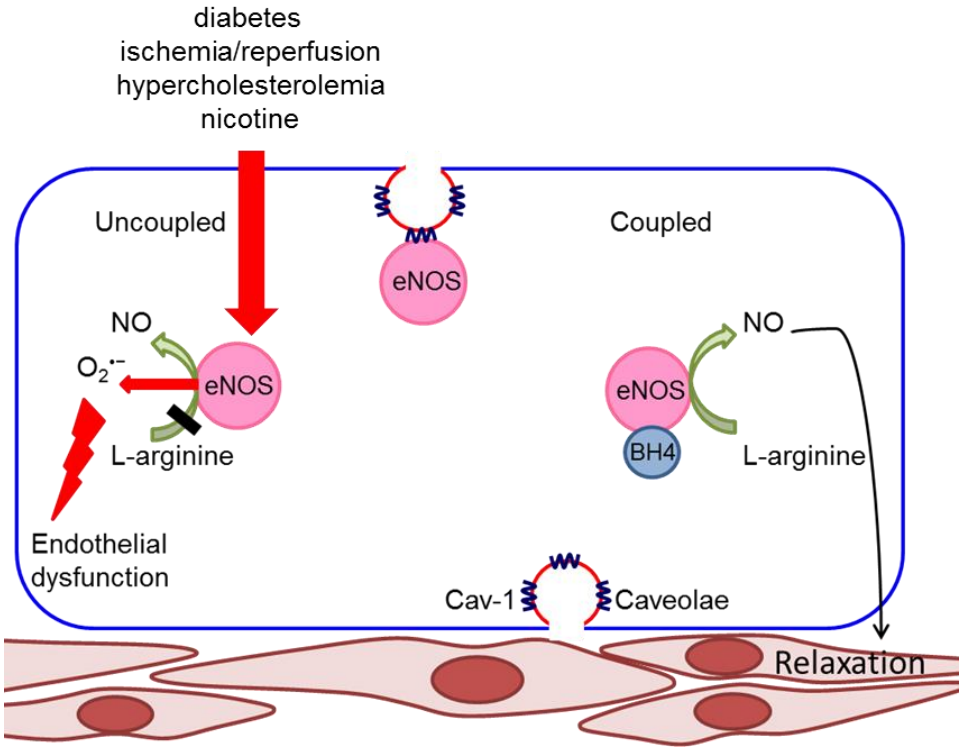

Figure 1.9 Schematic representation of endothelial nitric oxide signalling, redrawn from (Kietadisorn et al., 2012)

In a non-inflammatory state, eNOS is bound to the caveolin-1 (Cav-1) and is localised at the plasma membrane in its inactive form. Ca^{2+} uptake leads to eNOS activation, dissociation from the caveolar membrane and release into the cell. BH4 binds to the oxidase domain of eNOS and activates the enzyme to generate nitric oxide (NO) from L-arginine. NO diffuses to the underlying smooth muscle leading to relaxation. However, during stress, the bioactivity of BH4 is reduced, which leads to reduced NO generation, increased superoxide production and endothelial dysfunction.

As the oxidative stress in diabetes is the cause of cardiovascular complications, previous studies have focused on using antioxidant supplementation to improve the function of endothelial cells. The use of vitamin C (250 mg) and vitamin E (600 mg) as antioxidants failed to reduce the risk of heart failure (Heart Protection Study Collaborative, 2002). Moreover, the use of a high dose (>400 IU/ day) of vitamin E may raise mortality (Miller et al., 2005). Feron et al. (2001) used atorvastatin to enhance eNOS activity. Low-density lipoprotein (LDL) cholesterol increases the interaction between Cav-1 and eNOS. This leads to a decrease in NO generation and an increase in endothelial cell dysfunction. However, atorvastatin has been found to induce a reduction in Cav-1 expression which in turn promotes NO production (Feron et al., 2001). Furthermore, it has been reported that diabetes-induced zinc deficiency leads to diabetic complications (Islam and Loots, 2007). Chelating zinc with the Zn-buffering protein MT-1 helps in reducing diabetes-related complications and DNA damage (Islam and Loots, 2007). Thus, targeting ROS signalling events could represent a potential approach in reducing the risk of diseases caused by the overproduction of ROS.

1.9 The aims of the current study

i. To generate a TRPM2 construct containing an extracellular human influenza hemagglutinin (HA) epitope to investigate the cellular distribution and trafficking of TRPM2 channels.

ii. To investigate the role of TRPM2 channels in intracellular dynamics of Ca^{2+} and Zn^{2+} and mitochondrial fragmentation during high glucose stress on endothelial cells.

iii. To investigate the role of TRPM2 channels, Ca^{2+} and Zn^{2+} in high glucose-induced endothelial cell death.

1.10 Hypothesis of current study

High glucose induced oxidative stress induces mitochondrial fragmentation and cell death through TRPM2 channel activation and intracellular Zn^{2+} elevation.

1.11 Overview of the thesis

In this thesis I inserted an HA tag into the S1-S2 loop of TRPM2 channels and evaluated the function and expression of the resulting construct, TRPM2-HA. I then examined how TRPM2 channel activation by oxidative stress affects mitochondrial Zn^{2+} uptake, mitochondrial fragmentation and cell death.

Chapter 2 outlines the materials and methods used in this study.

Chapter 3 shows that the insertion of human influenza hemagglutinin-tag into the TRPM2 channel did not affect the structure, function or subcellular localisation of the channel.

Chapter 4 demonstrates that exposure of endothelial cells to H_2O_2 or high glucose conditions led to lysosomal membrane permeability (LMP), resulting in a marked decrease in lysosomal Zn^{2+} and redistribution of Zn^{2+} to mitochondria. The resultant rise in mitochondrial Zn^{2+} led to extensive mitochondrial fragmentation. The silencing of TRPM2 channels with siRNA prevented intracellular Zn^{2+} redistribution and mitochondrial fragmentation. Chapter 4 also demonstrates that a fraction of TRPM2 channels is localised to the mitochondria, where they control mitochondrial fission. Zn^{2+} released from lysosomes enters mitochondria via TRPM2 channels and increases mitochondrial fragmentation by promoting the recruitment of cytoplasmic Drp1. The data imply a novel mechanism for how oxidative stress leads to excessive mitochondrial fragmentation mediated by mitochondrial TRPM2 ion channels.

Chapter 5 illustrates the relevance of TRPM2 and Zn^{2+} redistribution to H_2O_2 and high glucose-induced mitochondrial ROS production and endothelial cell death. Blockers of TRPM2, TRPM2-targeted siRNA and chelation of Zn^{2+} significantly inhibited oxidative stress-induced cell death. The mechanism involves activation of TRPM2 channels leading to increased Ca^{2+} entry, intracellular Zn^{2+} release and mitochondrial ROS production. Chapter 5 also shows that there is a link between oxidative stress and the level of TRPM2 channel expression at the plasma membrane.

Chapter 6 provides a summary of the work and an outline of future directions.

2 | Materials and methods

2.1 Materials

2.1.1 Molecular biology materials

Supercompetent XL1-Blue cells purchased from Agilent Technologies (USA) were used for transformation. The QlAprep Spin Miniprep Kit, Qiagen HiSpeed Plasmid Midi Kit and Gel Extraction Kit were purchased from Qiagen, UK. All oligonucleotide primers used for pcDNA3.1-HA-TRPM2 sequencing and for inserting the HA-epitope were custom-made by Sigma-Aldrich® (Table 2.1). Phusion High Fidelity DNA Polymerase, *Dpn* I, 10× DNA ligase buffer and T4 DNA ligase were purchased from New England BioLabs (UK). The HF buffer used in the PCR was purchased from Stratagene (Cambridge, UK). Avian myeloblastosis virus reverse transcriptase (AMV-RT) and random primers were obtained from Promega. Taq DNA polymerase was from New England BioLabs. siRNA-1 (ON-TARGETplus Human TRPM2 (7226)) was from Thermo Scientific; siRNA-2 for human TRPM2 (5′- GAAAGAAUGCGUGUAUUUUGUAA -3′) was custom-made by Dharmacon; scrambled siRNA was from Ambion. DNA marker (HyperLadder I) was purchased from Bioline (London, UK). Luria-Bertani (LB) broth was purchased from Fisher Bioreagents (USA) and LB agar was purchased from Sigma-Aldrich® (USA). Ampicillin was purchased from Sigma-Aldrich®. Sequencing of pcDNA3.1-HA-TRPM2 was carried out by Beckman Coulter Genomics (UK).

2.1.1.1 Plasmid clones

Human TRPM2 cDNA in the pcDNA3.1 vector was kindly provided by Dr. Lin-Hua-Jiang of the University of Leeds, UK. TRPM2-HA clone lacking two codons was generated by Tim Munsey (University of Leeds, UK). hERG-HA was generated by Dr. David Elliot (University of Leeds, UK) and has been described before (Karnik et al., 2013). TRPM2-EE and TRPM2-FLAG were from Dr. Lin-Hua Jiang and have been described before (Mei et al., 2006). pMito-Cherry was constructed from pMito-CFP (Clontech) by Honglin Rong (University of Leeds, UK). Drp1-GFP clone containing shRNA to knock-down the

endogenous Drp1 (Slupe et al., 2013), and its dominant negative (K38A) version, was a kind gift from Dr. Stefan Strack (University of Iowa, USA). Lamp1-GFP was obtained from Dr, P. Boquet (Institut National de la Santé et de la Recherche Médicale, France).

Table 2.1 Primers used

A- Primers used for pcDNA-HA-TRPM2 plasmid sequencing

Name of primer	Primer sequence '5-3'
T7	TAATACGACTCACTATAGGG
Sequence 1	TCCTCTCTCTGGACTTCAT
Sequence 2	ACATGAAGTTTGTGTCTCAC
Sequence 3	GCACTCATCTCCAACAAGCCT
Sequence 4	GCCGAGTACATACTGGATGA
Sequence 5	GACGCCATGGTGGACCTG
Sequence 6	ACTTGCTGAAGTGCGGCA

B- Primers (5'phosphorylated) used for insertion of two missing amino-acids into the HA-epitope

Primers	Sequence '5-3'
Forward primer	**P'-GTC**CCAGACTACGCTCACCTCCAA
Reverse primer	**P'-GTC**GTAGGGGTAGATTTCCTGGGC

C- PCR primers of TRPM2

Primers	Sequence '5-3'
Forward primer	CCATCCGTGACCTTCTCATT
Reverse primer	CTCTGAGCCCAGATGATTCC

D- PCR primers of human actin

Primers	Sequence '5-3'
Forward primer	CCTCGCCTTTGCCGATCC
Reverse primer	GGATCTTCATGAGGTAGTCAGTC

2.1.2 Cell biology materials

2.1.2.1 Cell lines

HEK293- MSRII cells were obtained from Glaxo-Smith-Kline (Stevenage, UK). HEK293 cells were obtained from ATCC (ATCC CRL-1573). HEK293 cells stably expressing TRPM2 under the control of tetracycline were provided by Dr. AM Scharenberg (Washington University, USA). HUVECs were obtained from Lonza (USA). HeLa cells were obtained from the European Cell Culture Collection (Cambridge, UK). INS-1 cells were a kind gift of CB Wollheim (University Medical Centre, Geneva, Switzerland). Lung microvascular endothelial cells (lung ECs) were isolated from 8-10 week old wild-type (C57BL/6) and TRPM2 knock-out (TRPM2 KO) mice by immuno-selection.

2.1.2.2 Cell culture medium and growth factors

Cell culture media DMEM (Dulbecco's Modified Eagle Medium) + GlutaMAX-1, RPMI-1640 + Glutamax™ and DPBS (Dulbecco's phosphate buffered saline) were purchased from Invitrogen (Gibco Life Technologies, UK). EGM-2 was purchased from Lonza (USA). FBS (foetal bovine serum) was purchased from Sigma-Aldrich®.

For transfection

Lipofectamine® 2000 was purchased from Life Technologies™.

2.1.2.3 Molecular probes and pharmacological reagents

LysoTracker® Red DND-99, MitoTracker® Red CMXROS and ER-tracker™ Red, BAPTA-AM (1,2-bis(o-aminophenoxy)ethane-N,N,N',N'-tetraacetic acid), Opti-MEM®, Pluronic®F127, Fura-2-AM, Fluo4-AM and Fluozin3™-AM, Hoechst 33342, H_2DCFDA were purchased from Life Technologies™. MitoSOX™ Red was purchased from Thermo Fisher. DAPI (4,6-diamidino-2-phenylindole)-Fluoromount-G™ was purchased from Southern Biotech. Annexin V-GFP was a kind gift from Prof. Christoph Borner, Institute for Molecular Medicine, University of Freiburg (Geissler et al., 2013). Alexa Fluor^{488} conjugated transferrin was purchased from Invitrogen. n-(p-amylcinnamoyl) anthranilic acid (ACA), PARP Inhibitor VIII, PJ34 were purchased from Calbiochem. G418 (Geneticin sulphate) was purchased from Invitrogen (UK) and stored as 50 µg/ml at -20°C. Zeocin and Blasticidin were purchased from InvivoGen. All other chemicals were either from Sigma-Aldrich® or Calbiochem.

Ca^{2+} and Zn^{2+} indicator dyes

In this study, two Ca^{2+} indicator dyes were used which are Fura-2-AM and Fluo-4-AM. Fura-2-AM is a ratiomentric dye widely used for quantitative intracellular Ca^{2+} measurements (Martin et al., 2006; Paredes et al., 2008). Affinity of Fura-2 for Ca^{2+} is within the range of endogenous resting levels of Ca^{2+} (K_D 145 nM) (Martin et al., 2006). This dye chemically modified to its acetomethoxy (AM) ester form to enable it to cross the cell membrane (Paredes et al., 2008). Once inside the cell, cytosolic esterases cleave the AM group trapping fluorescent Fura-2 within the cell (Paredes et al., 2008). However, Fura-2 has been shown to interact with Zn^{2+} with a hundred-fold higher affinity than Ca^{2+} (Martin et al., 2006; Paredes et al., 2008).

Fluo-4-AM is a fluorescent cytosolic Ca^{2+} probe. Its affinity for Ca^{2+} (K_D 345 nM) is lower than that for Fura-2-AM (Gee et al., 2000). Fluo-4-AM is a useful probe for fluorescent imaging because it is excited by a single wavelength (Gee et al., 2000) while Fura-2 is excited by dual wavelength (Martin et al., 2006) (see section 2.2.2.13). It has been reported that Ca^{2+} sensitive dyes are less specific to their target than dyes that target Zn^{2+} (Martin et al., 2006).

FluoZin-3-AM is a membrane permeable fluorescent probe used to detect Zn^{2+}. It has a very high affinity for Zn^{2+} (K_D 15 nM) and is highly specific for Zn^{2+} (Zhao et al., 2008). Ca^{2+} and Mg^{2+} at physiological levels do not appear to disrupt FluoZin-3's ability to bind Zn^{2+} (Zhao et al., 2008). Moreover, increasing the concentration of Ca^{2+} up to 10 mM does not prevent FluoZin-3 from detecting low concentrations (~100 pM) of Zn^{2+} (Zhao et al., 2008).

In the present study the above fluorescent probes were used in conjunction with chelators of Ca^{2+} (BAPTA-AM) and Zn^{2+} (TPEN and clioquinol). Table 2.2 lists the reagents used and their properties.

Table 2.2 Ca^{2+} and Zn^{2+} intracellular chelators

Chelator	Affinity	Reference
BAPTA-AM	K_D values of BAPTA-AM Zn^{2+}: 7.9 x 10^{-9} M Ca^{2+}: 1.1 x 10^{-7} M	(Qian and Colvin, 2015)
TPEN	Affinities (K_A) for various metal ions are as follows. Mn^{2+}:$10^{10.27}$ M^{-1} Fe^{2+} : $10^{14.61}$ M^{-1} Zn^{2+}: $10^{15.58}$ M^{-1} Mg^{2+}: $10^{1.7}$ M^{-1} Ca^{2+}: $10^{4.4}$ M^{-1}	(Arslan et al., 1985)
Clioquinol	K_D values of clioquinol Zn^{2+}: 7 × 10^{-8} M Cu^{2+}: 1.2 × 10^{-10} M	(Di Vaira et al., 2004)

2.1.2.4 Antibodies

Primary antibodies

Rat anti-HA high affinity monoclonal antibody (clone 3F10) (1:500) was purchased from Roche. Rabbit polyclonal anti-CD31 (1:300) was purchased from Abcam. Mouse monoclonal anti-LAMP-1(1:5000) was purchased from BD Biosciences. Mouse

monoclonal anti-VDAC-1 (1:100,000) was purchased from Abcam. Rabbit polyclonal anti-calnexin (1:5000) was purchased from Abcam. Mouse monoclonal anti-EE (1:1000) was purchased from Covance. Mouse monoclonal Anti-FLAG M2 (1:500) was purchased from Sigma-Aldrich®. Mouse monoclonal anti-cathepsin B (1:100) was purchased from Calbiochem. Rabbit monoclonal anti-cytochrome *c* (1:100) was purchased from Cell Signalling. The numbers in parenthesis following the antibodies indicate dilutions used.

Secondary antibodies

Anti-rat Cy3-conjugated secondary antibody (1:500), anti-mouse Cy3-conjugated secondary antibody (1:500) and anti-rabbit Cy3-conjugated secondary antibody (1:500) were purchased from Jackson ImmunoResearch. Alexa Fluor^{594} mouse anti-HA IgG (1:300), Alexa Fluor^{488} donkey anti-mouse IgG (1:500) and Alexa Fluor^{488} donkey anti-rabbit IgG (1:500) were purchased from Life Technologies™. HRP-conjugated goat anti-rat IgG (1:1000), HRP-conjugated goat anti-mouse IgG (1:10000) and HRP-conjugated goat anti-rabbit IgG (1:10000) were purchased from Sigma-Aldrich®. Goat anti-rat IgG 10 nm gold (1:50) was purchased from Agar Scientific.

2.1.2.5 Plates and pipettes

6-, 24- and 69-well plates were purchased from Sarstedt. The FluoroDish^{TM} glass bottomed cell culture dishes were purchased from World Precision Instruments.

2.1.3 Buffer and solutions

Table 2.3 Buffers and solutions used

A- 10x phosphate buffered saline (PBS)

Ingredients (stock solution)	Quantity per 1 L
NaCl (MW:58.44)	80 g
KCl (MW:74.55)	2 g
KH_2PO_4 (MW:136.09)	2 g

Na_2HPO4 (MW:141.96)	11.48 g

B- Tris-saline

Ingredients	Quantity per 50 ml
1 M Tris pH7.4	2.5 ml
3 M NaCl	2.5 ml
H_2O	45 ml

C- Ice-cold transfer buffer

(Store at 4°C)

Ingredients	Quantity
10x TGS (BIO-RAD)	1 part
Methanol	2 part
H_2O	7 part

D- 1.5 mM Ca^{2+} standard buffered saline (SBS), pH7.4

Ingredients	Quantity per 1 L
130mM NaCl	7.60 g
5mM KCl	0.37 g
1.2mM $MgCl_2$	2 ml of 1M
8mM Glucose	1.44 g
10mM HEPES	2.38 g
1.5mM $CaCl_2$	1.5 ml of 1 M

E- 0 mM Ca^{2+} (SBS), pH7.4

Ingredients	Quantity per 1 L
130 mM NaCl	7.60 g
5 mM KCl	0.37 g
1.2 mM $MgCl_2$	2 ml of 1M
8 mM Glucose	1.44 g
10 mM HEPES	2.38 g
0.4 mM EDTA	0.15 g

F- KCl buffer

(Store at 4°C)

Ingredients	Quantity per 100 ml
125 mM KCl	0.931 g
2 mM K_2HPO4	0.0348 g
5 mM HEPES	0.119 g
5 mM $MgCl_2$	0.5 ml of 1 M
0.02 mM EDTA	0.744 g
5 mM succinic acid	0.081 g
5 mM glutamate	0.0735 g
0.05 mM ATP pH 7.0	0.00275 g

G- KCl free buffer

(Store at 4°C)

Ingredients	Quantity per 100 ml
2 mM K_2HPO4	0.0348 g
5 mM HEPES	0.119 g
5 mM $MgCl_2$	0.5 ml of 1 M
0.02 mM EDTA	0.744 g
5 mM succinic acid	0.081 g
5 mM glutamate	0.0735 g
200 µM EGTA	0.0076 g
0.05 mM ATP pH 7.0	0.00275 g

2% Paraformaldehyde (PFA)

0.1 g paraformaldehyde powder (Sigma-Aldrich®) was added to 1 ml 0.05 M NaOH pre warmed at 60°C. After dissolving, 50 µl of 1M HCl, 0.5 ml 10x PBS and 3.5 ml Milli-Q water were added and mixed. pH paper was used to check that the pH was ~7.0.

2.2 Methods

2.2.1 Molecular biology methods

2.2.1.1 Insertion polymerase chain reaction (PCR)

The PCR used in this study was to add two missing codons of the HA-epitope into an incomplete construct generated by Tim Munsey. Phusion DNA polymerase was used for PCR.

2.2.1.2 Oligonucleotides

The length of the primer: the number of the primer bases was around 18-22 (N), which is short enough to bind easily to the template and long enough to be sufficiently specific.
GC content: the number of guanosine and cytosine bases in the primer was kept around 40-60% of the primer sequence.
Tm of the primer = 81.5+0.41 (GC%)-674/N

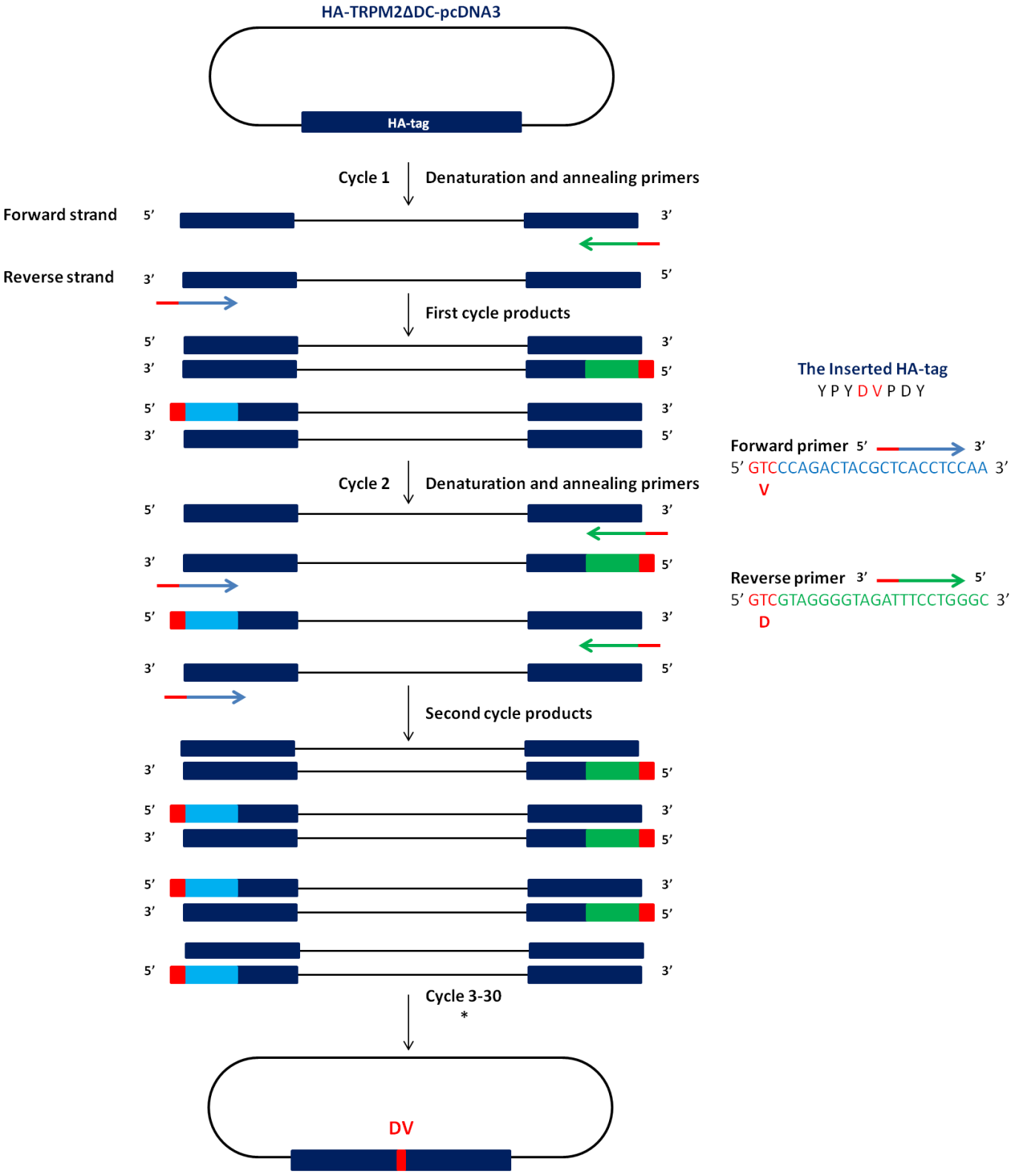
HA-TRPM2ΔDC-pcDNA3
HA-tag
Cycle 1
Denaturation and annealing primers
Forward strand
Reverse strand
5′
3′
First cycle products
Cycle 2
Denaturation and annealing primers
Second cycle products
Cycle 3-30
*
DV
The Inserted HA-tag
Y P Y D V P D Y
Forward primer 5′ 3′
5′ GTCCCAGACTACGCTCACCTCCAA 3′
V
Reverse primer 3′ 5′
5′ GTCGTAGGGGTAGATTTCCTGGGC 3′
D

Figure 2.1 A schematic of the PCR used to insert two missing amino acids (DV) into the HA-epitope

In cycle 1, during denaturation, the DNA was separated into two single strands. During annealing, the reverse primer bound to the forward strand while the forward primer bound to the reverse strand. Following cycle 1, the length of each original strand was raised by one amino acid codon. In cycle 2, during denaturation and annealing, the DNA was separated and the primers bound to each single strand. Cycles 3-30 were repeated to generate multiple copies of the strands with amino acid codons added, one at either end. The ends of the PCR products were joined together by incubating the PCR products with T4 DNA ligase after digestion and gel extraction. This gave rise to a plasmid with complete HA-epitope that could be transformed into XL I-Blue cells.

2.2.1.3 PCR reaction

The PCR reaction mix (20 µl) was prepared according to the instructions of the manufacturer of the DNA polymerase enzyme used. The PCR mix (see Table 2.3) was heated to 98°C to denature the template DNA and to allow separation of the strands. Temperature was then lowered to the Tm "annealing temperature". This temperature allowed the primers to anneal to their target site on the template strand. Extension at 68°-72°C allowed the DNA polymerase to make new copies of the DNA strands by extending the primers. The final extension at 72°C allowed completion of any incomplete stands. Finally, the samples were held at 4°-10°C.

Table 2.4 Components of the reaction mixture

PCR reaction mix components	Final concentration
DNA template	10 ng
5× Phusion HF buffer	1×
Forward primer	0.5 µM
Reverse primer	0.5 µM
dNTPs	200 µM
Phusion DNA Polymerase	2 units/ µl

2.2.1.4 Digestion of template DNA

Template DNA was digested using *Dpn* I restriction enzyme. 25 µl of PCR product, from a total volume 50 µl, was incubated with 1 µl of *Dpn* I (10 units/µl) for one hour at 37°C.

2.2.1.5 Gel electrophoresis

Agarose gel electrophoresis is a way of separating, analysing and semi-quantifying DNA fragments. It can also be used to check the specificity of the primers used for DNA amplification. 2 µl of DNA after digestion with *Dpn* I was analysed by 1% agarose gel electrophoresis.

2.2.1.6 Agarose gel preparation

1% agarose gel was prepared by dissolving 1 g agarose in 100 ml of 1×TAE buffer by microwaving. It was then left it to cool down to about 60°C. 5 µl (10 mg ml^{-1})/100 ml of ethidium bromide (Sigma; E-8751) was added and mixed. The molten gel was poured into a gel tray, a comb was inserted and the gel was left to set for 1 hr at room temperature. The comb was removed after the gel was set.

2.2.1.7 Sample preparation and electrophoresis

An electrophoresis tank was filled with 1x TAE buffer and the gel placed into the tank. 6 µl of DNA marker (HyperLadder I) was loaded into the first well in order to estimate the size of DNA run in parallel lanes. DNA samples were loaded into individual wells (1 µl of 6x sample buffer mixed with 2 µl of DNA and 3 µl of autoclaved water). The gel was run at 60 mV for about 2 hr. The DNA bands were visualised on a Bio-Rad UV transilluminator.

2.2.1.8 Gel extraction

After the large scale digested PCR product (25 µl) was run on the agarose gel, the gel was placed under a UV illuminator. This was to help in identifying the fragments of interest stained with ethidium bromide. The band was isolated using a clean scalpel and placed in an Eppendorf tube. DNA from the gel slice was extracted and purified using a QlAquick Gel Extraction Kit, following the protocol provided by the manufacturer.

2.2.1.9 Ligation

8 µl of purified PCR product was incubated with 1 µl of 10× ligase buffer and 1 µl (1 U) of T4 DNA ligase. The mixture was incubated for 2 hr at room temperature.

2.2.1.10 Transformation plasmid DNA

XL1-Blue competent cells were thawed on ice (100 µl). 5 µl of the ligated PCR product was added to competent cells. The mixture was incubated on ice for 20-30 min and then heat-shocked for 40 sec in a water bath at 42°C. Next, the mixture was incubated on ice for 2 min. Five volumes of pre-wormed LB were added to the cell suspension and incubated for 1 hr at 37°C in a shaking incubator at 225-250 rpm. The sample was centrifuged at 7,000 rpm for 1 min in a Heraeus microcentrifuge. 150 µl was then removed from the sample and the pellet was re-suspended into the remaining medium. The transformation mixture was plated onto a pre-warmed LB-ampicillin agar plate and incubated overnight at 37°C.

LB-agar was prepared by suspending 8.75 g of LB agar in 250 ml of water and sterilizing by autoclaving. The molten agar was cooled to 45°C. Ampicillin was added to a final concentration of 100 µg/ml and poured into petri-dishes (~25 ml per plate). The plates were stored at 4°C up to 4 weeks.

2.2.1.11 Plasmid preparation

Single colonies from the transformed plate were inoculated into LB medium (5-100 ml) containing 50 µg/ml ampicillin and grown overnight at 37°C and 200 rpm. Miniprep and midiprep kits were used to purify plasmid DNA from bacterial cultures. A miniprep kit (QlAprep Spin Miniprep Kit) was used for small scale plasmid DNA preparation, while a midiprep kit (Qiagen HiSpeed Plasmid Midi Kit) was used for the large scale plasmid preparation, according to the instruction of the manufacturer.

2.2.1.12 Sequencing

DNA prepared from several clones on the transformed plate was custom-sequenced and the resulting sequence was aligned against the reference sequence using ClustalW2 (see Appendix).

2.2.1.13 RT–PCR to determine mRNA levels

RNA preparation

RT-PCR for TRPM2 and actin (housekeeping gene) was performed on RNA isolated from cells transfected with desired siRNA. The cell pellet derived from two wells of a 6-well plate was lysed with 1 ml Trizol reagent (Sigma-Aldrich®). The lysate was passed through the pipette several times. The sample was incubated for 5 min at 15-30°C. 0.2 ml of chloroform:isoamyl alcohol (24:1) per 1 ml Trizol was added. The tube was shaken by hand for 15 sec and then incubated for 2-3 min at 15-30°C, before centrifugation at 12,000 x*g* for 15 min at 2-8°C. After centrifugation, the colourless upper aqueous phase was transferred to a fresh tube. 0.5 ml of isopropyl alcohol was added to precipitate RNA. The sample was incubated for 10 min at 15-30°C and then centrifuged at 12,000 x*g* for 10 min at 2-8°C. After centrifugation, the pellet was washed with 75% ethanol (prepared in RNase-free water) and then left to air-dry for 5-10 min. RNA was dissolved in 10 µl RNase-free water by incubating for 10 min at 55-60°C.

RT reaction and PCR reaction

5 µg of total RNA in a 10 µl volume was heated for 5-10 min at 65°C and then chilled on ice. cDNA was synthesised from 5 µg of total RNA using 1 µg random primers and 5 units of AMV reverse transcriptase in 20 µl volume. 6 µl of the cDNA product was subjected to 33 cycles of PCR using 1 unit of Taq DNA polymerase and 100 ng of each primer in a final volume of 20 µl. Each PCR cycle comprised 95°C for 30 sec, 65°C for 45 sec and 72°C for 60 sec, with a final extension at 72°C for 5 min. The primers used for TRPM2 and for human actin are shown in Table 2.1. PCR products were analysed using 1% agarose gel electrophoresis.

2.2.2 Cell biology techniques

2.2.2.1 Cell culture

HEK293-MSRII cells, HEK-TRPM2^{tet} cells, HEK293, HEK293FT and HeLa cells were cultured in DMEM medium supplemented with 10% FBS, 100 units/ml penicillin and 100

µg/ml streptomycin. G418 at 50 µg/ml was used for HEK293-MSRII cells. Zeocin at 200 µg/ml and blasticidin at 0.4 µg/ml was used for HEK-TRPM2^{Tet} cells. HUVECs at passages 3-6 and ECs (isolated from mice by immunoselection using CD146 antibody-coated magnetic beads (Miltenyi Biotec) (Li et al., 2014)) were cultured in Endothelial cell Basal Medium (EBM-2) supplemented with 2% FBS, human epidermal growth factor (hEGF), human fibroblast growth factor-B (hFGF-B), gentamicin sulphate, amphotericin-B (GA-1000), hydrocortisone, ascorbic acid and heparin. INS-1 cells were cultured in RPMI 1640+Glutamax^{TM} medium supplemented with 10% FBS, 1 mM sodium pyruvate, 50 µM 2-mercaptoethanol, 10 mM HEPES, 100 units/ml penicillin and 100 µg/ml streptomycin. Cells were cultured in 25 cm^2 and 75 cm^2 culture flasks in a humidified incubator with 5% CO_2 and 95% air at 37ºC. Growth media were replaced every 3 days for all cell lines. The cells were passaged at 75% confluency. HUVECs were used between passage numbers 3 and 6, while other cell lines were used until passage number 40.

2.2.2.2 Isolation of lung endothelial cells

Generation of TRPM2 KO mice has been described (Zou et al., 2013). Mice were bred and maintained under UK Home Office licence and ethical procedures. Mice were killed by cervical dislocation. Lung microvascular endothelial cells (lung ECs) were isolated from 8-10 week old wild-type (C57BL/6) and TRPM2 knock-out (TRPM2 KO) mice by immunoselection with anti-CD146 antibody coated magnetic beads (Miltenyi Biotec) according to the protocol described (Li et al., 2014).

Isolation of single cell suspension (1 mouse)

The lungs were harvested and collected into ice-cold HBSS (10 ml). In a tissue culture hood, the tissue was transferred to a petri-dish containing 3 ml of 1 mg/ml collagenase in HBSS. The lungs were minced to 1 mm^2 pieces using a scalpel blade. The pieces of tissue were suspended in 10 ml of 1 mg/ml collagenase and incubated in a shaking water-bath at 37°C for 45 min. Tissue aggregates were broken down by repeated pipetting of the suspension. The cell suspension was filtered through a 70 µM sieve into a 50 ml Falcon tube. The sieve was rinsed with 10 ml PBS-BSA (3.3 ml 7.5% BSA

(Sigma) plus 46.7 ml PBS) and the tissue was discarded. The sample was centrifuged at 1200 rpm for 5 min to pellet cells. The cell pellet was washed once with PBS-BSA.

Incubation of the isolated cells with LSEC (CD146) microbeads

After centrifugation and PBS-BSA wash, the cell pellet was suspended in 100 µl PBS-BSA and transferred to 1.5 ml Eppendorf tube (on ice). 15 µl of LSEC microbeads was added and incubated by using a tube rotator at 4°C (cold room) for 20 min. 1 ml of PBS-BSA was added and the sample was centrifuged at 4000 rpm for 5 min. The supernatant was discarded and the pellet was resuspended in 500 µl PBS-BSA.

Loading onto MiniMACS (MS) magnet column

A MiniMACS magnet was attached to the MultiStand and the MiniMACS (MS) column was inserted (wings to the front). A 15 ml Falcon tube was placed under the MS column. 500 µl of PBS-BSA was applied and run through the MS column. Then, the cell suspension was applied onto the MS column (unbound cells were able to pass through). The column was washed three times by adding 500 µl PBS-BSA buffer each time. To collect the bound cells, the MS column was removed from the separator and placed into a 15 ml Falcon tube. 500 µl of PBS-BSA was added to the MS column and cells flushed out immediately into a 15 ml tube by applying the plunger of the column. The isolated cells were centrifuged at 4000 rpm for 5 min and the supernatant was removed. The cell pellet was suspended in 600 µl EGM-2 medium and plated into 2 wells of a 6-well plate coated with 1% fibronectin (Sigma) (each well contained 2.5 ml EGM-2 medium). Medium was replaced with 2 ml of fresh medium after 6 hr of incubation when the cells adhered to the plate. After 24 hr, medium was replaced with fresh medium and incubated for 3 days.

2.2.2.3 Transfection

All transfections were performed using Lipofectamine 2000. Cells were allowed to attach to 13 mm glass cover-slips or 35 mm FluoroDish^{TM} glass bottomed dishes (live cell imaging), sterilised and pre-coated with 0.01% poly-L-lysine (diluted 1:10; Sigma P4832) (HEK293 cells) or 0.1% gelatin (HUVECs) or 2 µg/ml fibrinectin (lung ECs).

HEK293-TRPM2^{tet} cells were treated for 48 hr with 1 µg/ml tetracycline to induce expression of TRPM2 channels (Manna et al., 2015). On the day of transfection, cell confluency was approximately 50-70%.

Transfections were performed on cells grown in a 24-well plate or 35 mm FluoroDish^{TM}. For each well of a 24-well plate, 0.5 µl of Lipofectamine 2000 was added to 25 µl Opti-MEM, and 0.3-0.4 µg of plasmid DNA was added to 25 µl Opti-MEM (in separate tubes) and incubated for 5 min at room temperature. For transfection in 35 mm FluoroDish^{TM}, 1 µl Lipofectamine 2000 was added to 50 µl Opti-MEM and 0.8 µg of plasmid DNA per to 50 µl Opti-MEM and incubated for 5 min at room temperature. The Lipofectamine 2000-Opti-MEM and plasmid DNA-OptiMEM were mixed, and the resulting transfection mixtures were incubated for 30 min at room temperature. The mixtures were added to the cells containing 450 µl (in the 24-well plate) or to 900 µl of Opti-MEM (in the 35 mm FluoroDish^{TM}). Cells were incubated for 6-7 hr at 37ºC after transfection. Then, the medium was replaced with complete medium and incubation continued for 48-72 hr, during which cells were treated as required before imaging.

For siRNA-TRPM2 transfection

1 µl of Lipofectamine 2000 was added to 50 µl Opti-MEM (A), and 1 µl of 50 µM human TRPM2 siRNA was added to 50 µl Opti-MEM (B), and incubated for 5 min at room temperature. (A) was mixed with (B) and incubated for 30 min at room temperature. The resulting mixture (C) was added to the cells containing Opti-MEM and incubated for 7 hr at 37ºC; see Table 2.4. Then, medium was changed to complete medium and incubation continued for 48-72 hr.

Table 2.5 The required siRNA resuspension volumes

	Mixtures (C) (each well)	Medium serum free (each well)	Total (each well)
24 well plate	50 µl	450 µl	500 µl
35 mm FluoroDish	100 µl	900 µl	1000 µl

For scrambled siRNA

13 µl of Lipofectamine 2000 was added to 650 µl Opti-MEM serum-free medium (A) and 1 µl of scrambled siRNA was added to 600 µl Opti-MEM serum free medium (B); both (A) and (B) were incubated for 5 min at room temperature. Then, 300 µl of (A) was mixed with 300 µl of (B) and incubated for 30 min at room temperature. The mixtures (C) were added to the cells containing Opti-MEM and incubated for 3 hr at 37ºC; see Table 2.5. The medium was changed to complete medium and incubation continued for 48 hr.

Table 2.6 The required scrambled siRNA resuspension volume

	Mixtures (C) (each well)	Opti-Mem (each well)	Total (each well)
24 well plate	40 µl	80 µl	120 µl
35 mm FluoroDish	100 µl	200 µl	300 µl

2.2.2.4 Immuno-fluorescence staining

Transfected cells on pre-treated glass cover-slips were washed three times with phosphate-buffered saline containing calcium and magnesium, 1 mM each (PBS). Cells were fixed with 2% PFA for 10 min at room temperature. Where required, cells were permeabilised by adding 0.25% Triton X-100/10 mM Tris/150 mM NaCl, pH7.4 and incubating for 5 min. Triton-X100 permeabilises the plasma membrane and allows the antibody to access the intracellular targets (Marty et al., 2014). The fixative was quenched by adding 300 µl of Tris-saline to each well. Cells were washed three times with PBS. Nonspecific binding sites were blocked with 1% ovalbumin/PBS for 1 hr before incubation for 1-2 hr with the desired primary antibody diluted in 1% ovalbumin/PBS. Cells were then washed thrice with PBS and incubated in the dark with appropriate secondary antibodies diluted in 1% ovalbumin/PBS. After washing, cover-slips were dipped into Milli-Q water, excess water was removed, and the cover-slips were mounted onto microscope slides in 7 µl DAPI-Fluoromount-G, dried overnight in the dark at room temperature and imaged.

2.2.2.5 Live cell staining with fluorescence probes

Intracellular Zn^{2+} redistribution

Intracellular distribution of Zn^{2+} was assessed by live imaging after staining the cells with FluoZin-3 for Zn^{2+} and the organelles with vital stains. HUVECs grown on FluoroDish™ dishes were washed with EBM-2 medium and incubated at 37°C for 2-4 hr in the dark in EBM-2 containing 1 µM FluoZin-3-AM and 0.02% (w/v) Pluronic F-127 ± 1 mM H_2O_2 ± pharmacological treatment (150 µM 2-APB or 10 µM PJ-34). Cells were then washed twice (15 min each) with EBM-2 and incubated at 37°C for 30 min with organelle marker dyes: MitoTracker Red CMXROS (200 nM) or LysoTracker Red DND-99 (200 nM) or ER-Tracker (1 µM) diluted in EBM-2. After washing with EBM-2, cells were imaged. HEK-293 cells were similarly loaded with the dyes, but using the DMEM medium.

To examine the effect of glucose, HUVECs were incubated in EGM-2 or EGM-2 containing 33 mM glucose or 5 mM glucose plus 28 mM mannitol for 24 hr at 37°C. Cells were then loaded with FluoZin-3-AM for 4 hr and further incubated in the respective media. Organelles were labelled with markers as above during the last 30 min of incubation. The total incubation time including all steps was 48 hr. To examine zinc pyrithione (Zn-PTO) induced Zn^{2+} redistribution, cells were incubated in EGM-2 or EGM-2 containing 0.7 µM $ZnCl_2$ plus 50 µM pyrithione for 2 hr at 37°C, prior to washing and loading FluoZin-3-AM (2 hr) and organelle markers. To examine the effect of H_2O_2, cells were incubated with H_2O_2 (see figure legends for concentrations) for 2-3 hr at 37°C, prior to loading FluoZin-3-AM (2 hr) and organelle markers. Where appropriate, cells were co-treated with TRPM2 channel inhibitors including 150 µM 2-APB or 10 µM PJ-34 or metal chelators including 0.3 µM TPEN, or pre-transfected with siRNA (see relevant figure legends for details). Images were captured at 37ºC using Zeiss LSM700 confocal microscope fitted with a 63× oil objective. Co-localisation of Zn^{2+} fluorescence and organelle fluorescence and number of lysosomes were determined using the Imaris software.

Intracellular Ca^{2+} staining

HUVECs were cultured in 35 mm Fluorodish^{TM} glass bottomed dishes. Cells were washed with EBM-2 medium not containing growth factors. Then, 1 ml of indicator dye (1 ml EBM-2 medium mixed with 1 µl 1 mM Fluo-4-AM and 1 µl 20% w/v pluronic F-127) with or without 1 µM calcium ionophore A23187 was added. Cells were incubated for 1 hr at 37ºC in the dark. The cells were washed twice with EBM-2 medium not containing growth factors; each wash required 15 min incubation at 37ºC in the dark. For organelle staining, samples were loaded with 200 nM LysoTracker or 200 nM MitoTracker diluted in EBM-2 medium not containing growth factors. Images were captured at 37ºC using a Zeiss LSM700 confocal microscope fitted with a 63× oil objective.

2.2.2.6 Mitochondrial morphology assessment

Morphology of mitochondria was assessed from images of cells stained with MitoTracker Red or transfected with pMito-Cherry or with pMito-CFP. In some experiments, cells were transfected with pMito-Cherry because MitoTracker Red staining was diffuse in the presence of H_2O_2, making changes in mitochondrial morphology difficult to assess. pMito-CFP is a cyan fluorescent mitochondrial marker. However, in some experiments, pMito-Cherry (red) was used to allow determination of its co-localisation with the green Zn^{2+} marker (FluoZin-3-AM).

Aspect ratio (AR, ratio between the major and minor axis) and form factor (FF, degree of branching) were determined using ImageJ 1.44p from individual mitochondria after reducing nonspecific noise of the fluorescence signal as reported previously (Koopman et al., 2005). FF is defined as $((Perimeter^2)/(4\pi*Area))$. Mitochondrial morphology measurements were made from over 70 individual mitochondria taken from at least 3-4 independent experiments. The mitochondria were counted as fragmented if the FF was below 2.5. A cell was considered as having fragmented mitochondria when ≥ 50% of its total number of mitochondria were fragmented (Trudeau et al., 2011).

2.2.2.7 Mitochondrial staining of mouse aorta

Aortas isolated from 8-10 week old wild-type (C57BL/6) and TRPM2-KO mice were cut open longitudinally and cut into ~5 mm pieces. After two washes with SBS, pieces of aorta were exposed to EGM-2 containing 33 mM glucose for 72 hr before loading with MitoTracker Red for 30 min at 37°C. After washing with SBS, they were fixed in 4% paraformaldehyde (1 hr), blocked overnight at 4°C with 1% ovalbumin/PBS, washed with PBS (3 times 10 min each) and mounted onto microscope slides in DAPI-Fluoromount-G. Control pieces were exposed to 8 mM glucose. Confocal Images were captured from the luminal surface using conditions described later under Image acquisition and analysis (see Section 2.2.2.16).

2.2.2.8 Drp1 recruitment to mitochondria

To examine glucose-induced Drp1 recruitment to mitochondria, cells were transfected with Drp1-GFP or DN-Drp1(K38A)-GFP with and without human TRPM2 siRNA-1 or TRPM2 siRNA-2. Transfected cells were incubated in EGM-2 or EGM-2 containing 33 mM glucose or 5 mM glucose plus 28 mM mannitol for 24 hr at 37°C. 0.3 µM TPEN was included in some experiments and incubation continued for a further 24 hr. For H_2O_2, cells transfected with Drp1-GFP or DN-Drp1(K38A)-GFP with and without human TRPM2 siRNA-1 were incubated with 1 mM H_2O_2 for 2-3 hr. Cells were then washed with EBM-2 and incubated at 37°C for 30 min with MitoTracker Red (200 nM) diluted in EBM-2. After washing, cells were imaged in EBM-2 for Drp1-GFP and MitoTracker Red.

2.2.2.9 Determination of lysosomal membrane permeability (LMP) and mitochondrial membrane permeability (MMP)

The extent of LMP was assessed by determining the decrease in the number of LysoTracker positive lysosomes following various treatments and also by examining the cells for cytoplasmic release of cathepsin B. LysoTracker positive lysosomes per cell were counted using the Imaris software.

Cells on pre-treated glass cover-slips were treated with 1 mM H_2O_2 in the presence or absence of 150 µl 2-APB for 4 hr at 37°C. Cells were fixed and permeabilised as described above in Section 2.2.2.3. To determine LMP, cells were immunostained with mouse anti-cathepsin B antibody and anti-mouse Cy3-conjugated secondary antibody. MMP was determined by immunostaining the cells with rabbit anti-cytochrome *c* antibodies and anti-rabbit Cy3-conjugated secondary antibody. Cells were imaged with a confocal microscope. Changes in the red fluorescence per cell were quantified using ImageJ.

2.2.2.10 Cell death assay

Cell death was assessed by staining the dead cells with propidium iodide (PI) and live cells with Hoechst 33342 as described previously (Manna et al., 2015). Cells were treated with medium alone (control) or medium with H_2O_2 (1 mM, 6 hr) or high glucose (33 mM glucose, 48 hr). Where appropriate, cells were co-treated with TRPM2 channel inhibitors or Zn^{2+} chelators, or pre-transfected with siRNA (see relevant figure legends for details). Cells were incubated with PI (5 µg ml^{-1}) and Hoechst 33342 (4 µM) in EBM-2 for 30 min before washing with EBM-2 and recording the images using confocal or epifluorescence microscope (EVOS® FL Cell Imaging System, Life technologies), fitted with a 20x/40x lens. PI positive (dead) cells were expressed as percent of Hoechst 33342 stained (total) cells. Images were collected from at least 3 fields of view using appropriate filters and analysed using ImageJ.

2.2.2.11 ROS measurement

Total ROS production was determined using the cell-permeant 2',7'-dichlorodihydrofluorescein diacetate (H_2DCFDA) (Jheng et al., 2012). This dye is a stable nonpolar compound (Bass et al., 1983). It diffuses into the cells and where it is hydrolysed to yield dichlorodihydrofluorescein (DCFH) (Bass et al., 1983). Intracellular ROS oxidises DCFH to the fluorescent compound DCF (Bass et al., 1983). The intensity of the fluorescence is proportional to the amount of ROS (Bass et al., 1983).

Cells grown in a 96-well plate were treated with high glucose (33 mM glucose, 48 hr) or 5 mM glucose plus 28 mM mannitol (control). Where appropriate, cells were co-treated with Zn^{2+} chelators (0.3 µM TPEN) or antioxidant (10 mM NAC) or pre-transfected with human TRPM2 siRNA or scrambled siRNA. To examine zinc pyrithione (Zn-PTO) induced effects, cells were incubated in EGM-2 or EGM-2 containing 0.7 µM $ZnCl_2$ plus 50 µM pyrithione for 1 hr. Where required, cells were co-treated with a Zn^{2+} chelator (0.3 µM TPEN) or antioxidant (10 mM NAC) or pre-transfected with human TRPM2 siRNA. Following the various treatments, cells were incubated with 10 µM H_2DCFDA diluted in EBM-2 for 30 min at 37˚C followed by three washes with EBM-2. Cells were imaged using EVOS® FL Cell Imaging System (Life technologies) fitted with a 40× lens. Images were analysed with ImageJ software. The results were expressed as the mean fluorescence intensity/cell.

2.2.2.12 Mitochondrial ROS measurement

Mitochondrial ROS was determined by staining cells with the MitoSox™ Red fluorescent dye. MitoSox™ Red is a fluoroprobe used to detect superoxide generation from mitochondria in different pathophysiological conditions (Mukhopadhyay et al., 2007). Staining can be detected and quantified using confocal microscopy and flow cytometry (Mukhopadhyay et al., 2007).

Cells were grown on cover-slips in a 24-well plate. Cells were treated with high glucose (33 mM glucose, 48 hr) or 5 mM glucose plus 28 mM mannitol (control). Where appropriate, cells were co-treated with antioxidant (10 mM NAC) or pre-transfected with human TRPM2 siRNA or scrambled siRNA. They were then incubated with 1 µM MitoSox™ Red diluted in appropriate medium for 30 min at 37˚C followed by three washes with the medium. Cells were fixed with 2% PFA and blocked with PBS-1% ovalbumin for 1 hr at room temperature. Images were captured using a confocal microscope with a 63× lens and analysed by ImageJ.

2.2.2.13 Intracellular Ca^{2+} and Zn^{2+} measurements

Intracellular changes in [Ca^{2+}] and [Zn^{2+}] were monitored using Fura-2-AM and FluoZin-3-AM respectively (Al-Shawaf et al., 2010). HUVECs or HEK-TRPM2^{tet} cells, grown in 96-well plates, were incubated with Fura-2-AM (2 µM) or FluoZin-3-AM (3 µM) in SBS containing 0.02% Pluronic F-127 for 1 hr at 37°C. After washing twice with SBS for 30 min, 200 µl of SBS was added to each well. Fluorescence was recorded using the Flexstation® II multi-mode microplate reader (Molecular Devices, California, USA). Fluorescence was measured at 5-10 sec intervals using excitation wavelengths of 340 and 380 nm and an emission wavelength of 510 nm for Ca^{2+}. $[Zn^{2+}]_i$ was monitored at 530 nm (excitation wavelength 490 nm). After taking several control measurements for 1 min, 50 µl of the desired reagents made up at 5-fold the required final concentration were added to wells. For Ca^{2+}, the ratio of fluorescence intensities at 340 and 380 nm (F340/F380) was calculated. For Zn^{2+}, changes in emission at 530 nm were measured. HUVECs were pre-treated with 1 mM H_2O_2 for 2 hr and washed with SBS prior to Zn^{2+} fluorescence measurements. For Ca^{2+} free conditions, the extracellular solution was Ca^{2+}-free SBS containing 0.4 mM EGTA.

2.2.2.14 Subcellular fractionation

For subcellular fractionation, a Lysosome Enrichment Kit for Tissues and Cultured Cells (Catalog Number 89839; Thermo Scientific) was used. HEK-293-MSR cells (2 x 75 cm^2 flasks) transfected with pCDNA3.1-TRPM2-HA were harvested by centrifugation at 850 x*g* for 2 min.

The cell pellet (~200 mg wet weight) was gently resuspended in 600 µl of extraction buffer (LER-A, supplemented with 1% protease inhibitor cocktail, Roche) and incubated on ice for 2 min. The suspension was homogenised in a ball-bearing homogeniser (Isobiotech, 16 micron clearance) using 20 passages. The efficiency of cell lysis was checked using a light microscope by placing 5 µl of lysate onto a glass slide. To the lysate, 600 µl LER-B (also supplemented with 1% protease inhibitor cocktail) was added. The samples were centrifuged at 600 x*g* for 10 min at 4°C to remove the nuclei

and debris. The supernatant containing lysosomes, mitochondria and cytosol was subjected to density gradient centrifugation.

Samples preparation for density gradient centrifugation

All steps were performed in the cold room or on ice. Five gradients were prepared by mixing gradient dilution buffer (1 LER A:1 LER B) with Optiprep medium, as outlined in Table 2.6.

Table 2.7 The required Opti-prep volume and concentration for density gradient centrifugation

Optiprep medium volume (µl)	Gradient dilution buffer volume (µl)	Final volume (µl)	Optiprep final concentration (%)
283.3	716.7	1000	17
333.3	666.7	1000	20
191.7	308.3	500	23
450	550	1000	27
250	250	500	30

OptiPrep density gradient solutions were carefully pipetted into 5 ml ultracentrifuge tubes in the following order: 30%, 27%, 23%, 20% and 17%. The supernatants from the cell extracts were mixed with Optiprep (4:1) to make the final Optiprep concentration 15%. 1 ml of this was overlaid on the top of the gradient, and the tubes were centrifuged in SW 55 Ti rotor in a Beckmann ultracentrifuge at 40,000 rpm at 4°C for 4 hr. After centrifugation, two distinct bands were seen in the gradient; see Figure 2.1. 500 µl fractions collected from the top were diluted with 1 ml PBS and centrifuged at 14000 x*g* at 4°C for 1 hr. After centrifugation, supernatants of each fraction were collected and labelled as cytosolic fractions. Pellets containing the organelles were resuspended in 30 µl of 1×SDS sample buffer.

For mitochondrial imaging

Mitochondrial fraction (see Figure 2.2) was collected and diluted in KCl buffer. The sample was centrifuged at 14000 x*g* at 4°C for 1 hr. The pellets containing mitochondria were resuspended in KCl buffer and the supernatant was discarded.

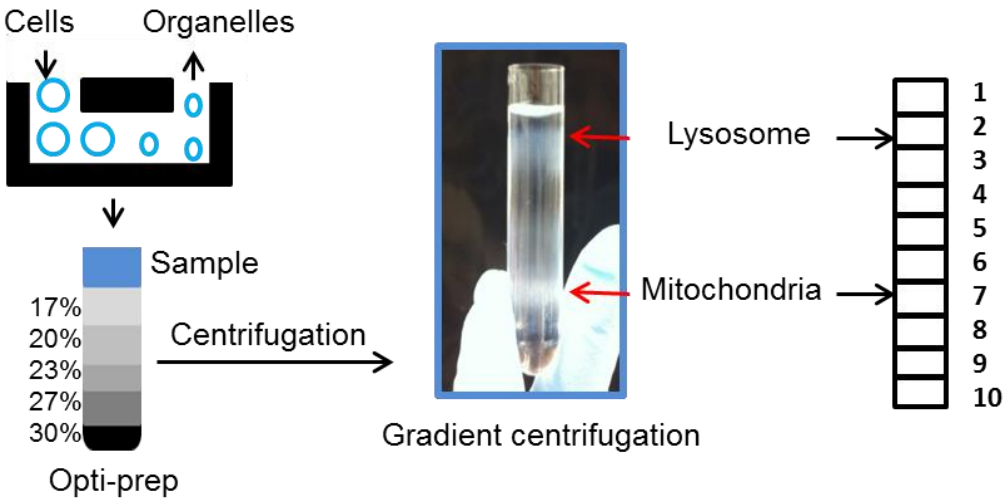

Figure 2.2 Samples preparation and density gradient centrifugation

Cell suspension was homogenised in a ball-bearing homogeniser to break the cells; debris and nuclei were removed by centrifugation. Five Optiprep solutions containing different concentrations of Optiprep were sequentially loaded in an ultracentrifugation tube, with high concentration at the bottom. Post-nuclear supernatant diluted with Optiprep was overlaid on the top of the density gradient. After centrifugation, two distinct bands were seen in the tube: the top band containing lysosomes (fraction 1-3) and the bottom band containing mitochondria (fraction 6-8). All fractions were collected and prepared for western blot analysis.

2.2.2.15 Western blot analysis

Sample preparation

To determine TRPM2-HA expression in HEK-MSR cells, the cells were cultured in a 24-well plate for 24 hr, transfected with TRPM2-HA and incubated for 48 hr. Cells were washed three times with PBS, scraped and then transferred into an Eppendorf tube. Cells were centrifuged for 5 min at 1,000 rpm at 4ºC. Supernatant was discarded and

the cell pellet re-suspended in 50 µl of 1× SDS sample buffer. After incubation for 5 min at 95ºC, samples were centrifuged at 13,000 *xg* for 5 min.

SDS-PAGE

Table 2.8 Gel preparation

A- 10% running gel

Solution Components	Component volumes (ml) per gel
Milli-Q water	1.9
30% acrylamide mix (Sigma)	1.7
1.5 M Tris (pH8.8) (Thermo Fisher)	1.3
10% SDS (Sigma)	0.05
10% ammonium persulfate (Sigma)	0.05
TEMED (Sigma)	0.002

The mixture was loaded in between the gel plates, overlaid with water-saturated butanol and allowed to stand for 30 min; see Table 2.7A.

B- 5% stacking gel

Solution Components	Component volumes (ml) per gel
Milli-Q water	0.68
30% acrylamide mix (Sigma)	0.17
1.0 M Tris (pH6.8) (Thermo Fisher)	1.3
10% SDS (Sigma)	0.01
10% ammonium persulfate (Sigma)	0.01
TEMED (Sigma)	0.001

Butanol was discarded and the running gel was overlaid with the 5% stacking gel; see Table 2.7B. Combs were placed and left to set for 1 hour.

Electrophoresis, western transfer and antibody labelling

Equal amounts of cell lysate protein were loaded into the wells of the gel. The gels were run at 160 V for 70 min. Proteins were transferred electrophoretically onto a 0.45 µm nitrocellulose membrane (BIO-RAD) at 50 mA for 90 min. Membranes were blocked

with Marvel dry milk (5%) in PBS containing 0.05% Tween-20 (PBS-T) for 1 hr at room temperature before incubating with HRP-conjugated primary antibodies. Alternatively, primary antibodies (non-HRP conjugated) diluted in the blocking buffer were added to the blots and then incubated at 4°C overnight. After washing with PBS-T for 1 hr at room temperature, the membranes were incubated for 1 hr at room temperature with appropriate HRP-conjugated secondary antibody diluted in the blocking buffer. After washing with PBS-T for 1 hr at room temperature, with several changes of PBS-T, the bound proteins were stained with a chemiluminescence reagent. For the source and dilutions of antibodies see Section 2.1.2.4.

Staining and developing

Lumigen PS-Atto solution A (400 µl) was mixed with Lumigen PS-Atto solution B (400 µl) and left in the dark for 2 min. The membrane was positioned on a glass plate, protein side up. PS-Atto was pipetted onto the membrane making sure that the membrane was completely covered with the mixture of solutions (A) and (B). The membrane was left in the dark for 2 min. As much residue was drained off as much as possible, and the plate covered in cling film. The film was exposed starting from one min to several min, and developed using X-ray film developer and fixer. Alternatively, chemiluminescence on the blots was captured using G-BOX Chemi XX6.

2.2.2.16 Zn^{2+} uptake by mitochondria

Zn^{2+} uptake by mitochondria was determined as described previously (Malaiyandi et al., 2005). Mitochondria were isolated from HEK-293-TRPM2^{tet} cells (~200 mg wet cell pellet) induced to express TRPM2 channels using the Optiprep density gradient centrifugation method, as described above. Mitochondrial fractions (6-8) were washed and resuspended in KCl-based buffer (see Table 2.2F). After loading with 50 µM FluoZin-3-AM for 20 min at 37ºC in substrate-free KCl free buffer containing 200 µM EGTA (see Table 2.2G), 100 µl of the suspension was placed in a FluoroDish^{TM} glass bottomed dish. After 7 min, 900 µl of KCl buffer was added and the fluorescence (excitation 490 nm/emission 530 nm) recorded continuously at 37°C using LSM 700 Zeiss confocal microscope; see Figure 2.2. After control recordings, 30 µl $ZnCl_2$ plus or

minus 200 µM H_2O_2 diluted in KCl buffer was carefully added and the recording of the field continued for 15 min. Background fluorescence was collected from mitochondria free regions. Increase in fluorescence was quantitated using ImageJ.

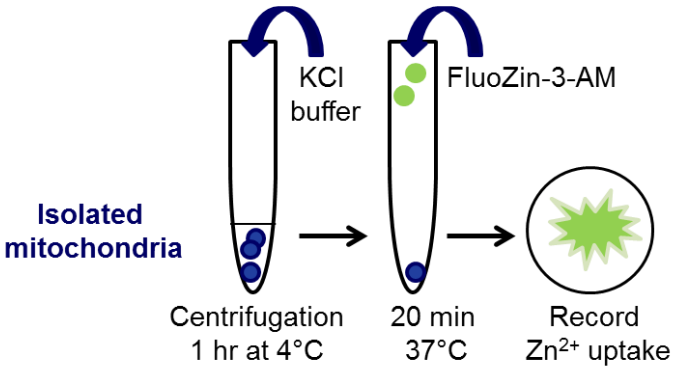

Figure 2.3 Sample preparation for mitochondrial imaging

Mitochondrial fractions were collected, centrifuged and washed with KCl buffer. The pellet was resuspended with FluoZin-3-AM prepared in KCl free buffer and incubated for 20 min at 37°C. Then, the suspension was placed in an empty FluoroDish glass bottomed dish. After 7 min, KCl buffer was added and Zn^{2+} uptake by isolated mitochondria was recorded.

2.2.2.17 Image acquisition

The images were captured randomly for presentation and analysis. Where necessary, images were cropped to illustrate details of subcellular structural changes.

Images of immunofluorescent live cells were collected with a LSM700 or LSM810 Zeiss inverted laser scanning confocal microscope equipped with an oil-immersion 63×/ NA 1.3 objective lens. DAPI (345 nm excitation, 458 emission) was excited with a diode laser at 405 nm, fitted with a 420-440 nm emission filter. MitoTracker Red, LysoTracker Red, ER Tracker Red, MitoSOX Red, Mito-Cherry and Cy3 (548 nm excitation, 562 nm emission) were excited using a He-Ne laser fitted with 543 nm filters. Alexa Fluor^{488}, FluoZin-3, Fluo4, pMito-CFP, Drp1-GFP and Lamp1-GFP (494 nm excitation, 519 nm emission) were excited with an Argon laser at 488 nm, fitted with a 500-530 nm emission filter.

2.2.2.18 Data analysis

Co-localisation analysis was performed using the Imaris software (Bitplane). ImageJ was used for quantification of mitochondrial morphology, Zn^{2+} uptake by isolated mitochondria and ROS levels. All experiments were performed at least 3 times (n) and the values presented as mean ± SEM. n/N in figure legends indicates the number of independent experiments (n) over the number of cells (N) analysed. Statistical significance was assessed using the Student's *t*-test (Microsoft Excel) or One-way Anova, (OriginPro .1) followed by Tukey post-hoc test. Probability (*P*) values are indicated with ∗, ∗∗, ∗∗∗, ∗∗∗∗, which correspond to values of 0.05, 0.01, 0.001 and 0.0001 respectively.

2.2.3 Electrophysiology techniques

2.2.3.1 Procedures of whole cell patch-clamp recording of TRPM2 channel currents

HEK293 cells were co-transfected with 400 µg TRPM2-HA and 100 ng EGFP (marker for transfected cells). Transfected cells were seeded onto cover-slips after transfection. 24-48 hr later, transfected cells were chosen for patch-clamp recording based on EGFP fluorescence.

Patch clamp recordings were made at room temperature, using Axopatch200B amplifier (Axon Instruments) and Digidata 1332A (Axon Instruments). The extracellular solution contained: 147 mM NaCl, 2 mM KCl, 1 mM $MgCl_2$, 2 mM $CaCl_2$, 10 mM HEPES and 13 mM glucose, pH 7.4. Cells were held at -40 mV and voltage ramps with a 1 sec duration from -120 mV to 80 mV were applied every 5 sec. 20 µM N-(p-Amylcinnamoyl) anthranilic acid (ACA) was applied at the end of the recording. Data analysis was carried out using pClamp9 software (Axon Instruments). Patch-clamp experiments were performed by Dr. Lin-Hua Jiang, Faculty of Biological Science, University of Leeds.

3 | Generation, expression and functional evaluation of HA tagged TRPM2 ion channels

3.1 Introduction

The TRPM2 channel is a plasma membrane ion channel. However, its expression has also been reported in lysosomes (Lange et al., 2009; Sumoza-Toledo et al., 2011; Sun et al., 2012). Its activation by oxidative stress has been linked widely to cell death due to Ca^{2+} entry (Kaneko et al., 2006; Manna et al., 2015; McHugh et al., 2003; Sun et al., 2012). Trafficking of TRPM2 ion channels to the plasma membrane and to lysosomes is not known. Likewise little is known about how the plasma membrane TRPM2 channels are internalised and what their fate is following internalisation.

Emerging evidence suggests that the TRPM2 channel functions both at the plasma membrane and the lysosome. Moreover, some cells have more channels in the lysosomal membranes than in the plasma membrane. For example, TRPM2 expression in dendritic cells is largely seen in the endosomal vesicles (punctate cytoplasmic distribution), whereas in neutrophils, TRPM2 expression was mainly found in the plasma membrane (Sumoza-Toledo et al., 2011; Zeng et al., 2010). The question is, how do TRPM2 channels reach lysosomes? In general, there are two different routes for intracellular trafficking to lysosomes. In the first route, proteins travel from the Golgi apparatus to late endosomes and then to lysosomes (Harter and Mellman, 1992; Mathews et al., 1992), while, in the second route, proteins travel from the Golgi apparatus to the plasma membrane and then to early endosomes, late endosomes and lysosomes (Harter and Mellman, 1992). Investigation of TRPM2 trafficking requires antibodies to the channel protein, ideally to an extracellular loop (Karnik et al., 2013; Mankouri et al., 2006). However, the commercial TRPM2 antibody (Bethyl laboratories, catalog #A300-413A) is not suitable to label TRPM2 channels at the plasma membrane, as the antibodies are directed to an intracellular segment. In addition, these commercial TRPM2 antibodies produce significant nonspecific labelling in both

immunohistochemistry and western blotting (observation in Sivaprasadarao's laboratory).

The present chapter aims to introduce an epitope (Fritze and Anderson, 2000; Karnik et al., 2013; Mankouri et al., 2006) into the extracellular loop of TRPM2 channels. There are many common tags that are often fused to protein of interest and can be detected with commercially available antibodies; examples of such tags include Influenza haemagglutinin A (HA), FLAG and Myc (Fritze and Anderson, 2000; Jarvik and Telmer, 1998). However, insertion of a tag without disturbing the structure, function or subcellular localisation can be challenging (Jarvik and Telmer, 1998; Reinhard et al., 2013). In this chapter, an HA tag was inserted into the S1-S2 loop of TRPM2 channels using recombinant techniques, and its expression and function were evaluated using cell biology techniques and whole-cell patch clamp recordings respectively.

3.2 Results

3.2.1 An investigation into the specificity of commercial anti-TRPM2 antibodies

To study the trafficking pathway of TRPM2 ion channel in health and disease, specificity of a commercial polyclonal rabbit anti-TRPM2 antibody (Bethyl Laboratories, catalog #A300-413A) was first examined. For this, HUVECs (which express TRPM2 channels natively) and HEK-293 cell lines (which do not express native TRPM2 channels) were used. The results in Figure 3.1 indicate that the commercial anti-TRPM2 antibody shows significant nonspecific labelling in HEK-293 cells that do not express native TRPM2. Moreover, this antibody was raised against an intracellular epitope; thus it is less suitable for direct detection of plasma membrane expression of TRPM2 channels.

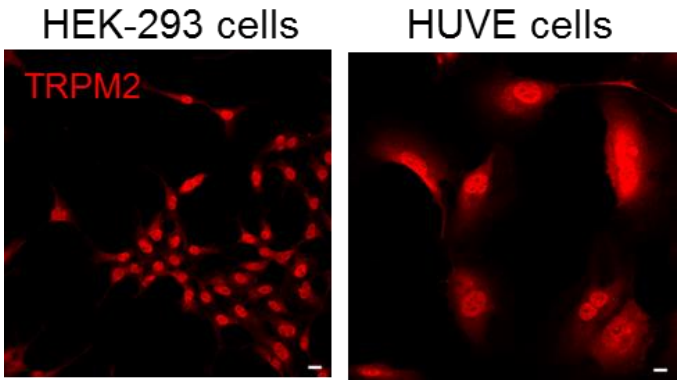

Figure 3.1 Nonspecific labelling of TRPM2 by anti-TRPM2 antibodies

HEK-293 cells and HUVECs were fixed with 2% PFA, permeabilised, and incubated with the polyclonal rabbit anti-TRPM2 (1:100) antibody. Cells were then stained with Cy3-conjugated anti-rabbit secondary antibody (1:500). Cells were imaged by confocal microscopy, scale bar, 10 µm. Representative images are shown; experiment was done twice.

3.2.2 Insertion of an extracellular HA epitope into the TRPM2 channel

As shown in Figure 3.1, TRPM2 antibody is not suitable to selectively label TRPM2 channels and study TRPM2 trafficking. Introduction of HA epitope into a TRPM2 channel would help in studying the localisation and trafficking of the channel. Therefore, an attempt was made to insert an HA-epitope (YPYDVPDYA) into the first extracellular loop, between segment 1 and segment 2 of TRPM2, by Timothy Munsey, University of Leeds. The construct in the pcDNA3 vector was sequenced and aligned with hTRPM2 using the ClustalW2. Unfortunately, it was found that two amino acids, an aspartate (D) and valine (V), were missing from the HA sequence (YPYDVPDYA). In order to insert the missing amino acids, primers were designed and PCR was carried out (see Figure 2.1) as described before (Sivaprasadarao and Findlay, 1993). After treating with *Dpn* I, the PCR product was analysed using agarose gel electrophoresis (Figure 3.2A). There is a clear indication of a band on the agarose gel, with a size between 8000–10000 bp.

The PCR product (Figure 3.2A) was cut from the agarose gel and purified using a commercial gel extraction kit. Recovery of DNA in the purified fraction was assessed by agarose gel electrophoresis (Figure 3.2B). A single band was seen on the gel. The purified product was incubated with T4 DNA ligase to join the DNA ends.

The ligated PCR product was transformed into competent XL I-Blue cells. Single colonies were picked and incubated in 5 ml culture tubes overnight at 37°C for small scale plasmid preparation, following the protocol of QIAprep Spin Mini-prep Kit. The plasmid preparations from five clones were analysed by agarose gel electrophoresis (Figure 3.2C). Two of these clones, 1 and 5, were fully sequenced, and aligned against the expected sequence of TRPM2-HA (see appendix). The sequences around the HA (Figure 3.2D) confirmed in both the clones the presence of D and V amino acids, the two amino acids that had been missing in the original construct made by Tim Munsey.

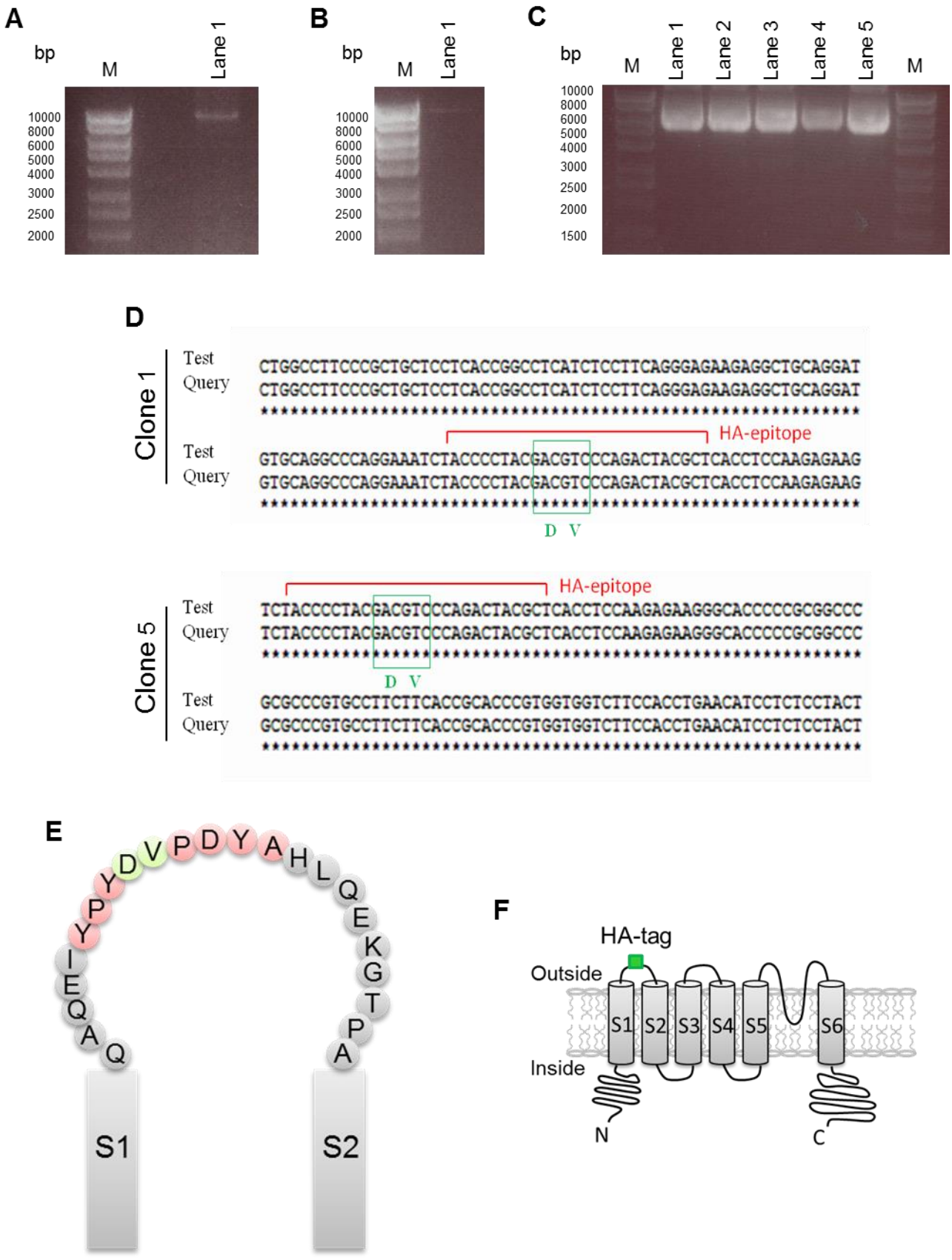
A
bp
M
Lane 1
10000
8000
6000
5000
4000
3000
2500
2000
B
bp
M
Lane 1
10000
8000
6000
5000
4000
3000
2500
2000
C
bp
M
Lane 1
Lane 2
Lane 3
Lane 4
Lane 5
M
10000
8000
6000
5000
4000
3000
2500
2000
1500
D
Clone 1
Test
Query
CTGGCCTTCCCGCTGCTCCTCACCGGCCTCATCTCCTTCAGGGAGAAGAGGCTGCAGGAT
CTGGCCTTCCCGCTGCTCCTCACCGGCCTCATCTCCTTCAGGGAGAAGAGGCTGCAGGAT
HA-epitope
GTGCAGGCCCAGGAAATCTACCCCTACGACGTCCCAGACTACGCTCACCTCCAAGAGAAG
GTGCAGGCCCAGGAAATCTACCCCTACGACGTCCCAGACTACGCTCACCTCCAAGAGAAG
D V
Clone 5
HA-epitope
TCTACCCCTACGACGTCCCAGACTACGCTCACCTCCAAGAGAAGGGCACCCCCGCGGCCC
TCTACCCCTACGACGTCCCAGACTACGCTCACCTCCAAGAGAAGGGCACCCCCGCGGCCC
D V
GCGCCCGTGCCTTCTTCACCGCACCCGTGGTGGTCTTCCACCTGAACATCCTCTCCTACT
GCGCCCGTGCCTTCTTCACCGCACCCGTGGTGGTCTTCCACCTGAACATCCTCTCCTACT
E
D V P D Y A H L Q E K G T P A Q A Q I E Q Y P Y D Y
S1
S2
F
HA-tag
Outside
Inside
S1
S2
S3
S4
S5
S6
N
C

Figure 3.2 Insertion of an extracellular HA epitope into TRPM2

(A) Agarose gel electrophoresis of the PCR product. Lane 1, 25 µl of PCR product digested with 10 units of *Dpn;* lane M, DNA ladder.

(B) Agarose gel electrophoresis of the purified PCR product. PCR product in Figure 3.1A was cut out of the gel under UV transilluminator and purified using Gel Extraction kit. 2µl of the purified DNA electrophoresed on 1% agarose gel.

(C) Minipreps of clones generated from transformation of the ligated PCR product from (B). The purified ligated PCR product was transformed into XL-I Blue cells and small scale plasmid DNA prepared (minipreps) from five clones and electrophoresed on 1% agarose gel (Lanes 1-5).

(D) Partial sequences of two minprep plasmid DNA samples. Sequence alignment of the pcDNA3-hTRPM2-HA (test) with the DNA (query) from Clone 1 (Lane 1) and Clone 5 (Lane 5) produced by ClustalW2. Green boxes indicate the inserted codons. Only the relevant portion of the DNA sequence is shown.

(E) Schematic of the location of HA-epitope (red) in extracellular loop 1 (grey) between segment 1 and segment 2 indicating D and V residues (green) in HA.

(F) Schematic of the topology of TRPM2 subunit showing the site of the hemagglutinin (HA) epitope insertion.

3.2.3 Examination of the HA-tagged TRPM2 protein expression in different cell lines

The above data confirmed insertion of the HA epitope into pcDNA3-TRPM2 channel (Figure 3.2). Epitope tagged proteins and antibodies have since been widely used to study the movement of proteins between different cellular compartments (Jarvik and Telmer, 1998). However, insertion of a tag may affect expression, cellular location or function of a protein (Jarvik and Telmer, 1998). To investigate the expression of a HA-tagged TRPM2 channel, cell biology experiments (immuno-fluorescent staining and western blot analysis) were carried out. HEK-MSR cells were transfected with the TRPM2-HA construct. 48 hr post transfection, the cells were fixed with 2% PFA with and without permeabilisation. Cells were first treated with PBS-1% ovalbumin to block nonspecific binding sites and then incubated with rat anti-HA antibody and stained with Cy3 conjugated secondary antibody. It was expected that non-permeabilised cells will show staining of TRPM2-HA at the plasma membrane, while permeabilised cells will indicate total TRPM2-HA expression. Figure 3.3A shows no detectable expression of TRPM2-HA at the plasma membrane in non-permeabilised cells; some cells, however, showed intracellular staining which could be attributed to accidental permeabilisation of cells during the experiment. Permeabilised cells showed clear staining which indicates that the HA-epitope inserted into TRPM2 is effectively recognised by the anti-HA antibodies (Figure 3.3B). Expression of TRPM2-HA was also confirmed by western blot analysis of transfected cells, where a band corresponding to the molecular weight of ~170 KDa is seen (Figure 3.3C); the size roughly corresponds to the theoretical molecular weight of TRPM2-HA which is 173515.78. No bands were seen in the non-transfected control cell lysate. TRPM2-HA could also be successfully expressed in other cell types including HUVECs, HeLa and INS-1 cells (Figure 3.3D).

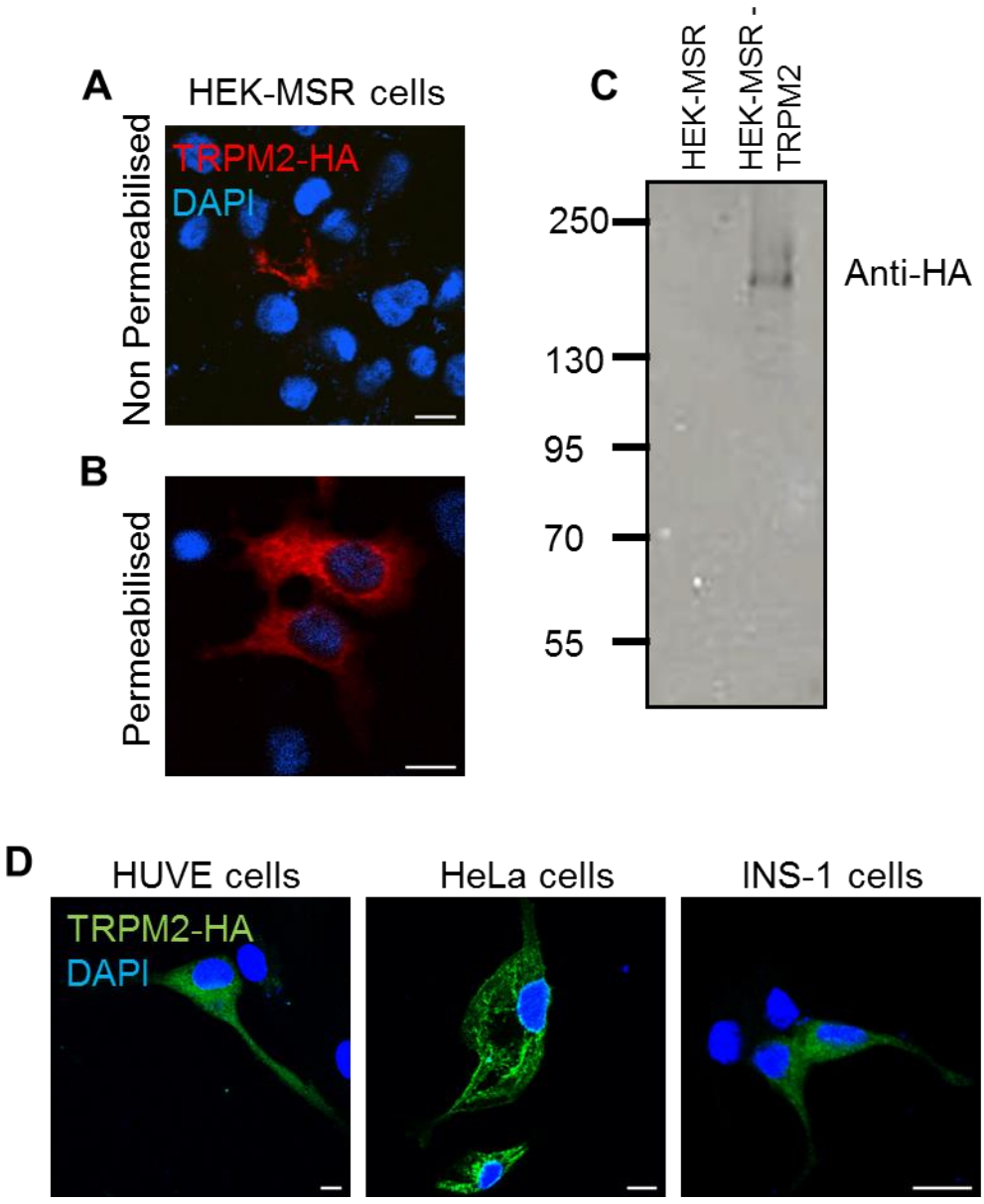
A
HEK-MSR cells
Non Permeabilised
TRPM2-HA
DAPI
B
Permeabilised
C
HEK-MSR
HEK-MSR - TRPM2
250
130
95
70
55
Anti-HA
D
HUVE cells
HeLa cells
INS-1 cells
TRPM2-HA
DAPI

Figure 3.3 Expression of TRPM2-HA in different cell lines

(A-B) Expression of TRPM2-HA in HEK-MSR cells. Cells were transfected with pcDNA3-TRPM2-HA. Cells were fixed with 2% PFA and permeabilised (B) or non-permeabilised (the cell stained was accidentally permeabilised) (A) with 0.25% Triton X-100. Cells were incubated with rat anti-HA and stained with Cy3 conjugated anti-rat secondary antibody. Images were taken by confocal microscope, scale bar, 10 µm, n=3.

(C) Western blot analysis of lysate from HEK-MSR cells, not transfected (control) and transfected with pcDNA3-TRPM2-HA. Immunostaining for the HA epitope revealed TRPM2-HA expression. Band at a molecular weight of ~170 kDa corresponds to the calculated size TRPM2-HA protein, n=3. Numbers on the left of the blot indicate size of marker proteins in kDa.

(D) TRPM2-HA expression in different cell lines. Different cell lines as indicated were transfected with TRPM2-HA. Cells were fixed with 2% PFA, permeabilised with 0.25% Triton X-100 and stained with AlexaFluor^{488} conjugated anti-rat secondary antibody. Images were taken by confocal microscope, scale bar, 10 µm, n=3. In all cases, representative images are shown.

3.2.4 Insertion of HA-tag does not affect cell membrane expression of TRPM2 channel

It is not clear from the above data whether the HA-tagged TRPM2 channels are expressed at the plasma membrane. This could be because HA-tagging prevents trafficking of the channel to the plasma membrane, or because its steady-state levels at the plasma membrane are too low to be detectable by immunostaining. To address this, internalisation of anti-HA antibodies was examined, along with the marker, the transferrin (Tfn) receptor. Internalisation of a transferrin receptor can be detected by confocal microscopy when the cells are pulsed with fluorescent transferrin, which binds the receptor and undergoes endocytosis into clathrin-coated vesicles (Mukherjee et al., 1997; Rajendran et al., 2010). If anti-HA antibodies bind TRPM2-HA at the plasma membrane and undergo internalisation, one would expect to see the antibodies in intracellular vesicles. If the vesicles also contain fluorescent transferrin, the results could suggest internalisation of TRPM2-HA into clathrin-coated vesicles. Thus HEK-TRPM2 cells were transfected with pcDNA3-TRPM2-HA and incubated with AlexaFluor^{488}-conjugated Tfn (marker of the Tfn receptor) for 15 min at 37°C. The cells were then washed and incubated with AlexaFluor^{594}-conjugated anti-HA antibodies. Live cell imaging (Figure 3.4) showed co-localisation of internalised TRPM2-HA channels with Tfn (yellow puncta). These data indicate that the internalised TRPM2-HA channels localise to distinct endosomes and are likely internalised by clathrin-mediated endocytosis. The results suggest that insertion of an HA epitope does not affect TRPM2 expression at the plasma membrane, although no distinct plasma membrane labelling could be seen when non-permeabilised cells were stained.

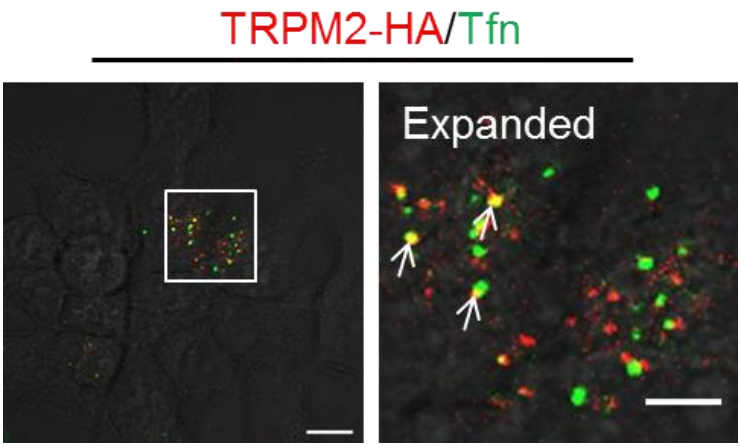

Figure 3.4 Internalised TRPM2-HA channels localise to transferrin-positive vesicles

HEK-MSR cells were transfected with pcDNA3-TRPM2-HA. Cells were incubated with 50 µg/ml AlexaFluor^{488} conjugated Tfn for 15 min at 37°C and then incubated with AlexaFluor^{594} anti-HA (1:300) for 15 min at RT. Cells were washed with SBS and imaged as a video by confocal microscopy at 37°C. The image represents a snapshot from the video (the CD is attached to the back cover of the thesis), n=2. Scale bar, 10 µm. Boxed regions are expanded, scale bar, 5 µm; representative images are shown.

3.2.5 Lysosomal TRPM2 expression

Previous studies have shown that TRPM2 ion channel is not only a plasma membrane ion channel but also a lysosomal ion channel (Lange et al., 2009). Immuno-fluorescent staining was carried out to test whether insertion of the HA-epitope affects location of TRPM2-HA expression in lysosomes. HEK-TRPM2 cells were transfected with pcDNA3-TRPM2-HA. The cells were fixed, incubated with rat anti-HA and mouse anti-CD63 (lysosomal marker) primary antibodies and stained with Cy3 conjugated anti-mouse secondary antibody and AlexaFlour^{488}-conjugated anti-rat secondary antibody. Confocal images in Figure 3.5 indicate intracellular expression of TRPM2-HA (green) that colocalises with CD63 (red). These data indicate that the HA-tag does not affect lysosomal trafficking of TRPM2 protein.

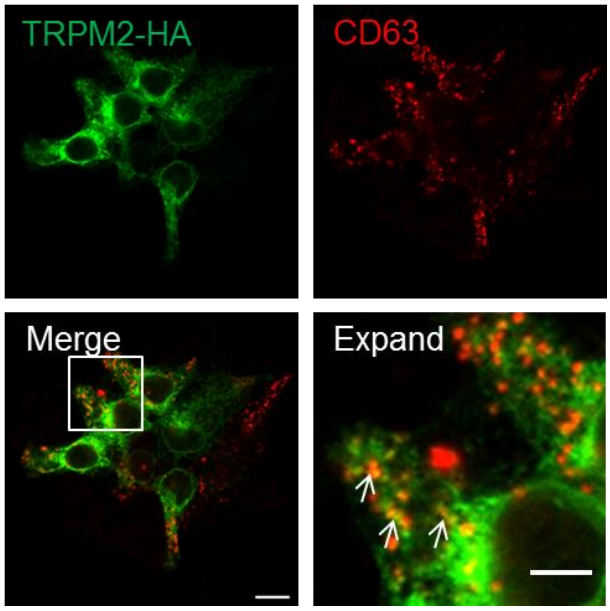

Figure 3.5 Expression of TRPM2-HA channels in lysosomes

HEK-MSR cells were transfected with pcDNA3-TRPM2-HA, fixed with 2% PFA, and permeabilised with 0.25% Triton X-100. Cells were incubated with rat anti-HA (1:500) and mouse anti-CD63 (1:500), one after the other, and stained with Cy3-conjugated anti-rat secondary antibody (1:500) and AlexaFlour^{488} conjugated anti-mouse (1:500) secondary antibodies. Cells were imaged by confocal microscopy, scale bar, 10 µm, n=3. Boxed regions are expanded, scale bar, 5 µm.

3.2.6 Insertion of HA-tag does not affect the function of TRPM2 channel

The aim of this experiment was to test whether the insertion of HA-tag into the S1-S2 loop affects the function of TRPM2 channel. Tetracycline-induced (+TRPM2-FLAG) and not-induced (-TRPM2-FLAG) HEK-TRPM2^{tet} cells were used as positive and negative controls. ADPR was applied though the patch pipette to activate the channels, and ACA was used to inhibit the ADPR-activated currents. As shown in Figure 3.6, there were no currents in not-induced cells. In tetracycline-induced cells, there was a robust current that was fully blocked by ACA. Currents of similar magnitude were detected in HEK-293 cells transfected with pcDNA3-TRPM2-HA. These results indicate that the insertion of an HA-epitope into TRPM2 channels does not perturb its function.

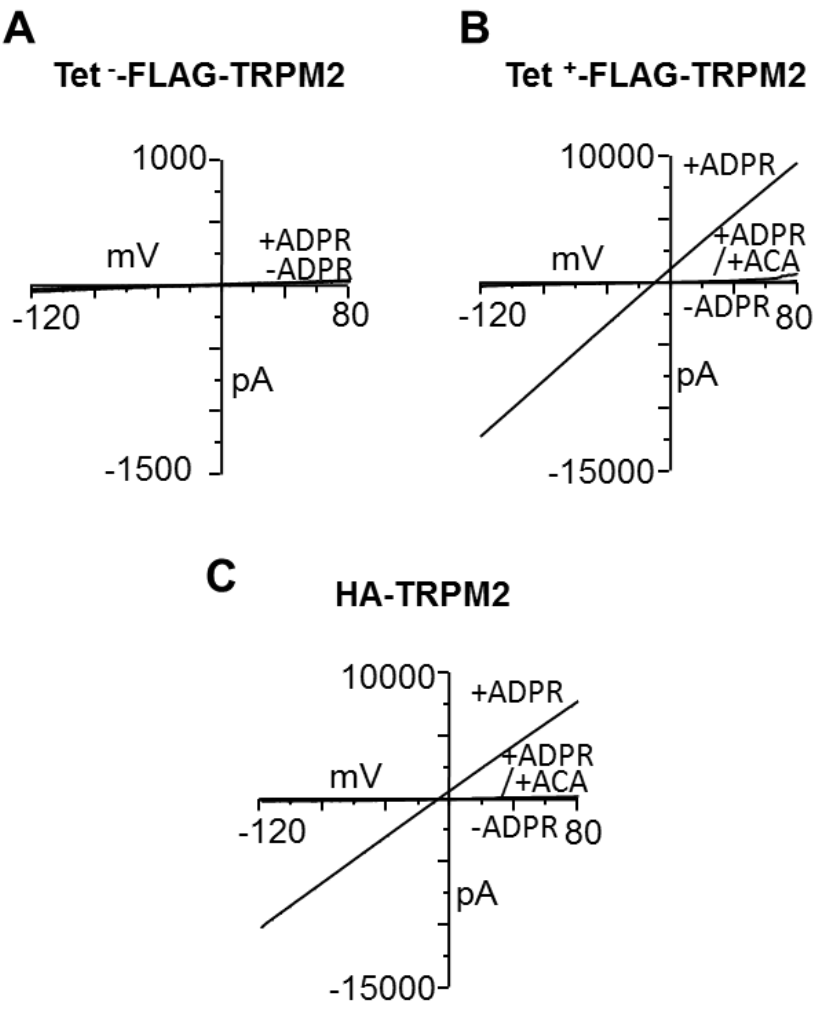

Figure 3.6 Effect of HA on the function of TRPM2 channels

(A-B) Whole-cell current measurements were made from induced (+TRPM2-FLAG) and not-induced (-TRPM2-FLAG) HEK-TRPM2^{tet} cells. (A) Current-voltage relationships without and with cytosolic 1 mM ADPR recorded from not-induced (-TRPM2-FLAG) HEK-TRPM2^{tet} cells. (B) Currents recorded from induced (+TRPM2) HEK-TRPM2^{tet} cells; recording was performed as in (A). ADPR-induced currents were inhibited by the application of 10 mM N-(p-amylcinnamoyl)anthranilic acid (ACA), n=3.

(C) Whole-cell current measurements from HEK-293 cells transfected with pcDNA3-TRPM2-HA. Currents induced by 1 mM ADPR and inhibited by 10 mM ACA, n=3.

I would like to acknowledge Dr. Lin-Hua Jiang, Faculty of Biological Science, University of Leeds for these recordings.

3.3 Discussion

Previous reports have shown that altered cellular trafficking of ion channels can lead to diseases such as cardiovascular and neuronal diseases (Hung and Link, 2011). Previous work implicated TRPM2 channels in diabetes, ischemia-reperfusion injury, vascular endothelial damage and brain injury (Dietrich and Gudermann, 2008; Manna et al., 2015; Ye et al., 2014). It is conceivable that altered trafficking of TRPM2 channels could contribute to these disease states. However, little is known about how TRPM2 channels traffic in a cell under normal conditions. Commercially available antibodies were found to be nonspecific (Figure 3.1) and are thus unsuitable for studies of TRPM2 trafficking. Furthermore these antibodies were raised against an intracellular epitope, which makes them less suitable for endocytic trafficking studies. For these reasons, in this chapter, HA epitope was inserted into the S1-S2 extracellular loop of the TRPM2 channel. The results show that the resulting TRPM2-HA construct is functional and suitable for trafficking studies.

3.3.1 TRPM2-HA expression, location and function

HA epitope was inserted into the first extracellular loop between S1 and S2 of a human TRPM2 sequence using PCR (Figure 3.2) and subsequent cloning of the PCR product. Epitope-tagged proteins and antibodies have been widely used to study the movement proteins between cellular compartments (Jarvik and Telmer, 1998). However, since insertion of a tag may affect expression, cellular location or function of a protein (Jarvik and Telmer, 1998), TRPM2-HA was expressed in a variety of cell lines and subjected to immunostaining and functional analysis.

Surface expression of TRPM2 channels was not detectable when non-permeabilised cells were labelled with anti-HA antibodies (Figure 3.3A). There could be several reasons why TRPM2-HA membrane expression was not discernible. Firstly, insertion of HA epitope may have prevented the channel from expression or trafficking to the cell surface. Secondly, the channels may move rapidly from the cell membrane to other organelles, so at steady-state, their levels could be too low to be detectable at the

plasma membrane. Finally, the epitope in the loop could be inaccessible to the antibody (Jarvik and Telmer, 1998).

In permeabilised cells, TRPM2-HA staining was robust (Figure 3.3B), indicating that insertion of the HA did not affect expression of the protein. This was further confirmed by the western blotting of transfected cells which showed a band, the size (~170 kDa) of which corresponds to the molecular weight calculated from the amino acid sequence (Figure 3.3C). Thus insertion of the HA-epitope did not affect TRPM2 expression and recognition by the anti-HA antibody. Although TRPM2-HA expression could not be detected by the anti-HA antibody labelling, whole cell patch-clamp analysis of transfected cells showed ADPR-induced cation currents that were inhibited by the TRPM2 inhibitor, ACA (Figure 3.6). The size of the currents were similar to currents from TRPM2 channels lacking the HA epitope. These results indicate that insertion of HA epitope does not inhibit trafficking of the channel to the plasma membrane and its function.

Besides the plasma membrane, expression of native TRPM2 channels was also reported in lysosomes of dendritic cells (Sumoza-Toledo et al., 2011) and INS-1 cells (Lange et al., 2009; Manna et al., 2015). Using CD63 as a marker, expression of TRPM2-HA in lysosomes could be demonstrated (Figure 3.5). Taken together, the results indicate that insertion of the HA tag does not affect normal trafficking and function of the channel and is thus suitable to investigate TRPM2 trafficking under different conditions.

3.3.2 Internalisation of plasma membrane TRPM2-HA channels

Although TRPM2-HA channels could not be detected at the cell surface by immunostaining, patch-clamp data revealed that they traffic to the cell surface. To investigate if TRPM2-HA channels undergo internalisation, an antibody uptake assay (Mankouri et al., 2006) was used. The data from live cell imaging of HEK-TRPM2-HA transfected cells (Figure 3.4) revealed that TRPM2-HA channels undergo internalisation

into endocytic vesicles that are positive for the early endosomes marker, transferrin receptor. These data confirmed that TRPM2-HA ion channels are expressed at the plasma membrane and delivered from the cell surface to early endosomes. During endocytosis, many receptors including transferrin receptors are localised to clathrin-coated vesicles (Mukherjee et al., 1997; Rajendran et al., 2010). Thus, these data also suggest that TRPM2-HA is internalised via clathrin-mediated endocytosis.

To conclude, the results of this chapter demonstrate that insertion of an HA tag into the S1-S2 loop of TRPM2 channels does not affect its trafficking to the plasma membrane and lysosomes. The results also provide the first indication that these channels are likely internalised via clathrin-mediated endocytosis. Thus the TRPM2-HA construct made in this study should be useful for detailed studies into trafficking of the channel under normal conditions and in disease states. However, the inability to detect surface expression of TRPM2-HA channels using anti-HA antibodies makes it somewhat difficult to study the trafficking of plasma membrane TRPM2 channels.

4 TRPM2 channels regulate the integrities of lysosomes and mitochondria

4.1 Introduction

Mitochondria are essential organelles that play key roles in cell life and cell death. They exist as a dynamic network and are mainly responsible for the production of energy. However, the structural integrity of mitochondria is constantly threatened by environmental and metabolic stresses. Mitochondria have the ability to cope with these threats by undergoing continuous cycles of fission and fusion (Archer, 2013; Dorn, 2015; Friedman and Nunnari, 2014; Youle and van der Bliek, 2012).

The fission machinery, in conjunction with mitophagy, helps remove damaged parts of mitochondria, and protects the cell from toxicity due to damaged mitochondria (Youle and Narendra, 2011). Mitochondrial fission is driven by the dynamin-related protein 1 (Drp1) (Chan, 2012). There are several mitochondrial proteins that act as a recruiter or receptor of Drp1; these include mitochondrial fission protein 1 (FIS1), mitochondria fission factor (MFF) and mitochondrial dynamics proteins (MiDs; MiD49 and MiD51) (Chan, 2012; Palmer et al., 2011). Drp1 is mainly located in the cytoplasm, but is recruited to the mitochondrial outer membrane during fission (Chan, 2012). Fusion promotes joining of healthy parts of mitochondria and restores the functional network. Fusion occurs in two steps, wherein the outer membrane and the inner membrane fuse in separate events. Mitofusin1 (Mfn1) and Mitofusin2 (Mfn2), which are located in the outer membrane, are responsible for the fusion of the outer membrane, whereas Optic atrophy 1 (OPA1), which is located in the inner membrane and intermembrane space, is responsible for inner membrane fusion (Archer, 2013; Chan, 2012; Friedman and Nunnari, 2014; Youle and van der Bliek, 2012). Imbalance between the fusion and fission events leads to mitochondrial elongation or mitochondrial fragmentation, both of which affect mitochondrial function. Disruption of fusion-fission equilibrium can impair cell homeostasis, and contribute to a wide range of diseases, in particular the late-age

onset diseases (Archer, 2013; Dorn, 2015). For example, a shift in the fusion-fission equilibrium towards fission has been reported in neuronal (Parkinson's, Alzheimer's) diseases, cardiovascular disease, diabetes and cancer (Archer, 2013; Friedman and Nunnari, 2014; Youle and van der Bliek, 2012). Thus these findings suggest that mitochondrial dynamics represent a valid drug target for a wide range of age-related illnesses.

The shift from fusion to fission has been attributed to the increase in cellular oxidative stress due to increased production of reactive oxygen species (ROS) by the aging cell. However, targeting the proteins involved in the fusion and fission events may prove difficult because knock-out of these proteins is embryonically lethal (Chen et al., 2003; Rahn et al., 2013; Wakabayashi et al., 2009). Compared with what is known about the molecular mechanism of mitochondrial fission, little is known about how oxidative stress regulates this process; thus a better understanding of the regulatory mechanisms may reveal novel drug targets.

It has been well established that hyperglycemic conditions and over-production of ROS induce mitochondrial fragmentation by increasing the intracellular Ca^{2+} concentration, thereby leading to increased apoptosis (Dorn, 2015; Friedman and Nunnari, 2014; Youle and van der Bliek, 2012). Some studies reported that oxidative stress leads to intracellular zinc accumulation, mitochondrial dysfunction and apoptosis (Weiss et al., 2000). The mechanisms by which Ca^{2+} and Zn^{2+} regulate these events are unclear.

In this chapter, the hypothesis that oxidative stress induces mitochondrial fragmentation by activating the TRPM2 cation channel has been tested. The rationale behind this hypothesis is the knowledge that TRPM2 channels are potently activated during oxidative stress (Sumoza-Toledo and Penner, 2011; Takahashi et al., 2011), and the resulting changes in intracellular Ca^{2+} and Zn^{2+} levels affect cell homeostasis, leading to apoptotic cell death (Manna et al., 2015; Sumoza-Toledo and Penner, 2011; Takahashi et al., 2011), which is the primary cause of most late age-onset diseases. To address this aim, human umbilical vein endothelial cells (HUVECs) were exposed to H_2O_2 or

high concentrations of glucose (diabetic conditions) as it has been shown previously that high glucose leads to apoptotic cell death by increasing cellular levels of ROS. The role of TRPM2 channels in H_2O_2 and high glucose-induced mitochondrial fragmentation (Du et al., 1998; Manna et al., 2015) was tested using pharmacological and RNAi approaches. The role of TRPM2 mediated changes in Ca^{2+} and Zn^{2+} signals was tested using chemical chelators of these ions. The results show that by mobilising the mitotoxic Zn^{2+} from lysosomal stores to mitochondria, TRPM2 channels increase mitochondrial fission. Unexpectedly, besides the plasma membrane and lysosomes, TRPM2 channels were also found in the mitochondria. Studies into the role of mitochondrial TRPM2 channels revealed that these channels promote mitochondrial Zn^{2+} accumulation leading to mitochondrial fragmentation.

In this chapter, different concentrations of H_2O_2 for different cell lines were used. The rationale behind this is the fact that different cells respond to different concentrations of H_2O_2 in terms of their ability to induce cell death (apoptosis) and mitochondrial fragmentation. This may be related to differences in ROS regulation in different cell types (Halliwell et al., 2000). Thus, in this study, HEK-TRPM2 cells and HUVECs were exposed to different concentrations of H_2O_2 and incubated for different lengths to detect phenotypic changes.

4.2 Results

4.2.1 Time course of H_2O_2-induced changes in mitochondrial morphology

To examine H_2O_2-induced changes in mitochondrial morphology, HUVECs were transfected with pMito-CFP. Transfected cells were exposed to 3 mM H_2O_2 and images were taken at 15 min time intervals by confocal microscopy. The images in Figure 4.1 show that oxidative stress induced branching of the mitochondrial network at the 15 min time point (red arrows). However, this newly formed branch disappeared at the 30 min time point (red arrows). These changes were then followed by progressive mitochondrial fission to small rounded structures (yellow arrows), some of which fused at early time points (purple arrow). At later time points, some of the rounded mitochondrial fragments began to disappear (blue arrows). These results are in agreement with the previous reports on neurons exposed to nitric oxide and on myocytes exposed to hydrogen peroxide (Barsoum et al., 2006; Fan et al., 2010).

To conclude, H_2O_2 has a profound effect on mitochondrial morphology. Brief exposure to H_2O_2 elicited a positive response by promoting branching. Prolonged exposure, however, caused extensive mitochondrial fission, followed by the gradual disappearance of fragmented mitochondria.

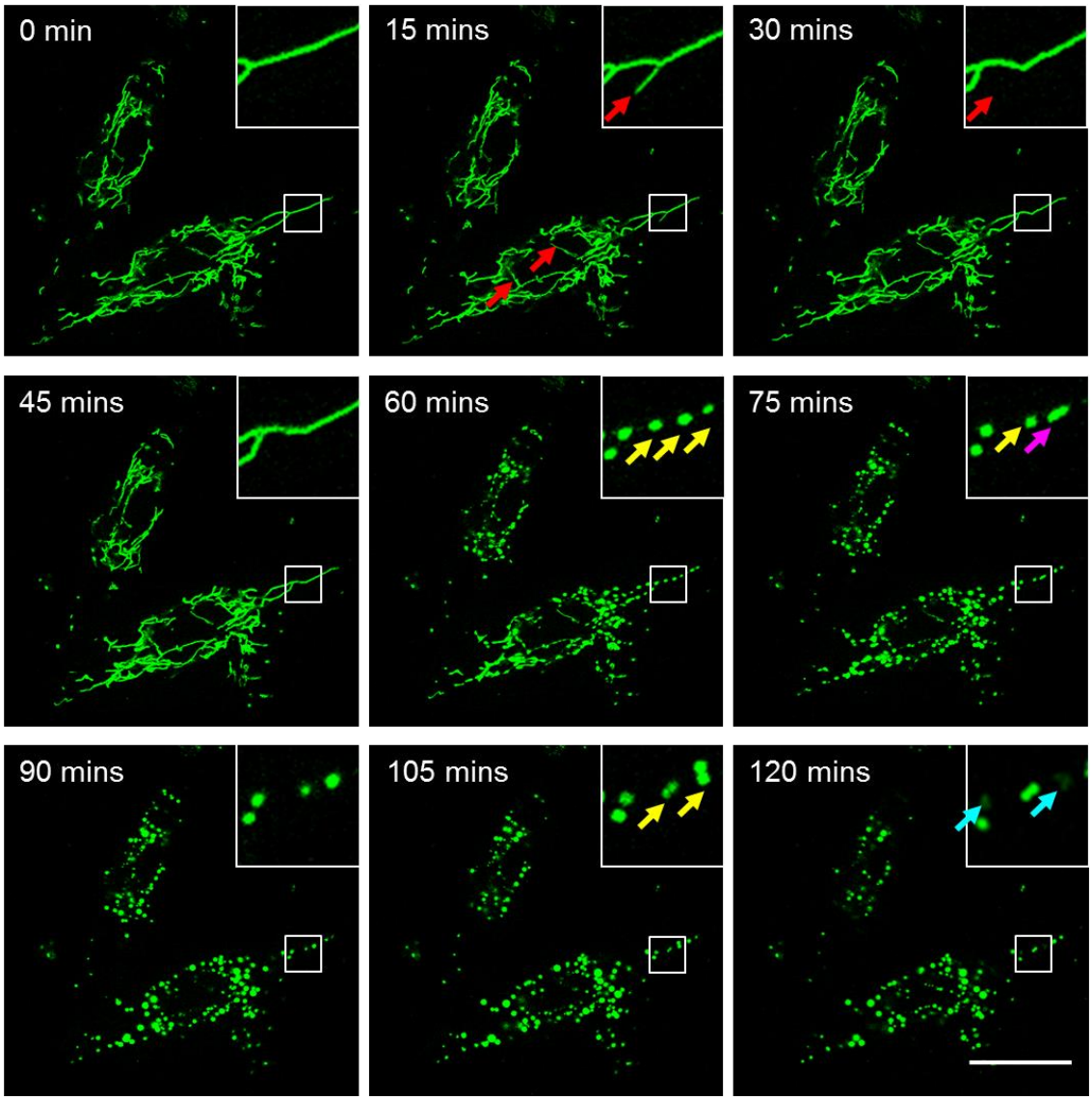

Figure 4.1 Sequential events of H_2O_2-induced mitochondrial fission and fusion in HUVECs

HUVECs were transfected with pMito-CFP (colour changed to green for clarity), and the mitochondria of two individual cells were imaged before (time = 0 min) and after H_2O_2 (3 mM) application. Confocal mages acquired at 15 min intervals are shown. Scale bar, 10 µm. Appearance of single mitochondrion, fission, fusion and mitochondrial disappearance events are indicated with arrows (red arrows indicate branching of mitochondrial network, yellow arrows indicate mitochondrial fission, purple arrows indicate mitochondrial fusion and blue arrows indicate mitochondrial disappearance). Representative images are shown; experiment was performed two times.

4.2.2 Expression of TRPM2 channels in HUVECs and RNAi silencing

To examine whether TRPM2 channels play a role in oxidative stress-induced mitochondrial fragmentation in endothelial cells, firstly, TRPM2 expression and function were tested in HUVECs. Calcium imaging and RT-PCR gave evidence of TRPM2 channel expression in HUVECs (Figure 4.2). Application of exogenous 3 mM H_2O_2 to HUVECs induced a rise in cytosolic [Ca^{2+}], which was absent in the presence of TRPM2 blockers (2-aminoethoxydiphenyl borate (2-APB) and N-(p-amylcinnamoyl)anthranilic acid (ACA)) (Figure 4.2A). RT-PCR performed on RNA isolated from HUVECs showed a band (293 bp) expected from TRPM2 messenger RNA. A similar size band was obtained from HUVECs transfected with scrambled (negative control) siRNA, but not from cells transfected with TRPM2 siRNA (Figure 4.2B). The efficiency of TRPM2-siRNA was further confirmed by calcium imaging. Figure 4.2C shows a reduction in Ca^{2+} entry in HUVECs transfected with TRPM2 siRNA, but not scrambled siRNA. These findings are in agreement with the previous reports that endothelial cells express TRPM2 ion channels (Hecquet and Malik, 2009) that are activated by H_2O_2 (Hecquet and Malik, 2009) and inhibited by 2-APB (Togashi et al., 2008) and ACA (Kraft et al., 2006) blockers.

To conclude, these findings confirm TRPM2 expression in endothelial cells and its activation by H_2O_2.

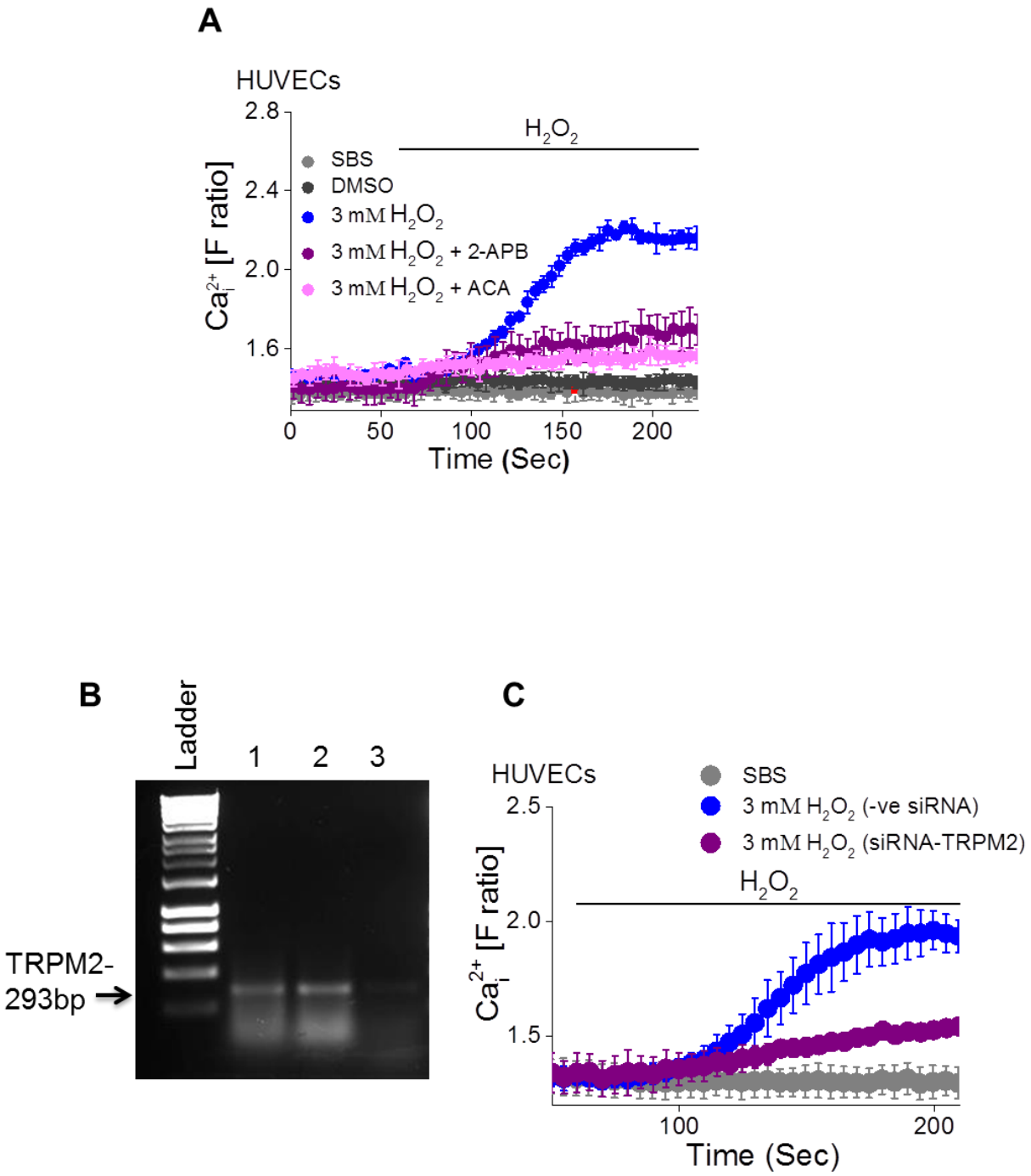
A
HUVECs
2.8
2.4
2.0
1.6
Ca_i^{2+} [F ratio]
H_2O_2
SBS
DMSO
3 mM H_2O_2
3 mM H_2O_2 + 2-APB
3 mM H_2O_2 + ACA
0
50
100
150
200
Time (Sec)
B
Ladder
1
2
3
TRPM2-
293bp
C
HUVECs
SBS
3 mM H_2O_2 (-ve siRNA)
3 mM H_2O_2 (siRNA-TRPM2)
2.5
2.0
1.5
Ca_i^{2+} [F ratio]
H_2O_2
100
200
Time (Sec)

Figure 4.2 Expression of TRPM2 channels in HUVECs and RNAi silencing

(A) Functional analysis of TRPM2 expression by Ca^{2+} imaging. HUVECs were loaded with Fura-2 AM, washed and incubated with TRPM2 blockers (150 µM 2-APB or 10 µM ACA) for 30 min at room temperature. Addition of 3 mM H_2O_2 (shown as horizontal bar) elicited a marked time-dependent increase in F340/F380 fluorescence ratio (due to rise in intracellular Ca^{2+}, Ca^{2+}_i). Rise in Ca^{2+}_i is absent in cells treated with the TRPM2 blockers. Symbols represent mean fluorescence ratio and the associated bars represent SEM, n=2.

(B) Demonstration of silencing of TRPM2 mRNA expression by RNAi.

Lanes 1-3: RT-PCR products from mRNA isolated from non-transfected HUVECs (lane 1) or HUVECs transfected with scrambled (negative control) siRNA (lane 2) or siRNA targeted to TRPM2 (lanes 3). The results show absence of a TRPM2 band (lane 3) in TRPM2 siRNA transfected samples, but not scrambled siRNA controls (lane 2).

(C) Demonstration of RNAi silencing of TRPM2 expression by calcium imaging. Experiments were performed as in (A), except the cells were transfected with scrambled siRNA or siRNA targeted to the TRPM2 channel. The results show efficient suppression of TRPM2 expression by TRPM2 siRNA, which is consistent with the RT-PCR results, n=3.

4.2.3 Inhibition of TRPM2 channels prevents H_2O_2-induced mitochondrial fragmentation

It was shown earlier that H_2O_2 induces endothelial mitochondrial fragmentation and activates TRPM2 ion channels. The aim of this experiment was to examine the role of TRPM2 ion channels in H_2O_2-induced mitochondrial fragmentation. To obtain a quantitative description of mitochondrial dynamics, HUVECs were transfected with pMito-Cherry, which codes for a mitochondria-directed fluorescent reporter protein. Cells were exposed to 1 mM H_2O_2 for 3 hr. The results show that the number of cells susceptible to H_2O_2-induced mitochondrial fragmentation was markedly reduced when TRPM2 channels were inhibited with siRNA or pharmacological agents (2-APB; TRPM2 blocker) (Figure 4.3A and E). For objective assessment of mitochondrial morphology, the aspect ratios (major axis/minor axis) and the form factors (a measure of degree of branching) of mitochondria were measured (Yu et al., 2008). The results show that H_2O_2 caused a significant reduction in both the aspect ratio and form factor of mitochondria and that TRPM2 inhibition significantly rescued these changes (Figure 4.3B-D).

These results provide compelling evidence that TRPM2 channels mediate oxidant-induced mitochondrial fragmentation. This is a fundamentally important finding because although mitochondrial dynamics has received enormous interest in recent years (Archer, 2013; Friedman and Nunnari, 2014; Youle and van der Bliek, 2012), the signalling mechanisms underlying mitochondrial fission are far from clear.

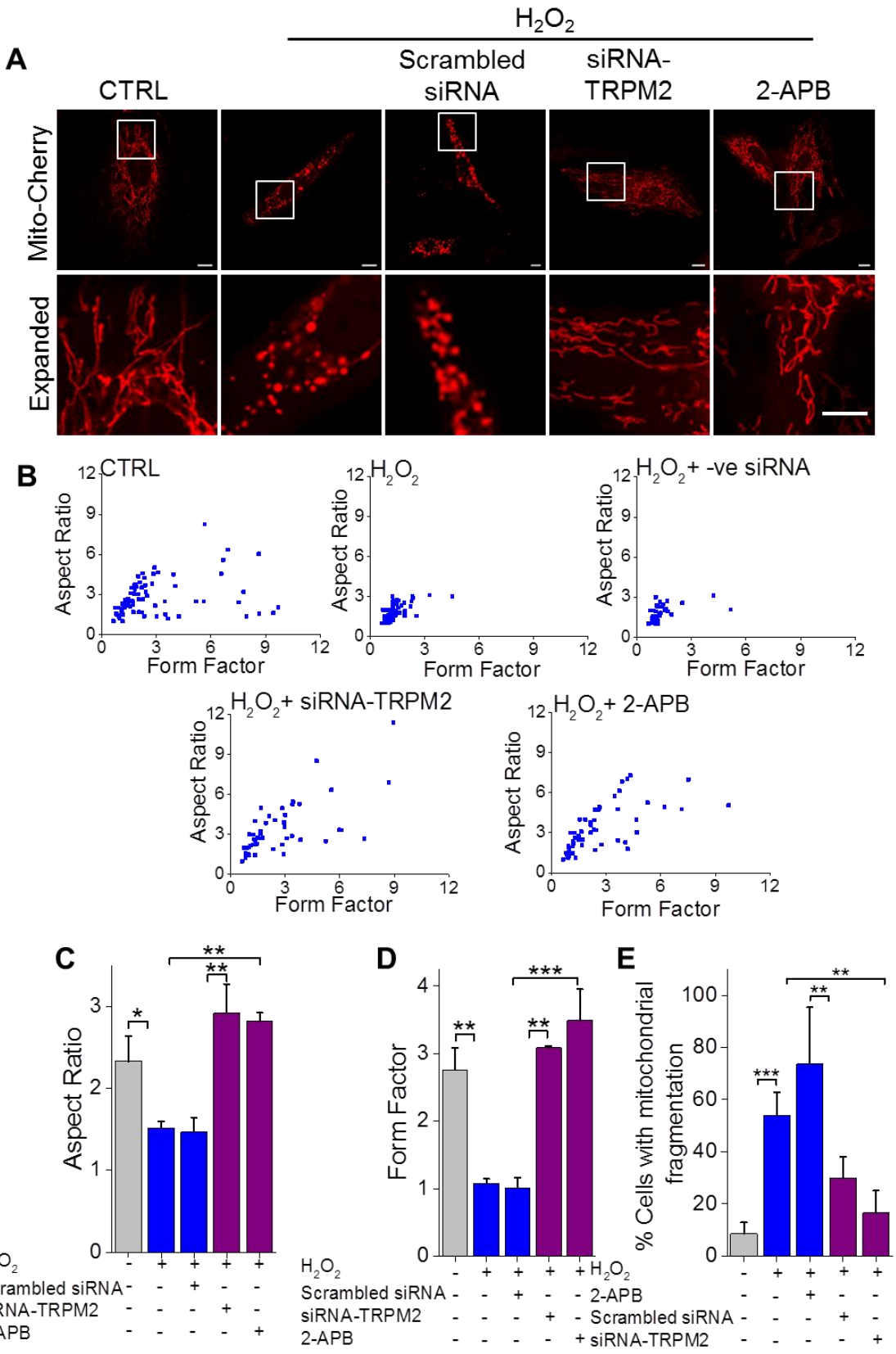
A
H_2O_2
CTRL
Scrambled siRNA
siRNA-TRPM2
2-APB
Mito-Cherry
Expanded
B
CTRL
H_2O_2
H_2O_2+ -ve siRNA
H_2O_2+ siRNA-TRPM2
H_2O_2+ 2-APB
Aspect Ratio
Form Factor
C
Aspect Ratio
D
Form Factor
E
% Cells with mitochondrial fragmentation
H_2O_2
Scrambled siRNA
siRNA-TRPM2
2-APB

Figure 4.3 Inhibition of TRPM2 channels prevents H_2O_2-induced mitochondrial fragmentation

(A) Inhibition of TRPM2 channels prevents H_2O_2-induced mitochondrial fragmentation. HUVECs were transfected with pMito-Cherry (a mitochondrial marker) and incubated with 1 mM H_2O_2 for 3 hr at 37°C in the presence and absence of a TRPM2 blocker (150 μM 2-APB). Alternatively, cells were co-transfected with pMito-Cherry and scrambled siRNA or siRNA targeted to TRPM2 channels. Representative confocal images are shown. Scale bar, 10 μm, n=3. Boxed regions are magnified in the lower panels. Scale bar, 5 μm.

(B) Plots of form factor against aspect ratio calculated from ≥ 70 mitochondria, n=3.

(C) Aspect ratio calculated from ≥ 70 mitochondria, n=3.

(D) Form factor calculated from ≥ 70 mitochondria, n=3.

(E) Percent cells displaying mitochondrial fragmentation determined from ≥ 100 cells, n=3.

Bars represent means ± SEM, statistical analysis was performed by one-way ANOVA with Tukey's post-hoc test *p <0.05, **P < 0.01, and ***P < 0.001.

4.2.4 Ectopic expression of TRPM2 channels confers mitochondrial fragmentation on HEK-293 cells

The above data showed that silencing of TRPM2 expression prevents oxidative stress-induced mitochondrial fragmentation. To confirm the role of TRPM2 channels, a recombinant approach was used. Previous studies have shown that HEK-293 cells do not express TRPM2 channels and can be engineered to express TRPM2 channels under the control of a tetracycline inducible promoter (Perraud et al., 2001). Thus these engineered cells, termed HEK-TRPM2^{tet} cells, express TRPM2 channels when induced with tetracycline. HEK-TRPM2^{tet} cells were incubated with 200 µM H_2O_2 and loaded with MitoTracker Red (mitochondrial marker) to examine mitochondrial morphology. Lower concentrations of H_2O_2 were used here because, unlike HUVECs, induced HEK-TRPM2^{tet} cells are highly susceptible to oxidant induced cell death (Manna et al., 2015). The results show no detectable effect of H_2O_2 on mitochondrial morphology of these cells (Figure 4.4A, labelled (-)TRPM2). However, when TRPM2 expression was induced by treating the cells with tetracycline, extensive fragmentation was seen (Figure 4.4B, labelled +TRPM2). To confirm that tetracycline treatment causes TRPM2 activation in HEK-TRPM2^{tet} cells, calcium imaging was carried out. Figure 4.4C-D shows that 1 mM H_2O_2 caused a significant rise in cytosolic Ca^{2+} in the cells induced to express TRPM2 channels but not in the cells not expressing TRPM2 channels. The results confirm that mitochondrial fragmentation is dependent on TRPM2 channel activation.

To conclude, H_2O_2 failed to induce mitochondrial fragmentation in HEK-293 cells lacking TRPM2 channels, but induction of TRPM2 expression led to significant mitochondrial fragmentation. These results confirm that H_2O_2-induced mitochondrial fragmentation is mediated by TRPM2 channels.

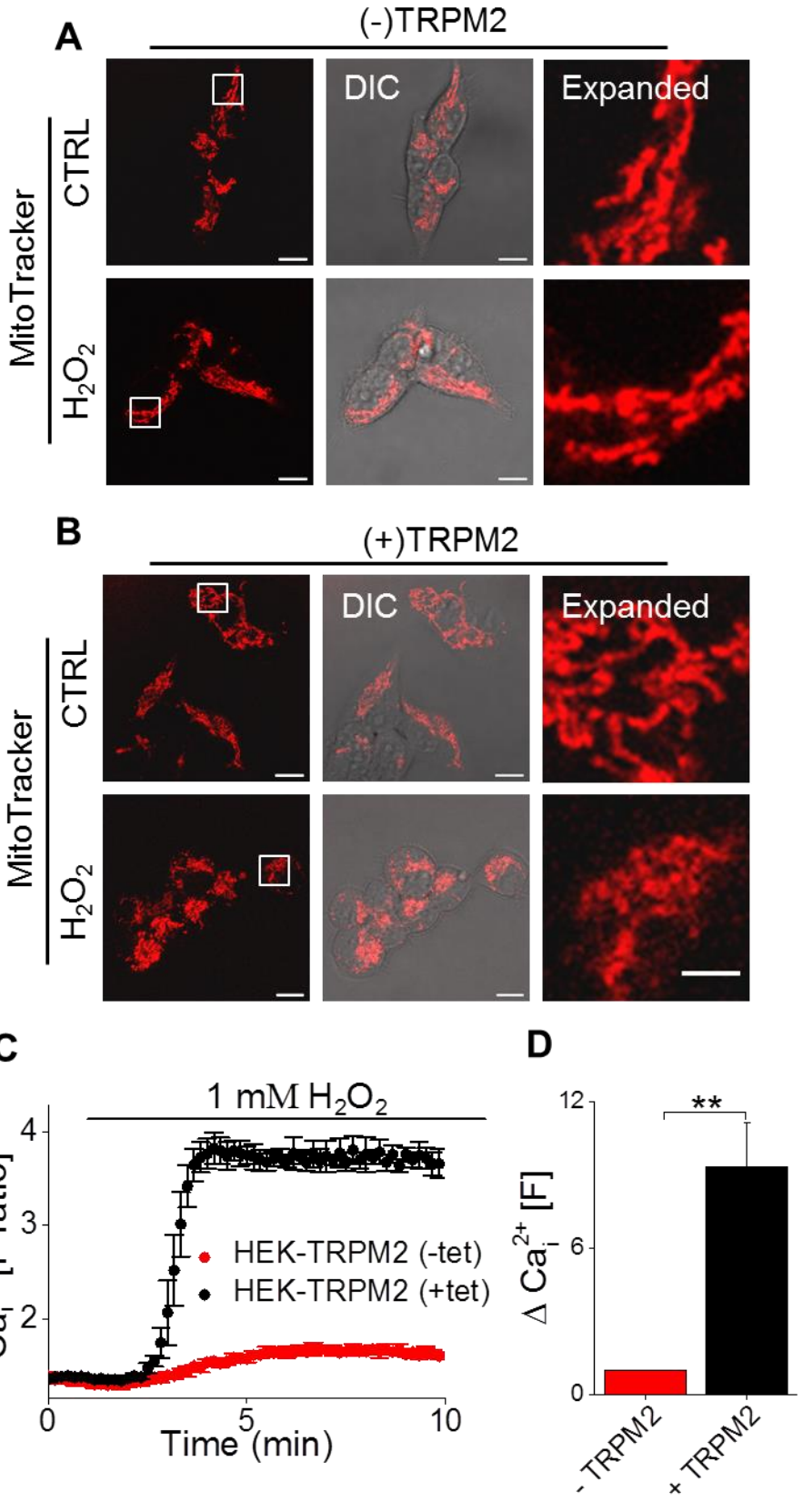
A
(-)TRPM2
DIC
Expanded
MitoTracker
CTRL
H_2O_2
B
(+)TRPM2
DIC
Expanded
MitoTracker
CTRL
H_2O_2
C
1 mM H_2O_2
Ca_i^{2+} [F ratio]
HEK-TRPM2 (-tet)
HEK-TRPM2 (+tet)
Time (min)
D
ΔCa_i^{2+} [F]
**
- TRPM2
+ TRPM2

Figure 4.4 Mitochondrial fragmentation is dependent on TRPM2 channel activation

(A-B) HEK-TRPM2^{tet} cells (cells engineered to express TRPM2 upon induction with tetracycline) were incubated with SBS alone (CTRL) or 200 µM H_2O_2 for 90 min and then loaded with MitoTracker Red for 30 min before imaging. Representative confocal images show that H_2O_2 induces no mitochondrial fragmentation in cells not expressing TRPM2 channels (-TRPM2; A), but extensive fragmentation in cells induced to express TRPM2 channels (+TRPM2; B), n=3. Scale bar, 10 µM. The middle panel shows the images merged with the corresponding DIC (differential interference contrast) images. Boxed sections are expanded in the far right panels; scale bar, 5 µm.

(C) TRPM2-dependent Ca^{2+} increased in HEK-TRPM2^{tet} cells. HEK-TRPM2^{tet} cells were induced (+tet) or not-induced (-tet) to express TRPM2 channels. Both groups of cells were loaded with Fura-2 AM for 1 hr at 37°C and washed for 30 min at room temperature. Fluorescence ratio (F340/F380) was recorded under control conditions and during the application of 1 mM H_2O_2 (shown as horizontal bar) in SBS containing 1.5 mM Ca^{2+}. Symbols represent mean fluorescence and the associated bars represent SEM.

(D) Mean ± SEM of change in Ca^{2+} calculated from the data in (C), n = 3. Statistical analysis was performed by Student's t-test, $^{**}P < 0.01$.

4.2.5 TRPM2 channels mediate oxidative stress-induced mitochondrial fragmentation

4.2.5.1 High glucose induces formation of ROS in HUVECs

In diabetes, endothelial cells experience oxidative stress due to increased blood glucose levels (Ouedraogo et al., 2006). Studies have shown that exposure of endothelial cells to high glucose (HG) triggers mitochondrial fragmentation and that these effects are mediated by the increased ROS production (Shenouda et al., 2011; Yu et al., 2008). To confirm the role of TRPM2 channels in mitochondrial fragmentation under pathophysiological conditions, cells were incubated in normal and high glucose medium. Fasting plasma glucose levels in healthy individuals is <6.1 mM, while diabetic patients have plasma glucose levels >7.0 mM (Tirosh et al., 2005; American Diabetes, 2004). In neonatal diabetes, glucose levels can exceed 30 mM concentration (Vaxillaire et al., 2004). Studies have shown cellular uptake of glucose is saturated at 30-35 mM glucose concentration (Heilig et al., 1995). Accordingly, in this study, 5.5 mM (control) and 33 mM glucose (representing diabetic levels) were used. Similar doses were used in previous studies (Ho et al., 2005; Lin et al., 2004). ROS production was determined by using the cell-permeant H_2DCFDA. DCF levels were measured in HUVECs exposed to 5.5 mM glucose and 33 mM glucose for 48 hr and 72 hr. Mannitol was used as osmotic control. The data in Figure 4.5 show that there was a significant increase in the mean of DCF florescence/cell after 48 hr compared with the corresponding control. There was a small, but insignificant increase in ROS when the incubation period was extended to 72 hr.

These data confirm that prolonged exposure to high glucose induces ROS production in HUVECs.

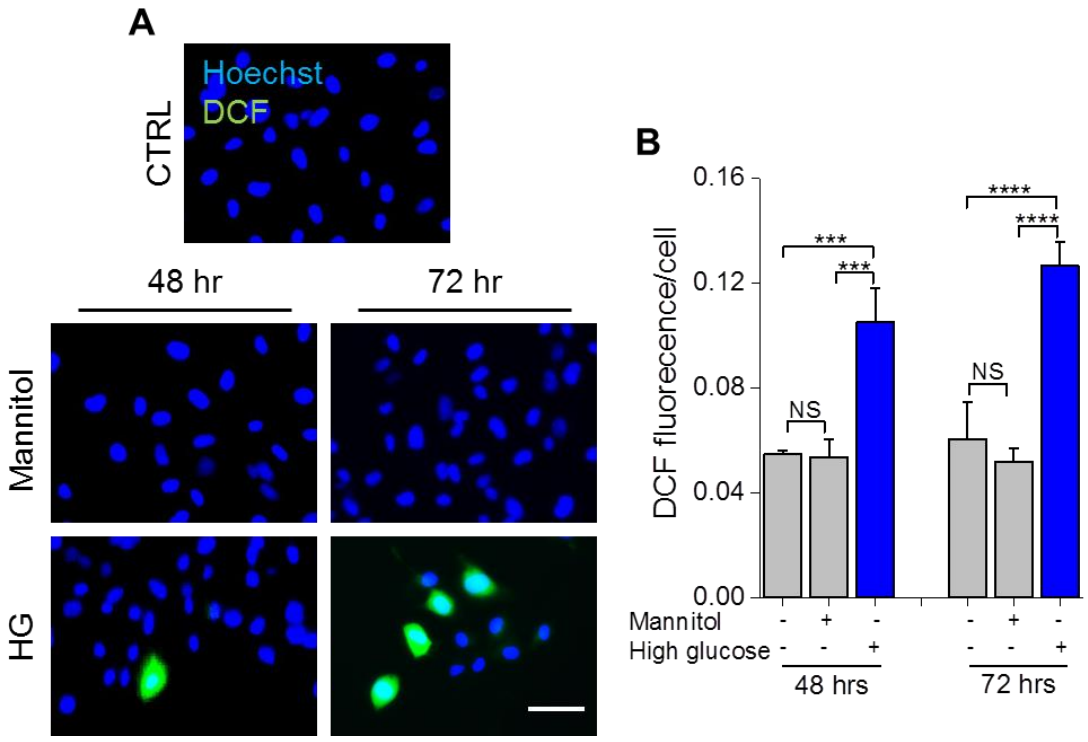

Figure 4.5 Glucose induces intracellular ROS generation

(A) HG-induced ROS production. HUVECs were exposed to medium alone (CTRL) or medium with 28 mM mannitol plus 5 mM glucose, or medium with 33 mM glucose (HG). Incubation was for 48 hr or 72 hr at 37°C. Cells were stained with the cell-permeant 2',7'-dichlorodihydrofluorescein diacetate (H_2DCFDA) ROS reporter to detect mean DCF fluorescence per cell. Images were captured with an epifluorescent microscope (EVOS) and analysed by ImageJ software.

(B) Mean ± SEM of fluorescence intensity/cell corresponding to data in (A), n = 3. Number of cells scored for each condition is ≥ 100 cells.

Statistical analysis was performed by one-way ANOVA with Tukey's post-hoc test, **p* <0.05, ***P* < 0.01 and ****P* < 0.001.

4.2.5.2 Hyperglycaemic conditions cause effects similar to H_2O_2 on endothelial cells

To investigate whether TRPM2 channels mediate stress-induced endothelial mitochondrial fragmentation, pMito-Cherry was expressed in HUVECs. Effect of high glucose (HG) on mitochondrial morphology was assessed by measuring the aspect ratio (AR: length to width ratio) and form factor (FF: a measure of degree branching) of the mitochondria (Yu et al., 2008).

Control cells showed an extensive mitochondrial network with long, branched tubular networks. High glucose (HG, 33 mM), but not mannitol (control for osmotic pressure effects), caused extensive mitochondrial fragmentation (Figure 4.6A and E). Changes in the length and branching of the mitochondrial network were quantified by determining the AR and FF. HG caused significant reduction in both the AR and the FF (Figure 4.6B, C and D). Inhibition of TRPM2 channels with 2-aminoethoxydiphenyl borate (2-APB) or suppression of TRPM2 expression using siRNA inhibited mitochondrial fragmentation significantly (Figure 4.6A and E).

Taken together, these data revealed a previously unrecognised role for TRPM2 channels in oxidative stress-induced mitochondrial fragmentation.

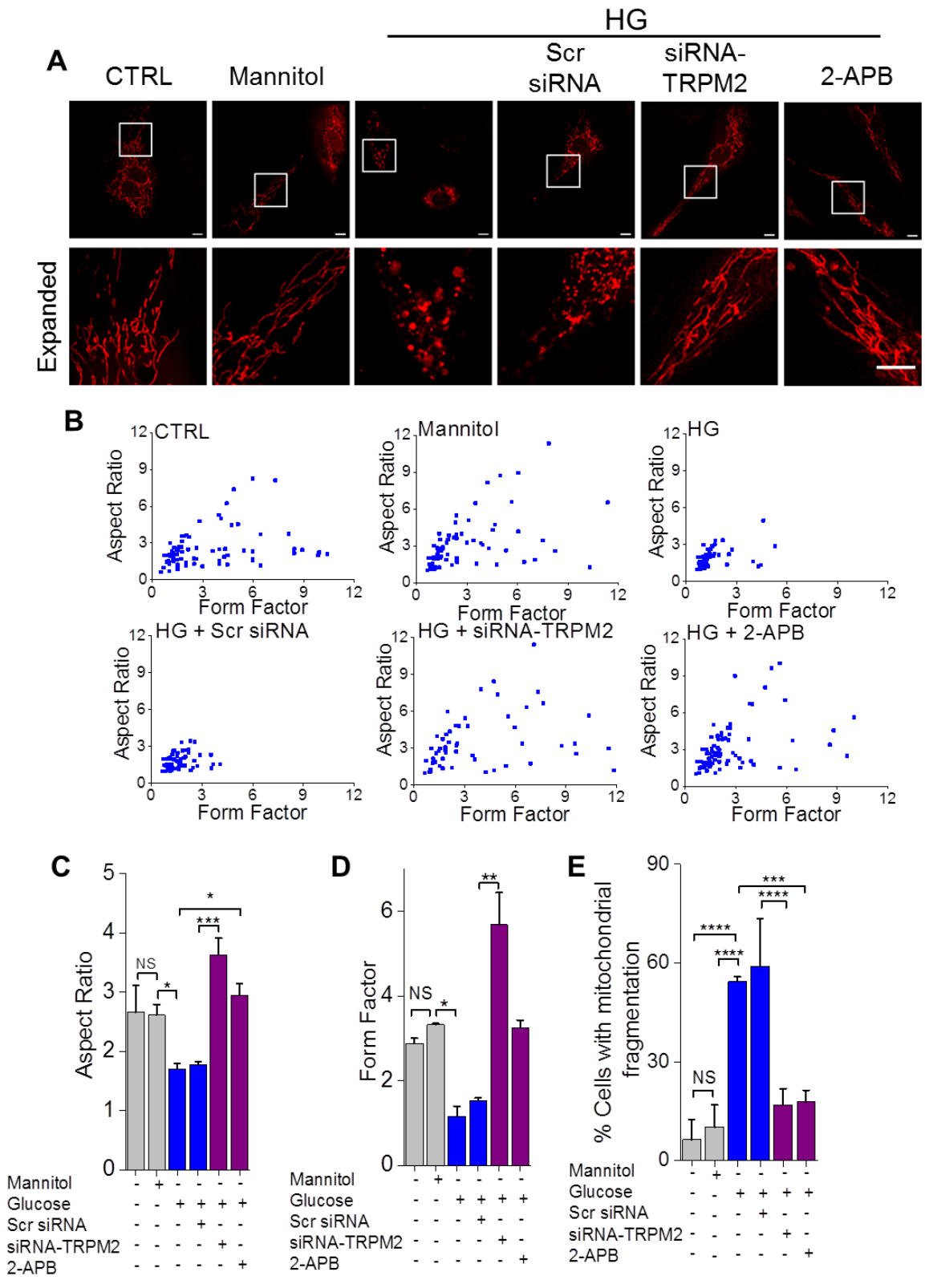
A
HG
CTRL
Mannitol
Scr siRNA
siRNA-TRPM2
2-APB
Expanded
B
CTRL
Mannitol
HG
HG + Scr siRNA
HG + siRNA-TRPM2
HG + 2-APB
Aspect Ratio
Form Factor
C
Aspect Ratio
NS
*
***
Mannitol
Glucose
Scr siRNA
siRNA-TRPM2
2-APB
D
Form Factor
NS
*
**
E
% Cells with mitochondrial fragmentation
NS
****
***

Figure 4.6 Inhibition of TRPM2 channels prevents high glucose-induced mitochondrial fragmentation

(A) HUVECs were transfected with pMito-Cherry and incubated with 5 mM glucose (CTRL), or mannitol (28 mM + 5 mM glucose) or HG (33 mM, indicated with a horizontal bar) for 24 hr. Where indicated, cells were co-transfected with siRNA or treated with 37.5 µM 2-APB. Representative confocal images are shown; scale bar, 10 µm; n=3. Boxed regions are magnified in the lower panels. Scale bar, 5 µm.

(B) Plots of form factor against aspect ratio calculated from ≥ 70 mitochondria, n=3.

(C) Aspect ratio calculated from ≥ 70 mitochondria, n=3.

(D) Form factor calculated from ≥ 70 mitochondria, n=3.

(E) Percent cells displaying mitochondrial fragmentation determined from ≥ 130 cells, n=3.

Bars are the means ± SEM, statistical analysis was performed by one-way ANOVA with Tukey's post-hoc test, **p* <0.05, ***P* < 0.01, ****P* < 0.001, and *****P* < 0.0001.

4.2.6 Knock-out of TRPM2 channels prevents high glucose-induced mitochondrial fragmentation in mouse pulmonary endothelial cells

The effect of HG on the mitochondria of primary endothelial cells isolated from the lungs of wild-type and TRPM2 knock-out (TRPM2 KO) mice was next examined. This was done to confirm the findings obtained from the cell lines. The identity of isolated endothelial cells was confirmed by immunostaining for the endothelial marker, CD-31/PECAM-1 (green) (Li et al., 2014), and examining mitochondrial morphology by staining with MitoTracker Red (Figure 4.7). Similar to HUVECs, HG caused extensive mitochondrial fragmentation in primary endothelial cells (Figure 4.7A, B, C). By contrast, endothelial cells isolated from TRPM2 KO mice were remarkably resistant to HG-induced mitochondrial fragmentation (Figure 4.7D, E, F). Interestingly, the form factor of mitochondria of TRPM2-deficient endothelial cells was significantly greater (~1.3-fold; $p < 0.05$) than that for mitochondria in wild-type endothelial cells; furthermore, this value changed little even after the HG challenge (Figure 4.7G).

Finally, the effect of high glucose on the endothelial cells of intact aorta was examined. For this, aortas were dissected from mice, cut open longitudinally, exposed to high glucose and stained with MitoTracker Red. Confocal imaging of the endothelial layer of the sections (Figure 4.8A and B) showed extensive mitochondrial fragmentation in the endothelial cells of aortas derived from wild-type mice, and no detectable fragmentation in aortas of TRPM2 KO mice. These data demonstrate that endothelial cells in intact aortas respond to high glucose in the same way as the isolated cells and that TRPM2 channels mediate high glucose-induced mitochondrial fragmentation.

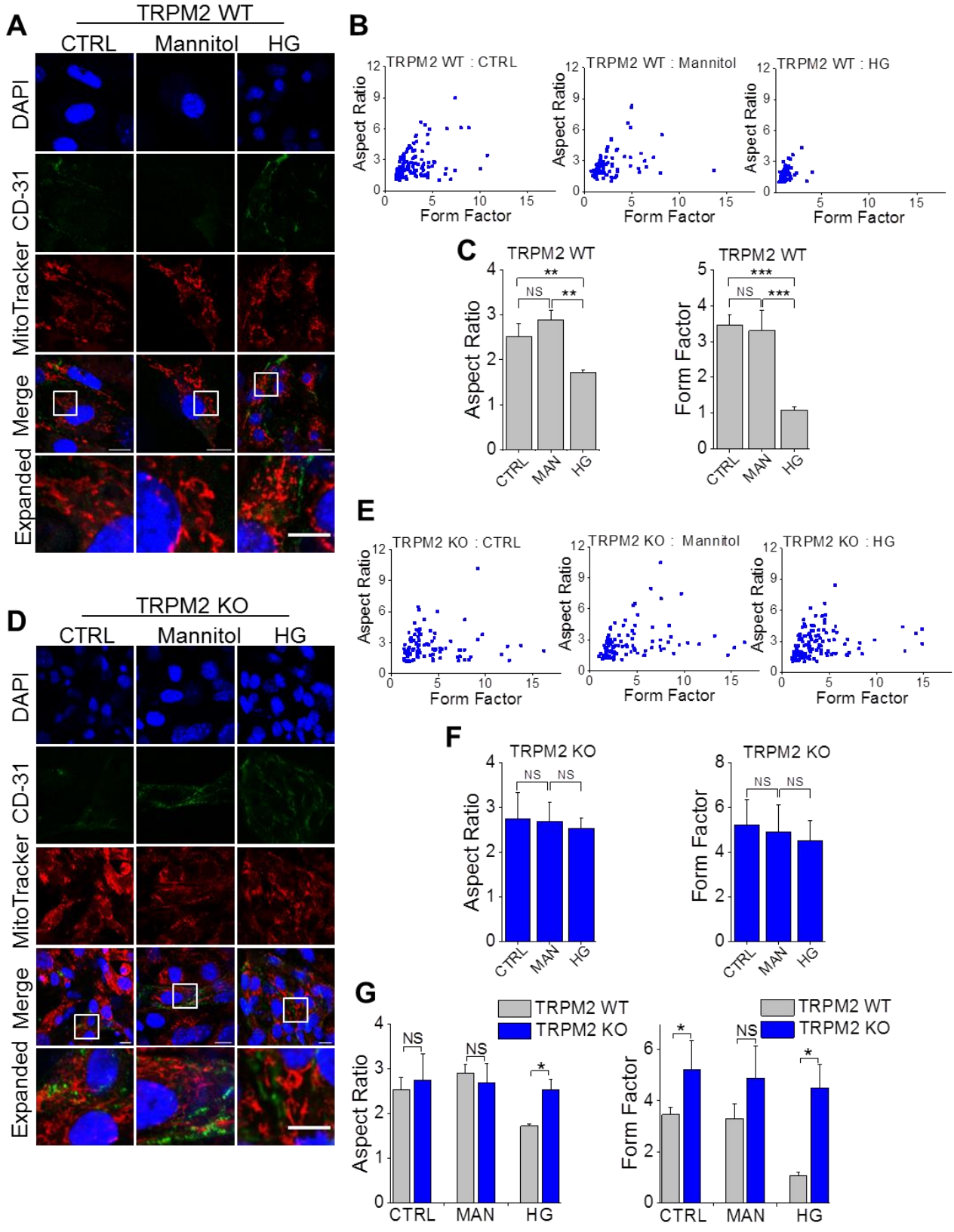
A
TRPM2 WT
CTRL
Mannitol
HG
DAPI
CD-31
MitoTracker
Merge
Expanded
B
TRPM2 WT : CTRL
TRPM2 WT : Mannitol
TRPM2 WT : HG
Aspect Ratio
Form Factor
C
TRPM2 WT
Aspect Ratio
Form Factor
NS
**
***
CTRL
MAN
HG
D
TRPM2 KO
E
TRPM2 KO : CTRL
TRPM2 KO : Mannitol
TRPM2 KO : HG
F
TRPM2 KO
G
TRPM2 WT
TRPM2 KO
*

Figure 4.7 Knock-out of TRPM2 channels prevents high glucose-induced mitochondrial fragmentation in mouse pulmonary endothelial cells

(A) Primary endothelial cells isolated from lungs of wild-type mice were treated with mannitol and HG as described in Figure 4.6 and incubated for 3 days. The cells were then stained for mitochondria with MitoTracker Red and, after fixing with 2% PFA, immunostained with anti-CD31 antibodies (green) to identify endothelial cells; nuclei were stained with DAPI (blue). Representative images are shown (8 mice: cells from 2-3 mice were pooled for each experiment; n =3). Scale bar, 10 µM. Boxed regions in the merged images are magnified in the bottom panels. Scale bar, 5 µm.

(B) Plots of form factor against aspect ratio calculated from ≥ 70 mitochondria, n=3.

(C) Aspect ratio calculated from ≥ 70 mitochondria, n=3.

(D) Primary endothelial cells isolated from lungs of TRPM2-KO mice were treated and stained as in (A) (7 mice: cells from 2-3 mice were pooled for each experiment; n =3). Scale bar, 10 µM. Boxed regions in the merged images are magnified in the bottom panels. Scale bar, 5 µm.

(E) Plots of form factor against aspect ratio calculated from ≥ 70 mitochondria, n=3.

(C) Aspect ratio calculated from ≥ 70 mitochondria, n=3.

(G) Comparison of mitochondrial aspect ratio and form factor between the wild-type and TRPM2-deficient pulmonary endothelial cells during various treatments.

Bars are the means ± SEM, statistical analysis was performed by one-way ANOVA with Tukey's post-hoc test, **p* <0.05, ***P* < 0.01 and ****P* < 0.001.

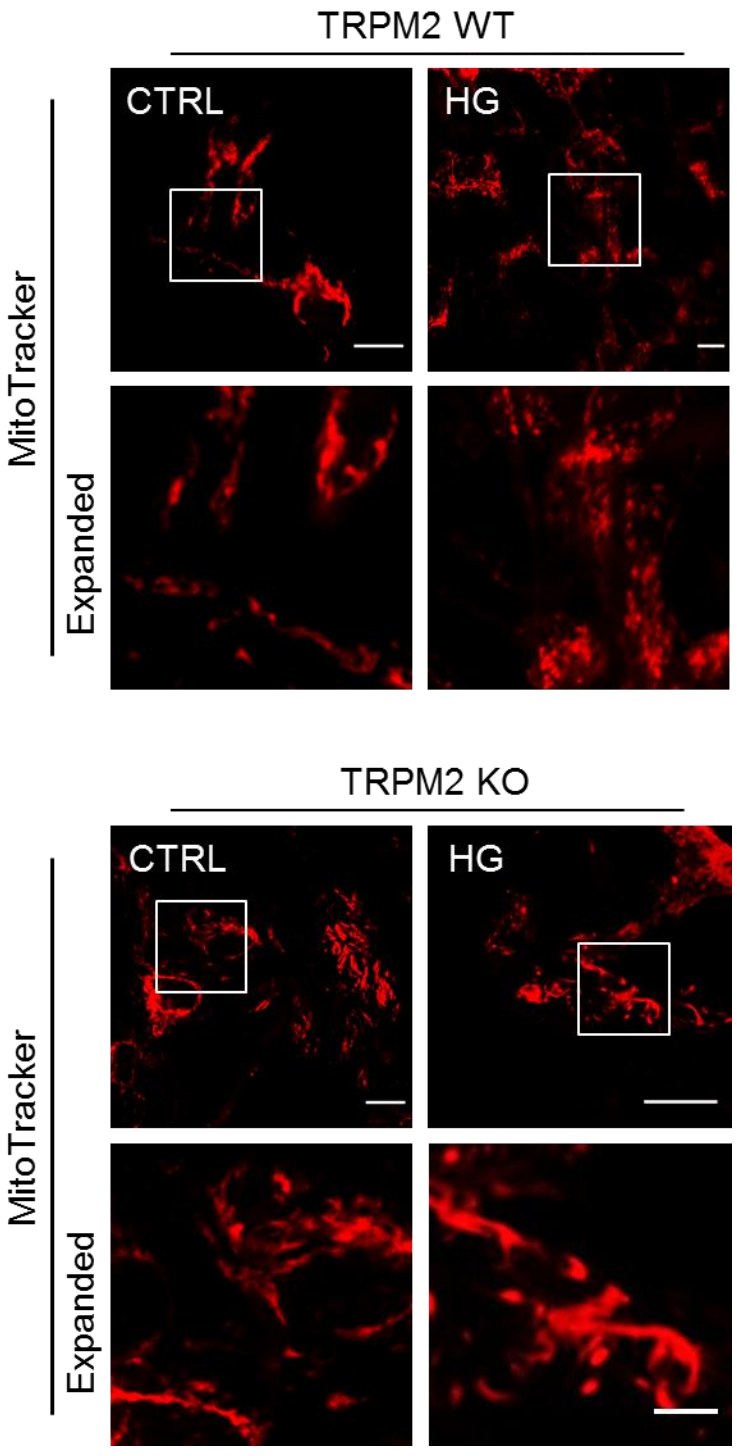
TRPM2 WT
CTRL
HG
MitoTracker
Expanded
TRPM2 KO
CTRL
HG
MitoTracker
Expanded

Figure 4.8 Knock-out of TRPM2 channels prevents high glucose-induced mitochondrial fragmentation in endothelial cells of intact aortas

Slices of aortas isolated from wild-type (TRPM2 WT) and TRPM2 knock-out (TRPM2 KO) mice were stained *in situ* for mitochondria with MitoTracker Red and fixed with 4% PFA. For high glucose, aortas were maintained in 33 mM glucose (HG) containing EGM-2 medium at 37°C for 3 days. Images of the luminal aspect of the sections were taken. Scale bar, 10 µM. Boxed regions are magnified in the lower panels. Scale bar, 5 µm.

4.2.7 TRPM2 channels regulate mitochondrial fragmentation through Zn^{2+} ions

As mentioned in the introduction, activation of TRPM2 channels raises the cytosolic levels of both Ca^{2+} and Zn^{2+} (Manna et al., 2015; Sumoza-Toledo and Penner, 2011; Takahashi et al., 2011). Previous studies have described a role for Ca^{2+} in mitochondrial fragmentation, but little is known about the role, if any, of Zn^{2+} in mitochondrial fragmentation. To examine the role of Zn^{2+}, HUVECs were transfected with pMito-Cherry and the effect of Zn^{2+} chelators was tested. The data in Figure 4.9 indicate that specific chelation of Zn^{2+} alone with a low (0.3 µM) concentration of TPEN (N,N,N',N'-tetrakis (2-pyridinylmethyl)-1,2-ethanediamine) (Manna et al., 2015; Sensi et al., 2009) was sufficient to abolish the ability of HG to induce mitochondrial fragmentation. Higher concentrations of TPEN were found to be toxic (Ho et al., 2008). The role of TRPM2-mediated Zn^{2+} rise on the mitochondria of mouse lung primary endothelial cells was next examined. Similar to HUVECs, HG caused extensive mitochondrial fragmentation in the primary endothelial cells; TRPM2 inhibition with 2-APB or siRNA as well as Zn^{2+} chelation prevented HG-induced mitochondrial fragmentation (Figure 4.10). These data indicate that HG induces endothelial mitochondrial fragmentation by affecting TRPM2-mediated changes in Zn^{2+} homeostasis.

For further confirmation of TRPM2-mediated mitochondrial fragmentation through Zn^{2+} ions, HUVECs were exposed to H_2O_2 in the presence and absence of Zn^{2+} chelators (0.3 µM TPEN or 2 µM clioquinol). The results (Figure 4.11) show that the effect of H_2O_2 on endothelial cells is similar to that of high glucose.

To conclude, Zn^{2+} represents the molecular link between TRPM2 activation and endothelial mitochondrial fragmentation.

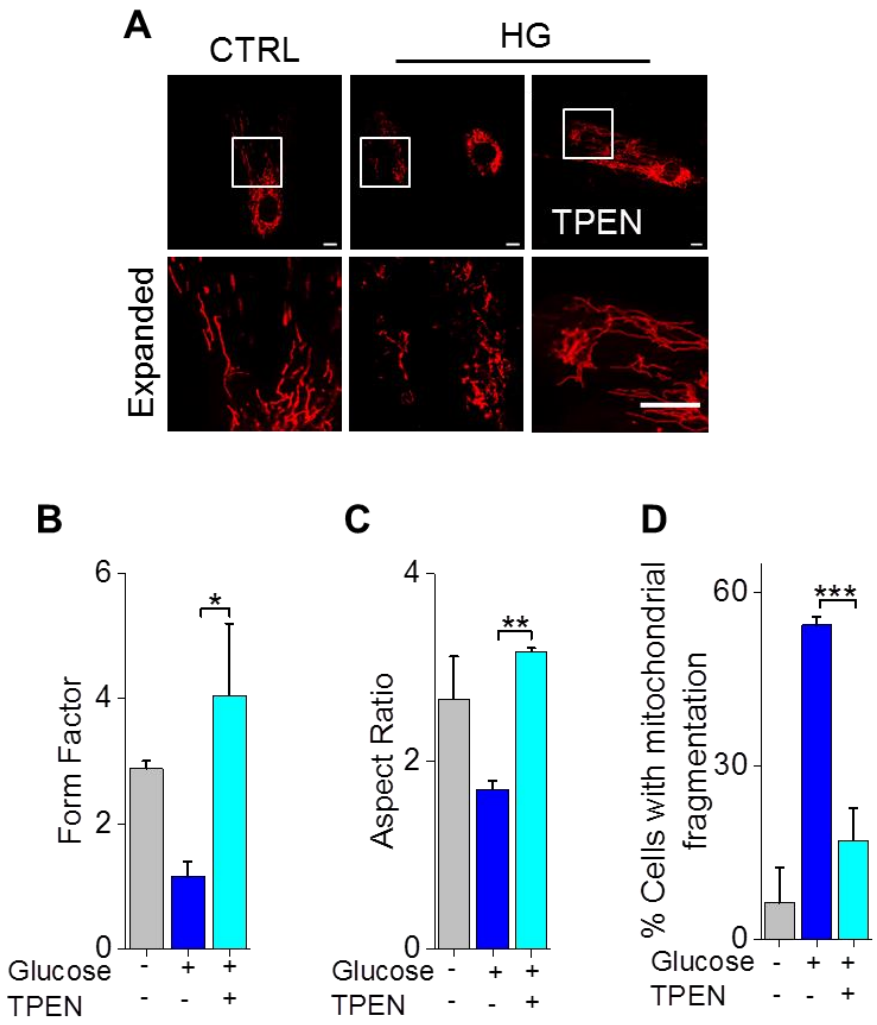

Figure 4.9 Zn^{2+} mediates mitochondrial fragmentation in HUVECs

(A) Zn^{2+} chelation by TPEN prevents HG-induced mitochondrial fragmentation in HUVECs. Cells were transfected with pMito-Cherry and incubated with 5 mM glucose (CTRL) or HG (33 mM) with and without of 0.3 µM TPEN. Representative confocal images are shown; scale bar, 10 µm. Boxed regions are magnified in the lower panels. Scale bar, 5 µm.

(B-C) Form factor (B), aspect ratio (C) calculated from ≥ 70 mitochondria, n =3.

(D) Percentage of cells showing mitochondrial fragmentation, n/N = 3/130 cells.

Bars are the means ± SEM, statistical analysis was performed by one-way ANOVA with Tukey's post-hoc test (B-D); *p <0.05, **P < 0.01 and ***P < 0.001.

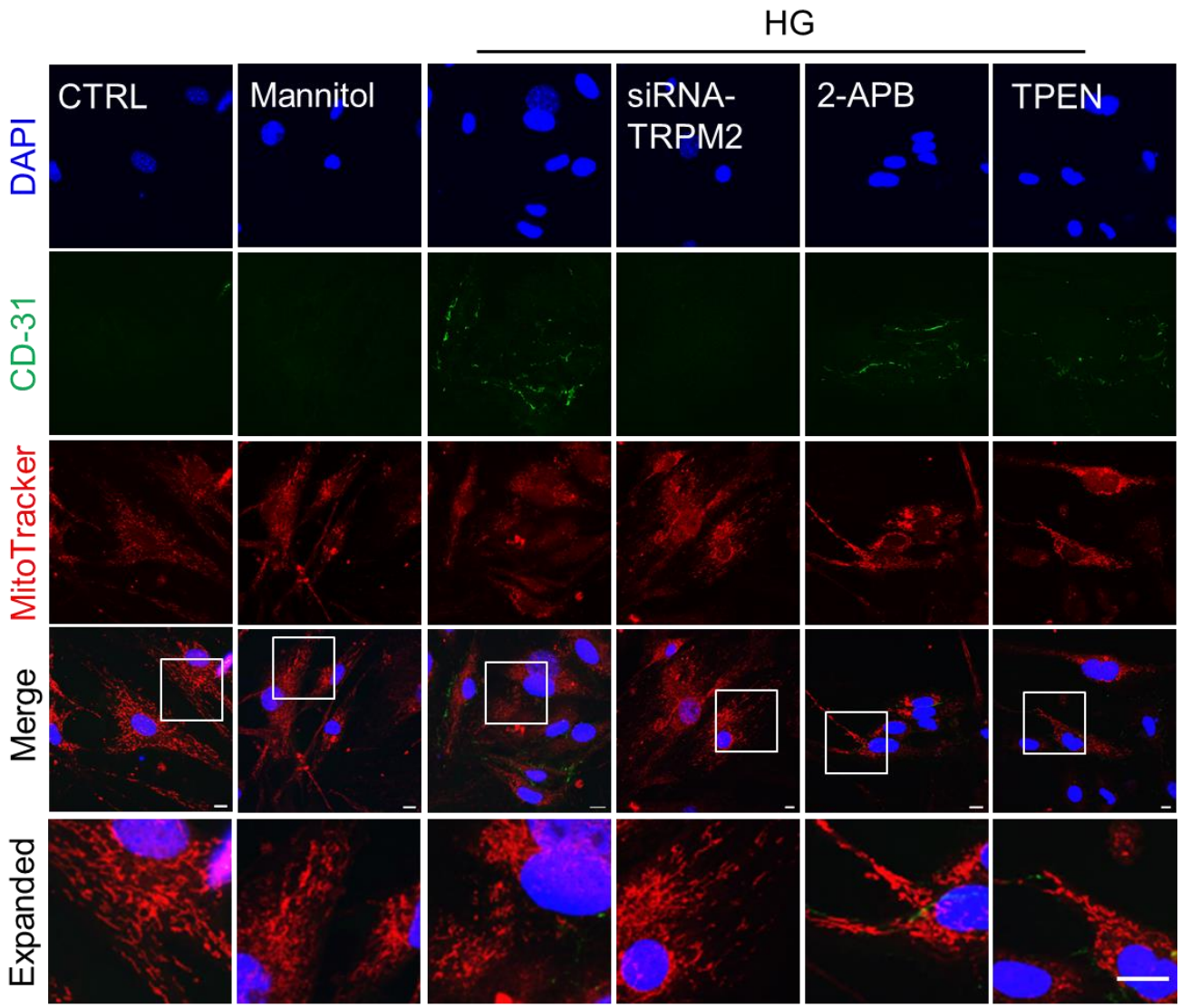

Figure 4.10 Zn^{2+} chelation prevents high glucose-induced mitochondrial fragmentation in primary endothelial cells isolated from lungs of wild-type mice

Primary endothelial cells isolated from lungs of wild-type mice were treated with mannitol and HG as described in Figure 4.6 and incubated for 3 days in the presence and absence of a TRPM2 blocker (37.5 µM 2-APB) or a Zn^{2+} chelator (0.3 µM TPEN) or the cells pre-transfected with siRNA-TRPM2. Cells were then stained and fixed as described in Figure 4.7. Scale bar, 10 µM; representative images are shown, the experiment was performed two times. Boxed regions in the merged images are magnified in the bottom panels. Scale bar, 5 µm.

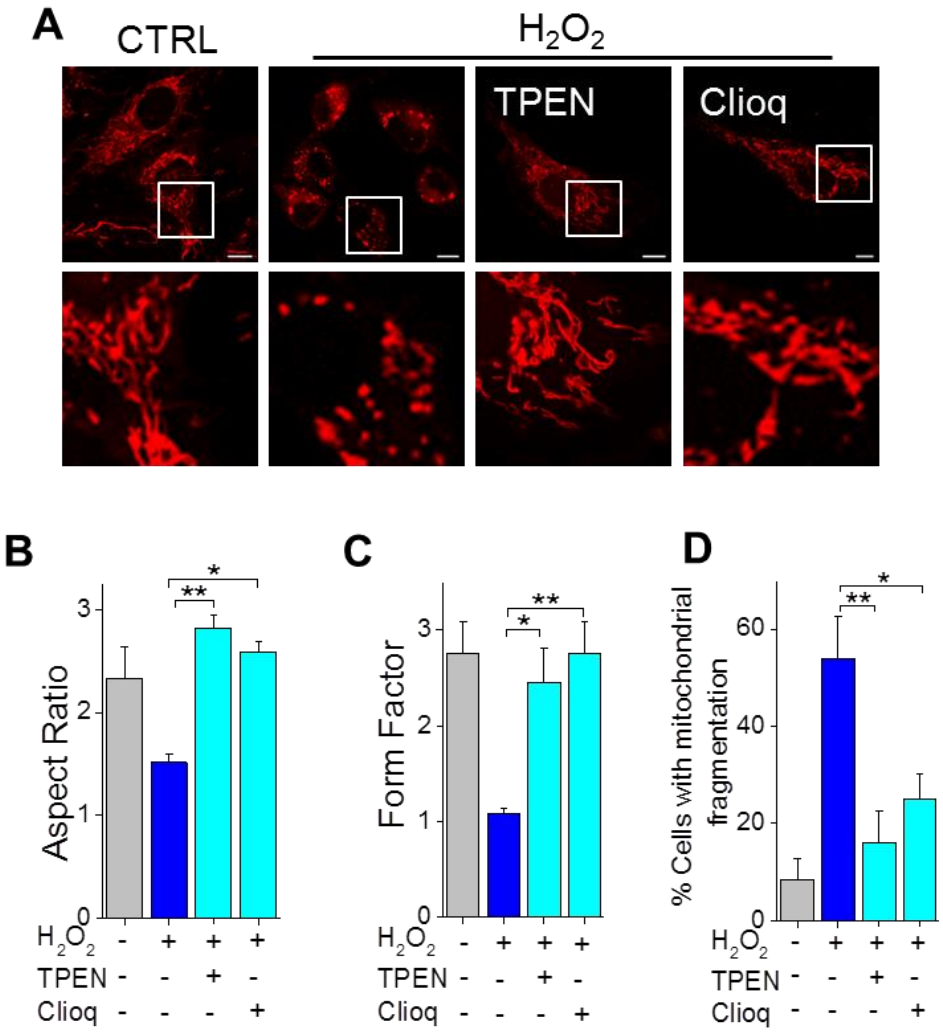

Figure 4.11 Zn^{2+} chelation prevents H_2O_2-induced mitochondrial fragmentation

(A) HUVECs were transfected with pMito-Cherry (mitochondrial marker) and incubated with 1 mM H_2O_2 for 3 hr at 37°C in the presence and absence of zinc chelators (0.3 µM TPEN or 2 µM clioquinol). Representative confocal images are shown. Scale bar, 10 µm. Boxed regions are magnified in the lower panels. Scale bar, 5 µm.

(B-C) Form factor (B), aspect ratio (C) calculated from ≥ 70 mitochondria, n =3.

(D) Percentage of cells showing mitochondrial fragmentation, n/N = 3/100 cells.

Bars are the means ± SEM, statistical analysis was performed by one-way ANOVA with Tukey's post-hoc test *p <0.05 and **P < 0.01.

4.2.8 Zn^{2+}-induced mitochondrial fragmentation is independent of extracellular Zn^{2+} entry

The data presented above confirm that TRPM2-induced mitochondrial fragmentation is mainly mediated by Zn^{2+} as chelation of Zn^{2+} was able to prevent mitochondrial fragmentation. The source of this Zn^{2+} could be extracellular or intracellular. Previous studies have reported that activation of plasma membrane TRPM2 channels can induce Zn^{2+} entry (Yu et al., 2012). Therefore, the effect of depletion of extracellular Zn^{2+} with diethylenetriamine pentaacetate (DTPA, a membrane impermeable Zn^{2+} chelator) (Manna et al., 2015) on mitochondrial fragmentation was examined. Cells were exposed to H_2O_2 in the presence and absence of DTPA for 3 hr. The data in Figure 4.12 show that DTPA was unable to prevent mitochondrial fragmentation.

Thus extracellular Zn^{2+} does not contribute to oxidative stress-induced changes in mitochondrial morphology.

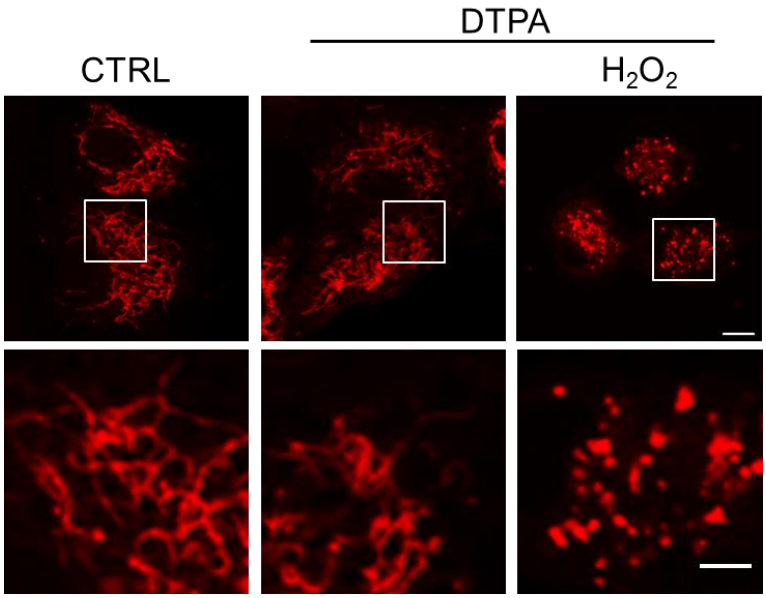

Figure 4.12 H_2O_2-induced rise in mitochondrial Zn^{2+} is not dependent on extracellular Zn^{2+} entry

HUVECs were exposed for 3 hr at 37°C to medium alone (CTRL) or to medium containing 1 mM DTPA with and without 1 mM H_2O_2. Cells were then stained for mitochondria (MitoTracker Red). Images show that H_2O_2 causes an increase in mitochondrial fragmentation. Mitochondrial fragmentation was unaffected by DTPA, indicating that extracellular Zn^{2+} entry does not cause mitochondrial fragmentation. Scale bar, 10 µm. n=2. Boxed regions in the images are magnified in the far bottom panels. Scale bar, 5 µm.

4.2.9 TRPM2 activation induces lysosomal membrane permeabilisation and redistribution of lysosomal Zn^{2+} to mitochondria

4.2.9.1 Lysosomes are the major source of free form of Zn^{2+}

The lack of effect of DTPA on H_2O_2-induced mitochondrial fragmentation suggests that the source of Zn^{2+} is intracellular. Within the cell, the majority of Zn^{2+} is normally protein bound (Wiseman et al., 2007). However, in some cells, including neuronal cells (Lee et al., 2009) and the INS-1 pancreatic β-cell line (Manna et al., 2015), free Zn^{2+} exists in lysosomes. To examine the intracellular distribution of free Zn^{2+}, HUVECs were co-stained for free Zn^{2+} and organelles. FluoZin3-AM (green), a Zn^{2+} specific dye was used to stain Zn^{2+}; intracellular compartments were stained with organelle-specific dyes (red): LysoTracker Red for lysosomes, MitoTracker Red for mitochondria, and ER-Tracker for the ER. The resulting co-localisation data (Figure 4.13) show that under normal conditions, free Zn^{2+} is mainly concentrated in lysosomes compared with the other compartments including the cytoplasm.

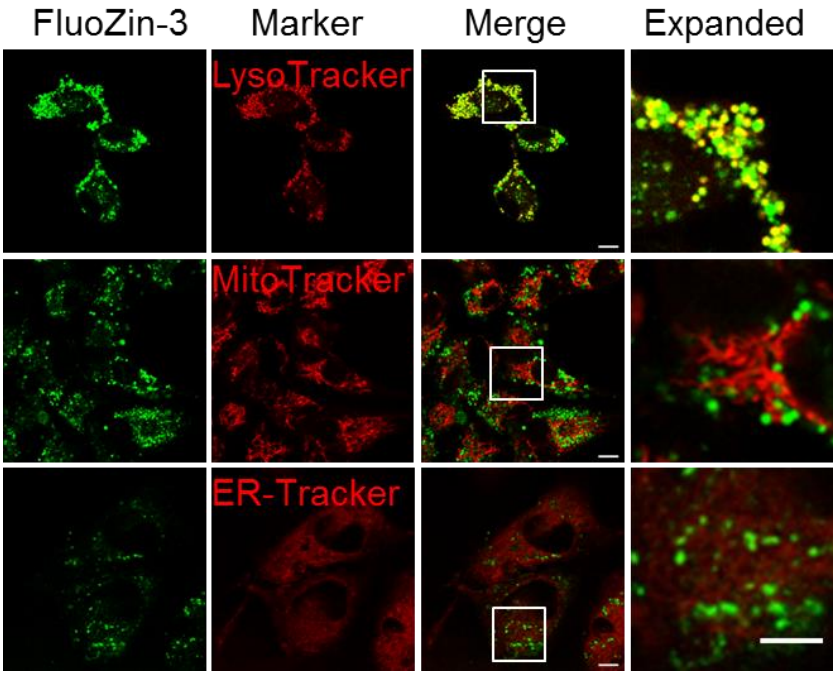

Figure 4.13 Lysosomes are the major site of Zn^{2+} storage

Fluorescence images of HUVECs co-stained for Zn^{2+} (FluoZin-3; green) and intracellular organelles (red): lysosomes (LysoTracker), mitochondria (MitoTracker) and the ER (ER Tracker). Merged images show marked localisation of Zn^{2+} to lysosomes (yellow), but not to mitochondria or the ER. Scale bar, 10 µm. Boxed regions in the merged images are magnified in the far right panels. Scale bar, 5 µm.

4.2.9.2 Oxidative stress-induced LMP depends on TRPM2 activation

To examine the role of intracellular organelles in Zn^{2+} release, HUVECs were loaded with FluoZin-3-AM and LysoTracker Red or MitoTracker Red. When HUVECs were exposed to HG (33 mM) or H_2O_2 (1 mM), there was a marked decline in the lysosome-associated Zn^{2+} (Figure 4.14A and Figure 4.15A and D). Remarkably, this decline in lysosomal Zn^{2+} was inhibited by siRNA targeted to TRPM2 channels, but not by scrambled siRNA (Figure 4.14A and Figure 4.15A). Pharmacological inhibitors (TRPM2 blockers; 2-APB and PJ-34) showed results similar to those of siRNA-TRPM2 (Figure 4.15A). The reduction in lysosomal Zn^{2+} staining was accompanied by a simultaneous decrease in LysoTracker staining (Figure 4.14B and Figure 4.15B). This suggests potential loss of membrane integrity (i.e., increased lysosomal membrane permeabilisation LMP) during oxidative stress. Although previous studies have shown increased LMP during oxidative stress (Boya et al., 2003; Boya and Kroemer, 2008; Repnik et al., 2014), little is known about the underlying mechanisms. The current notion seems to be that oxidative stress causes LMP through direct chemical damage of lysosomal membranes (Repnik et al., 2014). Contrary to this notion, evidence presented in this chapter suggests that LMP is a regulated process, as lysosomal Zn^{2+} loss is attenuated by TRPM2 inhibition.

To confirm the unexpected role of TRPM2 in LMP, HEK-293-$TRPM2^{tet}$ cells were used. In the absence of induction of TRPM2 (Figure 4.16A and B, labelled -TRPM2), these cells were resistant to oxidant-induced LMP. However, when induced with tetracycline (+TRPM2), H_2O_2 caused a marked increase in LMP.

To conclude, these data demonstrate that oxidative stress-induced LMP is dependent on TRPM2 activation.

4.2.9.3 Redistribution of lysosomal Zn^{2+} to mitochondria

Figure 4.13 shows that there is little overlap between the FluoZin-3 stain and MitoTracker stain. This suggests that under normal conditions, mitochondria do not store appreciable amounts of free Zn^{2+}. However, exposure of HUVECs to HG (33 mM) or H_2O_2 (1 mM) stress leads to a significant rise in mitochondrial Zn^{2+} as well as an increase in mitochondrial fragmentation (Figure 4.14C and Figure 4.15C). Inhibition of TRPM2 channels attenuated both HG- and H_2O_2-induced rise in mitochondrial Zn^{2+} (Figure 4.14C-D and Figure 4.15C-D). Precisely how HG and H_2O_2 promote the rise in mitochondrial Zn^{2+} is not known, but one possibility is that Zn^{2+} released during LMP is promptly taken up by the mitochondria.

Taken together, these data reveal two novel findings: Firstly, LMP is not simply due to nonspecific oxidative attack on lysosomal membranes, but is regulated by TRPM2 channels. Secondly, Zn^{2+} released during LMP is mobilised to mitochondria which, in turn, appears to trigger mitochondrial fragmentation.

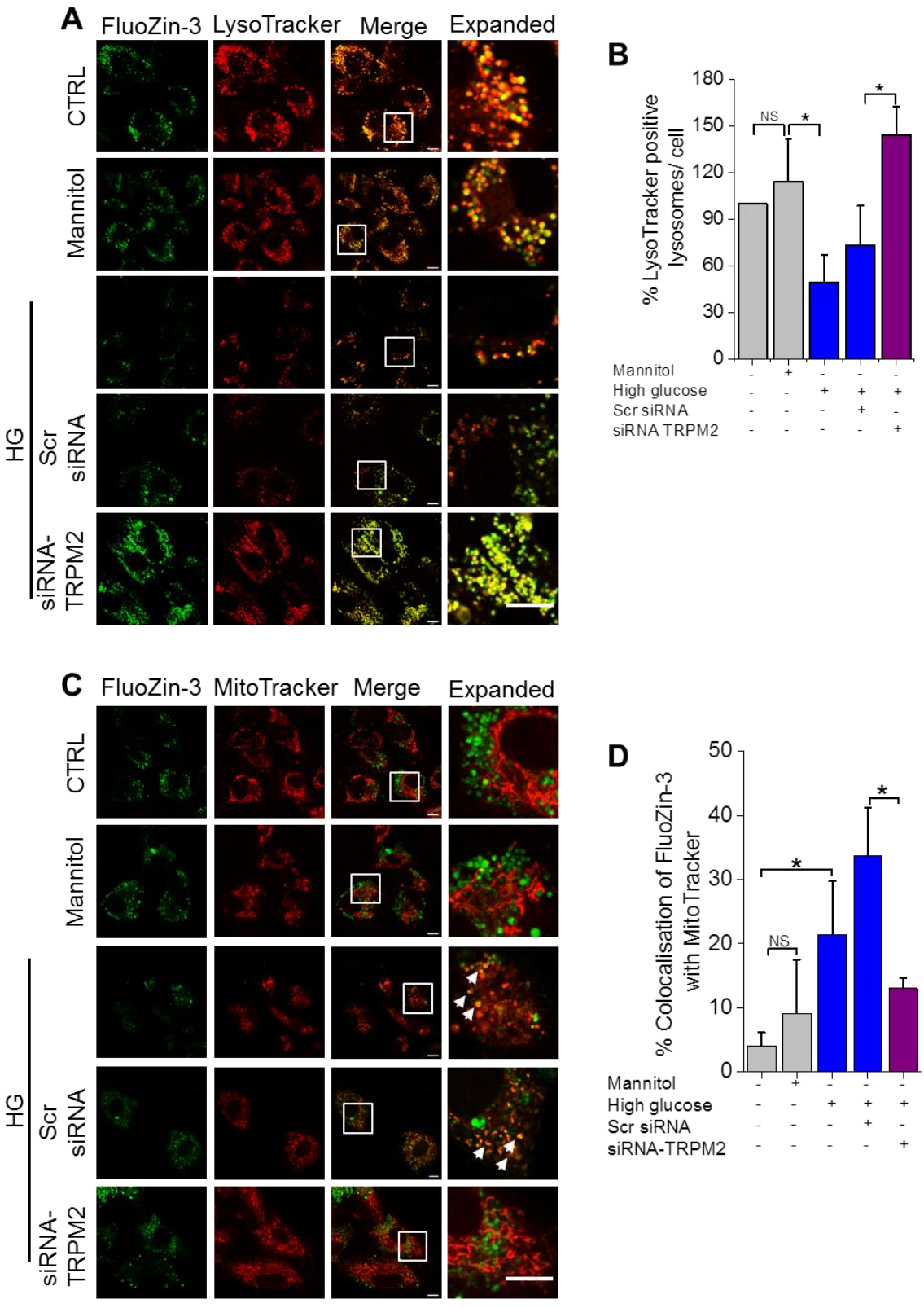
A
FluoZin-3
LysoTracker
Merge
Expanded
CTRL
Mannitol
HG
Scr siRNA
siRNA-TRPM2
B
% LysoTracker positive lysosomes/ cell
180
150
120
90
60
30
0
NS
*
*
Mannitol
High glucose
Scr siRNA
siRNA TRPM2
C
FluoZin-3
MitoTracker
Merge
Expanded
CTRL
Mannitol
HG
Scr siRNA
siRNA-TRPM2
D
% Colocalisation of FluoZin-3 with MitoTracker
50
40
30
20
10
0
NS
*
*
Mannitol
High glucose
Scr siRNA
siRNA-TRPM2

Figure 4.14 High glucose induces Zn^{2+} redistribution to mitochondria and triggers mitochondrial fragmentation

(A) HG causes a decrease in lysosomal Zn^{2+} and lysosomal number via activation of TRPM2 channels. HUVECs were treated as in Figure 4.3A, and incubated for 48 hr. Cells were loaded with FluoZin-3-AM and LysoTracker to detect Zn^{2+} and lysosomes respectively. Representative confocal images are shown; scale bar, 10 µm. Boxed regions in the merged images are magnified in the far right panels. Scale bar, 5 µm.

(B) Percent of LysoTracker positive lysosomes per cell, n/N = 3/≥110.

(C) High glucose increases mitochondrial Zn^{2+} and fragmentation via TRPM2 channel activation. Experiments were performed as in (A) except that MitoTracker staining was used in place of LysoTracker.

(D) Co-localisation of FluoZin-3 stain with MitoTracker; n/N values for various treatments are: CTRL, 3/155; Mannitol 3/91; HG, 3/119; scrambled siRNA, 3/108; siRNA-TRPM2, 3/148.

Bars are the means ± SEM, statistical analysis was performed by one-way ANOVA with Tukey's post-hoc test *p <0.05.

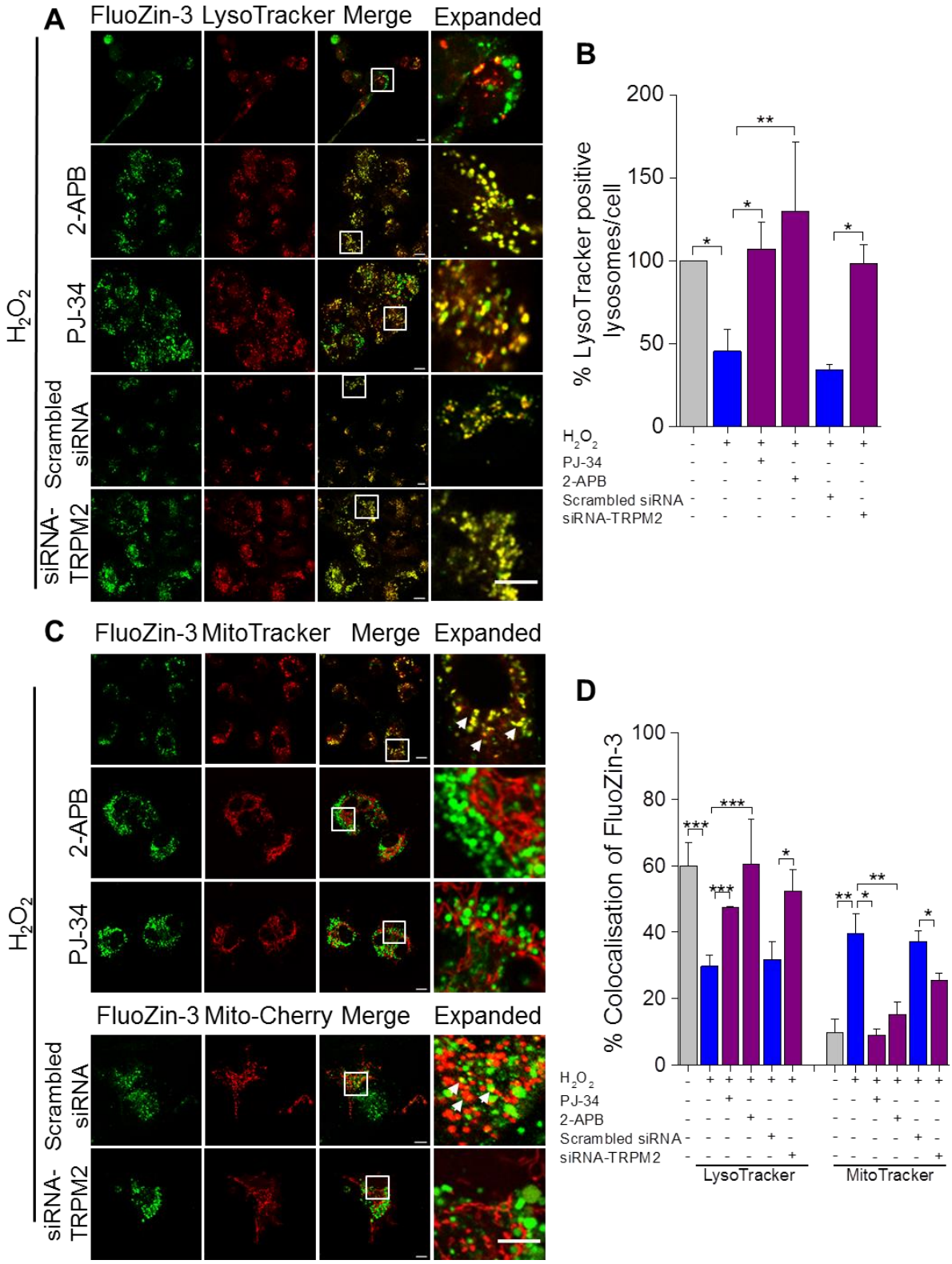
A
FluoZin-3
LysoTracker
Merge
Expanded
H2O2
2-APB
PJ-34
Scrambled siRNA
siRNA-TRPM2
B
% LysoTracker positive lysosomes/cell
200
150
100
50
0
H2O2
PJ-34
2-APB
Scrambled siRNA
siRNA-TRPM2
C
FluoZin-3
MitoTracker
Merge
Expanded
FluoZin-3
Mito-Cherry
Merge
Expanded
D
% Colocalisation of FluoZin-3
100
80
60
40
20
0
LysoTracker
MitoTracker

Figure 4.15 Activation of TRPM2 channels causes a reduction in lysosomal number and redistribution of Zn^{2+} to mitochondria

(A) Inhibition of TRPM2 channels attenuates H_2O_2-induced decrease in the lysosomal number and lysosomal Zn^{2+}. Live cell fluorescent images of HUVECs exposed to 1 mM H_2O_2 (4hr, 37°C) with and without the indicated TRPM2 inhibitors or pre-transfected with scrambled siRNA or siRNA targeted to TRPM2 channels (siRNA-TRPM2). Cells were stained for Zn^{2+} and lysosomes as described in the legend to Figure 4.14A. Scale bar, 10 µm. Boxed regions in the merged images are magnified in the far right panels. Scale bar, 5 µm.

(B) Percent LysoTracker positive lysosomes per cell, n/N = 3/≥48.

(C) Inhibition of TRPM2 channels prevents H_2O_2-induced increase in mitochondrial Zn^{2+}. Live cell imaging of HUVECs was performed as described in (A) except cells were stained with MitoTracker Red, instead of LysoTracker, or labelled with Mito-Cherry. Scale bar, 10 µm. Boxed regions in the merged images are magnified in the far right panels. Scale bar, 5 µm. Arrows indicate fragmented mitochondria containing Zn^{2+}.

(D) Percent co-localisation of lysosomal and mitochondrial markers with FluoZin-3-Zn^{2+} following the indicated treatments; n/N values for various treatments are as follows: for lysosomes: CTRL, 3/139; H_2O_2, 3/121; PJ34, 3/48; 2-APB, 3/112; scrambled siRNA, 3/91; siRNA-TRPM2, 3/222; and for mitochondria: CTRL, 3/105; H_2O_2, 3/122; PJ34 = 3/100; 2-APB, 3/88; scrambled siRNA, 3/127; siRNA-TRPM2, 3/68.

Bars are the means ± SEM, statistical analysis was performed by one-way ANOVA with Tukey's post-hoc test, **p* <0.05, ***P* < 0.01, and ****P* < 0.001.

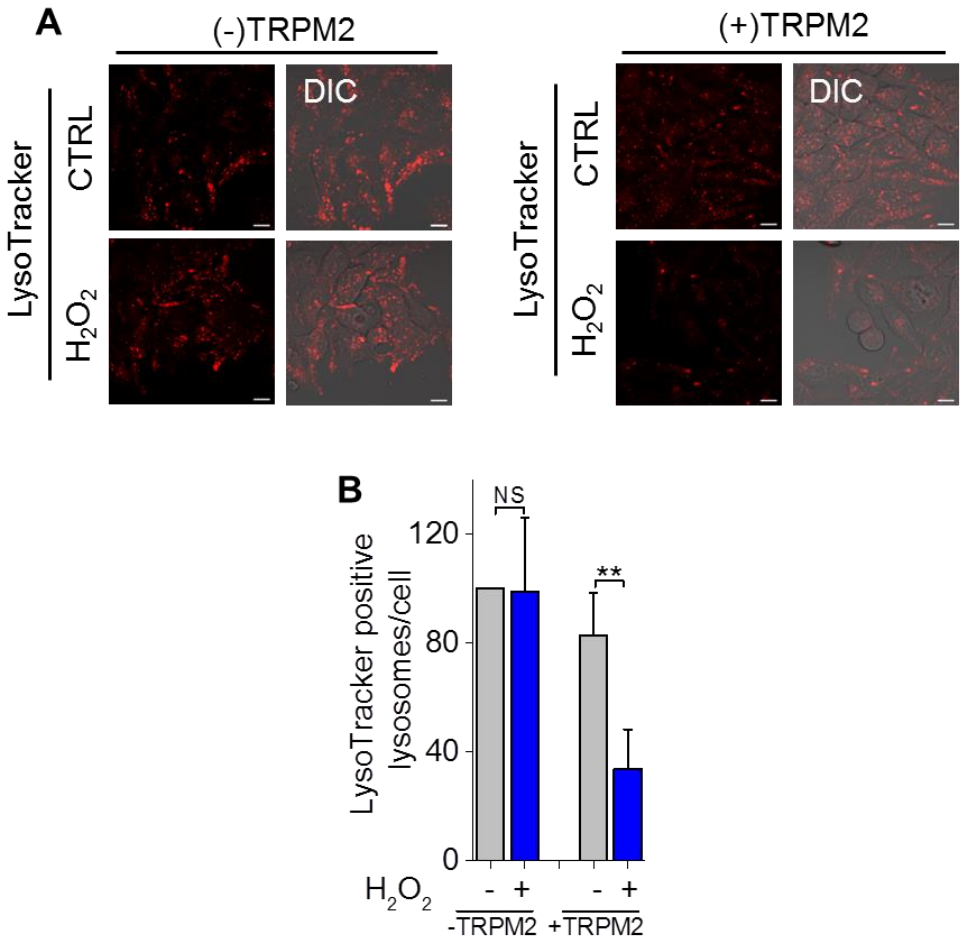

Figure 4.16 H_2O_2 activation of TRPM2 channels reduce the number of LysoTracker positive lysosomes

(A) LMP is dependent on TRPM2 expression. Not induced (-TRPM2) and induced (+TRPM2) HEK-TRPM2^{tet} cells were exposed to SBS alone (CTRL) or SBS with 200 µM H_2O_2 for 90 min at 37°C. Cells were then loaded with LysoTracker for 30 min, washed and imaged. Representative confocal images are shown; also shown are images overlaid with DIC images. Scale bar, 10 µm.

(B) Mean ± SEM corresponding to (A) show that H_2O_2 induced a significant reduction in the number of lysosomes per cell in TRPM2 expressing cells, but not in cells lacking TRPM2 expression (n/N =3/≥100 cells), ***p* <0.01, Student's t-test.

4.2.10 A23187 induces early LMP, but delayed mitochondrial fission

It has been reported that Ca^{2+} entry can activate lipases in lysosomes, thereby increasing the permeability of the lysosomes (Boya and Kroemer, 2008; Repnik et al., 2014). The TRPM2 dependence of LMP observed above could therefore be attributed to Ca^{2+} entry via plasma membrane TRPM2 channels. Since TRPM2 activation increases cytosolic levels of both Ca^{2+} and Zn^{2+}, it proved difficult to attribute H_2O_2-induced LMP to TRPM-mediated Ca^{2+} entry alone. To circumvent this, calcium and zinc ionophores were used to raise the cytosolic concentrations of Ca^{2+} and Zn^{2+}. Results from Ca^{2+} imaging (Figure 4.17A-C) show that application of exogenous A23187 induces a significant rise of $[Ca^{2+}]_i$. Effect of length of A23187 treatment on the integrity of lysosomes and mitochondria was examined using LysoTracker Red and MitoTracker Red. Results (Figure 4.17D-E) show a significant reduction in the percentage of LysoTracker positive lysosomes after 2 hr exposure to A23187, followed by a further decrease after 4 hr exposure. This finding is in agreement with previous reports that Ca^{2+} entry increases the permeability of lysosomes (Boya and Kroemer, 2008; Repnik et al., 2014). Although in 2 hr, A23187 caused LMP, there was no apparent change in mitochondrial morphology.

Mitochondrial fragmentation, however, was seen after 4 hr incubation with A23187. This could mean that Ca^{2+}-induced LMP may be required for mitochondrial fragmentation. Since LMP releases Zn^{2+}, the ability of Zn^{2+} chelator, TPEN, to prevent Ca^{2+}-induced mitochondrial fission was examined. As predicted, TPEN was able to fully prevent the effect of A23187 on mitochondrial fragmentation (Figure 4.16F-G). These findings are consistent with the idea that Zn^{2+} released during LMP triggers mitochondrial fragmentation. Conversely, when HUVECs were loaded with Zn^{2+} using Zn-PTO for 2 hr, there was extensive mitochondrial fragmentation that could be rescued by TPEN) (Figure 4.17F-G). Taken together, these results indicate that intracellular Ca^{2+} rise induces LMP, resulting in the release of Zn^{2+}, and the Zn^{2+} thus released causes mitochondrial fragmentation.

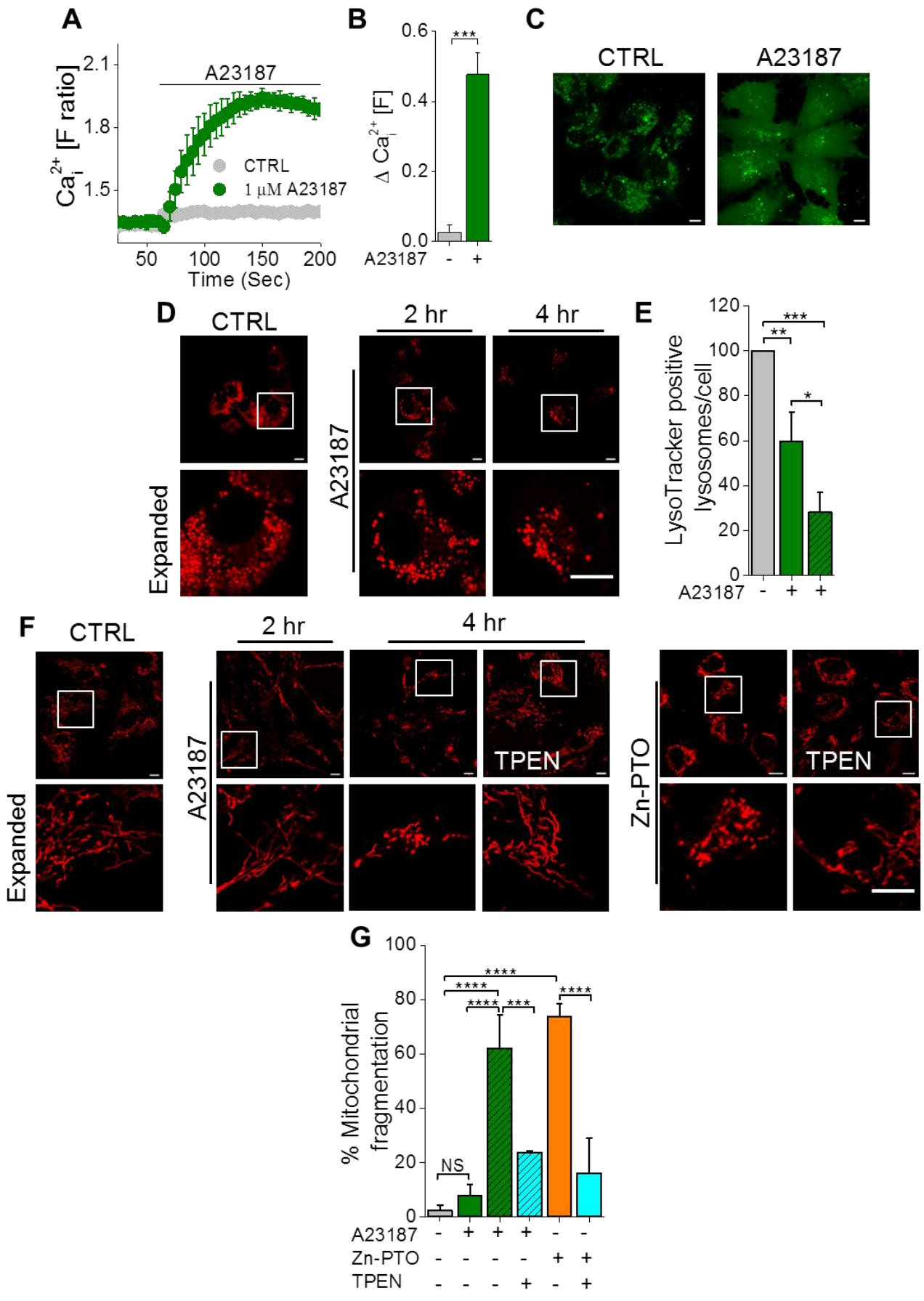
A
A23187
Ca_i^{2+} [F ratio]
2.1
1.8
1.5
CTRL
1 μM A23187
50
100
150
200
Time (Sec)
B
0.6
0.4
0.2
0.0
Δ Ca_i^{2+} [F]
***
A23187 - +
C
CTRL
A23187
D
CTRL
2 hr
4 hr
A23187
Expanded
E
120
100
80
60
40
20
0
LysoTracker positive lysosomes/cell
***
**
*
A23187 - + +
F
CTRL
2 hr
4 hr
A23187
Expanded
TPEN
Zn-PTO
TPEN
G
100
80
60
40
20
0
% Mitochondrial fragmentation
****
****
****
***
****
NS
A23187 - + + + - -
Zn-PTO - - - - + +
TPEN - - - + - +

Figure 4.17 A23187 induces early LMP but late Zn^{2+}-dependent mitochondrial fragmentation

(A) Addition of A23187 (shown with a horizontal bar) causes a rise in cytosolic Ca^{2+}.

(B) Mean ± SEM of change in Ca^{2+} fluorescence calculated from the data in (A), n = 3.

(C) Intracellular calcium imaging in HUVECs. Cells were treated for 2 hr at 37°C with medium alone (CTRL) or medium containing the calcium ionophore, A23187 (1 µM) plus Fluo-4-AM to detect Ca^{2+}. Representative confocal images are shown; scale bar, 10 µm.

(D) Raising the intracellular Ca^{2+} concentration induces LMP. HUVECs were treated for 2 hr and 4 hr at 37°C with medium alone (CTRL) or medium containing the calcium ionophore, A23187 (1 µM). Cells were then loaded with LysoTracker Red and imaged. Scale bar, 10 µm. Boxed regions are magnified in the lower panels. Scale bar, 5 µm.

(E) Mean ± SEM of percent cells displaying LysoTracker positive lysosomes in CTRL and A23187 treated cells, n=3, N≥100 cells.

(F) Longer incubation with A23187 is required to induce Zn^{2+}-dependent mitochondrial fission. HUVECs were treated for 2 hr and 4 hr at 37°C with medium alone (CTRL) or medium containing the calcium ionophore, A23187 (1 µM) or the zinc ionophore, zinc pyrithione (0.7 µM Zn^{2+}: 0.5 µM pyrithione). TPEN (0.3 µM) was included where indicated. Cells were then loaded with MitoTracker and imaged. Scale bar, 10 µm. Boxed regions are magnified in the lower panels. Scale bar, 5 µm.

(G) Mean ± SEM of percent cells displaying mitochondrial fragmentation in A23187 treated cells and zinc pyrithione treated cells. Cells were treated as in (F), n/N = 3/170 cells.

Statistical analysis was performed by Students t-test (B) or one-way ANOVA with Tukey's post-hoc test (E and G) or; *p <0.05, **P < 0.01, ***P < 0.001 and ****P < 0.0001.

4.2.11 TRPM2 channels are localised to mitochondria

4.2.11.1 Subcellular organelle fractionation to detect localisation of TRPM2 to mitochondria

To gain further insight into how TRPM2 channels promote redistribution of Zn^{2+} from lysosomes to mitochondria, subcellular localisation of TRPM2 channels was examined. For this, HA epitope-tagged TRPM2 (HA-TRPM2) channels were expressed in HEK-MSR cells (Figure 4.18A-B). The organelles were fractionated from these cells by Optiprep density gradient centrifugation and the individual fractions were examined for TRPM2 presence and protein markers of lysosomes (Lamp-1), mitochondria (VDAC-1) and ER (calnexin) by western blotting. The results in Figure 4.18C show a band corresponding to the size of TRPM2 (~170 KDa) in the fraction positive for the lysosomal marker, Lamp-1. This is not surprising given the previous immunostaining data on lysosomal expression of TRPM2 channels in other cell types (Lange et al., 2009; Manna et al., 2015) (see Chapter 3, Figure 3.5). Unexpectedly, the TRPM2 band was also observed in fractions positive for the mitochondrial marker protein VDAC-1. In fact, intensity of the TRPM2 band in the mitochondrial fractions was much stronger than that in the lysosomal fraction (Figure 4.18C). However, mitochondrial preparation was not pure as Lamp-1 bands were seen in fractions 7 and 8. This might be due to the fusion of lysosomes with mitochondria (Lee et al., 2012).

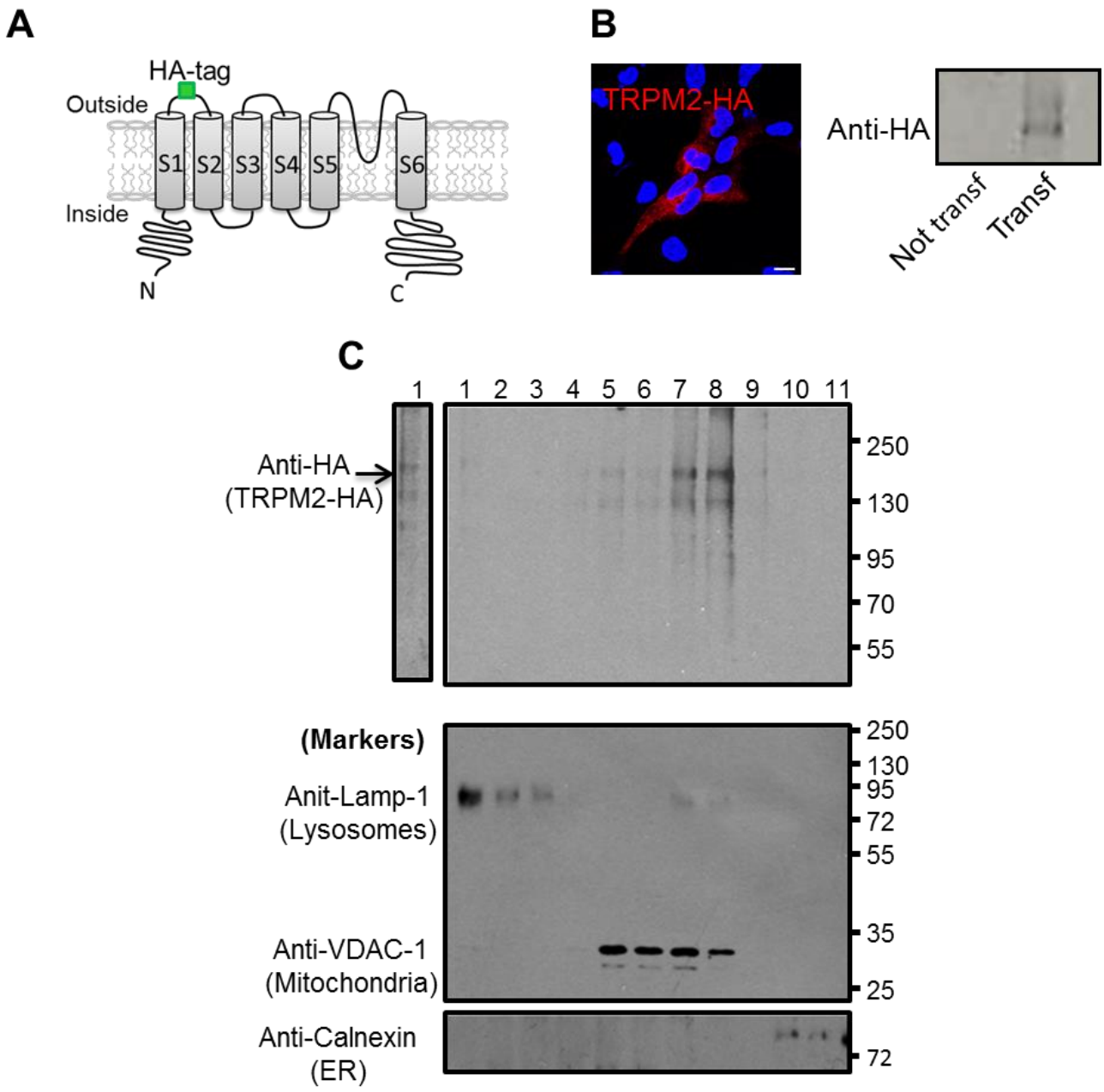
A
HA-tag
Outside
Inside
S1
S2
S3
S4
S5
S6
N
C
B
TRPM2-HA
Anti-HA
Not transf
Transf
C
1
1 2 3 4 5 6 7 8 9 10 11
Anti-HA
(TRPM2-HA)
250
130
95
70
55
(Markers)
250
130
95
72
55
Anit-Lamp-1
(Lysosomes)
35
Anti-VDAC-1
(Mitochondria)
25
Anti-Calnexin
(ER)
72

Figure 4.18 TRPM2 channels are present in mitochondria

(A) Schematic of the topology of TRPM2 subunit showing the site of the hemagglutinin (HA) epitope insertion.

(B) Immunodetection of TRPM2-HA expression in transiently transfected HEK-MSR cells. Western blot shows a ~170 KDa band corresponding to TRPM2-HA.

(C) Western blot analysis of Optiprep density gradient fractions (1-11) of lysates of HEK-MSR cells expressing TRPM2-HA. Fractions were blotted for the HA epitope (TRPM2-HA) and markers of lysosomes, mitochondria and ER using the indicated antibodies.

4.2.11.2 TRPM2-HA expression in mitochondria detected by immuno-fluorescence technique

To confirm mitochondrial location, TRPM2-HA was transfected into HUVECs and stained with anti-HA antibodies (green) and MitoTracker Red. Merged images and the quantification data confirm the presence of TRPM2 channels in mitochondria (yellow in Figure 4.19B-C, left column). However, no such staining was observed with the hERG potassium channel, also tagged with the HA-epitope in the analogous position (S1-S2 loop) (Figure 4.19D), indicating that insertion of the HA tag at this position is unlikely to cause mis-targeting of TRPM2 to mitochondria. Furthermore, TRPM2 channels tagged at the N- (FLAG tag) or the C- (EE tag) terminus with different epitopes showed similar mitochondrial localisation (Figure 4.19A-C, middle and right columns). These results provide the first demonstration of TRPM2 localisation to mitochondria.

For TRPM2 lysosomal expression, HA-TRPM2 was transfected into HUVECs and stained with anti-HA antibodies (green) and anti-CD-63 (lysosomal marker, red) antibodies. The merged image shows localisation of TRPM2 to lysosomes, a finding that is consistent with previous reports in other cell lines (Lange et al., 2009; Manna et al., 2015) (Figure 4.19E).

To conclude, TRPM2 is not only expressed in lysosomes, but also in mitochondria. Insertion of an HA tag does not cause mis-targeting of TRPM2 to mitochondria.

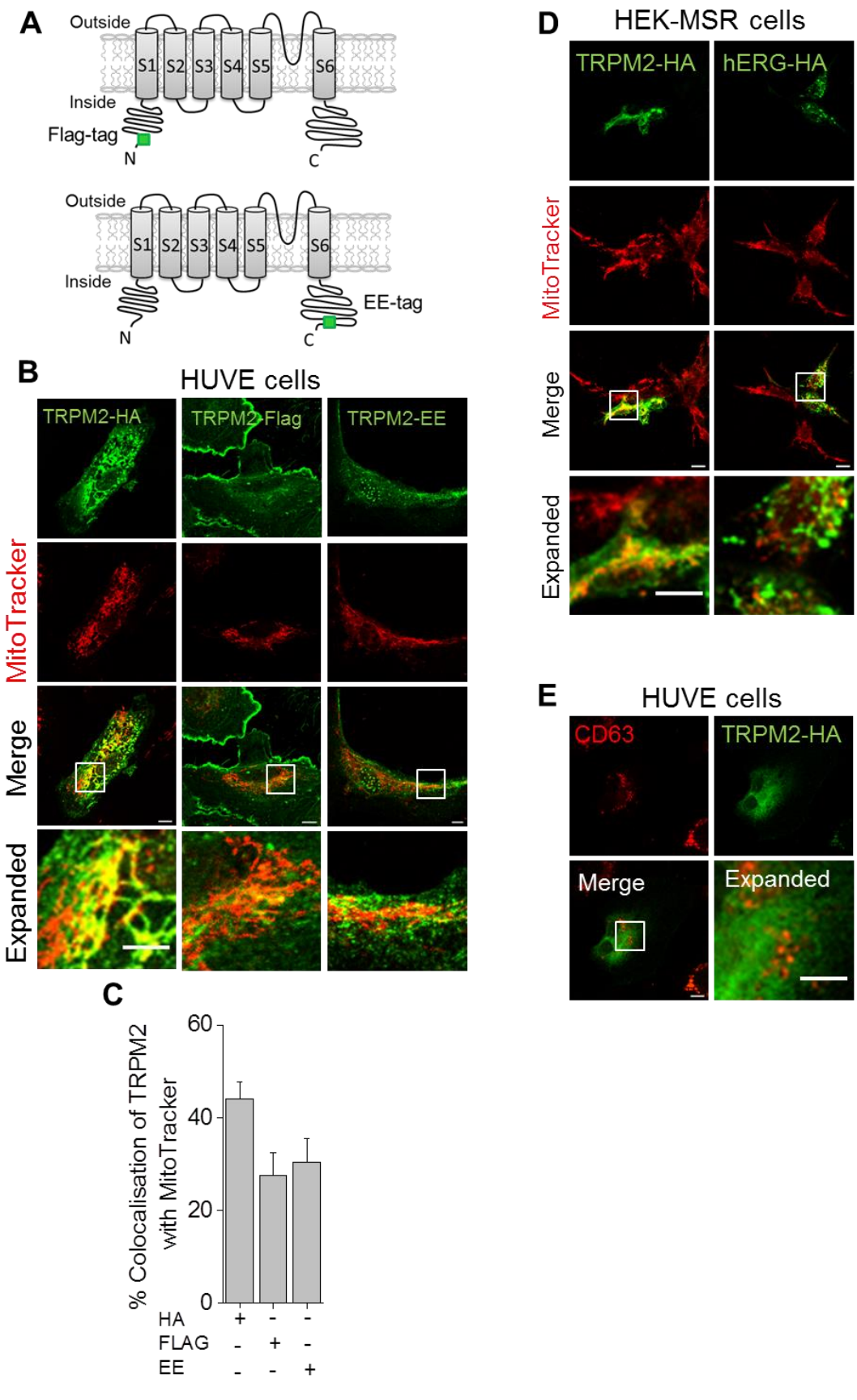
A
Outside
S1
S2
S3
S4
S5
S6
Inside
Flag-tag
N
C
Outside
S1
S2
S3
S4
S5
S6
Inside
EE-tag
N
C
B
HUVE cells
TRPM2-HA
TRPM2-Flag
TRPM2-EE
MitoTracker
Merge
Expanded
C
% Colocalisation of TRPM2 with MitoTracker
60
40
20
0
HA + - -
FLAG - + -
EE - - +
D
HEK-MSR cells
TRPM2-HA
hERG-HA
MitoTracker
Merge
Expanded
E
HUVE cells
CD63
TRPM2-HA
Merge
Expanded

Figure 4.19 TRPM2-HA immune-co-localisation to mitochondrial and lysosomes

(A) Schematic of the topology of TRPM2 subunit showing the sites of the EE and FLAG epitope.

(B) Immunolocalisation of tagged TRPM2 channels to mitochondria. HUVECs were transfected with TRPM2 tagged with the HA, FLAG or EE epitopes. Cells were loaded with MitoTracker (red), fixed with 2% PFA and permeabilised with 0.25% Triton X-100. Cells were then immunostained using antibodies against the epitopes. Representative confocal images are shown. Scale bar, 10 µm. Boxed regions in the merged images are magnified in the lower panel. Scale bar, 5 µm.

(C) Mean ± SEM of data from (B) expressed as the percentage of co-localisation of TRPM2-HA immunostaining with MitoTracker.

(D) HA-tagging does not mis-target TRPM2 channels to mitochondria. HEK-MSR cells transfected with TRPM2-HA or hERG-HA were stained for the HA-epitope and mitochondria as in (B). Representative images show co-localisation of TRPM2-HA, but not of hERG-HA channels, with MitoTracker. Scale bar, 10 µM. Boxed regions in the merged images are magnified in the lower panels. Scale bar, 5 µm.

(E) Immunolocalisation of tagged TRPM2 channels to lysosomes. HUVECs were transfected with pcDNA3-TRPM2-HA, fixed with 2% PFA, permeabilised with 0.25% Triton X-100. Cells were incubated with rat anti-HA (1:500) and mouse anti-CD63 (1:500) sequentially and stained with Cy3 anti-rat conjugated secondary antibody (1:500) and AlexaFlour^{488} anti-mouse (1:500) conjugated secondary antibodies. Cells were imaged by confocal microscopy, scale bar, 10 µm. Boxed regions are magnified. Scale bar, 5 µm.

4.2.12 Mitochondrial TRPM2 channels mediate $Zn2^{+}$ influx and mitochondrial fission

4.2.12.1 Mitochondrial Ca^{2+} uniporter (MCU)

The data presented above suggested that Zn^{2+} uptake by mitochondria triggers mitochondrial fragmentation. Previous studies have reported that the mitochondrial Ca^{2+} uniporter (MCU), which is located in the organelle's inner membrane, mediates mitochondrial Zn^{2+} uptake (Kirichok et al., 2004; Malaiyandi et al., 2005). The role of MCU in H_2O_2-induced Zn^{2+} uptake by mitochondria and mitochondrial fragmentation was examined using an MCU blocker and HEK-MSR cells transfected with TRPM2-HA. HEK-293 cells are known to express MCU natively (Madesh et al., 2013). Figure 4.20 shows that H_2O_2 leads to uptake of Zn^{2+} by mitochondria and mitochondrial fragmentation in HEK-MSR-TRPM2-HA cells. However, inhibition of MCU with ruthenium red (RuR) failed to inhibit H_2O_2-induced increase in mitochondrial Zn^{2+} and fragmentation, thus excluding a role for the uniporter in oxidative stress-induced mitochondrial Zn^{2+} influx. These data therefore suggest that there is another transporter or an ion channel to mediate mitochondrial Zn^{2+} uptake.

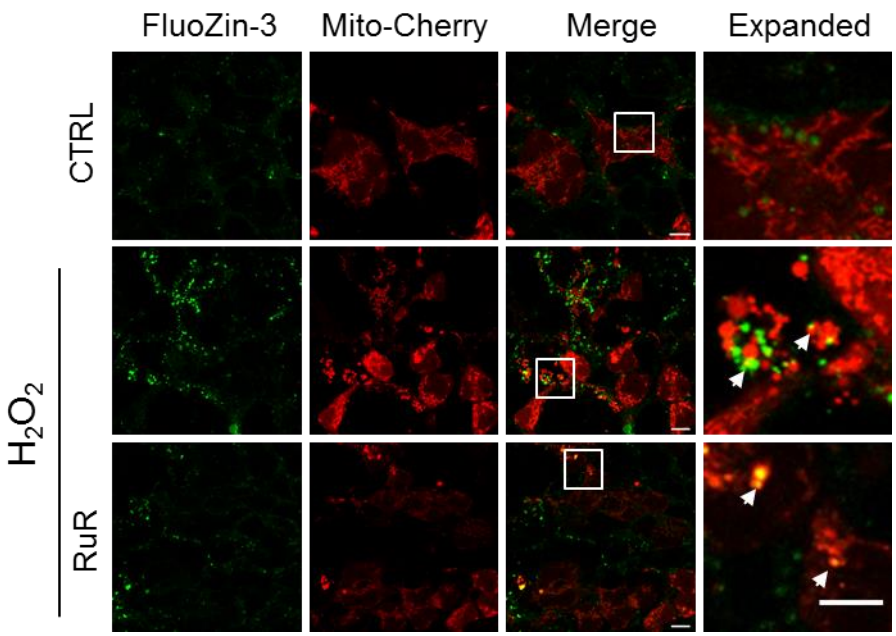

Figure 4.20 H_2O_2-induced rise in mitochondrial Zn^{2+} is Ca^{2+} uniporter-independent

HEK-MSR cells expressing TRPM2-HA were not treated (CTRL) or treated with 300 µM H_2O_2 for 3 hr in the absence or presence of 5 µM ruthenium red (RuR). Cells were then stained for Zn^{2+} (FluoZin-3) and mitochondria (Mito-Cherry). Merged confocal images show that H_2O_2 caused an increase in mitochondrial Zn^{2+} (yellow puncta, shown with arrows) that was unaffected by the Ca^{2+} uniporter blocker, RuR. The images also show that RuR failed to prevent mitochondrial fragmentation. Scale bar, 10 µm. Boxed regions in the merged images are magnified in the far right panels. Scale bar, 5 µm. Representative images are shown; the experiment was performed three times.

4.2.12.2 TRPM2 channels mediate mitochondrial $Zn2^{+}$ uptake

Since TRPM2 channels are located in mitochondria (Figure 4.18 and Figure 4.19) and TRPM2 channels are known to conduct Zn^{2+} (Yu et al., 2012), the possibility that TRPM2 channels could contribute to mitochondrial Zn^{2+} uptake during oxidative stress was investigated. For this, the cytoplasmic levels of free Zn^{2+} were raised in HUVECs using Zn-PTO, and changes in mitochondrial Zn^{2+} were examined. In this experiment, H_2O_2 was not included to activate TRPM2 channels because Zn-PTO, as has been shown previously (Clausen et al., 2013), and as was confirmed here (Figure 4.21C), can potently induce oxidative stress required to activate TRPM2 channels. The results show that Zn-PTO indeed induced Zn^{2+} accumulation in the mitochondria (Figure 4.21A), and the expected mitochondrial fragmentation (rescued by TPEN as in Figure 4.17F). Importantly, these effects of Zn-PTO were completely blocked by siRNA targeted to TRPM2 channels and by the anti-oxidant, N-acetyl cysteine (NAC) (Figure 4.21A-B). Absence of Zn^{2+} in TRPM2-depleted cells suggests that under this experimental condition, Zn-PTO does did not reach the mitochondria to raise mitochondrial Zn^{2+}. Thus these data suggest that TRPM2 channels mediate mitochondrial Zn^{2+} entry and fragmentation.

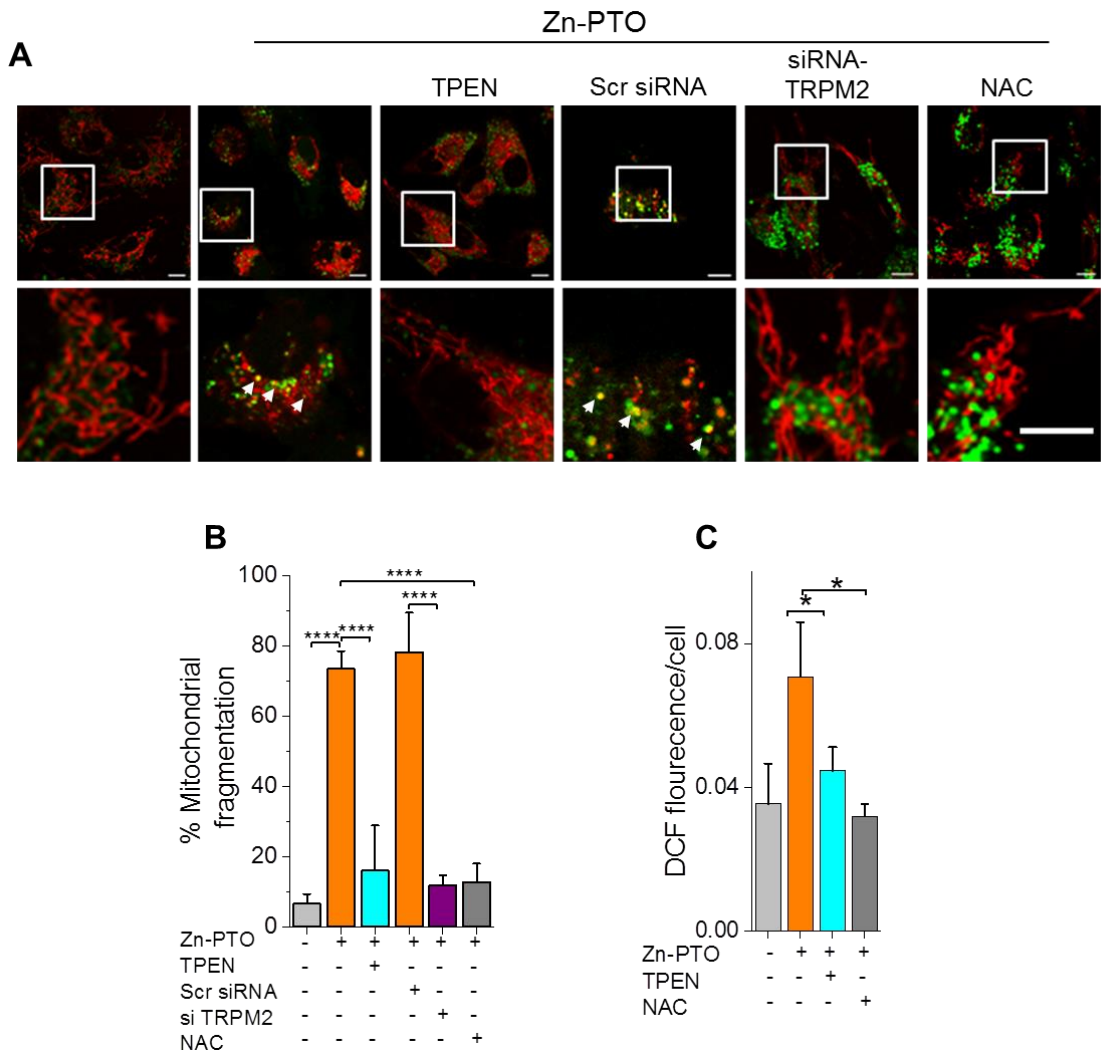

Figure 4.21 Mitochondrial TRPM2 channels are essential for mitochondrial Zn^{2+} uptake and fragmentation

(A) Fluorescent images of HUVECs treated for 2 hr with Zn-PTO (0.7 µM Zn^{2+}: 0.5 µM pyrithione) in the absence or presence of TPEN (0.3 µM TPEN) or N-acetyl cysteine (NAC, 10 mM), or transfected with scrambled or TRPM2-siRNA. Cells were stained for Zn^{2+} (green) and mitochondria (red). Scale bar, 10 µm. Boxed regions in the merged images are magnified in the lower panels. Scale bar, 5 µm; arrows indicate localisation of free Zn^{2+} in mitochondria.

(B) Mean ± SEM of data from (A) expressed as percentage of cells displaying mitochondrial fragmentation, n/N =3/100.

(C) Zn-PTO increases ROS production. HUVECs were treated as in (A) and ROS production measured using the H_2DCFDA reporter, n/N = 3/100.

Statistical analysis in B and C was performed by one-way ANOVA with Tukey's post-hoc test, **p* <0.05, ***P* < 0.01, ****P* < 0.001 and *****P* < 0.0001.

4.2.12.3 Zn^{2+} uptake by isolated mitochondria

Direct Zn^{2+} uptake by mitochondria isolated from HEK-293 cells overexpressing TRPM2 channels was examined in the presence and absence of H_2O_2 (TRPM2 activation). For this, mitochondria were isolated from HEK-$TRPM2^{Tet}$ cells, loaded with FluoZin-3-AM and placed in a glass bottom dish; increase in fluorescence in response to Zn^{2+} addition was then recorded by confocal microscopy (Malaiyandi et al., 2005). The results show that under control conditions, exogenous Zn^{2+} addition caused a significant increase (~0.3-fold) in Zn^{2+} fluorescence. However, H_2O_2 stimulus caused a further increase in the fluorescence (to ~0.8-fold) (Figure 4.22A-C), which could be attributed to TRPM2 mediated Zn^{2+} uptake. Further evidence using TRPM2 inhibitors and $TRPM2^{-/-}$ cells is required to confirm the role of TRPM2 channels in mitochondrial Zn^{2+} uptake.

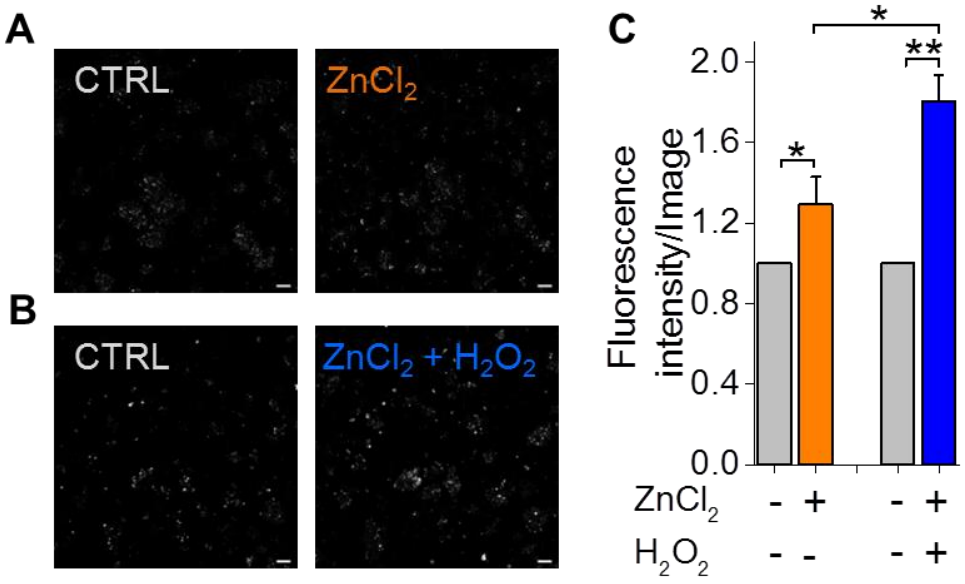

Figure 4.22 Zn^{2+} uptake by mitochondria isolated from HEK-293 cells overexpressing TRPM2 channels

(A-B) Mitochondria isolated from tetracycline-induced HEK-$TRPM2^{tet}$ cells were loaded with FluoZin-3 for 20 min at 37°C. Confocal images were taken before (CTRL) and 15 min after addition of 30 µM $ZnCl_2$ alone or 30 µM $ZnCl_2$ plus 200 µM H_2O_2. Scale bar, 10 µm.

(C) Mean ± SEM of data from (A) and (B) expressed as fluorescence (FluoZin3-Zn) intensity of the imaged fields, n= 3. Statistical analysis was performed by Student's *t*-test, **p* <0.05 and ***p* <0.01.

4.2.13 TRPM2-dependent rise in mitochondrial Zn^{2+} promotes Drp1 recruitment

Previous studies have shown that mitochondrial fragmentation is initiated by the recruitment of Drp1, a GTPase that catalyses mitochondrial fragmentation (Archer, 2013; Friedman and Nunnari, 2014; Slupe et al., 2013; Youle and van der Bliek, 2012). It was hypothesised that TRPM2-dependent mitochondrial Zn^{2+} uptake induces Drp1 recruitment. To test this, HUVECs were transfected with Drp1-GFP and the recruitment of Drp1-GFP from the cytoplasm to mitochondria was examined. The results demonstrate that HG, but not mannitol, promoted Drp1 mitochondrial recruitment, as measured by the co-localisation of MitoTracker Red fluorescence with Drp1-GFP (Figure 4.23A-B). HG-induced Drp1-GFP recruitment was suppressed by siRNA targeted to TRPM2 channels, but not by the scrambled siRNA. Under these conditions, HG treatment failed to induce recruitment of the dominant negative Drp1-GFP (Figure 4.23A-B). These data support a role for TRPM2 channels in Drp1 recruitment. Whether Zn^{2+} contributes to Drp1 recruitment was next investigated. Chelation of Zn^{2+} with TPEN markedly inhibited HG-induced Drp1-GFP recruitment (Figure 4.23A-B). Furthermore, delivery of Zn^{2+} via pyrithione stimulated mitochondrial recruitment of Drp1-GFP, but not its dominant negative version (Figure 4.23C-D).

Similar results were obtained when siRNA directed to a different region of the gene, siRNA-2, was used to suppress TRPM2 expression. Figure 4.24 A-C shows that siRNA-2-TRPM2 completely suppressed Drp1-GFP recruitment in HUVECs. Finally, silencing of TRPM2 expression also prevented H_2O_2 (direct oxidative stress) induced Drp1-GFP recruitment to mitochondria (Figure 4.25).

Taken together, the data indicate that TRPM2-mediated rise in mitochondrial Zn^{2+} promotes Drp1 recruitment and subsequent mitochondrial fragmentation.

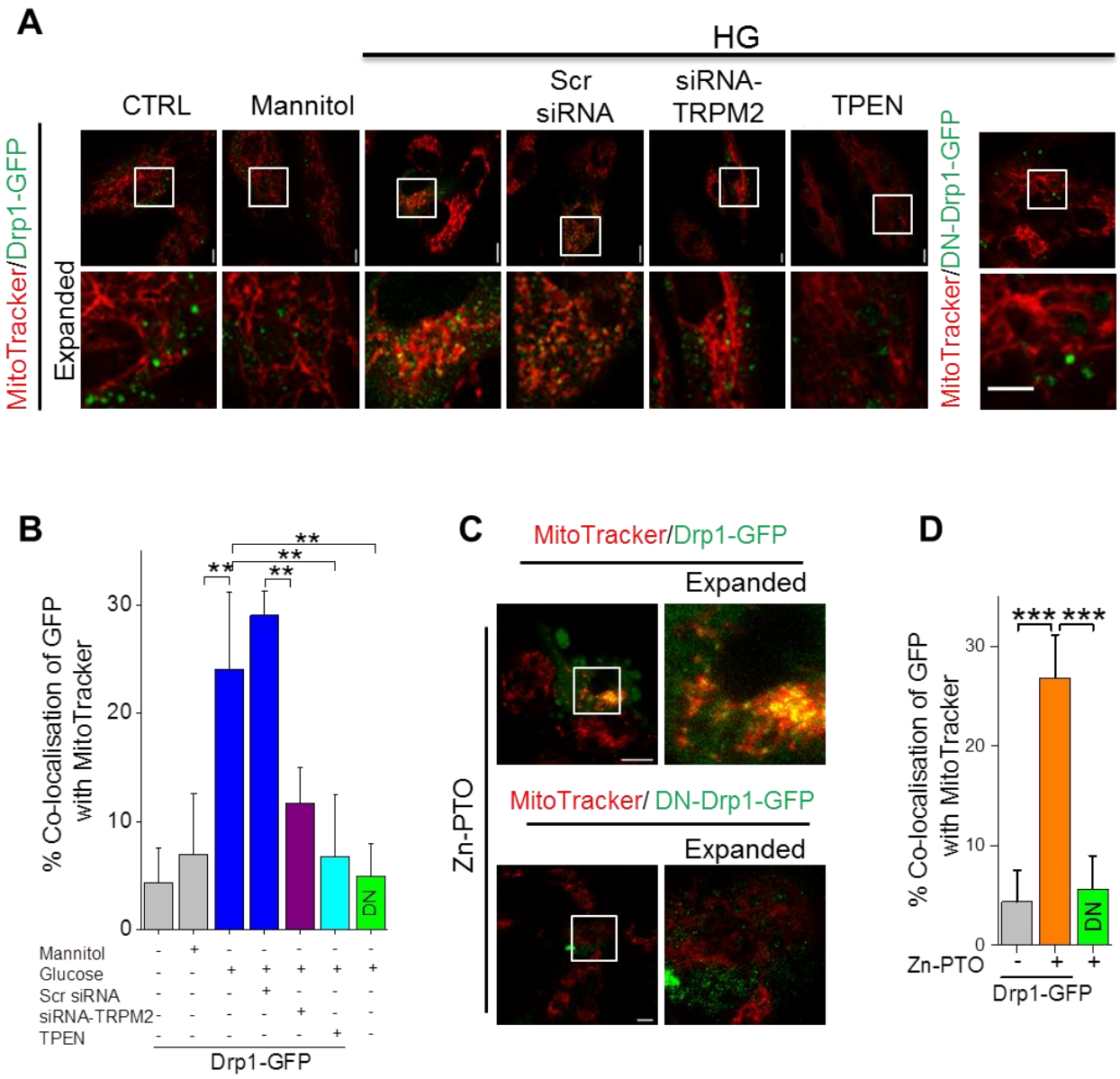
A
HG
CTRL
Mannitol
Scr siRNA
siRNA-TRPM2
TPEN
MitoTracker/Drp1-GFP
Expanded
MitoTracker/DN-Drp1-GFP
B
% Co-localisation of GFP with MitoTracker
30
20
10
0
**
**
**
**
DN
Mannitol
Glucose
Scr siRNA
siRNA-TRPM2
TPEN
Drp1-GFP
C
MitoTracker/Drp1-GFP
Expanded
Zn-PTO
MitoTracker/ DN-Drp1-GFP
Expanded
D
% Co-localisation of GFP with MitoTracker
30
20
10
0
***
***
DN
Zn-PTO
Drp1-GFP

Figure 4.23 High glucose-induced Drp1 recruitment is mediated by TRPM2 channels and Zn^{2+}

(A) Drp1-GFP recruitment to mitochondria is TRPM2 dependent. HUVECs transfected with Drp1-GFP or dominant negative (DN)-Drp1-GFP were treated as in Figure 4.12. Confocal images show cells stained with MitoTracker red. Scale bar, 10 µm. Boxed regions in the merged images are magnified in the bottom panels. Scale bar, 5 µm.

(B) Mean ± SEM of percentage co-localisation of GFP with MitoTracker calculated from the data in (A), n = 3.

(C) Zn^{2+} induces Drp1-GFP recruitment to mitochondria. HUVECs transfected with Drp1-GFP or DN-Drp1-GFP were treated with Zn-PTO as in Figure 4.21A for 1 hr and stained for mitochondria. Representative confocal images are shown. Scale bar, 10 µm. Boxed regions in the merged images are magnified in the right panels.

(D) Mean ± SEM of percentage co-localisation of GFP with MitoTracker Red calculated from the data in (C), n = 3. Statistical analysis was performed by one-way ANOVA with Tukey's post-hoc test, **p* <0.05, ***p* <0.01 and ****P* < 0.001.

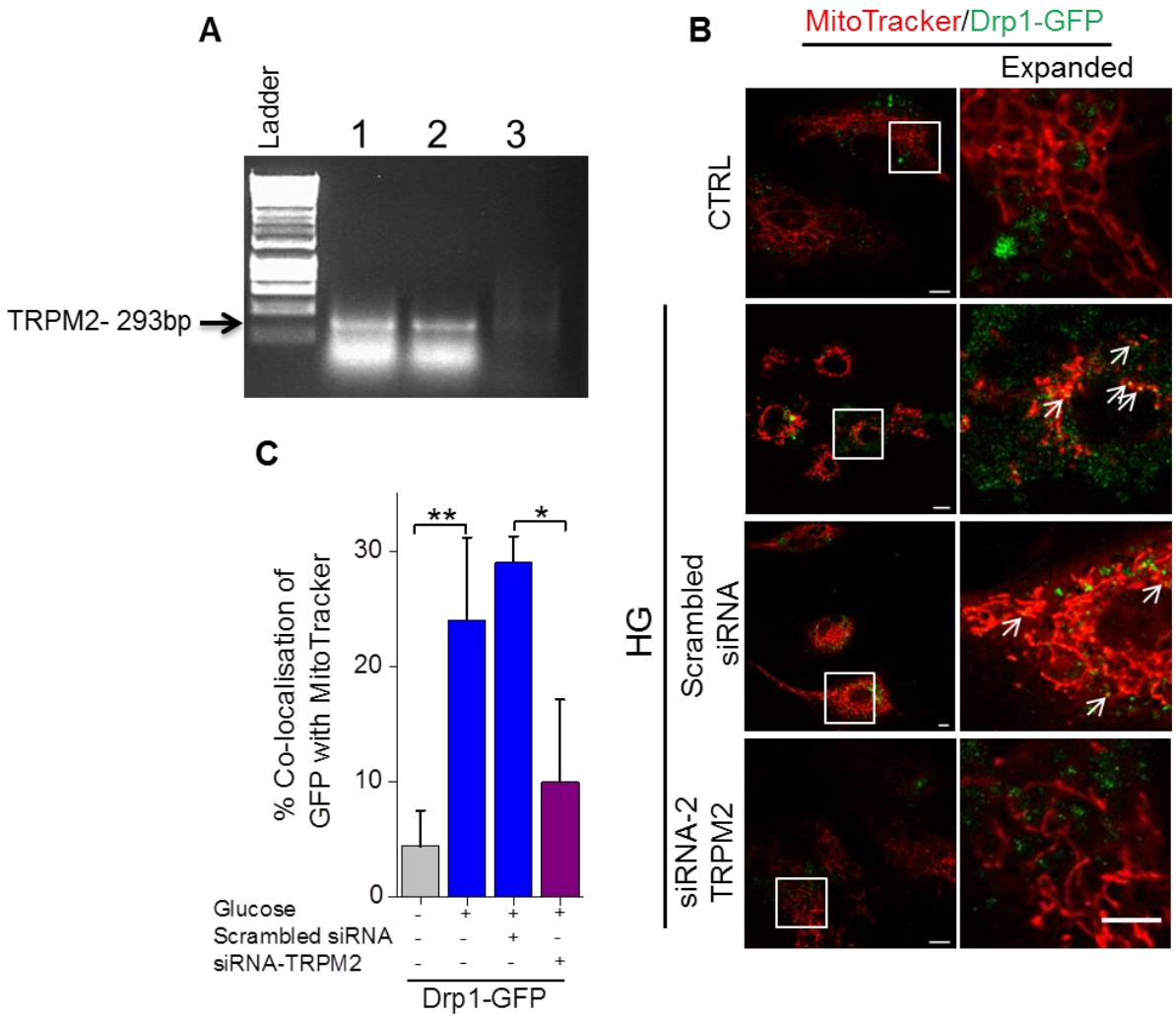

Figure 4.24 High glucose-induced Drp1 recruitment is mediated by TRPM2 channels

(A) Demonstration of silencing of TRPM2 mRNA expression by RNAi. 1: PCR product from TRPM2 plasmid. Lanes 2-3: RT-PCR products from mRNA isolated from HUVECs transfected with scrambled (negative control) siRNA (lane 2) or siRNA-2 targeted to TRPM2 (lanes 3).

(B) HUVECs were transfected with Drp1-GFP alone or together with scrambled siRNA or siRNA-2 targeted to TRPM2, as indicated. Cells were exposed to EGM-2 without (CTRL) or with additional glucose (HG, 33 mM, shown with a vertical bar) for 24 hr, before staining with MitoTracker Red. Representative merged (GFP and MitoTracker Red) images are shown. Scale bar, 10 µm. Boxed regions in the merged images are magnified in the right panels. Scale bar, 5 µm. Arrows show recruitment of Drp1 to mitochondria (yellow).

(C) Mean ± SEM of percentage co-localisation of GFP with MitoTracker calculated from the data in (B), n = 3. Statistical analysis was performed by one-way ANOVA with Tukey's post-hoc test, **p* <0.05 and ***p* <0.01.

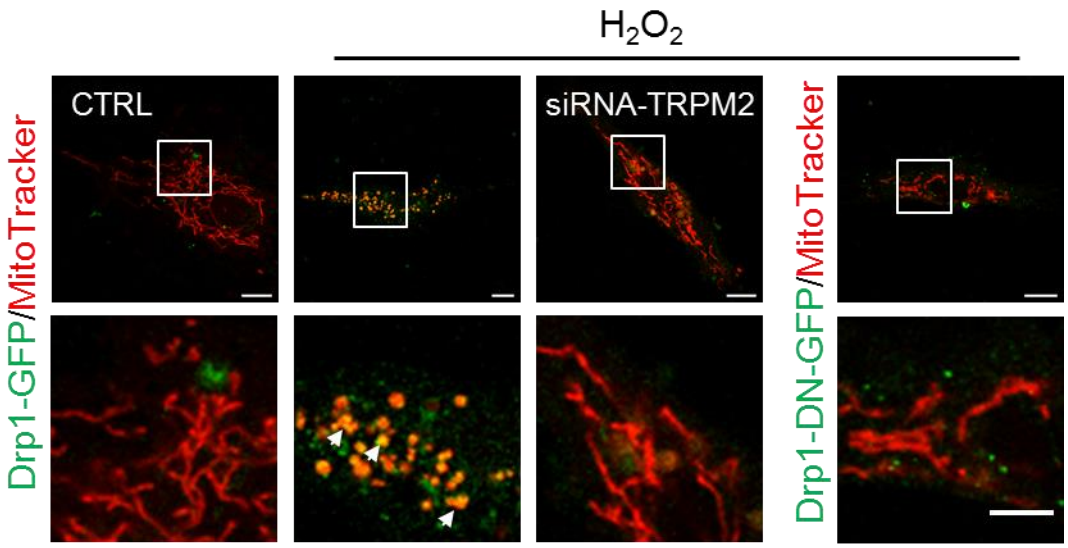

Figure 4.25 H_2O_2-induced Drp1 recruitment is mediated by TRPM2 channels

HUVECs were transfected with Drp1-GFP alone or together with siRNA-targeted to TRPM2, as indicated. Cells were exposed to EGM-2 alone (CTRL) or EGM-2 with 1 mM H_2O_2 for 2 hr, before staining with MitoTracker Red. Representative merged (GFP and MitoTracker Red) images are shown. Scale bar, 10 µm. Boxed regions in the merged images are magnified in the bottom panels. Scale bar, 5 µm. Arrows show recruitment of Drp1 to mitochondria (yellow).

4.3 Discussion

Emerging evidence suggests that increased mitochondrial fragmentation is a common defect in the majority of late age-onset diseases (Archer, 2013; Dorn, 2015). Oxidative stress, which increases as age increases, is an important trigger of mitochondrial fragmentation, but the underlying signalling mechanism is largely unknown. In this chapter, a key role for TRPM2 channels and mobilisation of mitotoxic free Zn^{2+} from lysosomes to mitochondria in mitochondrial fragmentation was demonstrated. The key findings are as follows: (i) oxidative stress-induced mitochondrial fragmentation is mediated by TRPM2 channels; (ii) knock-out of TRPM2 channels prevents high glucose-induced mitochondrial fragmentation in mouse pulmonary endothelial cells; (iii) chelation of Zn^{2+} alone was sufficient to prevent TRPM2-mediated mitochondrial fragmentation; (iv) TRPM2 activation induces lysosomal membrane permeabilisation and redistribution of lysosomal Zn^{2+} to mitochondria; (v) TRPM2 channels are localised to mitochondria where they mediate Zn^{2+} influx and mitochondrial fission; and (vi) TRPM2-dependent rise in mitochondrial Zn^{2+} promotes Drp1 recruitment. These findings have important implications for health, because mitochondrial fragmentation is associated with several age-related chronic illnesses including neuronal (Alzheimer's, Parkinson's), cardiovascular (atherosclerosis, myocardial infarction) and metabolic/inflammatory (diabetes) disorders. These results identify TRPM2 channel as a novel target that could be explored for therapeutic intervention of age-related illnesses.

In the current chapter, HUVECs were subjected to high glucose- and H_2O_2-induced oxidative stress, and their effects on mitochondrial dynamics were examined. Using pharmacological agents, RNA interference, and TRPM2 knock-out mice, it was demonstrated that the ROS-sensitive TRPM2 channel mediates HG- and H_2O_2-induced mitochondrial fragmentation (Figure 4.3, Figure 4.4, Figure 4.5, Figure 4.6 and Figure 4.7). It is known that activation of TRPM2 channels raises the cytoplasmic levels of Ca^{2+} and Zn^{2+} (Manna et al., 2015; Sumoza-Toledo and Penner, 2011; Takahashi et al., 2011). Although Ca^{2+} is the most widely used signalling ion, also implicated in mitochondrial dynamics (Cereghetti et al., 2008; Han et al., 2008; Slupe et al., 2013;

Szabadkai et al., 2006), it was found that chelation of Zn^{2+} alone was sufficient to prevent mitochondrial fragmentation (Figure 4.8, Figure 4.9 and Figure 4.10). Although the data obtained from HUVECs were sufficient to generate statistically significant results, there were not enough cells (≤ 20 cells) to perform significance tests on the primary cell data. Furthermore, the mitochondrial network in isolated primary cells is not as distinct as the cell lines to allow meaningful analysis of mitochondrial fragmentation.

Next, the question of where the Zn^{2+} signal was generated from, and how it was transmitted to mitochondria, was investigated. Data showed that the Zn^{2+} signal originates in lysosomes, and that oxidative stress causes a marked decrease in lysosomal Zn^{2+} (Figure 4.11, Figure 4.12 and Figure 4.13) with a concomitant rise in mitochondrial Zn^{2+} (Figure 4.12 and Figure 4.13).

Furthermore, chemical inhibition and RNAi silencing of TRPM2 channels prevented the mobilisation of lysosomal Zn^{2+} to mitochondria (Figure 4.12 and Figure 4.13) as well as mitochondrial fission. Taken together, these findings suggest that mobilisation of lysosomal Zn^{2+} to mitochondria may contribute to mitochondrial fission. Although inter-organelle Ca^{2+} redistribution, mediated by channels, transporters and pumps, have been described in the Ca^{2+} signalling field (Clapham, 2007), such dynamics are not known for Zn^{2+}. FluoZin-3 was used in these experiments as a Zn^{2+} reporter to determine the Zn^{2+} signal. It has demonstrated that FluoZin-3 failed to detect any fluorescence if the Ca^{2+} level is ≤ 10 mM (Gee et al., 2002). The estimated concentration of lysosomal Ca^{2+} is less than 1 mM (Xu and Ren, 2015). Thus, the fluorescence detected by FluoZin-3 is most likely from Zn^{2+}, but not Ca^{2+}. Thus the findings presented in this chapter reveal an intriguing role for inter-organelle Zn^{2+} dynamics (regulated by TRPM2 channels) in mitochondrial dynamics.

The decrease in lysosomal Zn^{2+} was accompanied by a decrease in LysoTracker staining (Figure 4.12 and Figure 4.13). LysoTracker uptake by lysosomes depends on the low pH of this organelle or its integrity. Thus an increase in pH or lysosomal membrane permeabilisation (LMP) can account for the decrease in oxidative stress

induced decrease in LysoTracker staining. As will be shown in the next Chapter (Figure 5.4), oxidative stress also causes release of cathepsin B into the cytoplasm, which is a biochemical indicator of LMP (Boya et al., 2003; Boya and Kroemer, 2008; Repnik et al., 2014), the underlying mechanisms are not clear. It has long been assumed that LMP is a result of nonspecific attack of oxidants on the lipids of lysosomal membranes. However, recent studies (Boya and Kroemer, 2008; Repnik et al., 2014) suggest that oxidants can activate phospholipase A2, leading to the hydrolysis of lysosomal membrane lipids and LMP (Zhao et al., 2001). Importantly, these lipases are activated by the cytosolic entry of extracellular Ca^{2+} (Boya and Kroemer, 2008). Given the finding from the current chapter that inhibition of TRPM2 channels attenuates LMP, it seemed reasonable to speculate that Ca^{2+} entry through the plasma membrane TRPM2 channels promotes LMP. Consistent with this idea, data from elevation of cytosolic levels of free Ca^{2+} (using ionophores, A23187) induced LMP after 2 hr, while mitochondrial fragmentation was induced after 4 hr (Figure 4.15). However, Zn^{2+} chelation was sufficient to prevent Ca^{2+}-induced mitochondrial fragmentation. Furthermore, direct elevation of cytosolic levels of free Zn^{2+} (using pyrithione) was enough to induce mitochondrial fragmentation within 2 hr (Figure 4.16). These findings led to the fundamentally important conclusion that ROS-induced mitochondrial fragmentation is regulated by TRPM2-mediated Zn^{2+} signalling but not Ca^{2+} signalling. Moreover, this finding also identified a regulatory role for TRPM2 channels in oxidant-induced LMP.

LMP causes release of lysosomal contents, including Zn^{2+}, into cytoplasm. Although previous studies have reported that mitochondrial Ca^{2+} uniporter mediates entry of cytosolic Zn^{2+} into mitochondria (Malaiyandi et al., 2005), its inhibition with ruthenium red failed to prevent H_2O_2-induced mitochondrial fragmentation (Figure 4.20). Given that mitochondrial Zn^{2+} rise is TRPM2 dependent, the possibility that TRPM2 channels might be localised to mitochondria was examined. Evidence from biochemical immunocytochemical and functional studies (Figure 4.18, Figure 4.19 and Figure 4.22) supports TRPM2 expression in mitochondria. Remarkably, in the absence of TRPM2 expression, oxidant-induced mitochondrial Zn^{2+} influx, as well as mitochondrial

fragmentation, were completely abolished (Figure 4.21). Taken together, the data suggest that Zn^{2+} released during LMP could enter mitochondria via mitochondrial TRPM2 channels.

How TRPM2-mediated Zn^{2+} entry regulates mitochondrial fragmentation was next investigated. Previous studies have shown that oxidative stress causes mitochondrial membrane depolarisation and that depolarisation drives mitochondrial fission by inducing cytoplasmic Drp1 recruitment to mitochondria (Archer, 2013; Cereghetti et al., 2008; Friedman and Nunnari, 2014; Slupe et al., 2013; Youle and van der Bliek, 2012). It is also known that excess Zn^{2+} causes mitochondrial depolarisation by inhibiting the electron transport chain (Sensi et al., 2009). These previous studies led to posit that TRPM2-mediated mitochondrial Zn^{2+} entry promotes Drp1 recruitment. Consistent with this speculation, in the absence of TRPM2-mediated rise in mitochondrial Zn^{2+}, oxidative stress failed to induce Drp-1 recruitment (Figure 4.23, Figure 4.24 and Figure 4.25). Previous studies have shown that excess mitochondrial fission is associated with mitochondrial membrane permeabilisation (MMP) and cell death (Suen et al., 2008), which will be investigated in the next chapter (chapter 5). Thus the finding that TRPM2-mediated rise in mitochondrial Zn^{2+} promotes Drp1 recruitment and therefore mitochondrial fission represents an important signalling mechanism underlying oxidative stress-induced apoptosis.

In summary, the discovery of a signalling role for TRPM2 channels and inter-organelle Zn^{2+} dynamics in mitochondrial fragmentation (Figure 4.26) provides important insights and new treatment avenues for a large group of late age-onset diseases (neurodegenerative diseases, cardiovascular disease, diabetes and cancer) because aging is associated with an increase in oxidative stress and mitochondrial fragmentation.

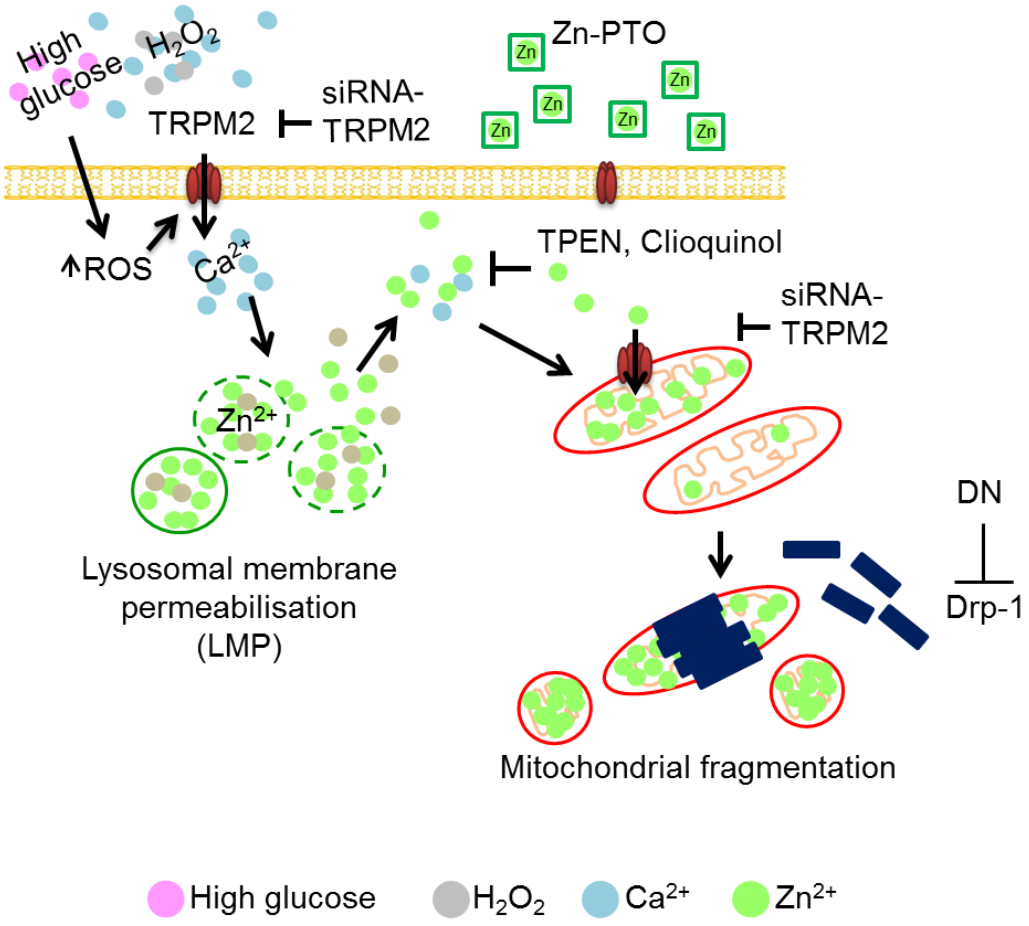

Figure 4.26 Schematic illustrating the role of TRPM2 channels and inter-organelle Zn^{2+} dynamics in oxidative stress-induced mitochondrial fragmentation

High glucose-induced rise in intracellular ROS leads to activation of plasma membrane TRPM2 channels and Ca^{2+} influx. The resultant rise in intracellular Ca^{2+} triggers lysosomal permeabilisation and Zn^{2+} release. Zn^{2+} thus released enters mitochondria via TRPM2 channels to induce recruitment of cytoplasmic Drp1, thereby increasing mitochondrial fragmentation. Genetic/chemical manipulations used to elucidate the mechanism are indicated. Similar results were obtained when exogenous oxidative stress (H_2O_2) was used as TRPM2 activator.

4.4 Preliminary data to be confirmed in the future

4.4.1 ROS-induced mitophagy is TRPM2 dependent

ROS are known to induce mitophagy (Scherz-Shouval and Elazar, 2007), where damaged and dysfunctional mitochondria are removed by lysosomes and eventually degraded (Scherz-Shouval and Elazar, 2007; Scherz-Shouval and Elazar, 2011; Youle and Narendra, 2011). This process is crucial to protect the cell from oxidative stress and to prevent cell death (Scherz-Shouval and Elazar, 2007). The potential role of TRPM2 channels in oxidative stress-induced mitophagy was examined. HUVECs were co-transfected with LAMP-1-GFP (lysosomal marker, green) and Mito-Cherry (mitochondrial marker, red) and exposed to H_2O_2 in the presence and absence of TRPM2 blockers. Parallel studies were also performed where HUVECs were transfected with control or TRPM2-directed siRNA. The results show that H_2O_2 not only causes mitochondrial fragmentation, but also leads to mitophagy; the latter is evident from the presence of mitochondria (Mito-Cherry labelled) in the lysosomes (LAMP-1-GFP labelled). TRPM2 blockers, in addition to silencing TRPM2-siRNA, prevented mitochondrial fragmentation and mitophagy (Figure 4.28). These data suggest that TRPM2 channels mediate ROS-induced mitophagy. However, these data are from preliminary experiments (performed twice) that need to be repeated using complementary biochemical studies.

To conclude, TRPM2 activation channels not only play a role in mitochondrial fragmentation but also in mitophagy.

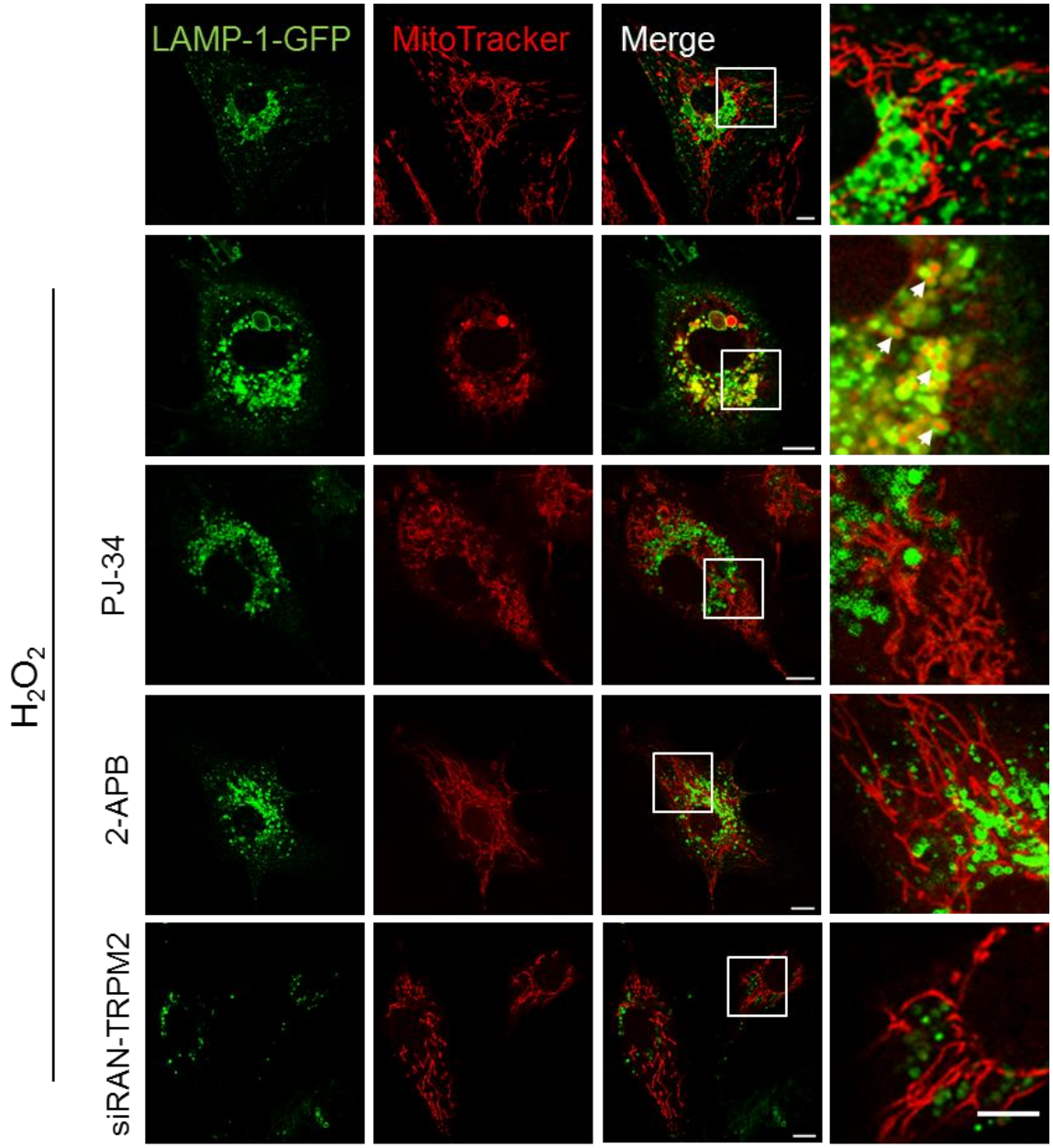

Figure 4.27 H_2O_2-induced mitophagy is prevented by inhibition of TRPM2 channels

HUVECs were co-transfected with Lamp-1-GFP and pMito-Cherry and incubated with 1 mM H_2O_2 for 3h at 37°C in the presence and absence of TRPM2 blockers (10 µM PJ-34 or 150 µM 2-APB). Alternatively, cells were pre-transfected with siRNA targeted to TRPM2 channels. Representative confocal images are shown. Scale bar, 10 µm. Boxed regions are magnified in the right panels. Scale bar, 5 µm.

5 | TRPM2-mediated, $Ca2^{+}$-potentiated Zn^{2+} release causes mitochondrial ROS amplification and endothelial cell apoptosis

5.1 Introduction

Reactive oxygen species (ROS) such as superoxide ($O_2^{\bullet-}$) and hydrogen peroxide (H_2O_2) play important roles in the normal physiology and patho-physiology of most organisms (Bedard and Krause, 2007; Li and Shah, 2004; Sena and Chandel, 2012; Trachootham et al., 2008). At low levels, they play beneficial roles by mediating cell signalling and survival (Trachootham et al., 2008), but at chronic high levels, they can cause cellular damage (D'Autreaux and Toledano, 2007; Sena and Chandel, 2012). Chronic elevation of ROS is associated with the pathogenesis of most age-related illnesses, including neuronal (Alzheimer's, Parkinson's) (Trushina and McMurray, 2007), cardiovascular (atherosclerosis, myocardial infarction) (Li and Shah, 2004; Lum and Roebuck, 2001) and metabolic/inflammatory (diabetes and hypertension) disorders (Giacco and Brownlee, 2010). A common feature of many of these illnesses is ROS-induced increase in cell death (Li and Shah, 2004). Prevention of excessive ROS production could therefore be regarded as a potential strategy to increase the healthy lifespan of organisms (Balaban et al., 2005; Giorgio et al., 2007).

There are many cellular mechanisms that contribute to vascular endothelial mitochondrial ROS generation, including NAD(P)H oxidase, xanthine oxidase, uncoupled endothelial nitric oxide (NO) synthase (eNOS) and mitochondrial electron leakage (Du et al., 1999; Finkel and Holbrook, 2000; Griendling, 2005; Li and Shah, 2004). However, the mitochondrial electron transport chain is the site of ROS generation in the most mammalian cells (Li and Shah, 2004). Electron transport chain consists of four protein complexes located in the inner mitochondrial membrane: complex I, complex II, complex III and complex IV. Superoxide ($O_2^{\bullet-}$) is generated by complex I and complex III (Finkel and Holbrook, 2000). It diffuses into the matrix of the

mitochondria and into the intermembrane space, while some superoxide escapes to the cytosol via voltage-dependent mitochondrial anion channel (VADC) (Raha and Robinson, 2000). Superoxide is converted to hydrogen peroxide (H_2O_2) by superoxide dismutase (SOD), which is subsequently detoxified to water (H_2O) by glutathione peroxidase (GPX) (Raha and Robinson, 2000). Recently, mitochondrial ROS generation has received more consideration as a potential key regulator for many diseases (Chouchani et al., 2014; Lin and Beal, 2006; Newsholme et al., 2007; Zhang and Gutterman, 2007).

ROS-induced apoptotic cell death is complex, involving several intracellular organelles (Du et al., 1999; Ferri and Kroemer, 2001). In the ER, ROS cause misfolding of proteins and induce the unfolded protein response (Haynes et al., 2004). In the nucleus, ROS induce cumulative damage to nuclear DNA (Kim et al., 2005; Yu et al., 2002). In the mitochondria, ROS induce depolarisation of membrane potential (ψ_m), breakdown of the mitochondrial network and mitochondrial membrane permeabilisation (MMP) (Boya et al., 2003; Ferri and Kroemer, 2001; Suen et al., 2008). MMP results in the release of apoptotic factors including cytochrome *c* into the cytoplasm (Boya et al., 2003; Suen et al., 2008; Wang, 2001). ROS also act on lysosomes, causing lysosomal membrane permeabilisation (LMP) and release of pro-apoptotic cathepsins (Boya et al., 2003; Ferri and Kroemer, 2001). Although some of these events are thought to cause cell death independently, there appears to be cross-talk between different organelles during ROS-induced apoptosis. For example, DNA damage leads to chronic activation of the DNA repair enzyme poly-ADP ribose polymerase (PARP). PARP transfers ADP-ribose moieties from NAD^+ to damaged proteins that are subsequently released by PARG (Kim et al., 2005). ADP-ribose triggers cell death by activating the mitochondria-mediated pathway. Similarly, cathepsins released during LMP can activate the t-bid protein that induces MMP and release of apoptotic factors (Kroemer et al., 2007). Thus molecular signals generated in the nucleus and lysosomes appear to cause cell death by acting on mitochondria.

In this chapter, I hypothesised that TRPM2 channels play a role in ROS-induced cell death by increasing LMP and MMP. To address this aim, human umbilical vein endothelial cells (HUVECs) were exposed to H_2O_2 or high concentration of glucose (diabetic conditions) as it has been shown previously that high glucose leads to apoptotic cell death by increasing cellular levels of ROS (Du et al., 1998). The role of TRPM2 channels in H_2O_2- and glucose-induced cell death was examined using pharmacological and RNAi approaches. TRPM2 channels generate signals, Ca^{2+} and Zn^{2+}, both of which are associated with cell death (Manna et al., 2015; Ye et al., 2014). Therefore, this chapter also examined the role of Ca^{2+} and Zn^{2+} signals in the induction of endothelial cell death.

5.2 Results

5.2.1 TRPM2-mediated, Ca^{2+}-potentiated Zn^{2+} release causes endothelial cell apoptosis

It has been well established that H_2O_2 activation of TRPM2 channels causes death of many cell types (Sumoza-Toledo and Penner, 2011; Takahashi et al., 2011). This has been attributed to a rise in cytosolic Ca^{2+} (Hara et al., 2002; Perraud et al., 2001; Sumoza-Toledo and Penner, 2011; Takahashi et al., 2011) as well as Zn^{2+} (Manna et al., 2015; Ye et al., 2014). Thus the role of TRPM2 channels and the two ions were examined in endothelial cell death using a cell death assay based on Hoechst 33342 and propidium iodide (PI) staining (Manna et al., 2015); Hoechst 33342 stains all cells (blue), whereas PI stains dead cells (red), allowing determination of percent cell death.

Figure 5.1A-B shows that H_2O_2 (1 mM; 6 hr) treatment causes a marked increase in cell death. Silencing of TRPM2 channels with siRNA, or inhibition with 150 µM 2-APB, or chelation of Zn^{2+} with 0.3 µM TPEN and 2 µM clioquinol, or chelation of Ca^{2+} with 2.5 µM BAPTA-AM and 2 mM EGTA, reduced endothelial cell death significantly. This finding indicates that H_2O_2-induced extracellular Ca^{2+} entry plays a significant role in oxidant-induced cell death. This finding is indeed in agreement with the numerous reports that TRPM2-mediated Ca^{2+} entry promotes cell death (Sumoza-Toledo and Penner, 2011; Takahashi et al., 2011). However, it does not explain the finding that chelation of Zn^{2+} alone can inhibit cell death. These findings led to the speculation that TRPM2-mediated Ca^{2+} entry augments Zn^{2+} release.

To test this, H_2O_2-induced Zn^{2+} release was examined by loading HUVECs with FluoZin3-AM and measuring the increase in fluorescence (due to rise in free Zn^{2+} levels) with FlexStation II. The results show that in the absence of extracellular Ca^{2+}, H_2O_2 caused a small but significant increase in Zn^{2+} release (Figure 5.1C-D). However, this increase was markedly enhanced by extracellular Ca^{2+} (Figure 5.1E-F), supporting the idea that Ca^{2+} entry augments Zn^{2+} release.

Cell death can occur by apoptosis or necrosis (van Engeland et al., 1998; Vanden Berghe et al., 2010). Images in Figure 5.1A suggest that cell death occurred predominantly by apoptosis. H_2O_2 caused marked changes to nuclear morphology and plasma membrane integrity. Compared with the normal nuclear morphology in control cells, cells treated with H_2O_2 showed significant nuclear fragmentation, which is a hallmark of apoptosis. Besides nuclear fragmentation, some cells showed loss of plasma membrane integrity, which is reflected by the fact that nuclei of these cells were stained with PI. Such phenotype indicates secondary necrosis, which follows apoptosis. A few others showed normal-looking nuclei, but stained red, indicating potential necrosis. To differentiate between various forms of cell death, cells were co-stained with PI and FITC-labeled annexin V (Figure 5.2); the latter binds phosphatidylserine exposed to the outer leaflet of the phospholipid bilayer and reports apoptosis (van Engeland et al., 1998). The results (Figure 5.2) confirm that cell death during the H_2O_2 treatment occurred predominantly by apoptosis as evident from annexin V staining. Again, both TRPM2 inhibitors (PJ34 and 2-APB) and the Zn^{2+} chelator, TPEN, prevented H_2O_2-induced apoptotic cell death. Collectively, these findings led to the conclusion that Ca^{2+}-potentiated Zn^{2+} release contributes to cell death (apoptosis).

In diabetes, endothelial cells are exposed to high glucose conditions. Studies have shown that high glucose has a number of deleterious effects on endothelial cells and that these are largely mediated by an increase in ROS production (Du et al., 1998). Given that H_2O_2 is a ROS, it is reasonable to speculate that the effects of high glucose would be similar to those of H_2O_2. To test this, HUVECs were exposed to normal (5 mM) and high (33 mM) glucose (HG) media or to a medium containing 5 mM glucose and 28 mM mannitol (to exclude any effects from osmotic changes). The results show that HG causes a significant increase in endothelial cell death. Furthermore, these effects were fully rescued by TRPM2 inhibition with 2-APB, PJ34 and siRNA targeted to TRPM2, as well as by Zn^{2+} chelation with TPEN (Figure 5.3A-B).

Taken together these data indicate that high glucose causes endothelial cell death through TRPM2-mediated changes in Zn^{2+} homeostasis. Whilst Ca^{2+} does contribute to

cell death, the data presented here suggest that its action is perhaps not direct. By augmenting the release of Zn^{2+}, extracellular Ca^{2+} entry appears to drive cell death.

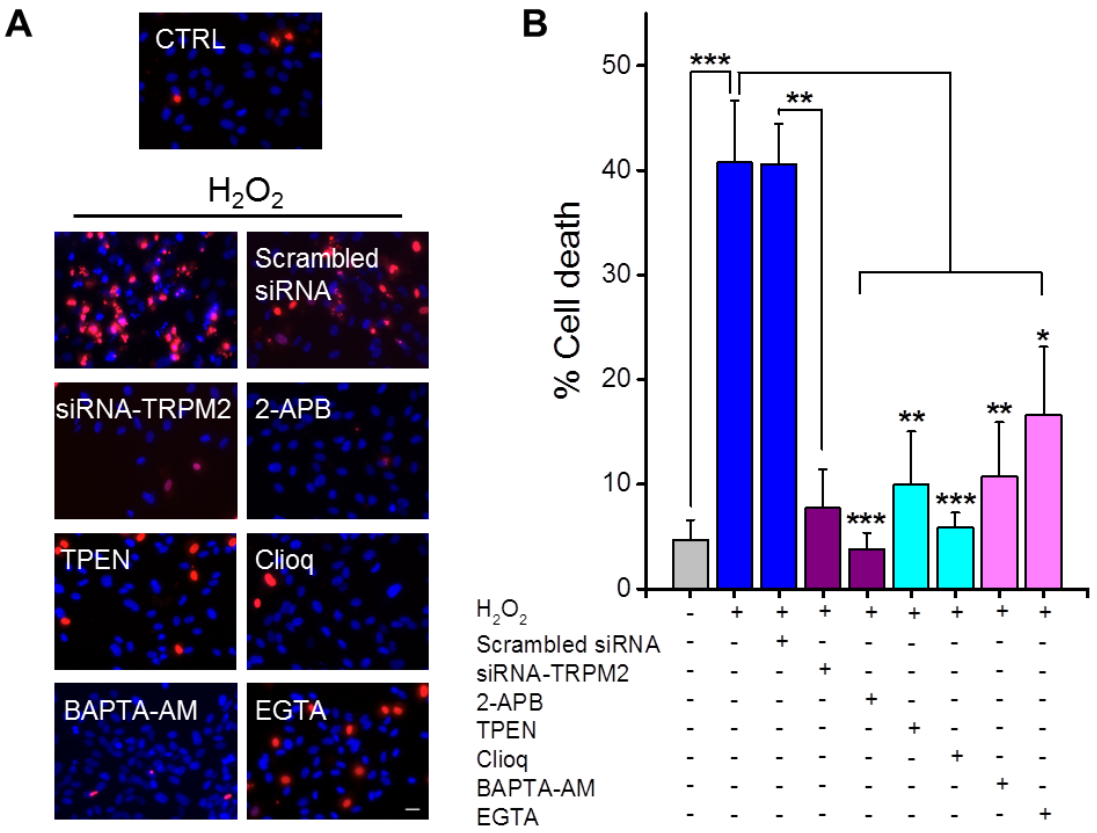
A
CTRL
H2O2
Scrambled siRNA
siRNA-TRPM2
2-APB
TPEN
Clioq
BAPTA-AM
EGTA
B
% Cell death
H2O2
Scrambled siRNA
siRNA-TRPM2
2-APB
TPEN
Clioq
BAPTA-AM
EGTA
C
SBS: Ca2+ -free
H2O2
CTRL
3 mM H2O2
Zni2+ [F]
Time (min)
D
HUVECs
Δ Zni2+ [F]
CTRL
H2O2
E
SBS: 1.5 mM Ca2+
H2O2
CTRL
3 mM H2O2
Zni2+ [F]
Time (min)
F
HUVECS
Δ Zni2+ [F]
CTRL
H2O2

Figure 5.1 Extracellular Ca^{2+} entry augments H_2O_2-induced Zn^{2+} release and endothelial cell death

(A) H_2O_2-induced cell death is dependent on TRPM2 activation, Zn^{2+} and Ca^{2+} entry. HUVECs were exposed to medium alone (CTRL) or to medium with1 mM H_2O_2 for 6 hr at 37°C in the presence of TRPM2 inhibitors or metal ion chelators (Zn^{2+} chelators: 0.3 µM TPEN or 2 µM clioquinol; Ca^{2+} chelators: 2.5 µM BAPTA-AM or 2 mM EGTA). Where indicated cells were transfected with scrambled siRNA or siRNA-TRPM2 prior to exposure to H_2O_2. Cells were stained with Hoechst 33342 (blue) and propidium iodide (PI) (red) to detect total number of cells and dead cells respectively. Images were captured with an epifluorescent microscope (EVOS). Scale bar, 10 µm.

(B) Mean ± SEM of percent cell death following the indicated treatments as in (A), n = 3. Number of cells scored ≥ 170 cells.

Statistical analysis was performed by one-way ANOVA with Tukey's post-hoc test, **p* <0.05, ***P* < 0.01, and ****P* < 0.001, and *****P* < 0.0001.

(C) H_2O_2-induced Zn^{2+} release from HUVECs. HUVECs, loaded with FluoZin-3-AM, were exposed to 3 mM H_2O_2 (time over which H_2O_2 was applied is indicated by the horizontal bar) and Zn^{2+} fluorescence (530 nm) was recorded using FlexStation II (Molecular Devices). The recording solution was Ca^{2+}-free SBS. Symbols represent mean values and errors bars represent SEM.

(D) Mean ± SEM of change in Zn^{2+} fluorescence calculated from the data in (C), n = 3.

(E) Experiment was performed as in (C) except that the recording solution contained 1.5 mM Ca^{2+}.

(F) Mean ± SEM of change in Zn^{2+} fluorescence calculated from the data in (E), n = 3.

Statistical analyses (D and F) were performed by Student's t-test, **p* <0.05.

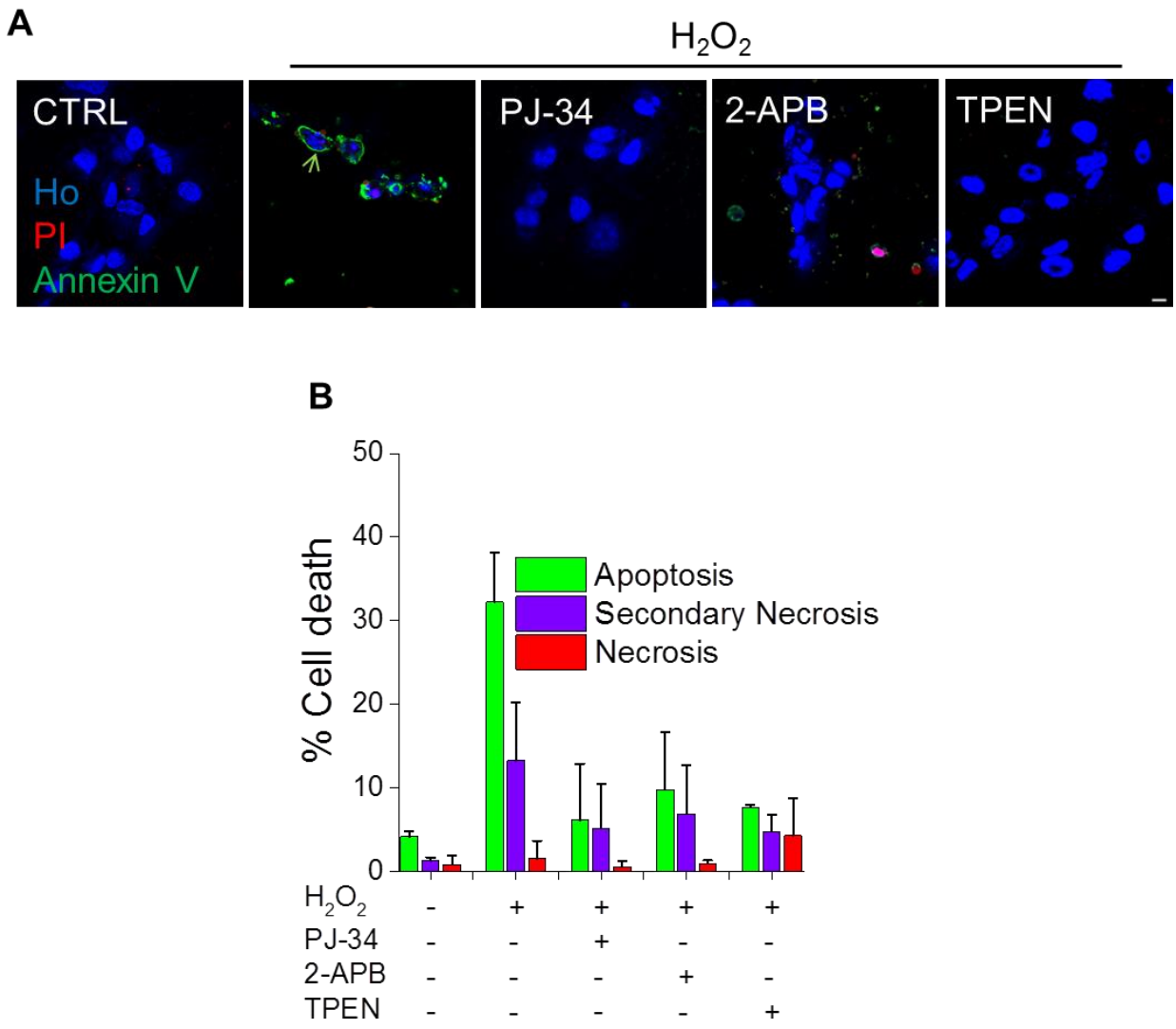

Figure 5.2 H_2O_2 causes apoptotic cell death in a TRPM2-dependent manner

(A) HUVECs were exposed to the medium alone (CTRL) or to H_2O_2 (plus or minus the indicated compounds: 10 µM PJ-34 or 150 µM 2-APB or 0.3 µM TPEN) and stained with Hoechst 33342 (blue), PI (red) and annexin-V-Alexa^{488} (green) to get a measure of total number of cells, necrotic cells and apoptotic (green arrow) cells respectively. Images were captured by confocal laser scanning microscope. Scale bar, 10 µm.

(B) Mean ± SEM of percent cell death by apoptosis (cells stained with annexin-V-Alexa^{488}), secondary necrosis (cell stained with both annexin-V-Alexa^{488} and PI) and necrosis (cell stained with PI) following the indicated treatments as in (A); n/N=2/≥ 170 cells.

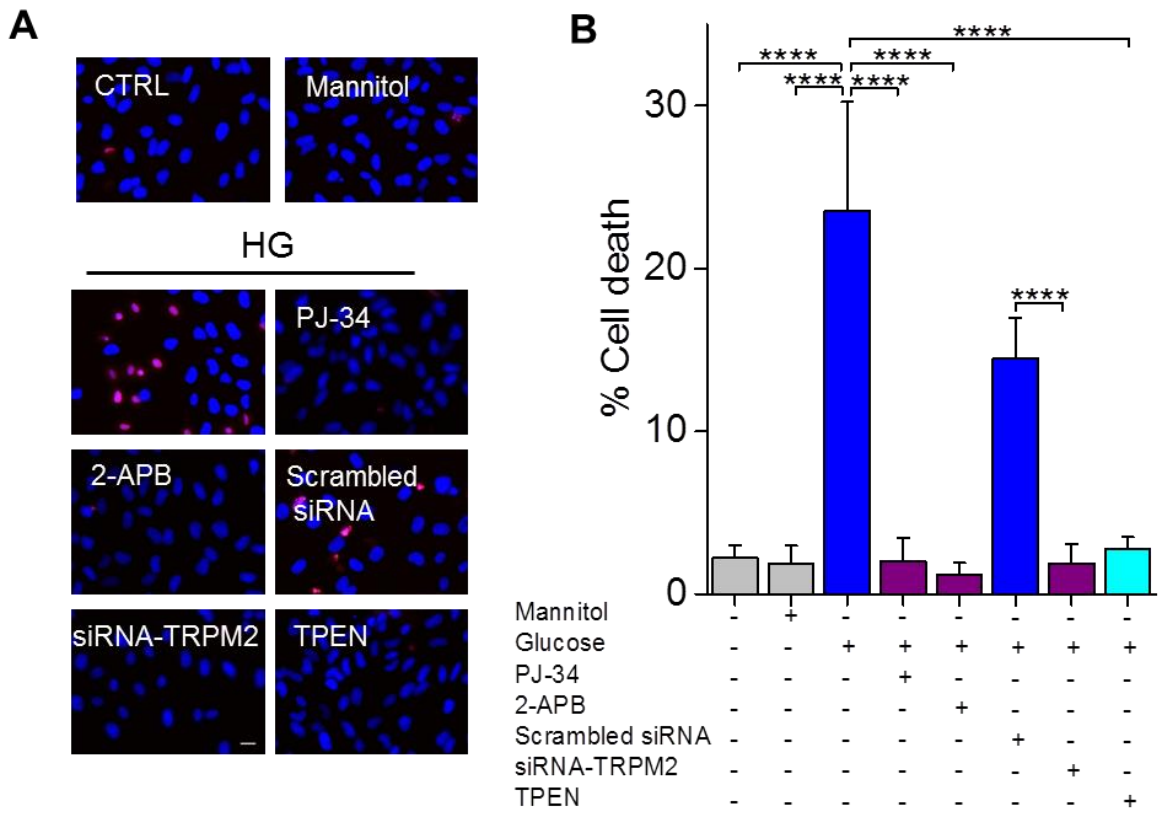

Figure 5.3 TRPM2 inhibition and Zn^{2+} chelation prevent high glucose-induced death of HUVECs

(A) High glucose-induced cell death is dependent on TRPM2 activation and Zn^{2+}. Cells were exposed to medium alone (CTRL) or medium with 28 mM mannitol plus 5 mM glucose, or medium with 33 mM glucose (HG) plus or minus the indicated treatments. Incubation was for 48 hr at 37°C. Cells were transfected with scrambled siRNA or siRNA-TRPM2 before exposure to glucose. Cells were stained with Hoechst 33342 (blue) and propidium iodide (PI) (red) to detect total number of cells and dead cells respectively. Images were captured with an epifluorescent microscope (EVOS). Scale bar, 10 µm.

(B) Mean ± SEM of percent cell death corresponding to data in (A), n = 3. Number of cells scored ≥ 300 cells.

Statistical analysis was performed by one-way ANOVA with Tukey's post-hoc test, **p* <0.05, ***P* < 0.01, ****P* < 0.001 and *****P* < 0.0001.

5.2.2 Role of TRPM2 channels in lysosomal membrane permeabilisation (LMP) and mitochondrial membrane permeabilisation (MMP)

Previous studies have suggested that oxidative stress leads to LMP, which in turn leads to MMP and, finally, to cell death (Boya et al., 2003; Galluzzi et al., 2009). As outlined in the previous section, TRPM2 activation by H_2O_2 induces endothelial cell death. The aim of this section was to examine whether TRPM2 channels regulate LMP and MMP. LMP was assessed by examining the release of lysosomal cathepsins B into the cytoplasm; MMP was determined by examining the release of mitochondrial cytochrome *c* into the cytoplasm. The results show that TRPM2 channel inhibition prevented H_2O_2-induced LMP and MMP as judged by the inhibition of cytosolic release of cathepsin B and cytochrome *c* respectively (Figure 5.4). Given the previous evidence that LMP triggers MMP (Boya et al., 2003), it is reasonable to suggest that the primary site of TRPM2 action in relation to cell death is likely lysosomes. These results suggest that activation of TRPM2 channels causes cell death by inducing LMP and MMP.

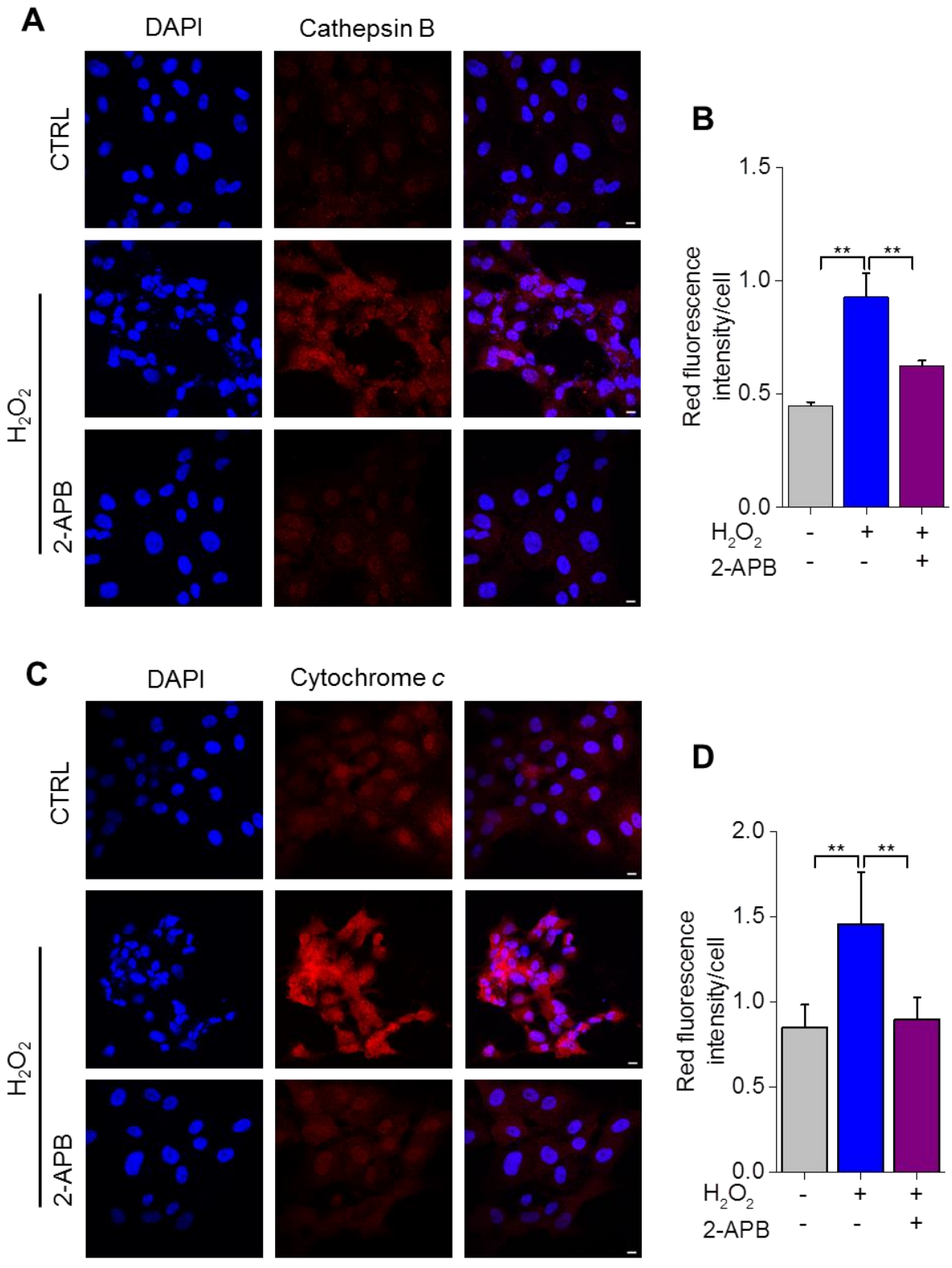
A
DAPI
Cathepsin B
CTRL
H_2O_2
2-APB
B
Red fluorescence intensity/cell
1.5
1.0
0.5
0.0
**
**
H_2O_2 - + +
2-APB - - +
C
DAPI
Cytochrome c
CTRL
H_2O_2
2-APB
D
Red fluorescence intensity/cell
2.0
1.5
1.0
0.5
0.0
**
**
H_2O_2 - + +
2-APB - - +

Figure 5.4 H_2O_2-induced lysosomal membrane permeabilisation (LMP) and mitochondrial membrane permeabilisation (MMP) is dependent on TRPM2 activation

(A) HUVECs were not treated (CTRL) or treated with H_2O_2 (1 mM) in the presence and absence of 150 µM 2-APB before immunostaining for cathepsin B and the nucleus with DAPI (see materials and methods); representative fluorescent images are shown. Cytoplasmic staining of cathepsins B indicates LMP; inhibition by 2-ABP indicates a role for TRPM2 channels.

(B) Fluorescence intensity per cell of cathepsin B stain from 63 cells, n = 3.

(C) HUVECs were not treated (CTRL) or treated with H_2O_2 in the absence or presence of 150 µM 2-APB before immunostaining for cytochrome *c*. Representative images are shown. Scale bar, 10 µm. Increase in the cytoplasmic levels of cytochrome *c* indicates MMP.

(D) Fluorescence intensity per cell of cytochrome *c* from 81 cells, n = 3.

Bars are the means ± SEM, statistical analysis in (B) and (D) were performed by one-way ANOVA with Tukey's post-hoc test, $^{**}P < 0.01$.

5.2.3 TRPM2 plays a role in intracellular ROS production

Mitochondria are the major site of ROS production. The mechanism of ROS production and its metabolism in mitochondria is well understood (Lesnefsky et al., 2001). However, what regulates mitochondrial ROS production is unclear. The results in Chapter 4 demonstrated that oxidative stress induces accumulation of Zn^{2+} in mitochondria and that this is TRPM2 dependent. Since Zn^{2+} is known to increase mitochondrial ROS production by inhibiting the electron transport chain (Donadelli et al., 2009), it is conceivable that TRPM2-mediated rise in mitochondrial Zn^{2+} contributes to mitochondrial ROS production. To test this possibility, the effect of depletion of TRPM2 channels using siRNA on high glucose-induced intracellular ROS generation was examined. HUVECs were initially maintained in EGM-2 medium containing 5.5 mM glucose (control; CTRL). For high glucose experiments, cells were incubated in 33 mM glucose. ROS generation was measured by using the cell-permeant 2',7'-dichlorodihydrofluorescein diacetate (H_2DCFDA). This dye is a stable nonpolar compound (Bass et al., 1983). It diffuses into the cells and where it is hydrolysed to yield dichlorodihydrofluorescein (DCFH). Intracellular ROS oxidises H_2DCF to the fluorescent compound DCF. The intensity of the fluorescence is proportional to the amount of ROS. The data in Figure 5.5A show that HG, but not mannitol, caused a significant increase in intracellular ROS which could be quenched with NAC. Importantly, siRNA-TRPM2, but not scrambled siRNA, completely inhibited cytosolic ROS production, indicating a role for TRPM2 channels in HG-induced ROS production.

In order to test if TRPM2-mediated Zn^{2+} entry into mitochondria causes ROS production, HUVECs were transfected with scrambled siRNA (negative control) or with siRNA-TRPM2. Cells were incubated with Zn-PTO (Zn-PTO; 0.7 µM Zn^{2+}: 0.5 µM pyrithione) to increase the cytosolic levels of Zn^{2+} in the cell. The data in Figure 5.5B show that silencing of TRPM2 expression blocked Zn-PTO-induced ROS production significantly, just like TPEN and NAC. Taken together, these data indicate that TRPM2 channel activation and Zn^{2+} elevation upregulate intracellular ROS production.

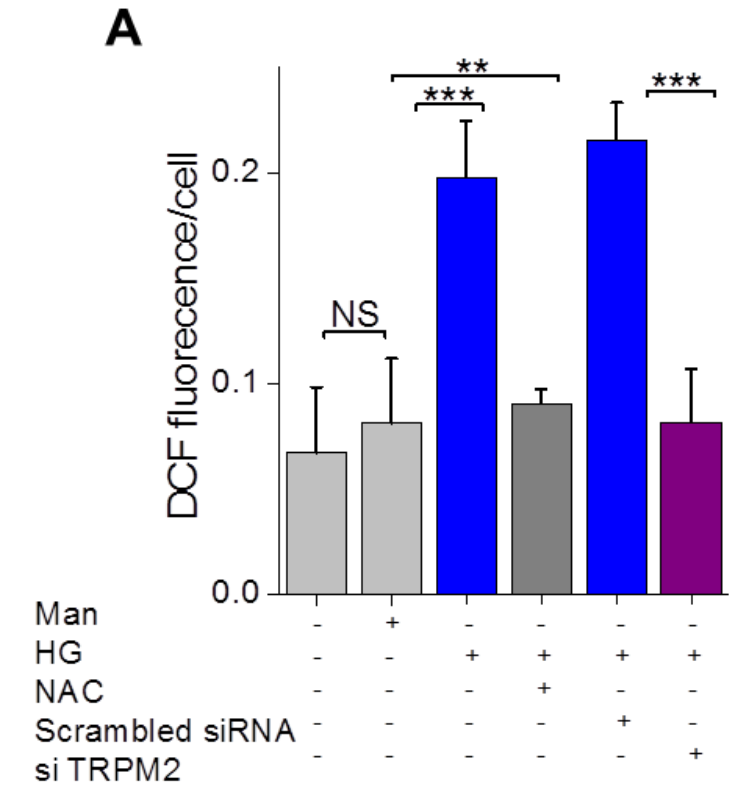
A
DCF fluorecence/cell
0.0
0.1
0.2
NS
**
***
***
Man
HG
NAC
Scrambled siRNA
si TRPM2

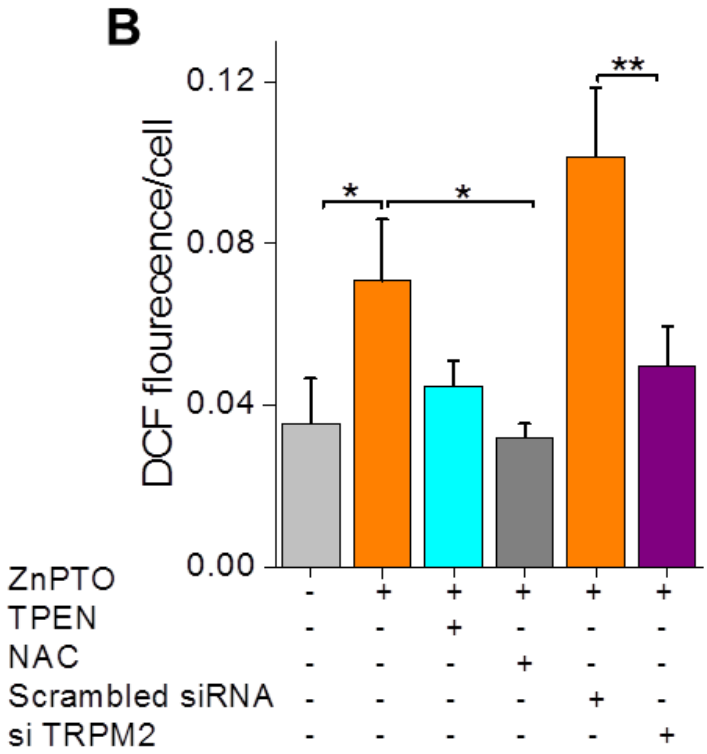
B
DCF flourecence/cell
0.00
0.04
0.08
0.12
*
*
**
ZnPTO
TPEN
NAC
Scrambled siRNA
si TRPM2

Figure 5.5 Intracellular ROS generation is mediated by TRPM2 activation

(A) HG-induced ROS production is prevented by the silencing of TRPM2 expression. HUVECs were exposed to medium alone (CTRL) or to medium with 28 mM mannitol plus 5 mM glucose, or to medium with 33 mM glucose (HG) plus or minus 10 mM NAC. Incubation was for 48 hr at 37°C. Cells were transfected with scrambled siRNA or siRNA-TRPM2 before exposure to glucose. Cells were stained with the H_2DCFDA ROS reporter to detect DCF fluorescence. Images were captured with an epifluorescent microscope (EVOS) and analysed by the ImageJ software. Data are presented as Mean ± SEM of fluorescence intensity/cell, n = 3. Number of cells scored ≥ 100.

(B) Zinc pyrithione-induced ROS production is prevented by the silencing of TRPM2 expression. HUVECs were treated for 1 hr with zinc pyrithione (Zn-PTO; 0.7 µM Zn^{2+}: 0.5 µM pyrithione) in the absence or presence of TPEN (0.3 µM TPEN) or N-acetyl cysteine (NAC, 10 mM), or HUVECs were transfected with scrambled or TRPM2 siRNA. Cells were stained and analysed as in (A). Data are presented as Mean ± SEM of fluorescence intensity per cell, n = 3. Number of cells scored ≥ 100.

Statistical analysis was performed by one-way ANOVA with Tukey's post-hoc test, **p* <0.05, ***P* < 0.01and ****P* < 0.001.

5.2.4 Mitochondrial ROS production

It has been well established that mitochondria are the major source of ROS (reactive oxygen species) in most mammalian cells (Li and Shah, 2004). Mitochondrial ROS are mainly generated by two complexes of the mitochondrial transport chain, complex I, which is the NADH-ubiquinone oxidoreductase, and complex III, which is the uniquinol-cytochrome *c* oxidoreductase (Finkel and Holbrook, 2000). Production of mitochondrial ROS contributes to oxidative damage to the membrane, DNA and mitochondrial proteins. The results in Figure 5.6 indicate that HG increases total ROS production, but does not indicate whether these ROS are of mitochondrial origin. To address this, MitoSOX^{TM} Red, a reagent specific for mitochondrial ROS (Munusamy and MacMillan-Crow, 2009), was used. It is a fluorogenic dye targeted to mitochondria specifically. It is suitable for live cells and produces red fluorescence when attacked by superoxide (Munusamy and MacMillan-Crow, 2009). HUVECs were initially maintained as maintained in Figure 5.3. The data show that HG, but not mannitol, causes an increase in mitochondrial ROS production, a finding that is in agreement with previous findings (Munusamy and MacMillan-Crow, 2009; Sun et al., 2010). This effect was prevented by TRPM2-siRNA; thus, TRPM2 channels appear to regulate mitochondrial ROS production. NAC (antioxidant)-treated cells, as expected, showed no MitoSOX Red staining (Figure 5.6A-B).

To confirm the role of TRPM2 channels in mitochondrial ROS production, the HEK-TRPM2^{tet} recombinant cell system was used. The results (Figure 5.6C-D) show that glucose has no effect on mitochondrial ROS production in not-induced (-TRPM2) cells, but cause a significant increase in cells induced to express TRPM2 channels (+TRPM2).

Similar results were obtained when cells were subjected to direct oxidative stress using H_2O_2 (Figure 5.6E-G). No difference was seen in the mean of MitoSOX Red intensity between control (CTRL) cells and cells treated with H_2O_2 in the absence of induction of TRPM2 channels (Figure 5.6E and G). By contrast, in cells induced to express TRPM2 channels, H_2O_2 caused an increase in mitochondrial ROS production (Figure 5.6F and

G). Interestingly, there is a marked shrinkage of nuclei which is a sign of apoptosis (Kroemer et al., 1998). This result is consistent with previous reports where H_2O_2 was shown to increase mitochondrial ROS generation (Tochigi et al., 2013). However, the present study indicates, for the first time, that TRPM2 ion channels play a key role in high glucose- and hydrogen peroxide-induced mitochondrial ROS production.

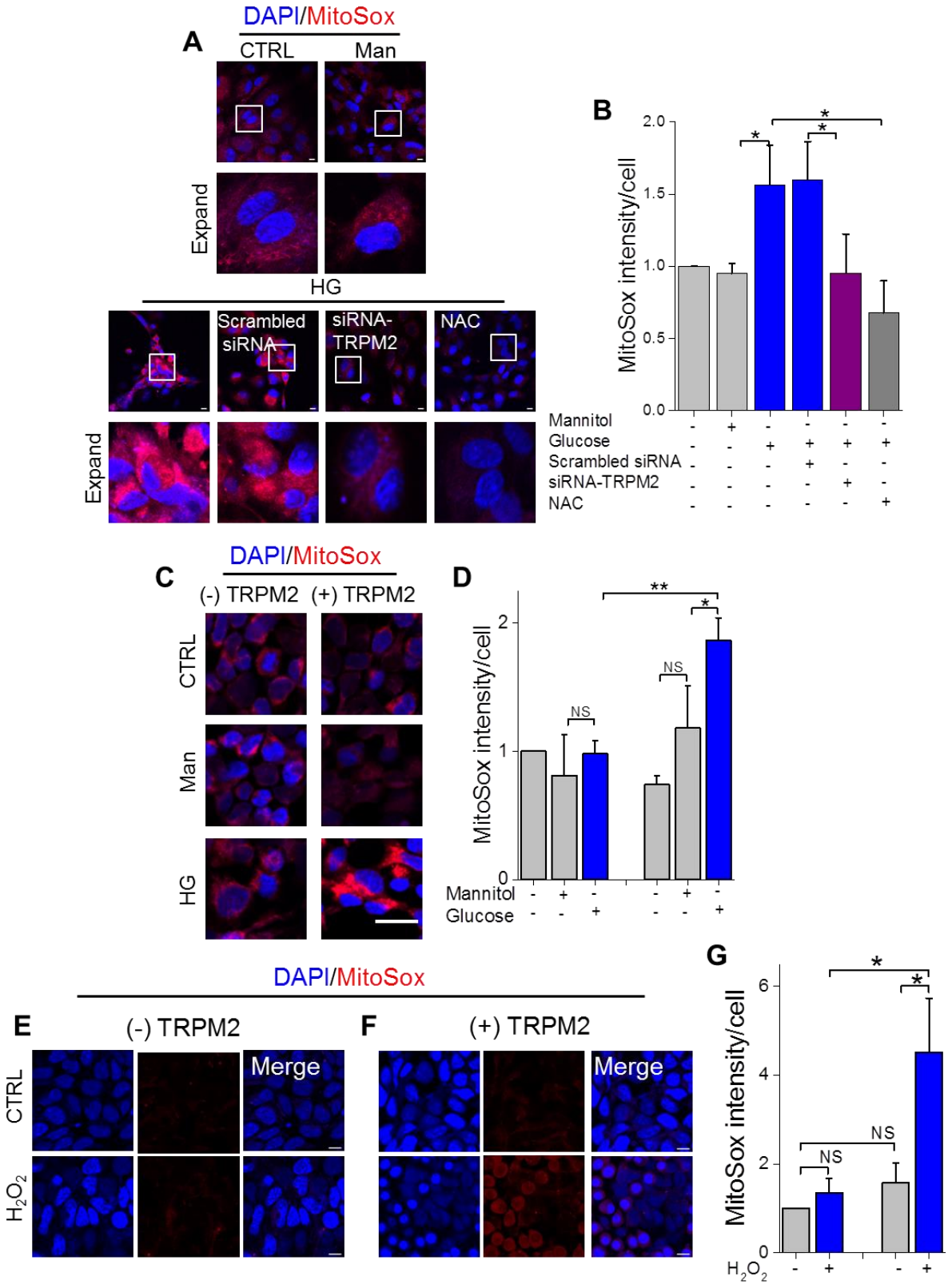
DAPI/MitoSox
A
CTRL
Man
Expand
HG
Scrambled siRNA
siRNA-TRPM2
NAC
Expand
B
MitoSox intensity/cell
2.0
1.5
1.0
0.5
0.0
Mannitol
Glucose
Scrambled siRNA
siRNA-TRPM2
NAC
DAPI/MitoSox
C
(-) TRPM2
(+) TRPM2
CTRL
Man
HG
D
MitoSox intensity/cell
2
1
0
NS
NS
Mannitol
Glucose
DAPI/MitoSox
E
(-) TRPM2
F
(+) TRPM2
CTRL
H_2O_2
Merge
Merge
G
MitoSox intensity/cell
6
4
2
0
NS
NS
H_2O_2

Figure 5.6 TRPM2 channels regulates mitochondrial ROS production

(A) TRPM2 channels mediate mitochondrial ROS generation**.** HUVECs were treated as in Figure 5.6. Mitochondrial ROS were determined by loading cells with 1 µM MitoSox^{TM} Red fluorescent dye for 30 min at 37°C. Cells were washed, fixed with 2% PFA and blocked with PBS-1% ovalbumin. Images were captured using a confocal microscope and analysed by ImageJ. The data show that silencing of TRPM2 channels prevented high glucose-induced Mito-ROS production. Scale bar, 10 µm. Boxed regions are magnified. Scale bar, 5 µm.

(B) Mean ± SEM of fluorescence intensity/cell corresponding to data in (A), n = 3. Number of cells scored ≥ 180 cells.

(C) HEK-TRPM2^{tet} cells were incubated with medium alone (CTRL) or with medium containing 30 mM glucose for 18 hr. Staining was performed as in (A). Representative confocal images show that high glucose induces significant increase in Mito-ROS levels in cells expressing TRPM2 channels (+TRPM2), but not in the cells not expressing TRPM2 channels (-TRPM2). Scale bar, 5 µm.

(D) Mean ± SEM of fluorescence intensity/cell corresponding to data in (C), n = 3. Number of cells scored ≥ 400.

(E-F) HEK-TRPM2^{tet} cells were incubated with SBS alone (CTRL) or SBS containing 200 µM H_2O_2 for 90 min. Staining was performed as in (A). Representative confocal images show that H_2O_2 induces no Mito-ROS production in cells not expressing TRPM2 channels (-TRPM2), but a marked increase in Mito-ROS levels in cells induced to express TRPM2 channels (+TRPM2). Scale bar, 10 µm.

(G) Mean ± SEM of fluorescence intensity/cell corresponding to data in (E and F), n = 3. Number of cells scored ≥ 400.

Statistical analysis (B, D and G) was performed by one-way ANOVA with Tukey's post-hoc test, **p* <0.05 and ***P* < 0.01.

5.2.5 Effect of Oxidative stress on plasma membrane TRPM2 ion channels

It is not known whether oxidative stress affects the steady-state levels of TRPM2 channels. To address this, the effect of oxidative stress on the surface expression of HA-tagged TRPM2 channels was examined. HEK-MSR cells were transfected with TRPM2-HA and incubated with 100 µM H_2O_2 overnight (~18 hr) or with 33 mM glucose for 48 hr (to allow sufficient intracellular ROS generation). TRPM2-HA expression was detected by staining the permeabilised cells with anti-HA antibodies. Images in Figure 5.7 show that in untreated cells (control) there was no detectable staining of TRPM2-HA channels at the cell surface, with the majority of staining being intracellular. By contrast, in both H_2O_2 and high glucose treated cells, there was clear staining of the cell surface. However, for reasons unclear, when unpermeabilised cells were stained for the extracellular HA epitope, there was no discernible membrane staining. These data suggest that oxidative stress may increase the plasma membrane expression of TRPM2 channels. However, further studies, including quantification of imaging data and surface biotinylation assays (Mankouri et al., 2006), are required to support this conclusion.

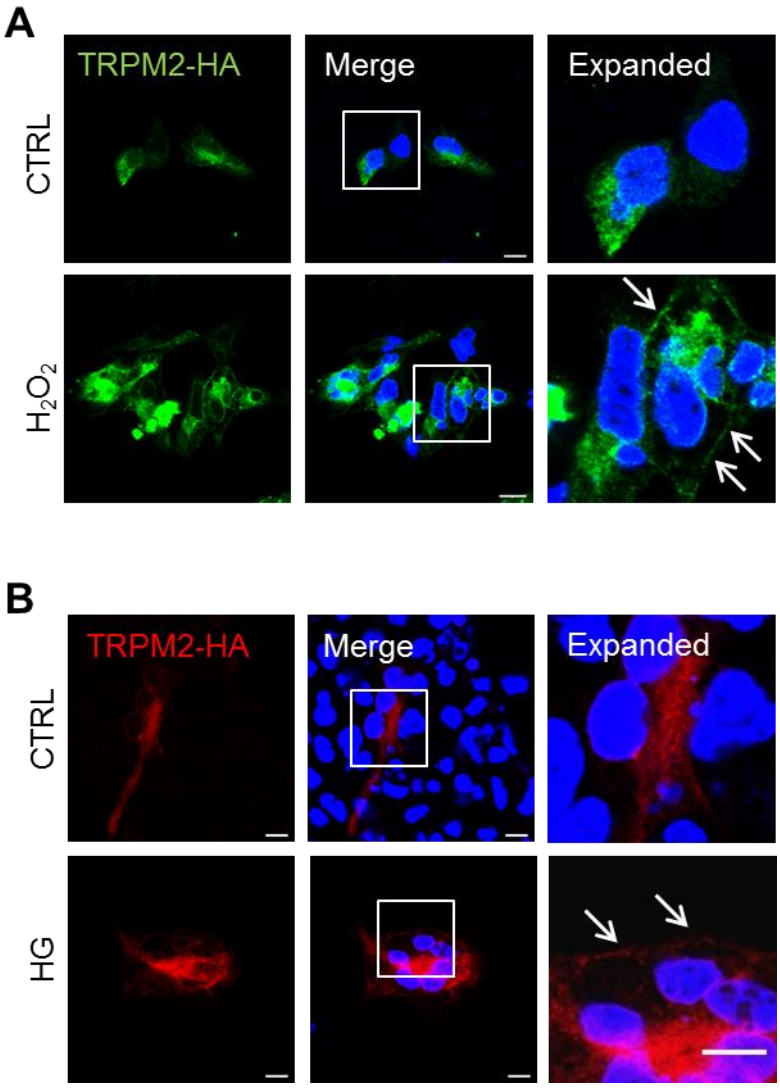

Figure 5.7 H_2O_2 enhanced detection of plasma membrane expression of TRPM2 channels

HEK-MSR cells were transfected with TRPM2-HA and incubated with 100 µM H_2O_2 overnight (18 hr) or with 33 mM glucose for 48 hr at 37°C. Cells were fixed, permeabilised, incubated with rat anti-HA, and stained with Alexa Fluor^{488} conjugated secondary antibody (A) or Cy3 conjugated secondary antibody (B).

Images show plasma membrane expression of TRPM2 channels (indicated with white arrows) in H_2O_2 (A) or HG (B) treated cells. Blue staining corresponds to nuclei. Scale bar, 10 µm, Boxed regions are magnified. Scale bar, 5 µm. Representative images are shown; experiment was performed three times.

5.2.6 Internalisation of TRPM2 channels

There are no previous reports on the internalisation of plasma membrane TRPM2 channels. If the channels are internalised, like most membrane proteins, they are expected to enter endosomes. For these experiments, HeLa cells were transfected with TRPM2-HA or hERG-HA. The latter was used as a positive control, as previous studies have shown that hERG-HA is efficiently internalised in these cells (Karnik et al., 2013). Transferrin receptor is routinely used as a marker of endosomes; when transferrin binds its receptor, the ligand-receptor complex is internalised by clathrin-mediated endocytosis (Mukherjee et al., 1997; Rajendran et al., 2010). Fluorescent-labelled transferrin is often used as marker to detect clathrin-coated endosomal vesicles (Mankouri et al., 2006; Mukherjee et al., 1997; Rajendran et al., 2010). To examine the internalisation of TRPM2-HA channels, surface TRPM2 channels were labelled with anti-HA antibodies and the internalised antibodies were detected using fluorescent secondary antibodies. AlexaFluor488-labelled transferrin was included during internalisation to see if the internalised TRPM2 channels entered the same compartments as transferrin. The results (Figure 5.8) show that TRPM2-HA channels were indeed internalised and that internalisation of TRPM2 channels was greater in the presence of H_2O_2, as revealed by the increase in the number of transferrin-positive endosomes containing TRPM2-HA channels (i.e. colocalisation between internalised TRPM2-HA and endocytosed fluorescent transferrin). However, in the control, from looking at different fields, internalisation of TRPM2 channels could not be seen. This might be due to less membrane expression of TRPM2 or the cells not being transfected. These data suggest that TRPM2 channels undergo clathrin-mediated endocytosis. However, the impact of H_2O_2 on the trafficking of TRPM2 channels, and the underlying mechanisms, need further investigation.

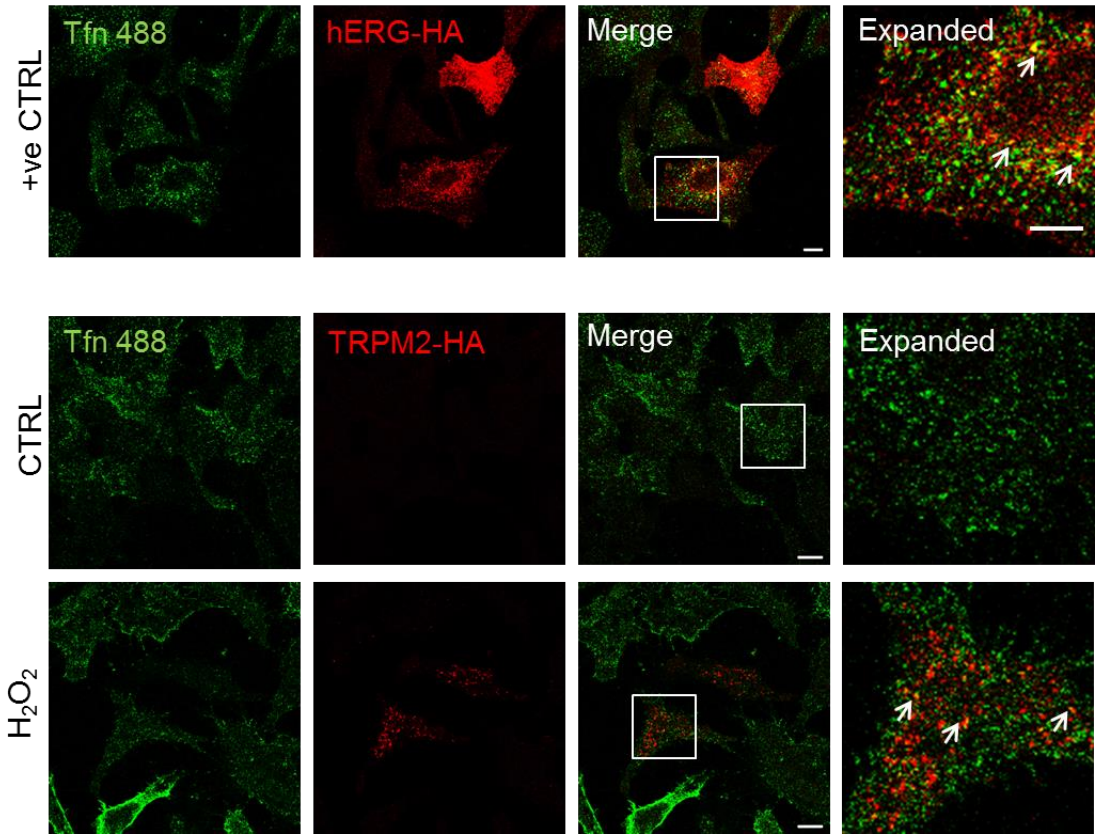

Figure 5.8 TRPM2 channels are internalised into transferrin positive vesicles

HeLa cells were transfected with hERG-HA (control; CTRL) or TRPM2-HA. The cells were blocked with 1% ovalbumin for 1 hr at 4°C. Cells were then incubated with rat anti-HA antibodies in the presence and absence of 200 µM H_2O_2 for 2 hr at 37°C. Alexa Fluor^{488}-conjugated transferrin was added during the last 15 min of incubation. Cells were fixed, permeabilised and the channels labelled with Cy3 conjugated anti-rat secondary antibodies. Representative confocal images are shown. Scale bar, 10 µM, n=2. Boxed regions are magnified. Scale bar, 5 µm.

5.3 Discussion

Oxidative stress leads to programmed cell death by generating a complex array of signals from different organelles of the cell (Avery, 2011; Ferri and Kroemer, 2001). In this chapter, the effect of H_2O_2 and high glucose (diabetic) stress on Ca^{2+} and Zn^{2+} dynamics and endothelial cell death (apoptosis) was investigated. The key findings are as follows: (i) activation of TRPM2 channels promotes cell death via apoptosis by affecting the dynamics of both Ca^{2+} and Zn^{2+}; (ii) TRPM2 activation and Ca^{2+} entry are important to enhance Zn^{2+} release from an intracellular source; (iii) chelation of Zn^{2+} alone was sufficient to prevent endothelial cell death; (iv) H_2O_2-induced cell death involves TRPM2-mediated LMP and MMP; (v) inhibition of TRPM2 channels prevents high glucose-induced mitochondrial ROS production, revealing an unsuspected role for TRPM2 channels in mitochondrial ROS generation; and, finally, (vi) H_2O_2 enhances TRPM2 translocation to the membrane. These findings have important implications for diabetes and a number of other degenerative diseases, where ROS generation features as a key pathological event.

5.3.1 TRPM2-mediated Zn^{2+} release enhances endothelial cell death

It has been reported that activation of TRPM2 channels by H_2O_2 induces apoptotic endothelial cell death because of cellular Ca^{2+} overload (Sun et al., 2012). However, the results of the present study show that besides BAPTA-AM and EGTA, Zn^{2+}-specific chelators (TPEN and clioquinol) were able to inhibit H_2O_2-induced apoptosis of HUVECs. Since chelation of Zn^{2+} alone was found to be sufficient to prevent cell death, these findings suggest that Zn^{2+} plays a major role in endothelial cell death. These results are consistent with the previous studies on the INS-1 pancreatic β- cell line (Manna et al., 2015).

Besides increasing the cytosolic levels of Ca^{2+}, H_2O_2 also caused an increase in the levels of free Zn^{2+} (Figure 5.1), a result that is consistent with the previous report with INS-1 cells (Manna et al., 2015) and the data presented in Chapter 4. The source of this

cytotoxic Zn^{2+} is likely intracellular because cell death occurred in the absence of free form of Zn^{2+} in the extracellular solution.

It has been reported previously that H_2O_2 causes DNA fragmentation and nuclear condensation which are apoptotic signs (Kapuscinski, 1995; Zhang and Xu, 2000). These effects of H_2O_2 have been shown to be reduced by silencing TRPM2 expression (Sun et al., 2012). The data presented in Figure 5.1 and Figure 5.2 indicate that H_2O_2-induced cell death is not only blocked by TRPM2 blockers and TRPM2-siRNA, but also by Zn^{2+} chelators. The data were confirmed by using a more physiologically relevant system (Figure 5.3), where cell death induced by high glucose (Ho et al., 2000) was reduced by blocking TRPM2 channels with PJ-34 and 2-APB and by silencing TRPM2 channels with TRPM2 siRNA. Notably, Zn^{2+} chelators blocked endothelial cell death significantly. These findings represent the first demonstration of the role of TRPM2 ion channels and Zn^{2+} in high glucose-induced endothelial cells death.

5.3.2 Inhibition of TRPM2 channels prevents H_2O_2-induced LMP and MMP

Current evidence indicates that LMP leads to MMP, and MMP, in turn, causes apoptosis (Boya and Kroemer, 2008). However, how LMP signals MMP is not fully understood. Previous studies reported that cathepsins released during LMP activate t-bid and promote recruitment of pro-apoptotic Bax proteins to the outer mitochondrial membrane (Boya et al., 2003; Boya and Kroemer, 2008). By forming pores in the outer membrane, Bax induces MMP and release of pro-apoptotic factors including cytochrome *c* (Boya and Kroemer, 2008). However, prevention of LMP with TRPM2 blockers was able to prevent MMP; this suggests that Zn^{2+} released during LMP likely serves as a signal for MMP (Figure 5.4). Consistent with this idea, as shown in the previous chapter's Figure 4.12 and Figure 4.13, Zn^{2+} released during LMP accumulates in mitochondria and Zn^{2+} is a known inducer of MMP (Sensi et al., 2009). Regardless of the mechanism, however, the data indicate that LMP is not a nonspecific mechanism (Boya et al., 2003; Boya and Kroemer, 2008), but instead it is a regulated process involving TRPM2-mediated signalling. Thus TRPM2-regulated Zn^{2+} is the potential elusive molecular link between LMP and MMP.

5.3.3 The TRPM2 channel is a key regulator of ROS production

It has been previously reported that high glucose-induced apoptosis is mediated by intracellular ROS production (Du et al., 1999). However, the underlying mechanism is still not clear. The current chapter investigated whether activation of TRPM2 channels enhances ROS production in endothelial cells, and if so, whether depletion of TRPM2 channels can prevent ROS generation during oxidative stress. The rationale behind this is the finding that TRPM2 channels mediate free Zn^{2+} accumulation in mitochondria (Chapter 4) and the fact that free Zn^{2+} inhibits the electron transport chain at sites where ROS are generated (Clausen et al., 2013). HUVECs were incubated with high glucose and ROS was monitoring by DCF-fluorescence dye. The results demonstrate that high glucose triggers ROS production (Figure 5.5A). This finding is in agreement with the previous studies (Ho et al., 2006). Importantly, silencing of TRPM2 channels with siRNA prevented high glucose-induced ROS generation.

To test the idea that TRPM2-mediated Zn^{2+} entry into mitochondria is responsible for ROS generation, HUVECs were treated with Zn-PTO to raise cytosolic Zn^{2+}, and the effect of silencing TRPM2 was examined. Zn-PTO caused a significant increase in intracellular ROS production, an effect that was prevented by Zn^{2+} chelator and antioxidant (Figure 5.5B); this finding is consistent with a previous report (Seo et al., 2001). As predicted, siRNA-TRPM2 caused a significant reduction in ROS generation. Thus, the present findings demonstrate a role for TRPM2 channels in ROS generation.

There are many endogenous sources of ROS production. Oxidants are generated from different cytosolic enzyme systems including NAD(P)H oxidase (NOX), xanthine oxidase, uncoupled endothelial nitric oxide (NO) synthase (eNOS) and mitochondrial electron leakage (Griendling, 2005; Li and Shah, 2004) and as result of the intracellular metabolism in mitochondria and peroxisomes (Finkel and Holbrook, 2000). The data presented in Figure 5.5A-B demonstrated that high glucose and raising intracellular Zn^{2+} cause a rapid increase in total cellular ROS production, and silencing of TRPM2 channels prevents these effects. It is possible that the rise is due to ROS production by

the mitochondria rather than NOX activation, because previous reports have shown that Ca^{2+} influx, but not intracellular Zn^{2+}, activates NOX (Clausen et al., 2013).

It is also possible that Ca^{2+} entry through plasma membrane TRPM2 channels increases cytoplasmic ROS by activating NOX5 by binding to EF hand motifs (Nauseef, 2008) as NOX5 is expressed in endothelial cells (BelAiba et al., 2007). Cytoplasmic ROS could in turn induce mitochondrial ROS production and amplify ROS generation through the process of ROS-induced ROS release (RIRR) (Zorov et al., 2014). However, according to the data presented in the current chapter, cytoplasmic ROS were not at detectable levels by DCF staining. It might due to the low level of NADPH oxidation.

The main source of mitochondrial ROS ($O_2^{\bullet-}$) is respiratory complexes I and III which are located in the inner mitochondrial membrane (Clausen et al., 2013; Finkel and Holbrook, 2000). Complex I receives electrons from NADH and generates NAD^+ (Yu and Bennett, 2014). These electrons are then transported to complex III via ubiquinone and finally to O_2 to generate water (Yu and Bennett, 2014). During this process, however, some electrons can escape to generate $O_2^{\bullet-}$. $O_2^{\bullet-}$ is converted to H_2O_2 by MnSOD and H_2O_2 is reduced to water by GPXs or catalase (Yu and Bennett, 2014) (see section 1.2.2). Being membrane permeable, H_2O_2 can escape into the cytoplasm.

Studies have shown that during pathological situations such as diabetes and Alzheimer's, the concentration of free Zn^{2+} is elevated in the primary pancreatic islet beta-cells and neuronal cells (Bellomo et al., 2011; Weiss et al., 2000). Zn^{2+} enables the production of ROS by inhibiting complex I. Inhibition of complex I prevents electron transport to complex III (Kushnareva et al., 2002). Therefore, its accumulation at complex I enhances ROS production (Kushnareva et al., 2002). So, it is possible that the observed rise in ROS (Figure 5.5A-B) is from the inhibition of complex I. In the previous chapter, it was shown that TRPM2 channels can exist in mitochondria where they promote Zn^{2+} entry into mitochondria. Thus Zn^{2+} entry through mitochondrial TRPM2 channels could inhibit complex I leading to ROS generation from mitochondria

(Figure 5.6) and the subsequent increase in cytosolic ROS. ROS is thought to escape from mitochondria via mitochondrial permeability transition pore (mPTP) (Zorov et al., 2014). Thus these findings provide a mechanistic insight into the regulation of mitochondrial ROS production.

5.3.4 Oxidative stress-enhanced detection of TRPM2 membrane expression

Studies have shown that trafficking of ion channels, receptors and transporters to the plasma membrane and subsequent endocytosis can be affected by ligands (Simons and Toomre, 2000; Valluru et al., 2005). Little is known about trafficking of TRPM2 channels. The results of this chapter show that the presence of H_2O_2 and high glucose treatment makes TRPM2 channels in the plasma membrane detectable (Figure 5.7). Although TRPM2 channels bearing an extracellular HA-tag were used in these studies, for reasons unclear, surface expression was not apparent in nonpermeabilised cells, but could be detected in permeabilised cells. Thus independent evidence using surface protein biotinylation experiments needs to be obtained to confirm H_2O_2 induced increase in surface expression of TRPM2 channels.

The Finding in Figure 5.7 was further confirmed by performing internalisation experiments where endocytosis of TRPM2-HA channels was followed along with the transferrin receptor, a well-established marker of endocytosis. The results demonstrated endocytosis of TRPM2-HA channels (Figure 5.8). Co-localisation of the internalised channels with the transferrin receptor suggested that TRPM2 channels are internalised via clathrin-mediated endocytosis (CME). Although endocytosis of several ion channels by CME has been demonstrated (Mankouri et al., 2006; Shimkets et al., 1997), this is the first demonstration of TRPM2 endocytosis. The increase in endosomal/lysosomal localisation in H_2O_2-treated cells was consistent with the presence of plasma membrane TRPM2 channels. However, it is possible that oxidative stress slows endocytic trafficking of TRPM2 channels, thereby increasing the steady-state expression of TRPM2 channels at the plasma membrane. Trafficking of TRPM2 channels was studied

by overexpressing TRPM2 channels and using the anti-HA antibody. However, overexpression of proteins may affect the trafficking pathway (Phan et al., 2008). Thus, further studies on the trafficking of natively expressed TRPM2 channels are required.

The contribution of increased plasma membrane trafficking to H_2O_2 signalling via TRPM2 activation and cell death remains to be examined. One would expect that increased trafficking to the cell surface would increase net Ca^{2+} influx, Ca^{2+}-induced Zn^{2+} release and cell death. To test this idea requires understanding of the mechanism by which oxidative stress enhances trafficking of TRPM2 channels to the plasma membrane and specific tools to inhibit such trafficking. Regardless of the mechanism, the results suggest that dynamic regulation of membrane TRPM2 channels may play a key role in cell death.

To conclude, the results presented in the current chapter demonstrate that H_2O_2 and high glucose stress can induce endothelial cell apoptosis by affecting Zn^{2+} homeostasis. The results also demonstrate a regulatory role for TRPM2 channels in mitochondrial ROS production (Figure 5.9). They also show that oxidative stress induces plasma membrane trafficking of TRPM2 channels. Finally, the data provide preliminary evidence that TRPM2 channels are internalised via clathrin-mediated endocytosis. The latter results suggest that oxidative stress-induced changes in trafficking of TRPM2 channels may play an important role in apoptosis and require further investigation.

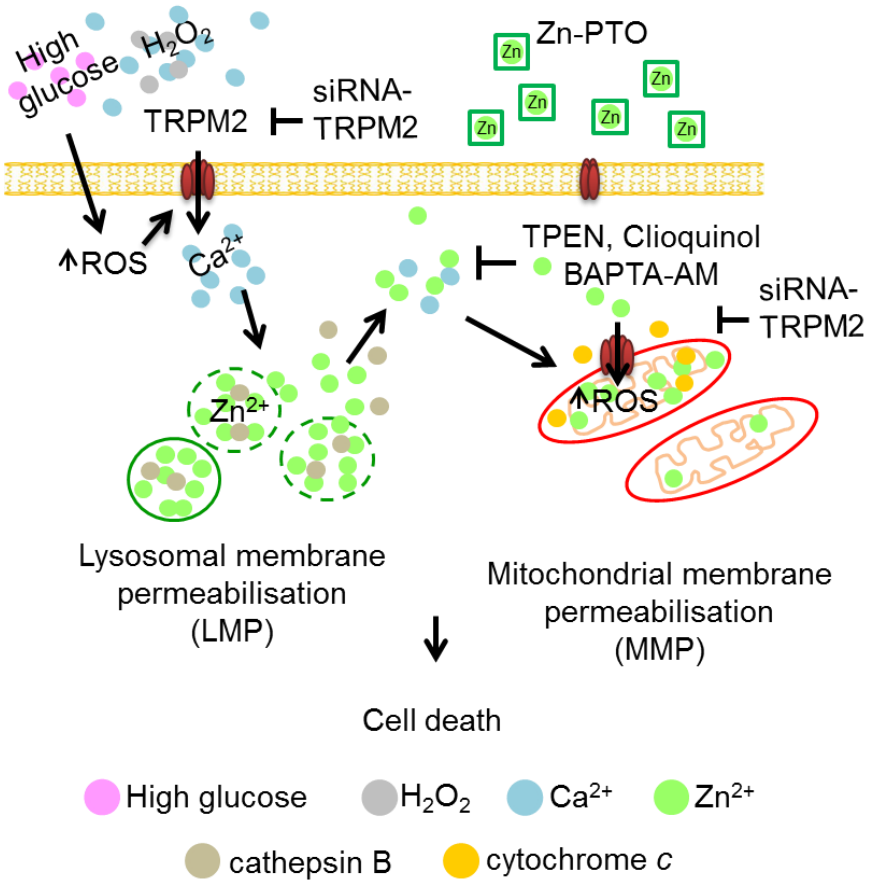

Figure 5.9 Possible pathway of TRPM2-mediated endothelial cell death

Activation of TRPM2 channels during oxidative stress (H_2O_2 or high glucose) induces Ca^{2+} influx across plasma membrane. Rise in intracellular Ca^{2+} initiates Zn^{2+} release into the cytoplasm. Ca^{2+} entry triggers LMP leading to MMP (cytochrome *c* release) and, in turn, to cell death. Cell death can be blocked by TRPM2 inhibitors (PJ-34 and 2-APB) or intracellular Zn^{2+} chelators (TPEN and clioquinol) or intracellular Ca^{2+} and Zn^{2+} chelator (BAPTA-AM). Oxidative stress induces amplification of mitochondrial ROS, which is regulated by activation of mitochondrial TRPM2 channels.

6 | Conclusion and further experiments

6.1 Summary of key findings

The data presented in Chapter 3 showed that the commercial anti-TRPM2 antibodies were not suitable to label TRPM2 channels in the plasma membrane of intact cells, as this antibody has been raised to an intracellular epitope and displays significant non-specific labelling in immunocytochemistry experiments. An HA epitope was therefore inserted into the S1-S2 extracellular loop of the TRPM2 channel using the PCR technique. The resultant construct, called TRPM2-HA, was used to transfect cells and examine intracellular distribution of the channel. It was found that TRPM2 channel expression was robust and the transfected cells showed a band with a size of ~170 kDa, which is in agreement with the previous findings (Fonfria et al., 2004). Previous studies have shown that the TRPM2 ion channel is not only a plasma membrane ion channel but also a lysosomal ion channel (Lange et al., 2009; Manna et al., 2015). However, TRPM2-HA membrane expression was not detected by immunostaining of intact (unpermeabilised) cells. Patch clamp recording, however, revealed TRPM2 currents in TRPM2-HA-transfected HEK293 cells, demonstrating that insertion of an HA-epitope does not disrupt the function of the channel. Thus, the inability to detect TRPM2-HA at the plasma membrane by immunostaining is not due to the absence of the channel. In summary, the data in Chapter 3 showed that the TRPM2-HA construct is functional and suitable for trafficking studies. However, it proved difficult to conduct endocytosis experiments (originally envisaged) as there was a lack of detectable TRPM2-HA staining at the plasma membrane.

The data presented in Chapter 4 represented the results of the investigation of the second aim. Specifically, the second aim was to determine whether oxidative stress-induced TRPM2 activation mediates mitochondrial fragmentation. Part of the second aim was also to determine whether the TRPM2 channel plays a role in the intracellular dynamics of Zn^{2+}, which has previously been shown to mediate oxidative stress-induced pancreatic β-cell death (Manna et al., 2015). To address this aim, live cell imaging,

immunostaining, ion imaging, biochemical and immuno-gold labelling techniques were carried out.

The data presented in Chapter 4 showed that oxidative stress induced mitochondrial fragmentation in human umbilical vein endothelial cells (HUVECs) exposed to high glucose levels and that the effect was mediated by TRPM2 channels; pharmacological inhibition of TRPM2 function and RNAi silencing of TRPM2 expression prevented endothelial mitochondrial fragmentation. Furthermore, knock-out of TRPM2 channels prevented mitochondrial fragmentation in mouse pulmonary endothelial cells. These findings show for the first time the role of TRPM2 channels in mitochondrial fragmentation. Previous findings indicated that TRPM2 activation increased cytosolic levels of free Ca^{2+} and Zn^{2+}. Interestingly, however, chelation of Zn^{2+} alone was sufficient to prevent TRPM2-mediated mitochondrial fragmentation. This effect of Zn^{2+} in mitochondrial fragmentation after TRPM2 activation has not been previously reported; therefore, it was examined in greater detail. Through a combination of fluorescent Zn^{2+} imaging and labelling of intracellular organelles, it was demonstrated that free Zn^{2+} is largely stored in the lysosomes. Surprisingly, oxidative stress caused a marked decrease in lysosomal Zn^{2+}, with a concomitant rise in mitochondrial Zn^{2+}. Chemical inhibition and RNAi silencing of TRPM2 channels prevented lysosomal Zn^{2+} release and uptake by the mitochondria. Elevation of cytosolic Zn^{2+} using Zn^{2+}-ionophore also caused a rise in mitochondrial Zn^{2+} and fragmentation. Thus rise in mitochondrial Zn^{2+} appears to trigger mitochondrial fragmentation. The lysosomal Zn^{2+} decrease was accompanied by a decrease in the number of lysosomes. The direct effect of Zn^{2+} on mitochondrial fragmentation has been previously reported (Park et al., 2014), but the manner by which TRPM2 channel activation leads to changes in mitochondrial dynamics through the Zn^{2+} ion is a new finding. These data provide new insights into the relationship between Zn^{2+}, LMP and mitochondrial fragmentation.

Elevation of cytosolic levels of free Ca^{2+} (using ionophore A23187) demonstrated that Ca^{2+} induces LMP within 2 hr, while mitochondrial fragmentation occurred after 4 hr. However, Zn^{2+} chelation was sufficient to prevent Ca^{2+}-induced mitochondrial

fragmentation, and the elevation of cytosolic levels of free Zn^{2+} (using pyrithione) was enough to induce mitochondrial fragmentation within 2 hr. Thus, it is possible that Ca^{2+} entry through TRPM2 channels induces LMP and Zn^{2+} release. The resultant rise in cytosolic Zn^{2+} leads to mitochondrial fragmentation. Previous findings showed that direct Zn^{2+} uptake by the mitochondria is mediated by the mitochondrial Ca^{2+} uniporter (MCU) (Malaiyandi et al., 2005); however, blocking the MCU with ruthenium red failed to prevent oxidative stress-induced mitochondrial Zn^{2+} uptake, suggesting the presence of other mechanisms.

Since mitochondrial Zn^{2+} rise is TRPM2 dependent and there is evidence that TRPM2 channels mediate Zn^{2+} uptake, mitochondria were examined for TRPM2 expression. A combination of biochemical and immunocytochemical techniques demonstrated presence of TRPM2 in the mitochondria. Furthermore, in the absence of TRPM2 channels, Zn^{2+} failed to enter the mitochondria and cause mitochondrial fragmentation. However, the TRPM2 channel lacks canonical mitochondrial targeting signals (Diekert et al, 1999; Omura, 1998). A recent study has shown that the canonical transient receptor potential 3 (TRPC3) channel lacks targeting motifs, yet the channel is capable of trafficking to mitochondria (Feng et al., 2013).

While the data presented in Chapter 4 support a role for Zn^{2+} in mitochondrial fragmentation, a role for Ca^{2+} cannot be fully excluded because FluoZin-3 dye can not only bind Zn^{2+} (K_D 15 nM) (Zhao et al., 2008) but also bind Ca^{2+} although at supraphysiological concentrations (Bastian and Li, 2007). This is a limitation of the dye as Zn^{2+} reporter.

Studies have shown that Drp1, a protein responsible for mitochondrial fission, is recruited from cytoplasm to mitochondria during oxidative stress (Ishihara et al., 2009; Loson et al., 2013; Qi et al., 2013). Accordingly, the role of TRPM2 channels and Zn^{2+} in Drp1 recruitment to mitochondria was examined. The data showed that TRPM2 activation-dependent rise in mitochondrial Zn^{2+} promotes Drp1 recruitment. In the absence of TRPM2 or in the presence of a Zn^{2+} chelator, oxidative stress failed to

induce Drp1 recruitment to mitochondria. In summary, TRPM2 channel activation works as an upstream signal for Drp1 recruitment during oxidative stress. The data in Chapter 4 thus presented the discovery of a novel mechanism where activation of TRPM2 channels causes a redistribution of Zn^{2+} from lysosomes to mitochondria, resulting in endothelial mitochondrial fragmentation.

The last aim of the thesis was to investigate the mechanisms by which elevated cytosolic Ca^{2+} and Zn^{2+} results in endothelial cell death during high glucose stress. Previous report showed that TRPM2 activation leads to Ca^{2+} entry-induced endothelial cell death (Sun et al., 2012). Another report illustrated that high glucose leads to apoptotic cell death by increasing cellular levels of ROS (Du et al., 1998). To address the aim of Chapter 5, endothelial cells were exposed to H_2O_2 or a high concentration of glucose (diabetic conditions), and the role of TRPM2 channels in H_2O_2- and glucose-induced cell death was examined using pharmacological and RNAi approaches.

The data in Chapter 5 showed that the activation of TRPM2 channels promotes cell death via apoptosis by affecting the dynamics of both Ca^{2+} and Zn^{2+}. It was found that Ca^{2+} entry via TRPM2 channels is important to enhance Zn^{2+} release from intracellular sources, leading to cell death. Intracellular Zn^{2+} chelation was enough to prevent oxidative stress-induced cell death. This finding is in agreement with the previous reports (Manna et al., 2015; Ye et al., 2014), but the interplay between Ca^{2+} and Zn^{2+} was not clear. High glucose and H_2O_2-induced increase in LMP (cathepsin B release into the cytoplasm) and MMP (cytochrome *c* release) were prevented by inhibition of TRPM2 channels.

Previous reports have shown that high glucose-induced apoptosis is mediated by intracellular ROS production, but the mechanism is still not clear (Du et al., 1999). The possibility that TRPM2 channel activation enhances ROS generation was examined. A combination of ROS monitoring with fluorescent probes and live cell imaging indicated that inhibition of TRPM2 channels indeed prevents high glucose-induced mitochondrial ROS production. This finding revealed a previously unrecognised role of TRPM2

channels in mitochondrial ROS generation. Taken together, the data presented in this chapter provided a novel mechanism by which diabetic stress causes apoptotic cell death via TRPM2 channel activation and mitochondrial ROS production.

These results likely have implications for endothelial cell death in pathophysiological situations such as diabetes, where oxidative stress increases and induces endothelial diseases including atherosclerosis, stroke and peripheral vascular disease (PAD). The development of TRPM2 inhibitors is an important new direction to be investigated in the future.

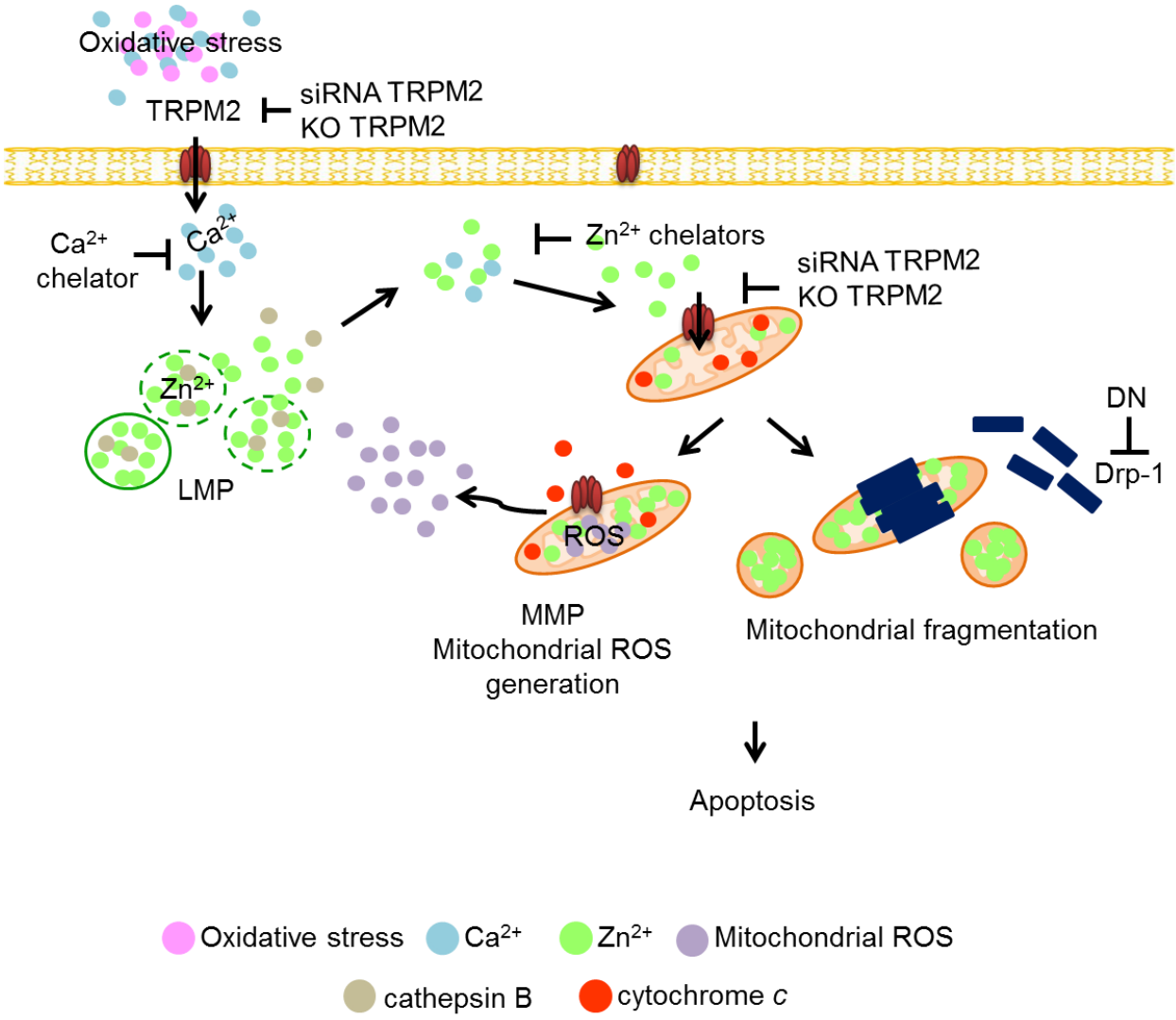

Figure 6.1 Mitochondria-mediated apoptosis is TRPM2 dependent

Oxidative stress induces TRPM2 activation in the plasma membrane thereby increasing Ca^{2+} entry. Excess intracellular Ca^{2+} induces lysosomal membrane permeability (LMP) by oxidation of membrane lipids directly or through activation of lipases (Johansson et al., 2010; Zhao et al., 2001). This leads to the release of hydrolases as well as zinc. Excess intracellular Zn^{2+} is taken up by mitochondria through mitochondrial TRPM2 channels. Silencing of TRPM2 expression or chelation of Zn^{2+} prevents Zn^{2+} redistribution from lysosomes to mitochondria. Zn^{2+} accumulation in mitochondria triggers mitochondrial ROS production and mitochondrial membrane permeability (MMP). Increase in mitochondrial Zn^{2+} leads to Drp1 recruitment to mitochondria and mitochondrial fragmentation. Finally, mitochondrial fragmentation leads to cell death. Cell death could be blocked by silencing TRPM2 expression or by TRPM2 inhibitors (PJ-34 and 2-APB), intracellular Zn^{2+} chelators (TPEN and clioquinol), and intracellular Ca^{2+} and Zn^{2+} chelator (BAPTA-AM). The sites of genetic intervention and pharmacological inhibition are shown.

6.2 Future work

The data presented in Chapter 4 showed that high glucose-induced mitochondrial fragmentation is mediated by TRPM2 channels. It would be interesting to examine if the damage could be reversed with chemical or biological inhibitors of TRPM2 channels.

Studies have shown that mitochondrial fragmentation increases in diabetic animals (Makino et al., 2010; Vincent et al., 2010; Wang et al., 2012). It would be interesting to investigate if knock-out of TRPM2 channels in diabetic animals would mitigate these effects.

The data presented in Chapter 4 revealed a previously unrecognised role for TRPM2 channels in mitochondrial dynamics. TRPM2 mediated changes in intracellular Zn^{2+} redistribution from lysosomes to mitochondria appears to underlie oxidative induced mitochondrial fragmentation. TRPM2 expression in mitochondria could be detected by biochemical and imaging techniques. However, there is no direct evidence that mitochondrial TRPM2 channels mediate Zn^{2+} entry into mitochondria. Direct patch clamping electrophysiology could provide evidence for this, but patching mitochondria is technically challenging (Kirichok et al., 2004).

Previous studies have shown that ROS production enhances mitophagy (Scherz-Shouval and Elazar, 2007; Scherz-Shouval and Elazar, 2011; Youle and Narendra, 2011). Preliminary data presented in Chapter 4 demonstrated that ROS-induced mitophagy is TRPM2 dependent. These data need to be confirmed using biochemical and microscopy-based studies, using autophagosome markers such as LC3 (Kim et al., 2007; Mizushima, 2004).

The data presented in Chapter 5 demonstrated that TRPM2 inhibition prevents H_2O_2- and high glucose-induced mitochondrial ROS production. However, other groups have reported conflicting, mitochondrial ROS level was higher in KO TRPM2 myocytes compared with WT TRPM2 myocytes (Miller et al., 2014). Further studies into the role of TRPM2 channels in mitochondrial ROS production using endothelial

cells isolated from wild-type and TRPM2 knock-out mice may help address this controversy. Furthermore, the mechanism by which TRPM2 channels regulate mitochondrial ROS production remains to be investigated.

7 | Appendix

ClustalW2 sequence alignment of human TRPM2-HA with Clone 1 of TRPM2-HA

```
Clone1          MEPSALRKAGSEQEEGFEGLPRRVTDLGMVSNLRRSNSSLFKSWRLQCPFGNNDKQESLS 60
hTRPM2-HA       MEPSALRKAGSEQEEGFEGLPRRVTDLGMVSNLRRSNSSLFKSWRLQCPFGNNDKQESLS 60
                ************************************************************

Clone1          SWIPENIKKKECVYFVESSKLSDAGKVVCQCGYTHEQHLEEATKPHTFQGTQWDPKKHVQ 120
hTRPM2-HA       SWIPENIKKKECVYFVESSKLSDAGKVVCQCGYTHEQHLEEATKPHTFQGTQWDPKKHVQ 120
                ************************************************************

Clone1          EMPTDAFGDIVFTGLSQKVKKYVRVSQDIPSSVIYHLMTQHWGLDVPNLLISVTGGAKNF 180
hTRPM2-HA       EMPTDAFGDIVFTGLSQKVKKYVRVSQDIPSSVIYHLMTQHWGLDVPNLLISVTGGAKNF 180
                ************************************************************

Clone1          NMKPRLKSIFRRGLVKVAQTTGAWIITGGSHTGVMKQVGEAVRDFSLSSSYKEGELITIG 240
hTRPM2-HA       NMKPRLKSIFRRGLVKVAQTTGAWIITGGSHTGVMKQVGEAVRDFSLSSSYKEGELITIG 240
                ************************************************************

Clone1          VATWGTVHRREGLIHPTGSFPAEYILDEDGQGNLTCLDSNHSHFILVDDGTHGQYGVEIP 300
hTRPM2-HA       VATWGTVHRREGLIHPTGSFPAEYILDEDGQGNLTCLDSNHSHFILVDDGTHGQYGVEIP 300
                ************************************************************

Clone1          LRTRLEKFISEQTKERGGVAIKIPIVCVVLEGGPGTLHTIDNATTNGTPCVVVEGSGRVA 360
hTRPM2-HA       LRTRLEKFISEQTKERGGVAIKIPIVCVVLEGGPGTLHTIDNATTNGTPCVVVEGSGRVA 360
                ************************************************************

Clone1          DVIAQVANLPVSDITISLIQQKLSVFFQEMFETFTESRIVEWTKKIQDIVRRRQLLTVFR 420
hTRPM2-HA       DVIAQVANLPVSDITISLIQQKLSVFFQEMFETFTESRIVEWTKKIQDIVRRRQLLTVFR 420
                ************************************************************

Clone1          EGKDGQQDVDVAILQALLKASRSQDHFGHENWDHQLKLAVAWNRVDIARSEIFMDEWQWK 480
hTRPM2-HA       EGKDGQQDVDVAILQALLKASRSQDHFGHENWDHQLKLAVAWNRVDIARSEIFMDEWQWK 480
                ************************************************************

Clone1          PSDLHPTMTAALISNKPEFVKLFLENGVQLKEFVTWDTLLYLYENLDPSCLFHSKLQKVL 540
hTRPM2-HA       PSDLHPTMTAALISNKPEFVKLFLENGVQLKEFVTWDTLLYLYENLDPSCLFHSKLQKVL 540
                ************************************************************

Clone1          VEDPERPACAPAAPRLQMHHVAQVLRELLGDFTQPLYPRPRHNDRLRLLLPVPHVKLNVQ 600
hTRPM2-HA       VEDPERPACAPAAPRLQMHHVAQVLRELLGDFTQPLYPRPRHNDRLRLLLPVPHVKLNVQ 600
                ************************************************************

Clone1          GVSLRSLYKRSSGHVTFTMDPIRDLLIWAIVQNRRELAGIIWAQSQDCIAAALACSKILK 660
hTRPM2-HA       GVSLRSLYKRSSGHVTFTMDPIRDLLIWAIVQNRRELAGIIWAQSQDCIAAALACSKILK 660
                ************************************************************

Clone1          ELSKEEEDTDSSEEMLALAEEYEHRAIGVFTECYRKDEERAQKLLTRVSEAWGKTTCLQL 720
hTRPM2-HA       ELSKEEEDTDSSEEMLALAEEYEHRAIGVFTECYRKDEERAQKLLTRVSEAWGKTTCLQL 720
                ************************************************************

Clone1          ALEAKDMKFVSHGGIQAFLTKVWWGQLSVDNGLWRVTLCMLAFPLLLTGLISFREKRLQD 780
hTRPM2-HA       ALEAKDMKFVSHGGIQAFLTKVWWGQLSVDNGLWRVTLCMLAFPLLLTGLISFREKRLQD 780
                ************************************************************
```

```
Clone1          VQAQEIYPYDVPDYAHLQEKGTPAARARAFFTAPVVVFHLNILSYFAFLCLFAYVLMVDF 840
hTRPM2-HA       VQAQEIYPYDVPDYAHLQEKGTPAARARAFFTAPVVVFHLNILSYFAFLCLFAYVLMVDF 840
                ************************************************************

Clone1          QPVPSWCECAIYLWLFSLVCEEMRQLFYDPDECGLMKKAALYFSDFWNKLDVGAILLFVA 900
hTRPM2-HA       QPVPSWCECAIYLWLFSLVCEEMRQLFYDPDECGLMKKAALYFSDFWNKLDVGAILLFVA 900
                ************************************************************

Clone1          GLTCRLIPATLYPGRVILSLDFILFCLRLMHIFTISKTLGPKIIIVKRMMKDVFFFLFLL 960
hTRPM2-HA       GLTCRLIPATLYPGRVILSLDFILFCLRLMHIFTISKTLGPKIIIVKRMMKDVFFFLFLL 960
                ************************************************************

Clone1          AVWVVSFGVAKQAILIHNERRVDWLFRGAVYHSYLTIFGQIPGYIDGVNFNPEHCSPNGT 1020
hTRPM2-HA       AVWVVSFGVAKQAILIHNERRVDWLFRGAVYHSYLTIFGQIPGYIDGVNFNPEHCSPNGT 1020
                ************************************************************

Clone1          DPYKPKCPESDATQQRPAFPEWLTVLLLCLYLLFTNILLLNLLIAMFNYTFQQVQEHTDQ 1080
hTRPM2-HA       DPYKPKCPESDATQQRPAFPEWLTVLLLCLYLLFTNILLLNLLIAMFNYTFQQVQEHTDQ 1080
                ************************************************************

Clone1          IWKFQRHDLIEEYHGRPAAPPPFILLSHLQLFIKRVVLKTPAKRHKQLKNKLEKNEEAAL 1140
hTRPM2-HA       IWKFQRHDLIEEYHGRPAAPPPFILLSHLQLFIKRVVLKTPAKRHKQLKNKLEKNEEAAL 1140
                ************************************************************

Clone1          LSWEIYLKENYLQNRQFQQKQRPEQKIEDISNKVDAMVDLLDLDPLKRSGSMEQRLASLE 1200
hTRPM2-HA       LSWEIYLKENYLQNRQFQQKQRPEQKIEDISNKVDAMVDLLDLDPLKRSGSMEQRLASLE 1200
                ************************************************************

Clone1          EQVAQTARALHWIVRTLRASGFSSEADVPTLASQKAAEEPDAEPGGRKKTEEPGDSYHVN 1260
hTRPM2-HA       EQVAQTARALHWIVRTLRASGFSSEADVPTLASQKAAEEPDAEPGGRKKTEEPGDSYHVN 1260
                ************************************************************

Clone1          ARHLLYPNCPVTRFPVPNEKVPWETEFLIYDPPFYTAERKDAAAMDPMGDTLEPLSTIQY 1320
hTRPM2-HA       ARHLLYPNCPVTRFPVPNEKVPWETEFLIYDPPFYTAERKDAAAMDPMGDTLEPLSTIQY 1320
                ************************************************************

Clone1          NVVDGLRDRRSFHGPYTVQAGLPLNPMGRTGLRGRGSLSCFGPNHTLYPMVTRWRRNEDG 1380
hTRPM2-HA       NVVDGLRDRRSFHGPYTVQAGLPLNPMGRTGLRGRGSLSCFGPNHTLYPMVTRWRRNEDG 1380
                ************************************************************

Clone1          AICRKSIKKMLEVLVVKLPLSEHWALPGGSREPGEMLPRKLKRILRQEHWPSFENLLKCG 1440
hTRPM2-HA       AICRKSIKKMLEVLVVKLPLSEHWALPGGSREPGEMLPRKLKRILRQEHWPSFENLLKCG 1440
                ************************************************************

Clone1          MEVYKGYMDDPRNTDNAWIETVAVSVHFQDQNDVELNRLNSNLHACDSGASIRWQVVDRR 1500
hTRPM2-HA       MEVYKGYMDDPRNTDNAWIETVAVSVHFQDQNDVELNRLNSNLHACDSGASIRWQVVDRR 1500
                ************************************************************

Clone1          IPLYANHKTLLQKAAAEFGAHY 1522
hTRPM2-HA       IPLYANHKTLLQKAAAEFGAHY 1522
                **********************
```

ClustalW2 sequence alignment of human TRPM2-HA with Clone 5 of TRPM2-HA

```
Clone5          MEPSALRKAGSEQEEGFEGLPRRVTDLGMVSNLRRSNSSLFKSWRLQCPFGNNDKQESLS 60
hTRPM2-HA       MEPSALRKAGSEQEEGFEGLPRRVTDLGMVSNLRRSNSSLFKSWRLQCPFGNNDKQESLS 60
                ************************************************************

Clone5          SWIPENIKKKECVYFVESSKLSDAGKVVCQCGYTHEQHLEEATKPHTFQGIQWDPKKHVQ 120
hTRPM2-HA       SWIPENIKKKECVYFVESSKLSDAGKVVCQCGYTHEQHLEEATKPHTFQGIQWDPKKHVQ 120
                ************************************************************

Clone5          EMPTDAFGDIVFTGLSQKVKKYVRVSQDTPSSVIYHLMTQHWGLDVPNLLISVTGGAKNF 180
hTRPM2-HA       EMPTDAFGDIVFTGLSQKVKKYVRVSQDTPSSVIYHLMTQHWGLDVPNLLISVTGGAKNF 180
                ************************************************************

Clone5          NMKPRLKSIFRRGLVKVAQTTGAWIITGGSHTGVMKQVGEAVRDFSLSSSYKEGELITIG 240
hTRPM2-HA       NMKPRLKSIFRRGLVKVAQTTGAWIITGGSHTGVMKQVGEAVRDFSLSSSYKEGELITIG 240
                ************************************************************

Clone5          VATWGTVHRREGLIHPTGSFPAEYILDEDGQGNLTCLDSNHSHFILVDDGTHGQYGVEIP 300
hTRPM2-HA       VATWGTVHRREGLIHPTGSFPAEYILDEDGQGNLTCLDSNHSHFILVDDGTHGQYGVEIP 300
                ************************************************************

Clone5          LRTRLEKFISEQTKERGGVAIKIPIVCVVLEGGPGTLHTIDNATTNGTPCVVVEGSGRVA 360
hTRPM2-HA       LRTRLEKFISEQTKERGGVAIKIPIVCVVLEGGPGTLHTIDNATTNGTPCVVVEGSGRVA 360
                ************************************************************

Clone5          DVIAQVANLPVSDITISLIQQKLSVFFQEMFETFTESRIVEWTKKIQDIVRRRQLLTVFR 420
hTRPM2-HA       DVIAQVANLPVSDITISLIQQKLSVFFQEMFETFTESRIVEWTKKIQDIVRRRQLLTVFR 420
                ************************************************************

Clone5          EGKDGQQDVDVAILQALLKASRSQDHFGHENWDHQLKLAVAWNRVDIARSEIFMDEWQWK 480
hTRPM2-HA       EGKDGQQDVDVAILQALLKASRSQDHFGHENWDHQLKLAVAWNRVDIARSEIFMDEWQWK 480
                ************************************************************

Clone5          PSDLHPTMTAALISNKPEFVKLFLENGVQLKEFVTWDTLLYLYENLDPSCLFHSKLQKVL 540
hTRPM2-HA       PSDLHPTMTAALISNKPEFVKLFLENGVQLKEFVTWDTLLYLYENLDPSCLFHSKLQKVL 540
                ************************************************************

Clone5          VEDPERPACAPAAPRLQMHHVAQVLRELLGDFTQPLYPRPRHNDRLRLLLPVPHVKLNVQ 600
hTRPM2-HA       VEDPERPACAPAAPRLQMHHVAQVLRELLGDFTQPLYPRPRHNDRLRLLLPVPHVKLNVQ 600
                ************************************************************

Clone5          GVSLRSLYKRSSGHVTFTMDPIRDLLIWAIVQNRRELAGIIWAQSQDCIAAALACSKILK 660
hTRPM2-HA       GVSLRSLYKRSSGHVTFTMDPIRDLLIWAIVQNRRELAGIIWAQSQDCIAAALACSKILK 660
                ************************************************************

Clone5          ELSKEEEDTDSSEEMLALAEEYEHRAIGVFTECYRKDEERAQKLLTRVSEAWGKTTCLQL 720
hTRPM2-HA       ELSKEEEDTDSSEEMLALAEEYEHRAIGVFTECYRKDEERAQKLLTRVSEAWGKTTCLQL 720
                ************************************************************

Clone5          ALEAKDMKFVSHGGIQAFLTKVWWGQLSVDNGLWRVTLCMLAFPLLLTGLISFREKRLQD 780
hTRPM2-HA       ALEAKDMKFVSHGGIQAFLTKVWWGQLSVDNGLWRVTLCMLAFPLLLTGLISFREKRLQD 780
                ************************************************************
```

```
Clone5          VQAQEIYPYDVPDYAHLQEKGTPAARARAFFTAPVVVFHLNILSYFAFLCLFAYVLMVDF 840
hTRPM2-HA       VQAQEIYPYDVPDYAHLQEKGTPAARARAFFTAPVVVFHLNILSYFAFLCLFAYVLMVDF 840
                ************************************************************

Clone5          QPVPSWCECAIYLWLFSLVCEEMRQLFYDPDECGLMKKAALYFSDFWNKLDVGAILLFVA 900
hTRPM2-HA       QPVPSWCECAIYLWLFSLVCEEMRQLFYDPDECGLMKKAALYFSDFWNKLDVGAILLFVA 900
                ************************************************************

Clone5          GLTCRLIPATLYPGRVILSLDFILFCLRLMHIFTISKTLGPKIIIVKRMMKDVFFFLFLL 960
hTRPM2-HA       GLTCRLIPATLYPGRVILSLDFILFCLRLMHIFTISKTLGPKIIIVKRMMKDVFFFLFLL 960
                ************************************************************

Clone5          AVWVVSFGVAKQAILIHNERRVDWLFRGAVYHSYLTIFGQIPGYIDGVNFNPEHCSPNGT 1020
hTRPM2-HA       AVWVVSFGVAKQAILIHNERRVDWLFRGAVYHSYLTIFGQIPGYIDGVNFNPEHCSPNGT 1020
                ************************************************************

Clone5          DPYKPKCPESDATQQRPAFPEWLTVLLLCLYLLFTNILLLNLLIAMFNYTFQQVQEHTDQ 1080
hTRPM2-HA       DPYKPKCPESDATQQRPAFPEWLTVLLLCLYLLFTNILLLNLLIAMFNYTFQQVQEHTDQ 1080
                ************************************************************

Clone5          IWKFQRHDLIEEYHGRPAAPPPFILLSHLQLFIKRVVLKTPAKRHKQLKNKLEKNEEAAL 1140
hTRPM2-HA       IWKFQRHDLIEEYHGRPAAPPPFILLSHLQLFIKRVVLKTPAKRHKQLKNKLEKNEEAAL 1140
                ************************************************************

Clone5          LSWEIYLKENYLQNRQFQQKQRPEQKIEDISNKVDAMVDLLDLDPLKRSGSMEQRLASLE 1200
hTRPM2-HA       LSWEIYLKENYLQNRQFQQKQRPEQKIEDISNKVDAMVDLLDLDPLKRSGSMEQRLASLE 1200
                ************************************************************

Clone5          EQVAQTARALHWIVRTLRASGFSSEADVPTLASQKAAEEPDAEPGGRKKTEEPGDSYHVN 1260
hTRPM2-HA       EQVAQTARALHWIVRTLRASGFSSEADVPTLASQKAAEEPDAEPGGRKKTEEPGDSYHVN 1260
                ************************************************************

Clone5          ARHLLYPNCPVTRFPVPNEKVPWETEFLIYDPPFYTAERKDAAAMDPMGDTLEPLSTIQY 1320
hTRPM2-HA       ARHLLYPNCPVTRFPVPNEKVPWETEFLIYDPPFYTAERKDAAAMDPMGDTLEPLSTIQY 1320
                ************************************************************

Clone5          NVVDGLRDRRSFHGPYTVQAGLPLNPMGRTGLRGRGSLSCFGPNHTLYPMVTRWRRNEDG 1380
hTRPM2-HA       NVVDGLRDRRSFHGPYTVQAGLPLNPMGRTGLRGRGSLSCFGPNHTLYPMVTRWRRNEDG 1380
                ************************************************************

Clone5          AICRKSIKKMLEVLVVKLPLSEHWALPGGSREPGEMLPRKLKRILRQEHWPSFENLLKCG 1440
hTRPM2-HA       AICRKSIKKMLEVLVVKLPLSEHWALPGGSREPGEMLPRKLKRILRQEHWPSFENLLKCG 1440
                ************************************************************

Clone5          MEVYKGYMDDPRNTDNAWIETVAVSVHFQDQNDVELNRLNSNLHACDSGASIRWQVVDRR 1500
hTRPM2-HA       MEVYKGYMDDPRNTDNAWIETVAVSVHFQDQNDVELNRLNSNLHACDSGASIRWQVVDRR 1500
                ************************************************************

Clone5          IPLYANHKTLLQKAAAEFGAHY 1522
hTRPM2-HA       IPLYANHKTLLQKAAAEFGAHY 1522
                **********************
```

8 | References

Abe, K., and R. Puertollano. 2011. Role of TRP channels in the regulation of the endosomal pathway. *Physiology*. 26:14-22.

Al-Shawaf, E., J. Naylor, H. Taylor, K. Riches, C.J. Milligan, D. O'Regan, K.E. Porter, J. Li, and D.J. Beech. 2010. Short-term stimulation of calcium-permeable transient receptor potential canonical 5-containing channels by oxidized phospholipids. *Arteriosclerosis Thrombosis and Vascular Biology*. 30:1453-1444.

Alexandre, J., F. Batteux, C. Nicco, C. Chereau, A. Laurent, L. Guillevin, B. Weill, and F. Goldwasser. 2006. Accumulation of hydrogen peroxide is an early and crucial step for paclitaxel-induced cancer cell death both in vitro and in vivo. *International Journal of Cancer*. 119:41-48.

Amantini, C., M. Mosca, M. Nabissi, R. Lucciarini, S. Caprodossi, A. Arcella, F. Giangaspero, and G. Santoni. 2007. Capsaicin-induced apoptosis of glioma cells is mediated by TRPV1 vanilloid receptor and requires p38 MAPK activation. *Journal of Neurochemistry*. 102:977-990.

American Diabetes Association. 2009. Diagnosis and classification of diabetes mellitus. *Diabetes Care*. 32:62-67.

Archer, S.L. 2013. Mitochondrial dynamics-mitochondrial fission and fusion in human diseases. *N Engl J Med*. 369:2236-2251.

Arundine, M., and M. Tymianski. 2003. Molecular mechanisms of calcium-dependent neurodegeneration in excitotoxicity. *Cell Calcium*. 34:325-337.

Arslan, P., F. Divirgilio, M. Beltrame, R.Y. Tsien, and T. Pozzan. 1985. cytosolic Ca^{2+} homeostasis in ehrlich and yoshida carcinomas - a new, membrane-permeant chelator of heavy-metals reveals that these ascites tumor-cell lines have normal cytosolic free Ca^{2+}. *Journal of Biological Chemistry*. 260:2719-2727.

Avery, S.V. 2011. Molecular targets of oxidative stress. *Biochem J*. 434:201-210.

Ayub, K., and M.B. Hallett. 2004. The mitochondrial ADPR link between Ca^{2+} store release and Ca^{2+} influx channel opening in immune cells. *Faseb Journal*. 18:1335-1338.

Balaban, R.S., S. Nemoto, and T. Finkel. 2005. Mitochondria, oxidants, and aging. *Cell*. 120:483-495.

BalazsToth, and L. Csanady. 2010. Identification of direct and indirect effectors of the transient receptor potential melastatin 2. *Biol Chem*. 285:30091-30102.

Barsoum, M.J., H. Yuan, A.A. Gerencser, G. Liot, Y.E. Kushnareva, S. Graeber, I. Kovacs, W.D. Lee, J. Waggoner, J. Cui, A.D. White, B. Bossy, J.-C. Martinou, R.J. Youle, S.A. Lipton, M.H. Ellisman, G.A. Perkins, and E. Bossy-Wetzel. 2006. Nitric oxide-induced mitochondrial fission is regulated by dynamin-related GTPases in neurons. *Embo Journal*. 25:3900-3911.

Bass, D.A., J.W. Parce, L.R. Dechatelet, P. Szejda, M.C. Seeds, and M. Thomas. 1983. Flow cytometric studies of oxidative product formation by neutrophils - a graded response to membrane stimulation. *Journal of Immunology*. 130:1910-1917.

Bastian, C., and Y.V. Li. 2007. Fluorescence imaging study of extracellular zinc at the hippocampal mossy fiber synapse. *Neuroscience Letters*. 419:119-124.

Beck, A., M. Kolisek, L.A. Bagley, A. Fleig, and R. Penner. 2006. Nicotinic acid adenine dinucleotide phosphate and cyclic ADP-ribose regulate TRPM2 channels in T lymphocytes. *Faseb Journal*. 20:962-964.

Bedard, K., and K.H. Krause. 2007. The NOX family of ROS-generating NADPH oxidases: physiology and pathophysiology. *Physiol Rev*. 87:245-313.

BelAiba, R.S., T. Djordjevic, A. Petry, K. Diemer, S. Bonello, B. Banfi, J. Hess, A. Pogrebniak, C. Bickel, and A. Goerlach. 2007. NOX5 variants are functionally active in endothelial cells. *Free Radical Biology and Medicine*. 42:446-459.

Bellomo, E.A., G. Meur, and G.A. Rutter. 2011. Glucose regulates free cytosolic Zn^{2+} concentration, Slc39 (ZiP), and metallothionein gene expression in primary pancreatic islet beta-cells. *Journal of Biological Chemistry*. 286:25778-25789.

Berridge, M.J. 1993. Inositol trisphosphate and calcium signaling. *Nature*. 361:315-325.

Berridge, M.J., M.D. Bootman, and P. Lipp. 1998. Calcium - a life and death signal. *Nature*. 395:645-648.

Blaustein, M.P., and W.J. Lederer. 1999. Sodium calcium exchange: Its physiological implications. *Physiological Reviews*. 79:763-854.

Bleazard, W., J.M. McCaffery, E.J. King, S. Bale, A. Mozdy, Q. Tieu, J. Nunnari, and J.M. Shaw. 1999. The dynamin-related GTPase Dnm1 regulates mitochondrial fission in yeast. *Nature Cell Biology*. 1:298-304.

Boya, P., K. Andreau, D. Poncet, N. Zamzami, J.L. Perfettini, D. Metivier, D.M. Ojcius, M. Jaattela, and G. Kroemer. 2003. Lysosomal membrane permeabilization

induces cell death in a mitochondrion-dependent fashion. *Journal of Experimental Medicine*. 197:1323-1334.

Boya, P., and G. Kroemer. 2008. Lysosomal membrane permeabilization in cell death. *Oncogene*. 27:6434-6451.

Brooks, C., Q. Wei, S.G. Cho, and Z. Dong. 2009. Regulation of mitochondrial dynamics in acute kidney injury in cell culture and rodent models. *The Journal of clinical investigation*. 119:1275-1285.

Brumatti, G., C. Sheridan, and S.J. Martin. 2008. Expression and purification of recombinant annexin V for the detection of membrane alterations on apoptotic cells. *Methods*. 44:235-240.

Buetler, T.M., A. Krauskopf, and U.T. Ruegg. 2004. Role of superoxide as a signaling molecule. *News in Physiological Sciences*. 19:120-123.

Burgoyne, R.D. 2007. Neuronal calcium sensor proteins: generating diversity in neuronal Ca^{2+} signalling. *Nature Reviews Neuroscience*. 8:182-193.

Buttke, T.M., and P.A. Sandstrom. 1994. Oxidative stress as a mediator of apoptosis. *Immunology Today*. 15:7-10.

Cai, H., and D.G. Harrison. 2000. Endothelial dysfunction in cardiovascular diseases: the role of oxidant stress. *Circulation Research*. 87:840-844.

Cai, S., J. Khoo, S. Mussa, N.J. Alp, and K.M. Channon. 2005. Endothelial nitric oxide synthase dysfunction in diabetic mice: importance of tetrahydrobiopterin in eNOS dimerisation. *Diabetologia*. 48:1933-1940.

Caterina, M.J., M.A. Schumacher, M. Tominaga, T.A. Rosen, J.D. Levine, and D. Julius. 1997. The capsaicin receptor: a heat-activated ion channel in the pain pathway. *Nature*. 389:816-824.

Catterall, W.A. 2011. Voltage-gated calcium channels. *Cold Spring Harbor Perspectives in Biology*. 3(8), a003947.

Cereghetti, G.M., A. Stangherlin, O. Martins de Brito, C.R. Chang, C. Blackstone, P. Bernardi, and L. Scorrano. 2008. Dephosphorylation by calcineurin regulates translocation of Drp1 to mitochondria. *Proceedings of the National Academy of Sciences of the United States of America*. 105:15803-15808.

Chan, D.C. 2006. Mitochondrial fusion and fission in mammals. *In Annual Review of Cell and Developmental Biology*. 22: 79-99.

Chan, D.C. 2012. Fusion and fission: interlinked processes critical for mitochondrial health. *Annual Review of Genetics.* 46:265-287.

Chen, H., H. Yoshioka, G.S. Kim, J.E. Jung, N. Okami, H. Sakata, C.M. Maier, P. Narasimhan, C.E. Goeders, and P.H. Chan. 2011. Oxidative stress in ischemic brain damage: mechanisms of cell death and potential molecular targets for neuroprotection. *Antioxidants & Redox Signaling*. 14:1505-1517.

Chen, H.C., and D.C. Chan. 2005. Emerging functions of mammalian mitochondrial fusion and fission. *Human Molecular Genetics*. 14:283-289.

Chen, H.C., A. Chomyn, and D.C. Chan. 2005. Disruption of fusion results in mitochondrial heterogeneity and dysfunction. *Journal of Biological Chemistry*. 280:26185-26192.

Chen, H.C., S.A. Detmer, A.J. Ewald, E.E. Griffin, S.E. Fraser, and D.C. Chan. 2003. Mitofusins Mfn1 and Mfn2 coordinately regulate mitochondrial fusion and are essential for embryonic development. *Journal of Cell Biology*. 160:189-200.

Cheng, J., and A. Vieira. 2006. Oxidative stress disrupts internalization and endocytic trafficking of transferrin in a human malignant keratinocyte line. *Cell Biochemistry and Biophysics*. 45:177-184.

Choi, S.M., K.-O. Choi, Y.-K. Park, H. Cho, E.G. Yang, and H. Park. 2006. Clioquinol, a Cu(II)/Zn(II) chelator, inhibits both ubiquitination and asparagine hydroxylation of hypoxia-inducible factor-1 alpha, leading to expression of vascular endothelial growth factor and erythropoietin in normoxic cells. *Journal of Biological Chemistry*. 281:34056-34063.

Chouchani, E.T., V.R. Pell, E. Gaude, D. Aksentijevic, S.Y. Sundier, E.L. Robb, A. Logan, S.M. Nadtochiy, E.N.J. Ord, A.C. Smith, F. Eyassu, R. Shirley, C.-H. Hu, A.J. Dare, A.M. James, S. Rogatti, R.C. Hartley, S. Eaton, A.S.H. Costa, P.S. Brookes, S.M. Davidson, M.R. Duchen, K. Saeb-Parsy, M.J. Shattock, A.J. Robinson, L.M. Work, C. Frezza, T. Krieg, and M.P. Murphy. 2014. Ischaemic accumulation of succinate controls reperfusion injury through mitochondrial ROS. *Nature*. 515:431-435.

Church, S.L., J.W. Grant, L.A. Ridnour, L.W. Oberley, P.E. Swanson, P.S. Meltzer, and J.M. Trent. 1993. Increased manganese superoxide-dismutase expression suppresses the malignant phenotype of human-melanoma cells. *Proceedings of the National Academy of Sciences of the United States of America*. 90:3113-3117.

Clapham, D.E. 1995. Calcium signaling. *Cell*. 80:259-268.

Clapham, D.E. 2007. Calcium signaling. *Cell*. 131:1047-1058.

Clausen, A., T. McClanahan, S.G. Ji, and J.H. Weiss. 2013. Mechanisms of rapid reactive oxygen species generation in response to cytosolic Ca^{2+} or Zn^{2+} loads in cortical neurons. *Plos One*. 8(12): 83347.

Cohen, R.A., and X. Tong. 2010. Vascular oxidative stress: the common link in hypertensive and diabetic vascular disease. *Journal of Cardiovascular Pharmacology*. 55:308-316.

Cosentino-Gomes, D., N. Rocco-Machado, and J.R. Meyer-Fernandes. 2012. Cell signalling through protein kinase C oxidation and activation. *International Journal of Molecular Sciences*. 13:10697-11522.

Cousins, R.J., J.P. Liuzzi, and L.A. Lichten. 2006. Mammalian zinc transport, trafficking, and signals. *Journal of Biological Chemistry*. 281:24085-24089.

D'Autreaux, B., and M.B. Toledano. 2007. ROS as signalling molecules: mechanisms that generate specificity in ROS homeostasis. *Nat Rev Mol Cell Biol*. 8:813-824.

Dahmer, M.K. 2005. Caspases-2, -3, and -7 are involved in thapsigargin-induced apoptosis of SH-SY5Y neuroblastoma cells. *Journal of Neuroscience Research*. 80:576-583.

Davignon, J., and P. Ganz. 2004. Role of endothelial dysfunction in atherosclerosis. *Circulation*. 109:27-32.

De Duve, C. 2005. The lysosome turns fifty. *M S-Medecine Sciences*. 21:8-11.

De Duve, C., B.C. Pressman, R. Gianetto, R. Wattiaux, and F. Appelmans. 1955. Tissue fractionation studies. 6. Intracellular distribution patterns of enzymes in rat-liver tissue. *The Biochemical journal*. 60:604-617.

Denmeade, S.R., A.M. Mhaka, D.M. Rosen, W.N. Brennen, S. Dalrymple, I. Dach, C. Olesen, B. Gurel, A.M. DeMarzo, G. Wilding, M.A. Carducci, C.A. Dionne, J.V. Moller, P. Nissen, S.B. Christensen, and J.T. Isaacs. 2012. Engineering a prostate-specific membrane antigen-activated tumor endothelial cell prodrug for cancer therapy. *Science Translational Medicine*. 4 (140): 140ra86.

Di, A., XP. Gao, F. Qian, T. Kawamura, J. Han, C. Hecquet, R.D. Ye, S.M. Vogel, and A.B. Malik. 2012. The redox-sensitive cation channel TRPM2 modulates phagocyte ROS production and inflammation. *Nature Immunology*. 13:29-34.

Di Sano, F., E. Ferraro, R. Tufi, T. Achsel, M. Piacentini, and F. Cecconi. 2006. Endoplasmic reticulum stress induces apoptosis by an apoptosome-dependent but

caspase 12-independent mechanism. *Journal of Biological Chemistry*. 281:2693-2700.

Di Vaira, M., C. Bazzicalupi, P. Orioli, L. Messori, B. Bruni, and P. Zatta. 2004. Clioquinol, a drug for alzheimer's disease specifically interfering with brain metal metabolism: structural characterization of its Zinc(II) and Copper(II) complexes. *Inorg. Chem.* 43:3795–3797.

Diabetes Control Complications Trial, D.R.G. 1995. Effect of intensive diabetes management on macrovascular events and risk-factors in the diabetes control and complications trial. *American Journal of Cardiology*. 75:894-903.

Diekert, K., Kispal, G., Guiard, B., and Lill, R. 1999. An internal targeting signal directing proteins into the mitochondrial intermembrane space. *PNAS*. 96:11752-11757.

Dietrich, A., and T. Gudermann. 2008. Another TRP to endothelial dysfunction - TRPM2 and endothelial permeability. *Circulation Research*. 102:275-277.

Donadelli, M., E.D. Pozza, M.T. Scupoli, C. Costanzo, A. Scarpa, and M. Palmieri. 2009. Intracellular zinc increase inhibits p53(-/-) pancreatic adenocarcinoma cell growth by ROS/AIF-mediated apoptosis. *Biochimica Et Biophysica Acta-Molecular Cell Research*. 1793:273-280.

Dorn, G.W., II. 2015. Mitochondrial dynamism and heart disease: changing shape and shaping change. *Embo Molecular Medicine*. 7:865-877.

Droge, W. 2002. Free radicals in the physiological control of cell function. *Physiological Reviews*. 82:47-95.

Du, J., J. Xie, and L. Yue. 2009. Intracellular calcium activates TRPM2 and its alternative spliced isoforms. *Proceedings of the National Academy of Sciences of the United States of America*. 106:7239-7244.

Du, X.L., K. Stockklauser-Farber, and P. Rosen. 1999. Generation of reactive oxygen intermediates, activation of NF-Kappa B, and induction of apoptosis in human endothelial cells by glucose: Role of nitric oxide synthase? *Free Radical Biology and Medicine*. 27:752-763.

Du, X.L., G.Z. Sui, K. Stockklauser-Farber, J. Weiss, S. Zink, B. Schwippert, Q.X. Wu, D. Tschope, and P. Rosen. 1998. Introduction of apoptosis by high proinsulin and glucose in cultured human umbilical vein endothelial cells is mediated by reactive oxygen species. *Diabetologia*. 41:249-256.

Duby, J.J., R.K. Campbell, S.M. Setter, J.R. White, and K.A. Rasmussen. 2004. Diabetic neuropathy: An intensive review. *American Journal of Health-System Pharmacy*. 61:160-173.

Elgass, K., J. Pakay, M.T. Ryan, and C.S. Palmer. 2013. Recent advances into the understanding of mitochondrial fission. *Biochimica Et Biophysica Acta-Molecular Cell Research*. 1833:150-161.

Elmore, S. 2007. Apoptosis: A review of programmed cell death. *Toxicologic Pathology*. 35:495-516.

Fan, X., R. Hussien, and G.A. Brooks. 2010. H_2O_2-induced mitochondrial fragmentation in C2C12 myocytes. *Free Radical Biology and Medicine*. 49:1646-1654.

Fan, X., J. Ma, W. Wan, P. Zhang, C. Wang, and L. Wu. 2011. Increased intracellular calcium concentration causes electrical turbulence in guinea pig ventricular myocytes. *Science China-Life Sciences*. 54:240-247.

Farber, J.L. 1990. The role of calcium in lethal cell injury. *Chemical Research in Toxicology*. 3:503-508.

Feng, S., L. Hongyu, T. Yilin, H. Junbo, S. Yujuan, J. Abramowitz, M. Zhu, L. Birnbaumer, and Y. Wang. 2013. Canonical transient receptor potential 3 channels regulate mitochondrial calcium uptake**.** *PNAS.* 110:11011-11016.

Feron, O., C. Dessy, J.P. Desager, and J.L. Balligand. 2001. Hydroxy-methylglutaryl-coenzyme A reductase inhibition promotes endothelial nitric oxide synthase activation through a decrease in caveolin abundance. *Circulation*. 103:113-118.

Ferri, K.F., and G. Kroemer. 2001. Organelle-specific initiation of cell death pathways. *Nature Cell Biology*. 3:E255-E263.

Feske, S. 2007. Calcium signalling in lymphocyte activation and disease. *Nature Reviews Immunology*. 7:690-702.

Finkel, T. 2012. Signal transduction by mitochondrial oxidants. *Journal of Biological Chemistry*. 287:4434-4440.

Finkel, T., and N.J. Holbrook. 2000. Oxidants, oxidative stress and the biology of ageing. *Nature*. 408:239-247.

Fonfria, E., I.C.B. Marshall, C.D. Benham, I. Boyfield, J.D. Brown, K. Hill, J.P. Hughes, S.D. Skaper, and S. McNulty. 2004. TRPM2 channel opening in response to oxidative stress is dependent on activation of poly (ADP-ribose) polymerase. *British Journal of Pharmacology*. 143:186-192.

Frank, S., B. Gaume, E.S. Bergmann-Leitner, W.W. Leitner, E.G. Robert, F. Catez, C.L. Smith, and R.J. Youle. 2001. The role of dynamin-related protein 1, a mediator of mitochondrial fission, in apoptosis. *Developmental Cell*. 1:515-525.

Frazzini, V., E. Rockabrand, E. Mocchegiani, and S.L. Sensi. 2006. Oxidative stress and brain aging: is zinc the link? *Biogerontology*. 7:307-314.

Frederickson, C.J. 1989. Neurobiology of zinc and zinc-containing neurons. *International Review of Neurobiology*. 31:145-238.

Frederickson, C.J., J.Y. Koh, and A.I. Bush. 2005. The neurobiology of zinc in health and disease. *Nature Reviews Neuroscience*. 6:449-462.

Friedman, J.R., and J. Nunnari. 2014. Mitochondrial form and function. *Nature*. 505:335-343.

Fritze, C.E., and T.R. Anderson. 2000. Epitope tagging: General method for tracking recombinant proteins. *Applications of Chimeric Genes and Hybrid Proteins Pt B*. 327:3-16.

Galluzzi, L., K. Blomgren, and G. Kroemer. 2009. Mitochondrial membrane permeabilization in neuronal injury. *Nature Reviews Neuroscience*. 10:481-494.

Gee, K.R., K.A. Brown, W.N.U. Chen, J. Bishop-Stewart, D. Gray, and I. Johnson. 2000. Chemical and physiological characterization of fluo-4 Ca^{2+} indicator dyes. *Cell calcium*. 27:97-106.

Gee K.R., Z.L. Zhou, D. Ton-That, S.L. Sensi, J.H. Weiss. 2002. Measuring zinc in living cells. A new generation of sensitive and selective fluorescent probes. *Cell calcium.* 31:245-251.

Gees, M., B. Colsoul, and B. Nilius. 2010. The role of transient receptor potential cation channels in Ca^{2+} signaling. *Cold Spring Harbor Perspectives in Biology*. 2(10):003962.

Geissler, A., F. Haun, D.O. Frank, K. Wieland, M.M. Simon, M. Idzko, R.J. Davis, U. Maurer, and C. Borner. 2013. Apoptosis induced by the fungal pathogen gliotoxin requires a triple phosphorylation of Bim by JNK. *Cell Death and Differentiation*. 20:1317-1329.

Giacco, F., and M. Brownlee. 2010. Oxidative stress and diabetic complications. *Circ Res*. 107:1058-1070.

Giorgio, M., M. Trinei, E. Migliaccio, and P.G. Pelicci. 2007. Hydrogen peroxide: a metabolic by-product or a common mediator of ageing signals? *Nat Rev Mol Cell Biol*. 8:722-728.

Griendling, K.K. 2005. ATVB in focus - redox mechanisms in blood vessels. *Arteriosclerosis Thrombosis and Vascular Biology*. 25:272-273.

Griparic, L., N.N. van der Wel, I.J. Orozco, P.J. Peters, and A.M. van der Bliek. 2004. Loss of the intermembrane space protein Mgm1/OPA1 induces swelling and localized constrictions along the lengths of mitochondria. *Journal of Biological Chemistry*. 279:18792-18798.

Grohm, J., S.W. Kim, U. Mamrak, S. Tobaben, A. Cassidy-Stone, J. Nunnari, N. Plesnila, and C. Culmsee. 2012. Inhibition of Drp1 provides neuroprotection in vitro and in vivo. *Cell death and differentiation*. 19:1446-1458.

Han, X.J., Y.F. Lu, S.A. Li, T. Kaitsuka, Y. Sato, K. Tomizawa, A.C. Nairn, K. Takei, H. Matsui, and M. Matsushita. 2008. CaM kinase I alpha-induced phosphorylation of Drp1 regulates mitochondrial morphology. *The Journal of cell biology*. 182:573-585.

Hara, Y., M. Wakamori, M. Ishii, E. Maeno, M. Nishida, T. Yoshida, H. Yamada, S. Shimizu, E. Mori, J. Kudoh, N. Shimizu, H. Kurose, Y. Okada, K. Imoto, and Y. Mori. 2002. LTRPC2 Ca^{2+}-permeable channel activated by changes in redox status confers susceptibility to cell death. *Molecular Cell*. 9:163-173.

Harman, D. 1956. Aging: a theory based on free radical and radiation chemistry. *Journals of Gerontology*. 11:298-300.

Harter, C., and I. Mellman. 1992. Transport of the lysosomal membrane glycoprotein-lgp120 (LGP-A) to lysosomes does not require appearance on the plasma-membrane. *Journal of Cell Biology*. 117:311-325.

Haynes, C.M., E.A. Titus, and A.A. Cooper. 2004. Degradation of misfolded proteins prevents ER-derived oxidative stress and cell death. *Molecular Cell*. 15:767-776.

Heart Protection Study Collaborative, G. 2002. MRC/BHF heart protection study of antioxidant vitamin supplementation in 20,536 high-risk individuals: a randomised placebo-controlled trial. *Lancet*. 360:23-33.

Hecquet, C.M., and A.B. Malik. 2009. Role of H_2O_2-activated TRPM2 calcium channel in oxidant-induced endothelial injury. *Thrombosis and Haemostasis*. 101:619-625.

Heilig, C.W., L.A. Concepcion, B.L. Riser, S.O. Freytag, M. Zhu, P. Cortes, C.C. Hassett, J.D. Gilbert, K.S.S. Sastry, K.O. Heilig, and J.M. Grondin. 1995. overexpression of glucose transporters in rat mesangial cells cultured in a normal glucose milieu mimics the diabetic phenotype. *Journal of Clinical Investigation*. 96:1802-1814.

Heiner, I., J. Eisfeld, C.R. Halaszovich, E. Wehage, E. Jungling, C. Zitt, and A. Luckhoff. 2003. Expression profile of the transient receptor potential (TRP) family in neutrophil granulocytes: evidence for currents through long TRP channel 2 induced by ADP-ribose and NAD. *Biochemical Journal*. 371:1045-1053.

Hermosura, M.C., A.M. Cui, R.C.V. Go, B. Davenport, C.M. Shetler, J.W. Heizer, C. Schmitz, G. Mocz, R.M. Garruto, and A.-L. Perraud. 2008. Altered functional properties of a TRPM2 variant in Guamanian ALS and PD. *Proceedings of the National Academy of Sciences of the United States of America*. 105:18029-18034.

Hill, K., S. McNulty, and A.D. Randall. 2004. Inhibition of TRPM2 channels by the antifungal agents clotrimazole and econazole. *Naunyn-Schmiedebergs Archives of Pharmacology*. 370:227-237.

Hitomi, J., T. Katayama, Y. Eguchi, T. Kudo, M. Taniguchi, Y. Koyama, T. Manabe, S. Yamagishi, Y. Bando, K. Imaizumi, Y. Tsujimoto, and M. Tohyama. 2004. Involvement of caspase-4 in endoplasmic reticulum stress-induced apoptosis and a beta-induced cell death. *Journal of Cell Biology*. 165:347-356.

Ho, F.M., W.W. Lin, B.C. Chen, C.M. Chao, C.R. Yang, L.Y. Lin, C.C. Lai, S.H. Liu, and C.S. Liau. 2006. High glucose-induced apoptosis in human vascular endothelial cells is mediated through NF-kappa B and c-Jun NH2-terminal kinase pathway and prevented by PI3K/Akt/eNOS pathway. *Cellular Signalling*. 18:391-399.

Ho, F.M., S.H. Liu, C.S. Liau, P.J. Huang, and S.Y. Lin-Shiau. 2000. High glucose-induced apoptosis in human endothelial cells is mediated by sequential activations of c-Jun NH2-terminal kinase and caspase-3. *Circulation*. 101:2618-2624.

Ho, K.W., N.J. Ward, and D.J. Calkins. 2012. TRPV1: a stress response protein in the central nervous system. *American journal of neurodegenerative disease*. 1:1-14.

Huang, L.P., C.P. Kirschke, Y.F. Zhang, and Y.Y. Yu. 2005. The ZIP7 gene (Slc39a7) encodes a zinc transporter involved in zinc homeostasis of the Golgi apparatus. *Journal of Biological Chemistry*. 280:15456-15463.

Ho, Y., R. Samarasinghe, M.E. Knoch, M. Lewis, E. Aizenman, and D.B. DeFranco. 2008. Selective inhibition of mitogen-activated protein kinase phosphatases by zinc accounts for extracellular signal-regulated kinase 1/2-dependent oxidative neuronal cell death. *Molecular Pharmacology*. 74:1141-1151.

Hung, MC., and W. Link. 2011. Protein localization in disease and therapy. *Journal of Cell Science*. 124:3381-3392.

Inoue, K., Z. O'Bryant, and Z.-G. Xiong. 2015. Zinc-permeable ion channels: effects on intracellular zinc dynamics and potential physiological/pathophysiological significance. *Current Medicinal Chemistry*. 22:1248-1257.

Ishihara, N., M. Nomura, A. Jofuku, H. Kato, S.O. Suzuki, K. Masuda, H. Otera, Y. Nakanishi, I. Nonaka, Y. Goto, N. Taguchi, H. Morinaga, M. Maeda, R. Takayanagi, S. Yokota, and K. Mihara. 2009. Mitochondrial fission factor Drp1 is essential for embryonic development and synapse formation in mice. *Nat Cell Biol*. 11:958-966.

Islam, M.S., and D.T. Loots. 2007. Diabetes, metallothionein, and zinc interactions: A review. *Biofactors*. 29:203-212.

James, D.I., P.A. Parone, Y. Mattenberger, and J.C. Martinou. 2003. hFis1, a novel component of the mammalian mitochondrial fission machinery. *Journal of Biological Chemistry*. 278:36373-36379.

Janicke, R.U., M.L. Sprengart, M.R. Wati, and A.G. Porter. 1998. Caspase-3 is required for DNA fragmentation and morphological changes associated with apoptosis. *Journal of Biological Chemistry*. 273:9357-9360.

Jarvik, J.W., and C.A. Telmer. 1998. Epitope tagging. *Annual Review of Genetics*. 32:601-618.

Jay, D., H. Hitomi, and K.K. Griendling. 2006. Oxidative stress and diabetic cardiovascular complications. *Free Radical Biology and Medicine*. 40:183-192.

Jheng, H.F., P.J. Tsai, S.M. Guo, L.H. Kuo, C.S. Chang, I.J. Su, C.R. Chang, and Y.S. Tsai. 2012. Mitochondrial fission contributes to mitochondrial dysfunction and insulin resistance in skeletal muscle. *Mol Cell Biol*. 32:309-319.

Jiang, F., Y. Zhang, and G.J. Dusting. 2011a. NADPH oxidase-mediated redox signaling: roles in cellular stress response, stress tolerance, and tissue repair. *Pharmacological Reviews*. 63:218-242.

Jiang, L.H., N. Gamper, and D.J. Beech. 2011b. Properties and therapeutic potential of transient receptor potential channels with putative roles in adversity: focus on TRPC5, TRPM2 and TRPA1. *Current Drug Targets*. 12:724-736.

Johansson, A.-C., H. Appelqvist, C. Nilsson, K. Kagedal, K. Roberg, and K. Ollinger. 2010. Regulation of apoptosis-associated lysosomal membrane permeabilization. *Apoptosis*. 15:527-540.

Johnson, A., P. Phillips, D. Hocking, M.F. Tsan, and T. Ferro. 1989. Protein kinase inhibitor prevents pulmonary edema in response to hydrogen peroxide. *American Journal of Physiology*. 256:1012-1022.

Kaneko, S., S. Kawakami, Y. Hara, M. Wakamori, E. Itoh, T. Minami, Y. Takada, T. Kume, H. Katsuki, Y. Mori, and A. Akaike. 2006. A critical role of TRPM2 in neuronal cell death hy hydrogen peroxide. *Journal of Pharmacological Sciences*. 101:66-76.

Kapuscinski, J. 1995. DAPI - a DNA-specific fluorescent-probe. *Biotechnic & Histochemistry*. 70:220-233.

Karbowski, M., and R.J. Youle. 2003. Dynamics of mitochondrial morphology in healthy cells and during apoptosis. *Cell Death and Differentiation*. 10:870-880.

Kardosh, A., E.B. Golden, P. Pyrko, J. Uddin, F.M. Hofman, T.C. Chen, S.G. Louie, N.A. Petasis, and A.H. Schoenthal. 2008. Aggravated endoplasmic reticulum stress as a basis for enhanced glioblastoma cell killing by bortezomib in combination with celecoxib or its non-coxib analogue, 2,5-dimethyl-celecoxib. *Cancer Research*. 68:843-851.

Karnik, R., M.J. Ludlow, N. Abuarab, A.J. Smith, M.E.L. Hardy, D.J.S. Elliott, and A. Sivaprasadarao. 2013. Endocytosis of hERG is clathrin-independent and involves Arf6. *Plos One*. 8(12):85630.

Kashio M., T. Sokabe, K. Shintaku, T. Uematsuc, N. Fukutaa, N. Kobayashic, Y. Morid, and M. Tominaga. 2011. Redox signal-mediated sensitization of transient receptor potential melastatin 2 (TRPM2) to temperature affects macrophage functions. *PNAS*. 109:6745-6750.

Kerr, J.F.R., A.H. Wyllie, and A.R. Currie. 1972. Apoptosis - basic biological phenomenon with wide-ranging implications in tissue kinetics. *British Journal of Cancer*. 26:239-257.

Kietadisorn, R., R.P. Juni, and A.L. Moens. 2012. Tackling endothelial dysfunction by modulating NOS uncoupling: new insights into its pathogenesis and therapeutic possibilities. *American Journal of Physiology-Endocrinology and Metabolism*. 303:1505-1505.

Kim, I., S. Rodriguez-Enriquez, and J.J. Lemasters. 2007. Selective degradation of mitochondria by mitophagy. *Archives of Biochemistry and Biophysics*. 462:245-253.

Kim, M.Y., T. Zhang, and W.L. Kraus. 2005. Poly(ADP-ribosyl)ation by PARP-1: 'PAR-laying' NAD^+ into a nuclear signal. *Genes Dev*. 19:1951-1967.

Kirichok, Y., G. Krapivinsky, and D.E. Clapham. 2004. The mitochondrial calcium uniporter is a highly selective ion channel. *Nature*. 427:360-364.

Kolisek, M., A. Beck, A. Fleig, and R. Penner. 2005. Cyclic ADP-ribose and hydrogen peroxide synergize with ADP-ribose in the activation of TRPM2 channels. *Molecular Cell*. 18:61-69.

Koopman, W.J., S. Verkaart, H.J. Visch, F.H. van der Westhuizen, M.P. Murphy, L.W. van den Heuvel, J.A. Smeitink, and P.H. Willems. 2005. Inhibition of complex I of the electron transport chain causes O_2^--mediated mitochondrial outgrowth. *Am J Physiol Cell Physiol*. 288:1440-1450.

Kraft, R., C. Grimm, H. Frenzel, and C. Harteneck. 2006. Inhibition of TRPM2 cation channels by N-(p-amylcinnamoyl)anthranilic acid. *British Journal of Pharmacology*. 148:264-273.

Kraft, R., C. Grimm, K. Grosse, A. Hoffmann, S. Sauerbruch, H. Kettenmann, G. Schultz, and C. Harteneck. 2004. Hydrogen peroxide and ADP-ribose induce TRPM2-mediated calcium influx and cation currents in microglia. *American Journal of Physiology-Cell Physiology*. 286:129-137.

Kroemer, G., B. Dallaporta, and M. Resche-Rigon. 1998. The mitochondrial death/life regulator in apoptosis and necrosis. *Annual Review of Physiology*. 60:619-642.

Kroemer, G., L. Galluzzi, and C. Brenner. 2007. Mitochondrial membrane permeabilization in cell death. *Physiol Rev*. 87:99-163.

Kroemer, G., and J.C. Reed. 2000. Mitochondrial control of cell death. *Nature Medicine*. 6:513-519.

Ku, H.H., U.T. Brunk, and R.S. Sohal. 1993. Relationship between mitochondrial superoxide and hydrogen-peroxide production and longevity of mammalian-species. *Free Radical Biology and Medicine*. 15:621-627.

Kuhn, F.J.P., I. Heiner, and A. Luckhoff. 2005. TRPM2: a calcium influx pathway regulated by oxidative stress and the novel second messenger ADP-ribose. *Pflügers Archiv-European Journal of Physiology*. 451:212-219.

Kukic, I., S.L. Kelleher, and K. Kiselyov. 2014. Zn^{2+} efflux through lysosomal exocytosis prevents Zn^{2+}-induced toxicity. *Journal of Cell Science*. 127:3094-3103.

Lambeth, J.D. 2007. Nox enzymes, ROS, and chronic disease: An example of antagonistic pleiotropy. *Free Radical Biology and Medicine*. 43:332-347.

Lange, I., S. Yamamoto, S. Partida-Sanchez, Y. Mori, A. Fleig, and R. Penner. 2009. TRPM2 functions as a lysosomal Ca^{2+}-release channel in beta cells. *Science Signaling*. 2(71): ra23.

Lee, R.J., T. Shaw, M. Sandquist, and L.D. Partridge. 1996. Mechanism of action of the non-steroidal anti-inflammatory drug flufenamate on $[Ca^{2+}]_i$ and Ca^{2+}-activated currents in neurons. *Cell Calcium*. 19:431-438.

Lee, H.C. 2012. Cyclic ADP-ribose and Nicotinic Acid Adenine Dinucleotide Phosphate (NAADP) as Messengers for Calcium Mobilization. *Journal of Biological Chemistry*. 287:31633-31640.

Lee, S.-J., K.S. Cho, and J.-Y. Koh. 2009. Oxidative injury triggers autophagy in astrocytes: the role of endogenous zinc. *Glia*. 57:1351-1361.

Lee J., S. Giordano and J. Zhang. 2012. Autophagy, mitochondria and oxidative stress: cross-talk and redox signaling. *Biochem J*. 441:523–540.

Lesnefsky, E.J., S. Moghaddas, B. Tandler, J. Kerner, and C.L. Hoppel. 2001. Mitochondrial dysfunction in cardiac disease: Ischemia-reperfusion, aging, and heart failure. *Journal of Molecular and Cellular Cardiology*. 33:1065-1089.

Li, J., B. Hou, S. Tumova, K. Muraki, A. Bruns, M.J. Ludlow, A. Sedo, A.J. Hyman, L. McKeown, R.S. Young, N.Y. Yuldasheva, Y. Majeed, L.A. Wilson, B. Rode, M.A. Bailey, H.R. Kim, Z. Fu, D.A.L. Carter, J. Bilton, H. Imrie, P. Ajuh, T.N. Dear, R.M. Cubbon, M.T. Kearney, K.R. Prasad, P.C. Evans, J.F.X. Ainscough, and D.J. Beech. 2014. Piezol integration of vascular architecture with physiological force. *Nature*. 515:279-308.

Li, J.M., and A.M. Shah. 2003. ROS generation by nonphagocytic NADPH oxidase: Potential relevance in diabetic nephropathy. *Journal of the American Society of Nephrology*. 14:221-226.

Li, J.M., and A.M. Shah. 2004. Endothelial cell superoxide generation: regulation and relevance for cardiovascular pathophysiology. *American Journal of Physiology-Regulatory Integrative and Comparative Physiology*. 287:1014-1030.

Li, X., E. Gulbins, and Y. Zhang. 2012. Oxidative stress triggers Ca^{2+}-dependent lysosome trafficking and activation of acid sphingomyelinase. *Cellular Physiology and Biochemistry*. 30:815-826.

Liesa, M., M. Palacin, and A. Zorzano. 2009. Mitochondrial dynamics in mammalian health and disease. *Physiological Reviews*. 89:799-845.

Lin L., C. Lin, F. Ho and C. Liau. 2005. Up-regulation of the association between heat shock protein 90 and endothelial nitric oxide synthase prevents high glucose-induced apoptosis in human endothelial cells. *J Cell Biochem*. 94:194-201.

Lin, M.T., and M.F. Beal. 2006. Mitochondrial dysfunction and oxidative stress in neurodegenerative diseases. *Nature*. 443:787-795.

Lishko, P.V., E. Procko, X. Jin, C.B. Phelps, and R. Gaudet. 2007. The ankyrin repeats of TRPV1 bind multiple ligands and modulate channel sensitivity. *Neuron*. 54:905-918.

Loson, O.C., Z. Song, H. Chen, and D.C. Chan. 2013. Fis1, Mff, MiD49, and MiD51 mediate Drp1 recruitment in mitochondrial fission. *Molecular Biology of the Cell*. 24:659-667.

Lum, H., and K.A. Roebuck. 2001. Oxidant stress and endothelial cell dysfunction. *American Journal of Physiology-Cell Physiology*. 280:719-741.

Madesh, M., and G. Hajnoczky. 2001. VDAC-dependent permeabilization of the outer mitochondrial membrane by superoxide induces rapid and massive cytochrome c release. *Journal of Cell Biology*. 155:1003-1015.

Madesh, M., K. Mallilankaraman, P. Doonan, C. Cardenas, H.C. Chandramoorthy, M. Muller, R. Miller, N. Hoffman, R. Gandhirajan, M. Birnbaum, B. Rothber, D.-O.D. Mak, and J.K. Foskett. 2013. MICU1 is an essential gatekeeper for MCU-mediated mitochondrial Ca^{2+} uptake that regulates cell survival. *Biophysical Journal*. 104(1):301.

Makino, A., B.T. Scott, and W.H. Dillmann. 2010. Mitochondrial fragmentation and superoxide anion production in coronary endothelial cells from a mouse model of type 1 diabetes. *Diabetologia*. 53:1783-1794.

Malaiyandi, L.M., O. Vergun, K.E. Dineley, and I.J. Reynolds. 2005. Direct visualization of mitochondrial zinc accumulation reveals uniporter-dependent and -independent transport mechanisms. *Journal of Neurochemistry*. 93:1242-1250.

Malhotra, J.D., and R.J. Kaufman. 2007. Endoplasmic reticulum stress and oxidative stress: A vicious cycle or a double-edged sword? *Antioxidants & Redox Signaling*. 9:2277-2293.

Mankouri, J., T.K. Taneja, A.J. Smith, S. Ponnambalam, and A. Sivaprasadarao. 2006. Kir6.2 mutations causing neonatal diabetes prevent endocytosis of ATP-sensitive potassium channels. *Embo Journal*. 25:4142-4151.

Manna, P.T., T.S. Munsey, N. Abuarab, F. Li, A. Asipu, G. Howell, A. Sedo, W. Yang, J. Naylor, D.J. Beech, L.H. Jiang, and A. Sivaprasadarao. 2015. TRPM2 mediated intracellular Zn^{2+} release triggers pancreatic beta cell death. *Biochem J*. 466:537-546.

Maritim, A.C., R.A. Sanders, and J.B. Watkins. 2003. Diabetes, oxidative stress, and antioxidants: A review. *Journal of Biochemical and Molecular Toxicology*. 17:24-38.

Marty, N.J., H.J. Teresinski, Y.T. Hwang, E.A. Clendening, S.K. Gidda, E. Sliwinska, D. Zhang, J.A. Miernyk, G.C. Brito, D.W. Andrews, J.M. Dyer, and R.T. Mullen. 2014. New insights into the targeting of a subset of tail-anchored proteins to the outer mitochondrial membrane. *Frontiers in Plant Science*. 5.

Martyn, K.D., L.M. Frederick, K. von Loehneysen, M.C. Dinauer, and U.G. Knaus. 2006. Functional analysis of Nox4 reveals unique characteristics compared to other NADPH oxidases. *Cellular Signalling*. 18:69-82.

Martin, J.L., C.J. Stork, and Y.V. Li. 2006. Determining zinc with commonly used calcium and zinc fluorescent indicators, a question on calcium signals. *Cell calcium*. 40:393-402.

Mathews, P.M., J.B. Martinie, and D.M. Fambrough. 1992. The pathway and targeting signal for delivery of the integral membrane glycoprotein lep100 to lysosomes. *Journal of Cell Biology*. 118:1027-1040.

Mattson, M.P., B. Rychlik, C. Chu, and S. Christakos. 1991. Evidence for calcium-reducing and excito-protective roles for the calcium-binding protein calbindin-D(28K) in cultured hippocampal-neurons. *Neuron*. 6:41-51.

McCord, J.M., and Fridovic.I. 1969. Superoxide dismutase an enzymic function for erythrocuprein (hemocuprein). *Journal of Biological Chemistry*. 244:6049-6055.

McCord, J.M., R.S. Roy, and S.W. Schaffer. 1985. Free radicals and myocardial ischemia. The role of xanthine oxidase. *Advances in myocardiology*. 5:183-189.

McHugh, D., R. Flemming, S.Z. Xu, A.L. Perraud, and D.J. Beech. 2003. Critical intracellular Ca^{2+} dependence of transient receptor potential melastatin 2 (TRPM2) cation channel activation. *Journal of Biological Chemistry*. 278:11002-11006.

McMahon, R.J., and R.J. Cousins. 2000. Mammalian zinc transporters. *Journal of Nutrition*. 130:667-670.

McQuillan, A., N.J. Bass, G. Kalsi, J. Lawrence, V. Puri, K. Choudhury, S.D. Detera-Wadleigh, D. Curtis, and H.M.D. Gurling. 2006. Fine mapping of a susceptibility locus for bipolar and genetically related unipolar affective disorders, to a region containing the C21ORF29 and TRPM2 genes on chromosome 21q22.3. *Molecular Psychiatry*. 11:134-142.

Mei, Z.-Z., H.-J. Mao, and L.-H. Jiang. 2006. Conserved cysteine residues in the pore region are obligatory for human TRPM2 channel function. *American Journal of Physiology-Cell Physiology*. 291:1022-1028.

Meldolesi, J., and T. Pozzan. 1998. The endoplasmic reticulum Ca^{2+} store: a view from the lumen. *Trends in Biochemical Sciences*. 23:10-14.

Miller, B.A. 2004. Inhibition of TRPM2 function by PARP inhibitors protects cells from oxidative stress-induced death. *British Journal of Pharmacology*. 143:515-516.

Miller, B.A., N.E. Hoffman, S. Merali, X.-Q. Zhang, J. Wang, S. Rajan, S. Shanmughapriya, E. Gao, C.A. Barrero, K. Mallilankaraman, J. Song, T. Gu, I. Hirschler-Laszkiewicz, W.J. Koch, A.M. Feldman, M. Madesh, and J.Y. Cheung. 2014. TRPM2 channels protect against cardiac ischemia-reperfusion injury role of mitochondria. *Journal of Biological Chemistry*. 289:7615-7629.

Miller, E.R., R. Pastor-Barriuso, D. Dalal, R.A. Riemersma, L.J. Appel, and E. Guallar. 2005. Meta-analysis: High-dosage vitamin E supplementation may increase all-cause mortality. *Annals of Internal Medicine*. 142:37-46.

Min, C.K., D.R. Yeom, K.E. Lee, H.K. Kwon, M. Kang, Y.S. Kim, Z.Y. Park, H. Jeon, and D.H. Kim. 2012. Coupling of ryanodine receptor 2 and voltage-dependent anion channel 2 is essential for Ca^{2+} transfer from the sarcoplasmic reticulum to the mitochondria in the heart. *Biochemical Journal*. 447:371-379.

Mishra, P., and D.C. Chan. 2014. Mitochondrial dynamics and inheritance during cell division, development and disease. *Nature Reviews Molecular Cell Biology*. 15:634-646.

Mizushima, N. 2004. Methods for monitoring autophagy. *International Journal of Biochemistry & Cell Biology*. 36:2491-2502.

Molina, A.J., J.D. Wikstrom, L. Stiles, G. Las, H. Mohamed, A. Elorza, G. Walzer, G. Twig, S. Katz, B.E. Corkey, and O.S. Shirihai. 2009. Mitochondrial networking protects beta-cells from nutrient-induced apoptosis. *Diabetes*. 58:2303-2315.

Morris, D.R., and C.W. Levenson. 2012. Ion channels and zinc: mechanisms of neurotoxicity and neurodegeneration. *Journal of toxicology*. 2012:785647-785647.

Mouche, S., S.B. Mkaddem, W. Wang, M. Katic, Y.H. Tseng, S. Carnesecchi, K. Steger, M. Foti, C.A. Meier, P. Muzzin, C.R. Kahn, E. Ogier-Denis, and I. Szanto. 2007. Reduced expression of the NADPH oxidase NOX4 is a hallmark of adipocyte differentiation. *Biochimica Et Biophysica Acta-Molecular Cell Research*. 1773:1015-1027.

Mukherjee, S., R.N. Ghosh, and F.R. Maxfield. 1997. Endocytosis. *Physiological Reviews*. 77:759-803.

Mukhopadhyay, P., M. Rajesh, K. Yoshihiro, G. Hasko, and P. Pacher. 2007. Simple quantitative detection of mitochondrial superoxide production in live cells. *Biochemical and Biophysical Research Communications*. 358:203-208.

Munusamy, S., and L.A. MacMillan-Crow. 2009. Mitochondrial superoxide plays a crucial role in the development of mitochondrial dysfunction during high glucose exposure in rat renal proximal tubular cells. *Free Radical Biology and Medicine*. 46:1149-1157.

Nagamine, K., J. Kudoh, S. Minoshima, K. Kawasaki, S. Asakawa, F. Ito, and N. Shimizu. 1998. Molecular cloning of a novel putative Ca^{2+} channel protein (TRPC7) highly expressed in brain. *Genomics*. 54:124-131.

Nauseef, W.M. 2008. Biological roles for the NOX family NADPH oxidasesd. *Journal of Biological Chemistry*. 283:16961-16965.

Newsholme, P., E.P. Haber, S.M. Hirabara, E.L.O. Rebelato, J. Procopi, D. Morgan, H.C. Oliveira-Emilio, A.R. Carpinelli, and R. Curi. 2007. Diabetes associated cell stress and dysfunction: role of mitochondrial and non-mitochondrial ROS production and activity. *Journal of Physiology-London*. 583:9-24.

Nilius, B. 2007. TRP channels in disease. *Biochimica Et Biophysica Acta-Molecular Basis of Disease*. 1772:805-812.

Nilius, B., G. Owsianik, T. Voets, and J.A. Peters. 2007. Transient receptor potential cation channels in disease. *Physiological Reviews*. 87:165-217.

Nilius, B., J. Prenen, G. Droogmans, T. Voets, R. Vennekens, M. Freichel, U. Wissenbach, and V. Flockerzi. 2003. Voltage dependence of the Ca^{2+}-activated cation channel TRPM4. *Journal of Biological Chemistry*. 278:42728-42728.

Novo, E., and M. Parola. 2012. The role of redox mechanisms in hepatic chronic wound healing and fibrogenesis. *Fibrogenesis & tissue repair*. 5:1-4.

Okamoto, K., and J.M. Shaw. 2005. Mitochondrial morphology and dynamics in yeast and multicellular eukaryotes. *Annual Review of Genetics*. 39:503-536.

Omura, T. 1998. Mitochondria-targeting sequence, a multi-role sorting sequence recognized at all steps of protein import into mitochondria. *Biochem J.* 123:1010-1016.

Ong, S.-B., S. Subrayan, S.Y. Lim, D.M. Yellon, S.M. Davidson, and D.J. Hausenloy. 2010. Inhibiting mitochondrial fission protects the heart against ischemia/reperfusion injury. *Circulation*. 121:2012-2107.

Ono, H., F. Umeda, T. Inoguchi, and H. Ibayashi. 1988. Glucose inhibits prostacyclin production by cultured aortic endothelial-cells. *Thrombosis and Haemostasis*. 60:174-177.

Ott, M., J.D. Robertson, V. Gogvadze, B. Zhivotovsky, and S. Orrenius. 2002. Cytochrome c release from mitochondria proceeds by a two-step process. *Proceedings of the National Academy of Sciences of the United States of America*. 99:1259-1263.

Ouedraogo, R., X.D. Wu, S.Q. Xu, L. Fuchsel, H. Motoshima, K. Mahadev, K. Hough, R. Scalia, and B.J. Goldstein. 2006. Adiponectin suppression of high-glucose-induced reactive oxygen species in vascular endothelial cells - Evidence for involvement of a cAMP signaling pathway. *Diabetes*. 55:1840-1846.

Palade, G.E. 1953. An electron microscope study of the mitochondrial structure. *Journal of Histochemistry & Cytochemistry*. 1:188-211.

Palmer, C.S., L.D. Osellame, D. Laine, O.S. Koutsopoulos, A.E. Frazier, and M.T. Ryan. 2011. MiD49 and MiD51, new components of the mitochondrial fission machinery. *Embo Reports*. 12:565-573.

Palmiter, R.D., and S.D. Findley. 1995. Cloning and functional-characterization of a mammalian zinc transporter that confers resistance to zinc. *Embo Journal*. 14:639-649.

Paredes, R.M., J.C. Etzler, L.T. Watts, W. Zheng, and J.D. Lechleiter. 2008. Chemical calcium indicators. *Methods*. 46:143-151.

Park, J.-S., B. Koentjoro, D. Veivers, A. Mackay-Sim, and C.M. Sue. 2014. Parkinson's disease-associated human ATP13A2 (PARK9) deficiency causes zinc dyshomeostasis and mitochondrial dysfunction. *Human Molecular Genetics*. 23:2802-2815.

Perraud, A.L., A. Fleig, C.A. Dunn, L.A. Bagley, P. Launay, C. Schmitz, A.J. Stokes, Q.Q. Zhu, M.J. Bessman, R. Penner, J.P. Kinet, and A.M. Scharenberg. 2001. ADP-ribose gating of the calcium-permeable LTRPC2 channel revealed by Nudix motif homology. *Nature*. 411:595-599.

Perraud, A.L., C. Schmitz, and A.M. Scharenberg. 2003. TRPM2 Ca^{2+} permeable cation channels: from gene to biological function. *Cell Calcium*. 33:519-531.

Phan, N.Q., S.-J. Kima, and D.C. Bassham. 2008. Overexpression of Arabidopsis Sorting Nexin AtSNX2b Inhibits Endocytic Trafficking to the Vacuole. *Molecular Plant*. 1:961-976.

Putney, J.W. 2005. Capacitative calcium entry: sensing the calcium stores. *Journal of Cell Biology*. 169:381-382.

Qi, X., N. Qvit, Y.-C. Su, and D. Mochly-Rosen. 2013. A novel Drp1 inhibitor diminishes aberrant mitochondrial fission and neurotoxicity. *Journal of Cell Science*. 126:789-802.

Raha, S., and B.H. Robinson. 2000. Mitochondria, oxygen free radicals, disease and ageing. *Trends in Biochemical Sciences*. 25:502-508.

Rahn, J.J., K.D. Stackley, and S.S.L. Chan. 2013. Opa1 Is Required for Proper Mitochondrial Metabolism in Early Development. *Plos One*. 8(3):59218

Rajendran, L., HJ. Knoelker, and K. Simons. 2010. Subcellular targeting strategies for drug design and delivery. *Nature Reviews Drug Discovery*. 9:29-42.

Rathmann, W., and G. Giani. 2004. Global prevalence of diabetes: Estimates for the year 2000 and projections for 2030 - Response to Wild et al. *Diabetes Care*. 27:2568-2569.

Rehman, J., H.J. Zhang, P.T. Toth, Y. Zhang, G. Marsboom, Z. Hong, R. Salgia, A.N. Husain, C. Wietholt, and S.L. Archer. 2012. Inhibition of mitochondrial fission prevents cell cycle progression in lung cancer. *FASEB J*. 26:2175-2186.

Reinhard, K., J.-S. Rougier, J. Ogrodnik, and H. Abriel. 2013. Electrophysiological properties of mouse and epitope-tagged human cardiac sodium channel Na v1.5 expressed in HEK293 cells. *F1000Research*. 2:48.

Reiter, R.J. 1995. Oxidative processes and antioxidative defense-mechanisms in the aging brain. *Faseb Journal*. 9:526-533.

Repnik, U., M.H. Cesen, and B. Turk. 2014. Lysosomal membrane permeabilization in cell death: Concepts and challenges. *Mitochondrion*. 19:49-57.

Richter, C. 1993. Pro-oxidants and mitochondrial Ca^{2+}-their relationship to apoptosis and oncogenesis. *Febs Letters*. 325:104-107.

Rizzuto, R., and T. Pozzan. 2006. Microdomains of intracellular Ca^{2+}: Molecular determinants and functional consequences. *Physiological Reviews*. 86:369-408.

Roberts, J.C., J.B. Davis, and C.D. Benham. 2004. H-3 resiniferatoxin autoradiography in the CNS of wild-type and TRPV1 null mice defines TRPV1 (VR-1) protein distribution. *Brain Research*. 995:176-183.

Rodriguez, A., P. Webster, J. Ortego, and N.W. Andrews. 1997. Lysosomes behave as Ca^{2+}-regulated exocytic vesicles in fibroblasts and epithelial cells. *Journal of Cell Biology*. 137:93-104.

Ron, D., and P. Walter. 2007. Signal integration in the endoplasmic reticulum unfolded protein response. *Nature Reviews Molecular Cell Biology*. 8:519-529.

Rosenstock, T.R., A.C.P. Carvalho, A. Jurkiewicz, R. Frussa, and S.S. Smaili. 2004. Mitochondrial calcium, oxidative stress and apoptosis in a neurodegenerative disease model induced by 3-nitropropionic acid. *Journal of Neurochemistry*. 88:1220-1228.

Roth, J., M. Bendayan, and L. Orci. 1978. Ultrastructural localization of intracellular antigens by the use of protein a-gold complex. *Journal of Histochemistry & Cytochemistry*. 26:1074-1081.

Salin, M.L., and J.M. McCord. 1975. Free-radicals and inflammation - protection of phagocytosing leukocytes by superoxide-dismutase. *Journal of Clinical Investigation*. 56:1319-1323.

Sano, Y., K. Inamura, A. Miyake, S. Mochizuki, H. Yokoi, H. Matsushime, and K. Furuichi. 2001. Immunocyte Ca^{2+} influx system mediated by LTRPC2. *Science*. 293:1327-1330.

Santel, A., and M.T. Fuller. 2001. Control of mitochondrial morphology by a human mitofusin. *Journal of Cell Science*. 114:867-874.

Scaffidi, C., S. Kirchhoff, P.H. Krammer, and M.E. Peter. 1999. Apoptosis signaling in lymphocytes. *Current Opinion in Immunology*. 11:277-285.

Scherz-Shouval, R., and Z. Elazar. 2007. ROS, mitochondria and the regulation of autophagy. *Trends in Cell Biology*. 17:422-427.

Scherz-Shouval, R., and Z. Elazar. 2011. Regulation of autophagy by ROS: physiology and pathology. *Trends in Biochemical Sciences*. 36:30-38.

Sena, L.A., and N.S. Chandel. 2012. Physiological roles of mitochondrial reactive oxygen species. *Mol Cell*. 48:158-167.

Sensi, S.L., P. Paoletti, A.I. Bush, and I. Sekler. 2009. Zinc in the physiology and pathology of the CNS. *Nature Reviews Neuroscience*. 10:780-738.

Seo, S.R., S.A. Chong, S.I. Lee, J.Y. Sung, Y.S. Ahn, K.C. Chung, and J.T. Seo. 2001. Zn^{2+}-induced ERK activation mediated by reactive oxygen species causes cell death in differentiated PC12 cells. *Journal of Neurochemistry*. 78:600-610.

Sesaki, H., and R.E. Jensen. 1999. Division versus fusion: Dnm1p and Fzo1p antagonistically regulate mitochondrial shape. *Journal of Cell Biology*. 147:699-706.

Shenouda, S.M., M.E. Widlansky, K. Chen, G. Xu, M. Holbrook, C.E. Tabit, N.M. Hamburg, A.A. Frame, T.L. Caiano, M.A. Kluge, M.A. Duess, A. Levit, B. Kim, M.L. Hartman, L. Joseph, O.S. Shirihai, and J.A. Vita. 2011. Altered mitochondrial dynamics contributes to endothelial dysfunction in diabetes mellitus. *Circulation*. 124:444-453.

Shimkets, R.A., R.P. Lifton, and C.M. Canessa. 1997. The activity of the epithelial sodium channel is regulated by clathrin-mediated endocytosis. *Journal of Biological Chemistry*. 272:25537-25541.

Sies, H. 1997. Oxidative stress: Oxidants and antioxidants. *Experimental Physiology*. 82:291-295.

Simons, K., and D. Toomre. 2000. Lipid rafts and signal transduction. *Nature Reviews Molecular Cell Biology*. 1:31-39.

Sivaprasadarao, A., and J.B.C. Findlay. 1993. Expression of functional human retinol-binding protein in escherichia-coli using a secretion vector. *Biochemical Journal*. 296:209-215.

Slee, E.A., M.T. Harte, R.M. Kluck, B.B. Wolf, C.A. Casiano, D.D. Newmeyer, H.G. Wang, J.C. Reed, D.W. Nicholson, E.S. Alnemri, D.R. Green, and S.J. Martin. 1999. Ordering the cytochrome c-initiated caspase cascade: Hierarchical activation of caspases-2, -3, -6, -7, -8, and -10 in a caspase-9-dependent manner. *Journal of Cell Biology*. 144:281-292.

Slupe, A.M., R.A. Merrill, K.H. Flippo, M.A. Lobas, J.C.D. Houtman, and S. Strack. 2013. A calcineurin docking motif (LXVP) in dynamin-related protein 1 contributes to mitochondrial fragmentation and ischemic neuronal injury. *Journal of Biological Chemistry*. 288:12353-12365.

Smirnova, E., L. Griparic, D.L. Shurland, and A.M. van der Bliek. 2001. Dynamin-related protein Drp1 is required for mitochondrial division in mammalian cells. *Molecular Biology of the Cell*. 12:2245-2256.

Smirnova, E., D.L. Shurland, S.N. Ryazantsev, and A.M. van der Bliek. 1998. A human dynamin-related protein controls the distribution of mitochondria. *Molecular Biology of the Cell*. 9:197.

Smith, M.A., P.S. Herson, K. Lee, R.D. Pinnock, and M.L.J. Ashford. 2003. Hydrogen-peroxide-induced toxicity of rat striatal neurones involves activation of a non-selective cation channel. *Journal of Physiology-London*. 547:417-425.

Sohal, R.S., B.H. Sohal, and U.T. Brunk. 1990. Relationship between antioxidant defenses and longevity in different mammalian-species. *Mechanisms of Ageing and Development*. 53:217-227.

Song, Z.Y., H.C. Chen, M. Fiket, C. Alexander, and D.C. Chan. 2007. OPA1 processing controls mitochondrial fusion and is regulated by mRNA splicing, membrane potential, and Yme1L. *Journal of Cell Biology*. 178:749-755.

Strehler, E.E., and M. Treiman. 2004. Calcium pumps of plasma membrane and cell interior. *Current Molecular Medicine*. 4:323-335.

Suen, D.F., K.L. Norris, and R.J. Youle. 2008. Mitochondrial dynamics and apoptosis. *Genes Dev*. 22:1577-1590.

Sumimoto, H. 2008. Structure, regulation and evolution of Nox-family NADPH oxidases that produce reactive oxygen species. *Febs Journal*. 275:3984-3984.

Sumoza-Toledo, A., I. Lange, H. Cortado, H. Bhagat, Y. Mori, A. Fleig, R. Penner, and S. Partida-Sanchez. 2011. Dendritic cell maturation and chemotaxis is regulated by TRPM2-mediated lysosomal Ca^{2+} release. *Faseb Journal*. 25:3529-3542.

Sumoza-Toledo, A., and R. Penner. 2011. TRPM2: a multifunctional ion channel for calcium signalling. *Journal of Physiology-London*. 589:1515-1525.

Sumpio, B.E., J.T. Riley, and A. Dardik. 2002. Cells in focus: endothelial cell. *International Journal of Biochemistry & Cell Biology*. 34:1508-1512.

Sun, L., L. Xiao, J. Nie, F.-y. Liu, G.-h. Ling, X.-j. Zhu, W.-b. Tang, W.-c. Chen, Y.-c. Xia, M. Zhan, M.-m. Ma, Y.-m. Peng, H. Liu, Y.-h. Liu, and Y.S. Kanwar. 2010. p66Shc mediates high-glucose and angiotensin II-induced oxidative stress renal tubular injury via mitochondrial-dependent apoptotic pathway. *American Journal of Physiology-Renal Physiology*. 299:1014-1025.

Sun, L., H.-Y. Yau, W.-Y. Wong, R.A. Li, Y. Huang, and X. Yao. 2012. Role of TRPM2 in H_2O_2-induced cell apoptosis in endothelial cells. *Plos One*. 7(8):43186.

Szabadkai, G., A.M. Simoni, K. Bianchi, D. De Stefani, S. Leo, M.R. Wieckowski, and R. Rizzuto. 2006. Mitochondrial dynamics and Ca^{2+} signaling. *Biochimica et biophysica acta*. 1763:442-449.

Takahashi, N., D. Kozai, R. Kobayashi, M. Ebert, and Y. Mori. 2011. Roles of TRPM2 in oxidative stress. *Cell Calcium*. 50:279-287.

Tan, Y., N. Dourdin, C. Wu, T. De Veyra, J.S. Elce, and P.A. Greer. 2006. Ubiquitous calpains promote caspase-12 and JNK activation during endoplasmic reticulum stress-induced apoptosis. *Journal of Biological Chemistry*. 281:16016-16024.

Tochigi, M., T. Inoue, M. Suzuki-Karasaki, T. Ochiai, C. Ra, and Y. Suzuki-Karasaki. 2013. Hydrogen peroxide induces cell death in human TRAIL-resistant melanoma through intracellular superoxide generation. *International Journal of Oncology*. 42:863-872.

Togashi, K., Y. Hara, T. Tominaga, T. Higashi, Y. Konishi, Y. Mori, and M. Tominaga. 2006. TRPM2 activation by cyclic ADP-ribose at body temperature is involved in insulin secretion. *Embo Journal*. 25:1804-1815.

Togashi, K., H. Inada, and M. Tominaga. 2008. Inhibition of the transient receptor potential cation channel TRPM2 by 2-aminoethoxydiphenyl borate (2-APB). *British Journal of Pharmacology*. 153:1324-1330.

Trachootham, D., W. Lu, M.A. Ogasawara, R.D. Nilsa, and P. Huang. 2008. Redox regulation of cell survival. *Antioxid Redox Signal*. 10:1343-1374.

Travers, K.J., C.K. Patil, L. Wodicka, D.J. Lockhart, J.S. Weissman, and P. Walter. 2000. Functional and genomic analyses reveal an essential coordination between the unfolded protein response and ER-associated degradation. *Cell*. 101:249-258.

Tirosh, A., I. Shai, D. Tekes-Manova, E. Israeli, D. Pereg, T. Shochat, I. Kochba, A. Rudich, and G. Israeli Diabetes Res. 2005. Normal fasting plasma glucose levels and type 2 diabetes in young men. *New England Journal of Medicine*. 353:1454-1462.

Trudeau, K., A.J.A. Molina, and S. Roy. 2011. High glucose induces mitochondrial morphology and metabolic changes in retinal pericytes. *Investigative Ophthalmology & Visual Science*. 52:8657-8664.

Trushina, E., and C.T. McMurray. 2007. Oxidative stress and mitochondrial dysfunction in neurodegenerative diseases. *Neuroscience*. 145:1233-1248.

Tsien, R.Y. 1980. new calcium indicators and buffers with high selectivity against magnesium and protons - design, synthesis, and properties of prototype structures. *Biochemistry*. 19:2396-2404.

Turk, B., and V. Turk. 2009. Lysosomes as "Suicide Bags" in cell death: myth or reality? *Journal of Biological Chemistry*. 284:21783-21787.

Uchida, K., K. Dezaki, B. Damdindorj, H. Inada, T. Shiuchi, Y. Mori, T. Yada, Y. Minokoshi, and M. Tominaga. 2011. Lack of TRPM2 impaired insulin secretion and glucose metabolisms in mice. *Diabetes*. 60:119-126.

Ueda, S., S. Ozawa, K. Mori, K. Asanuma, M. Yanagita, S. Uchida, and T. Nakagawa. 2015. eNOS deficiency causes podocyte injury with mitochondrial abnormality. *Free Radical Biology and Medicine*. 87:181-192.

Uttara, B., A.V. Singh, P. Zamboni, and R.T. Mahajan. 2009. Oxidative stress and neurodegenerative diseases: a review of upstream and downstream antioxidant therapeutic options. *Current Neuropharmacology*. 7:65-74.

Vallee, B.L., and K.H. Falchuk. 1993. The biochemical basis of zinc physiology. *Physiological Reviews*. 73:79-118.

Valluru, L., J. Xu, Y.L. Zhu, S. Yang, A. Contractor, and G.T. Swanson. 2005. Ligand binding is a critical requirement for plasma membrane expression of heteromeric kainate receptors. *Journal of Biological Chemistry*. 280:6085-6093.

Vaxillaire M., C. Populaire, K. Busiah, H. Cave, AL. Gloyn, AT. Hattersley, P. Czernichow, P. Froguel and M. Polak. 2004. Kir6.2 mutations are a common cause of permanent neonatal diabetes in a large cohort of french patients. *Diabetes.* 53: 2719-2722.

van Engeland, M., L.J.W. Nieland, F.C.S. Ramaekers, B. Schutte, and C.P.M. Reutelingsperger. 1998. Annexin V-affinity assay: a review on an apoptosis detection system based on phosphatidylserine exposure. *Cytometry*. 31:1-9.

Vanden Berghe, T., N. Vanlangenakker, E. Parthoens, W. Deckers, M. Devos, N. Festjens, C.J. Guerin, U.T. Brunk, W. Declercq, and P. Vandenabeele. 2010. Necroptosis, necrosis and secondary necrosis converge on similar cellular disintegration features. *Cell Death and Differentiation*. 17:922-930.

Venkatachalam, K., and C. Montell. 2007. TRP channels. *Annual Review of Biochemistry.* 76:387-417.

Vincent, A.M., J.L. Edwards, L.L. McLean, Y. Hong, F. Cerri, I. Lopez, A. Quattrini, and E.L. Feldman. 2010. Mitochondrial biogenesis and fission in axons in cell culture and animal models of diabetic neuropathy. *Acta Neuropathologica*. 120:477-489.

Wakabayashi, J., Z. Zhang, N. Wakabayashi, Y. Tamura, M. Fukaya, T.W. Kensler, M. Iijima, and H. Sesaki. 2009. The dynamin-related GTPase Drp1 is required for embryonic and brain development in mice. *Journal of Cell Biology*. 186:805-816.

Wallwork, J.C. 1987. Zinc and the central-nervous-system. *Progress in Food and Nutrition Science*. 11:203-247.

Wang, J., K.A. Pareja, C.A. Kaiser, and C.S. Sevier. 2014. Redox signalling via the molecular chaperone BiP protects cells against endoplasmic reticulum-derived oxidative stress. *Elife*. 3:03496.

Wang, W.J., Y. Wang, J.Y. Long, J.R. Wang, S.B. Haudek, P. Overbeek, B.H.J. Chang, P.T. Schumacker, and F.R. Danesh. 2012. Mitochondrial fission triggered by hyperglycemia is mediated by rock1 activation in podocytes and endothelial cells. *Cell Metabolism*. 15:186-200.

Wang, X., B. Su, H.-g. Lee, X. Li, G. Perry, M.A. Smith, and X. Zhu. 2009. Impaired balance of mitochondrial fission and fusion in Alzheimer's disease. *Journal of Neuroscience*. 29:9090-9103.

Wang, X.D. 2001. The expanding role of mitochondria in apoptosis. *Genes & Development*. 15:2922-2933.

Waris, G., and H. Ahsan. 2006. Reactive oxygen species: role in the development of cancer and various chronic conditions. *Journal of carcinogenesis*. 5:14-14.

Wehage, E., J. Eisfeld, I. Heiner, E. Jungling, C. Zitt, and A. Luckhoff. 2002. Activation of the cation channel long transient receptor potential channel 2 (LTRPC2) by hydrogen peroxide - a splice variant reveals a mode of activation independent of ADP-ribose. *Journal of Biological Chemistry*. 277:23150-23156.

Wei, M.C., W.X. Zong, E.H.Y. Cheng, T. Lindsten, V. Panoutsakopoulou, A.J. Ross, K.A. Roth, G.R. MacCregor, C.B. Thompson, and S.J. Korsmeyer. 2001. Proapoptotic BAX and BAK: A requisite gateway to mitochondrial dysfunction and death. *Science*. 292:727-730.

Weiss, J.H., S.L. Sensi, and J.Y. Koh. 2000. Zn^{2+}: a novel ionic mediator of neural injury in brain disease. *Trends in Pharmacological Sciences*. 21:395-401.

Werner, E. 2004. GTPases and reactive oxygen species: switches for killing and signaling. *Journal of Cell Science*. 117:143-153.

Wilkinson, J.A., J.L. Scragg, J.P. Boyle., B. Nilius, and C. Peers. 2008. H_2O_2-stimulated Ca^{2+} influx via TRPM2 is not the sole determinant of subsequent cell death. *Eur J Physiol*. 455:1141–1151.

Wiseman, D.A., S.M. Wells, M. Hubbard, J.E. Welker, and S.M. Black. 2007. Alterations in zinc homeostasis underlie endothelial cell death induced by oxidative

stress from acute exposure to hydrogen peroxide. *American Journal of Physiology-Lung Cellular and Molecular Physiology*. 292:165-177.

Xia, R., Z.Z. Mei, H.-J. Mao, W. Yang, L. Dong, H. Bradley, D.J. Beech, and L.H. Jiang. 2008. Identification of pore residues engaged in determining divalent cationic permeation in transient receptor potential melastatin subtype channel. *Journal of Biological Chemistry*. 283:27426-27432.

Xu, H.X., and D.J. Ren. 2015. Lysosomal Physiology. Annual Review of Physiology. 77: 57-80.

Yang, W., P.T. Manna, J.E. Zou, J.H. Luo, D.J. Beech, A. Sivaprasadarao, and L.H. Jiang. 2011. Zinc inactivates melastatin transient receptor potential 2 channels via the outer pore. *Journal of Biological Chemistry*. 286:23789-23798.

Ye, M., W. Yang, J.F. Ainscough, X.P. Hu, X. Li, A. Sedo, X.H. Zhang, X. Zhang, Z. Chen, X.M. Li, D.J. Beech, A. Sivaprasadarao, J.H. Luo, and L.H. Jiang. 2014. TRPM2 channel deficiency prevents delayed cytosolic Zn^{2+} accumulation and CA1 pyramidal neuronal death after transient global ischemia. *Cell Death Dis*. 5:1541.

Yoon, Y., K.R. Pitts, S. Dahan, and M.A. McNiven. 1998. A novel dynamin-like protein associates with cytoplasmic vesicles and tubules of the endoplasmic reticulum in mammalian cells. *Journal of Cell Biology*. 140:779-793.

Youle, R.J., and D.P. Narendra. 2011. Mechanisms of mitophagy. *Nature Reviews Molecular Cell Biology*. 12:9-14.

Youle, R.J., and A.M. van der Bliek. 2012. Mitochondrial fission, fusion, and stress. *Science*. 337:1062-1065.

Yu, E.P.K., and M.R. Bennett. 2014. Mitochondrial DNA damage and atherosclerosis. *Trends in Endocrinology and Metabolism*. 25:481-487.

Yu, P., Q. Wang, L.-H. Zhang, H.-C. Lee, L. Zhang, and J. Yue. 2012. A cell permeable NPE caged ADP-ribose for studying TRPM2. *Plos One*. 7(12):51028.

Yu, S.W., H. Wang, M.F. Poitras, C. Coombs, W.J. Bowers, H.J. Federoff, G.G. Poirier, T.M. Dawson, and V.L. Dawson. 2002. Mediation of poly(ADP-ribose) polymerase-1-dependent cell death by apoptosis-inducing factor. *Science*. 297:259-263.

Yu, T., S.-S. Sheu, J.L. Robotham, and Y. Yoon. 2008. Mitochondrial fission mediates high glucose-induced cell death through elevated production of reactive oxygen species. *Cardiovascular Research*. 79:341-351.

Zeng, X., S.C. Sikka, L. Huang, C. Sun, C. Xu, D. Jia, A.B. Abdel-Mageed, J.E. Pottle, J.T. Taylor, and M. Li. 2010. Novel role for the transient receptor potential channel TRPM2 in prostate cancer cell proliferation. *Prostate Cancer and Prostatic Diseases*. 13:195-201.

Zhang, D.X., and D.D. Gutterman. 2007. Mitochondrial reactive oxygen species-mediated signalling in endothelial cells. *American Journal of Physiology-Heart and Circulatory Physiology*. 292:2023-2031.

Zhang, J.H., and M. Xu. 2000. DNA fragmentation in apoptosis. *Cell Research*. 10:205-211.

Zhang, K., and R.J. Kaufman. 2008. From endoplasmic-reticulum stress to the inflammatory response. *Nature*. 454:455-462.

Zhao, M., U.T. Brunk, and J.W. Eaton. 2001. Delayed oxidant-induced cell death involves activation of phospholipase A2. *Febs Letters*. 509:399-404.

Zorov, D.B., M. Juhaszova, and S.J. Sollott. 2014. Mitochondrial reactive oxygen species (ROS) and ROS-induced ROS release. *Physiol Rev*. 94:909-950.

Zou, J., J.F. Ainscough, W. Yang, A. Sedo, S.-P. Yu, Z.-Z. Mei, A. Sivaprasadarao, D.J. Beech, and L.H. Jiang. 2013. A differential role of macrophage TRPM2 channels in Ca^{2+} signalling and cell death in early responses to H_2O_2. *American Journal of Physiology-Cell Physiology*. 305:61-69.